Modeling and Prediction in Diabetes Physiology

Cescon, Marzia

2013

Document Version:
Publisher's PDF, also known as Version of record

Modeling and Prediction in Diabetes Physiology

Marzia Cescon

LUNDS
UNIVERSITET

Department of Automatic Control

PhD Thesis
ISRN LUTFD2/TFRT--1099--SE
ISSN 0280–5316

Department of Automatic Control
Lund University
Box 118
SE-221 00 LUND
Sweden

Printed in Sweden by MediaTryck.
Lund 2013

Abstract

Diabetes is a group of metabolic diseases characterized by the inability of the organism to autonomously regulate the blood glucose levels. It requires continuing medical care to prevent acute complications and to reduce the risk of long-term complications. Inadequate glucose control is associated with damage, dysfunction and failure of various organs.

The management of the disease is non trivial and demanding. With today's standards of current diabetes care, good glucose regulation needs constant attention and decision-making by the individuals with diabetes. Empowering the patients with a decision support system would, therefore, improve their quality of life without additional burdens nor replacing human expertise.

This thesis investigates the use of data-driven techniques to the purpose of glucose metabolism modeling and short-term blood-glucose predictions in Type I Diabetes Mellitus (T1DM). The goal was to use models and predictors in an advisory tool able to produce personalized short-term blood glucose predictions and on-the-spot decision making concerning the most adequate choice of insulin delivery, meal intake and exercise, to help diabetic subjects maintaining glycemia as close to normal as possible.

The approaches taken to describe the glucose metabolism were discrete-time and continuous-time models on input-output form and state-space form, while the blood glucose short-term predictors, i.e., up to 120 minutes ahead, used ARX-, ARMAX- and subspace-based prediction.

Acknowledgments

First of all I would like to acknowledge my supervisor Rolf Johansson for having introduced me to graduate studies and for the opportunity to join the DIAdvisor project. All the DIAdvisor collegues have been excellent sources of insightful discussions at many levels. Their expertise in various fields other than control theory allowed me to have a broader view on many topics and is therefore highly appreciated.

Special thanks go to Per Hagander for the support and encouragment during the last few years.

I would like to thank the persons that proofread the manuscript: Rolf Johansson, Per Hagander, Fredrik Ståhl, Giacomo Como, Enrico Bini and Carolina Lidstrom. Also, Leif Andersson deserves credit for the typesetting of this thesis.

The Department of Automatic Control is just the best one could ask for graduate studies. It is a creative and friendly environment, pervaded by a positive atmosphere and a confident attitude. I'm fortunate to have been a member of this talented group of people.

I owe my gratitude to all the Ph.D. fellows that in one way or another shared with me the daily life at work. In particular, I would like to thank Fredrik Ståhl with whom I have been so lucky to closely collaborate and travel around the world for the various project-related meetings and conferences. I'm very thankful to my office mate Meike Stemmann for letting me have two thirds of the office space and not tripping over my bike...of course much more than that!

I acknowledge my second family: the SK RAN athletes and La Famiglia for the good time together at home, at training camps and at competitions.

Last, I would like to thank my family for being supportive in all I have been doing and for making me feel your love despite the distance!

Marzia

Financial Support
The author is member of the LCCC Linnaeus Center and the ELLIIT Excellence Center at Lund University. This work was partly supported by the European project DIAdvisor^{TM}, FP7 IST-216592 and the Swedish Research Council by the LCCC Linnaeus Center and by the ELLIIT Excellence Center.

Contents

1

Introduction

1.1 Context and motivation

Diabetes Mellitus is a chronic disease of disordered glucose metabolism due to defects in either insulin secretion by the pancreatic β-cells or insulin action [Williams and Pickup, 1992]. Type I diabetes (T1DM), also called insulin-dependent diabetes mellitus (IDDM) is characterized by failing production of insulin, whereas type II diabetes is caused by decreased sensitivity of the tissues to the metabolic effect of insulin. The basic effect of insulin lack or insulin resistance is to prevent the efficient uptake and utilization of glucose by most cells of the body, mainly the skeletal muscles, resulting in abnormally high blood sugar levels (hyperglycemia). Sustained hyperglycemia is associated with acute ketoacidosis, nephropaty, rethinopaty, neuropathy and damages to the cardio-vascular system which are irreversibile once they develop and can mean serious disability for the person who experiences them [Williams and Pickup, 1992].

With an estimated 371 million affected adult people worldwide in 2012 [The International Diabetes Federation, 2013], diabetes mellitus is one of the most widespread diseases and caused 4.8 million deaths in 2012, ranking fifth by cause-specific mortality in most high-income countries, after communicable diseases, cardiovascular diseases, cancer and injury, being undoubtedly one of the most challenging health problems in the 21st century [The International Diabetes Federation, 2013]. As for healthcare expenditures, North America and the Caribbean spent an estimated USD 223 billion or 48% of the global healthcare expenditures for diabetes in 2011, while Europe spent about half that amount at USD 130 billion. These two regions combined had the highest expenditures due to diabetes in 2011 [The International Diabetes Federation, 2013]. Beside direct costs, indirect costs associated with lost workdays, restricted activity days, lower productivity at work, premature mortality and permanent disability reached 50% of the direct costs. The diabetes epidemic is expected to

increase at an alarming rate unless effective prevention and treatment measures are put in place.

1.2 Statement of the problem

The development of means intended to improve diabetes care and management results decisive in order to curb the diabetes epidemic, both from patients quality of life and economic perspectives. In particular, sustained minimization of the time spent in hyperglycemia while avoiding hypoglycemia can be attained developing an integrated approach which sets no additional burden on the patients and works proactively, considering not only the instantaneous effects of the control actions but also their consequences in the near future. Reaching this goal requires in the first place patient metabolism models tailored to the individual and the actual conditions capable to merge the information already available from the patients and reproduce their dynamics as faithfully as possible.

To this end, the work presented in this thesis investigate patient-specific mathematical models of diabetes glucose dynamics with the purpose of describing the relationships between meal carbohydrate, exogenously injected insulin and possibly energy expenditure due to physical activity [Spurr et al., 1988] and blood glucose evolution in T1DM. Models and algorithms presented herein have been developed and used within the European FP7 IP research project DIAdvisor [DIAdvisor, 2012], aiming for use in a decision support system, namely, the DIAdvisor™ tool [DIAdvisor, 2012].

1.3 Outline of the thesis and contributions

This section serves as an outline of the thesis and a summary of the contributions.

Chapter 2: Background

Chapter 2 provides background material on blood glucose regulation, the physiology of diabetes and diabetes care, including an overview of the DIAdvisor™ project. Further, in the second part of the chapter, the vast literature on diabetes modeling is summarized.

Chapter 3: Experimental Conditions and Clinical Data Acquisition

The experimental conditions and clinical data acquisition within DIAdvisor™ are dealt with in Chapter 3. The equipment adopted by

the study participants is described, the study related procedure are illustrated and the criteria for the selection of the patients are given. Finally, an analysis of the reliability of glucose sensor measurements concludes the chapter.

The core contributions of the thesis are described in Chapters 4 to 8 and can be divided into two main topics: glucose metabolism modeling and short-term blood glucose prediction.

Chapter 4: Modeling of the Gluco-regulatory System

Chapter 4 considers discrete-time data-based system identification of the glucose-regulatory system. Individual-specific models were identified from a selected patients population data. Objective of the study was to provide the DIAdvisor Consortium with a set of personalized model to be implemented in the first prototype of the DIAdvisor^{TM} tool.

Related publications

Cescon, M. (2011). *Linear Modeling and Prediction in Diabetes Physiology*. Licentiate Thesis TFRT--3250--SE. Department of Automatic Control, Lund University, Sweden.

Cescon, M. and R. Johansson (2009). "Glycemic trend prediction using empirical model identification". In: *Proc. 48th IEEE Conference on Decision and Control (CDC2009)*. Shanghai, P.R.China, pp. 3501–3506.

Cescon, M. and R. Johansson (2013). "Linear modeling and prediction in diabetes physiology." In: Marmarelis, V. et al. (Eds.). *Data-driven Modeling for Diagnosis and Treatment of Diabetes*. Springer. In press.

Cescon, M., F. Ståhl, R. Johansson, and M. Landin-Olsson (2009a). "Short-term diabetes blood glucose prediction based on blood glucose measurements". In: *Proc. 2nd International Conference on Advanced Technologies and Treatments for Diabetes (ATTD2009)*. Athens, Greece.

Cescon, M., F. Ståhl, M. Landin-Olsson, and R. Johansson (2009b). "Subspace-based model identification of diabetic blood glucose dynamics". In: *Proc. 15th IFAC Symposium on System Identification (SYSID2009)*. Saint-Malo, France, pp. 233–238.

Chapter 5: Subspace-based Linear Multi-step Predictors for Predictive Control

In the framework of the subspace-based identification of linear systems, the first step for the construction of a state-space model from observed input-output data involves the estimation of the output predictor. This algorithmic step was elaborated in Chapter 5 to introduce short-term multi-step predictors.

Related publications

Cescon, M. and R. Johansson (2010). "Multi-step-ahead multivariate predictors: a comparative analysis". In: *Proc. 49th IEEE Conference on Decision and Control (CDC2010)*. Atlanta, USA, pp. 2837–2842.

Cescon, M. and R. Johansson (2011). "On data-driven multistep subspace-based linear predictors". In: *Proc. 18th IFAC World Congress (IFAC2011)*. Milano, Italy, pp. 11447–11452.

Chapter 6: Subspace-based Linear Multi-step Predictors in Diabetes

Chapter 6 presents the application of subspace-based multi-step short-term predictors introduced in Chapter 5 to the problem of T1DM blood glucose time-series forecasting.

Related publications

Cescon, M. and R. Johansson (2013). "Subspace-based multi-step predictors for predictive control." In: Lovera, M. (Ed.). *Control-oriented modelling and identification: theory and applications*. The institution of engineering and technology (IET). Submitted.

Chapter 7: Continuous-time State-Space Identification

Chapter 7 reviews theory and algorithms for system identification of continuous-time state-space models from finite discrete-time possibly non-uniformly sampled input-output data. Two approaches are presented, based on previous contributions: one subspace-based and one realization-based.

Related publications

Cescon, M., R. Johansson, E. Renard, and A. Maran (2013). "Identification of individualized empirical models of carbohydrate and insulin effects on T1DM blood glucose dynamics". *International Journal of Control. Special Issue on Applications of Continuous-Time Model Identification and Estimation.* In press.

Johansson, R., M. Cescon, and F. Ståhl (2013). "Continuous-time model identification using non-uniformly sampled data". In: *11th IEEE AFRICON 2013*. Mauritius. September 2013.

Chapter 8: Modeling the Impact of Meal and Insulin Intakes on Glycemia

In Chapter 8 the impact of carbohydrate intakes and insulin injections on diabetes glycemia is modeled with second order plus time delay continuous-time transfer functions. The models were identified from

a novel meal test data collected within DIAdvisor™ by means of the continuous-time algorithm $\text{PBSID}_{\text{cont}}$ given in Chapter 7.

Related publications

Cescon, M. and R. Johansson (2012). "Patient-specific glucose metabolism models for model predictive control of T1DM glycemia". In: *Proc. 5th International Conference on Advanced Technologies and Treatments for Diabetes (ATTD2012)*. Barcelona, Spain.

Cescon, M. and R. Johansson (2013). "Meal and insulin effects on blood glucose dynamic modeling". In: *13th Diabetes Technology Meeting (DTM2013)*. San Francisco, CA, USA.

Cescon, M., R. Johansson, E. Renard, and J. Place (2012a). "Modeling the impact of a standardized breakfast on T1DM fasting blood glucose". In: *12th Diabetes Technology Meeting (DTM2012)*. Bethesda, MD, USA.

Cescon, M., R. Johansson, and E. Renard (2012b). "Personalized short-term blood glucose prediction in T1DM". In: *Proc. 5th International Conference on Advanced Technologies and Treatments for Diabetes (ATTD2012)*. Barcelona, Spain.

Cescon, M., R. Johansson, E. Renard, and A. Maran (2013a). "Identification of individualized empirical models of carbohydrate and insulin effects on T1DM blood glucose dynamics". *International Journal of Control. Special Issue on Applications of Continuous-Time Model Identification and Estimation.*

Cescon, M., R. Johansson, and E. Renard (2013b). "Individualized empirical models of carbohydrate and insulin effects on T1DM blood glucose dynamics". In: *7th IEEE Multi-Conference on Systems and Control (MSC2013)*. Hyderabad, India, pp. 258–263.

Cescon, M., R. Johansson, and E. Renard (2013c). "Low-complexity MISO models of T1DM glucose metabolism". In: *9th Asian Control Conference (ASCC2013)*. Istanbul, Turkey.

Johansson, R., M. Cescon, and F. Ståhl (2013). "Continuous-time model identification using non-uniformly sampled data". In: *11th IEEE AFRICON 2013*. Mauritius.

Chapter 9: Conclusions

Finally, Chapter 9 concludes the thesis with some closing remarks and the outline of possible further research directions.

Other relevant publications by the author on the topic:

Cescon, M. and E. Renard (2011). “Adaptive subspace-based prediction of T1DM glycemia”. In: *Proc. 50th IEEE Conference on Decision and Control and European Control Conference (CDC-ECC2012)*. Orlando, FL, pp. 5164–5169.

Cescon, M., M. Stemmann, and R. Johansson (2012a). “Impulsive predictive control of T1DM glycemia: an in-silico study”. In: *Reglermöte 2012*. Uppsala, Sweden.

Cescon, M., M. Stemmann, and R. Johansson (2012b). “Impulsive predictive control of T1DM glycemia: an in-silico study”. In: *2012 ASME 5th Annual Dynamic Systems and Control Conference (DSCC2012)*. Fort Lauderdale, FL, USA, p. 8550.

Ståhl, F., M. Cescon, R. Johansson, and E. Renard (2009). “Infinite horizon prediction of postprandial breakfast plasma glucose excursion”. In: *Proc. 9th Diabetes Technology Meeting (DTM2009)*. San Francisco, CA, A163.

2

Background

2.1 Introduction

Glucose is the primary substrate for energy in the insulin-independent tissues (IIT), i.e., central nervous system and red blood cells. It is, therefore, vital that an adequate amount of glucose is always present in the bloodstream to continuously supply the nutritional requirements of the IIT [Nussey and Whitehead, 2001]. This is achieved by homoeostatic regulation of the concentration of extracellular fluid glucose. Glucose concentration is increased by intestinal absorption following meals and by glucose production in the liver and decreased by glucose uptake from the peripheral tissues. In a healthy subject, the balance between glucose entering and leaving the bloodstream is guaranteed by the actions of a highly complex neuro-hormonal control system, i.e., the glucoregulatory system [Williams and Pickup, 1992], which maintains blood glucose concentration within relatively narrow limits at around 90 [mg/dL].

2.2 Blood glucose regulation

After a food intake, during the so-called absorptive state, some glucose absorbed from the gut is immediately used by cells as a source of energy. That fraction not directly utilized is either stored in the liver or muscles in the form of glycogen or converted to triglyceride in adipocytes. Glucose storage is promoted by the hormone insulin. Then, between meals, i.e., in the post-absorptive state, glucose is first obtained from glycogen stores and subsequently by hepatic production from amino acids, these actions being governed by the hormone glucagon. These processes maintain plasma glucose within tight limits, assuring a constant supply of fuel to the IIT. Figure 2.1 shows the glucose-insulin control system for the non-diabetic subject.

Insulin and glucagon actions

The two main drivers of the glucoregulatory system are the pancreas-secreted hormones insulin and glucagon.

Insulin is secreted by the β-cells when the glucose in blood rises to a high concentration. Triglycerides and fatty acids have only a small stimulatory effect on insulin release. In response to a glucose load, insulin secretion occurs in two phases: the first phase represents the release of insulin stored in secretory granules, while the second, approximately 10 minutes later, shows a more gradual and sustained increase in insulin release that can last for several hours [Nussey and Whitehead, 2001]. Insulin promotes glycogen synthesis in the liver and induces a rapid uptake of glucose in muscles and fat tissue. In the muscles glucose is converted to glycogen, while in the adipose tissue it is converted to fatty acids for storage as triglyceride. Meanwhile, mobilization of fuels is suppressed by insulin, by inhibiting the breakdown of glycogen in the liver, the release of amino acids from muscle and the release of free fatty acids from adipose tissue.

Glucagon, on the other hand, is released by the α-cells of the pancreas, in response to a decreased insulin secretion. It has opposing actions (counter-regulatory) to those of insulin, promoting, instead of suppressing, mobilization of fuels. Glucagon ultimately stimulates the breakdown of glycogen to glucose (glycogenolysis) and the production of glucose from amino acids (gluconeogenesis). In addition, it promotes the release of free fatty acids from adipose tissue.

The glucose and insulin systems interact by feedback control: if a glucose rise occurs after a meal, the β-cells secrete more insulin in response to increased plasma glucose concentration and in turn insulin signaling promotes glucose uptake by the liver, muscles and adipose tissue, inhibiting glucose production thereby bringing the plasma glucose level back toward a steady-state value. These control interactions are usually referred to as insulin sensitivity and β-cell responsiveness. When the blood glucose concentration begins to fall, the consequent rapid decrease in insulin secretion triggers in turn glucagon release by the α-cells of the pancreas. Glucagon promotes the breakdown of the liver glycogen back to glucose, which is then released into the bloodstream preventing glucose concentration from falling too low [Williams and Pickup, 1992].

The secretion of both insulin and glucagon is potentiated by the gastrointestinal hormones incretins, released in response to orally ingested nutrients. Other hormones that also play major roles in the regulation of blood glucose concentrations include cortisol, adrenaline and growth hormone, all of which act to raise blood glucose concentrations and are, thus, considered to be counter-regulatory [Nussey and Whitehead, 2001].

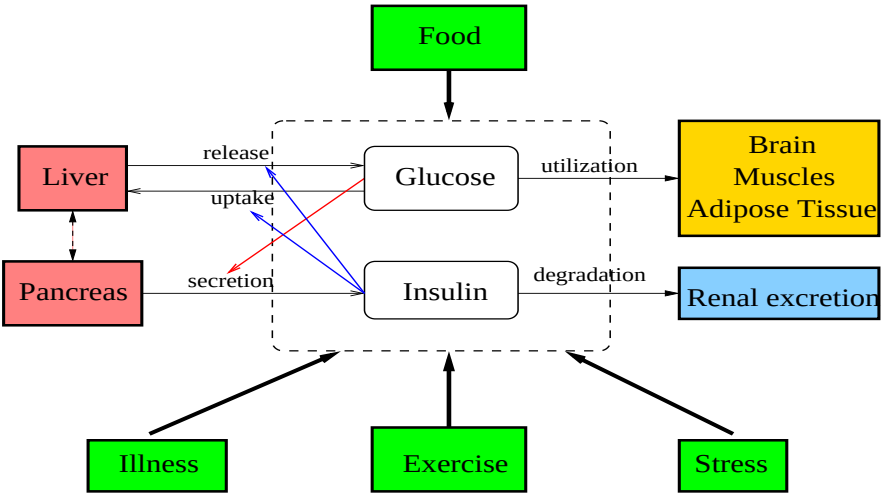

Figure 2.1 Glucose-insulin control system in the non-diabetic subject. 1. Increased blood glucose stimulates insulin secretion from the pancreas; 2. Insulin promotes liver uptake, storage and use of glucose; 3. Glucose is released back from the liver during fasting conditions

Overall, the mechanisms controlling the glucose-insulin systems stems from metabolic stimuli, gut hormones and neural reactions.

2.3 Diabetes mellitus

When the insulin feedback fails to function normally by either lack of insulin secretion or decreased sensitivity of the tissues to insulin, the metabolisms of carbohydrate, fat, and protein result impaired, leading to a group of metabolic diseases under the name of Diabetes Mellitus. In type I diabetes, also called insulin-dependent diabetes mellitus (IDDM), there is an absolute deficiency of insulin secretion, which is due to β-cell destruction. Insufficient insulin or insulin action for the body's need result in a chronically raised blood glucose concentration (hyperglycemia). Moreover, cell utilization of glucose falls and consequently utilization of fat and proteins for energy increases causing release of free fatty acids, cholesterol and phospholipids in the plasma. This produces long-term consequences for the body associated with damage, dysfunction and failure of various organs. Sustained hyperglycemia is associated with acute ketoacidosis, nephropaty, rethinopaty, neuropathy and damages to the cardiovascular system [Williams and Pickup, 1992]. The criteria for the diagno-

sis of T1DM are summarized as follows:

- American Diabetes Association [The American Diabetes Association, 2010]
  1. A1C [1] $\geq$ 6.5 % or
  2. FPG [2] $\geq$ 126 [mg/dL] or
  3. 2-h plasma glucose $\geq$ 200 [mg/dL] during an OGTT [3] or
  4. random plasma glucose $\geq$ 200 [mg/dL] in patient with symptoms of hyperglycemia
- World Health Organization [World Health Organization-International Diabetes Federation, 2006]
  1. FPG $\geq$ 126 [mg/dL] or
  2. 2-h plasma glucose $\geq$ 200 [mg/dL] during an OGTT

Diabetes care

Because insulin deficiency defines T1DM, insulin replacement is the hallmark of the therapy. Focusing on tight blood glucose targets, i.e., 70-140 [mg/dL] [The American Diabetes Association, 2013], the philosophy of insulin replacement is to mimic the physiological endogenous insulin secretion pattern of the non-diabetic person. In the non-diabetic subjects, insulin is secreted into the portal circulation at two rates: a slow basal secretion throughout the 24 hours and an augmented rate at meal times. This pattern can be achieved to some extent with the so-called basal-bolus regime: a basal dose of long-acting insulin (e.g., detemir [*Levemir*® 2013], glargine [*Lantus*® 2013]) is sufficient to keep a constant glucose concentration during fasting conditions and a prandial bolus of rapid-acting insulin (e.g., lispro [*Humalog*® 2013], aspart [*NovoLog*® 2013], glulisine [*Apidra*® 2013]) enhances an increased glucose uptake during and after meals. Actually, such a regime is the most common therapy for IDDM subjects. Patients on multiple-dose insulin (MDI) therapy use insulin pens (e.g., *NovoPen*® *4* [Novo Nordisk, 2013b], *FlexTouch*® [Novo Nordisk, 2013a], *ClikSTAR*® [Sanofi-Aventis, 2013], *Daily Dose* [Insulution, 2013]) to administer both long-acting insulin analogue for the basal dose once or twice a day and rapid-acting insulin for boluses and corrections. Alternatively, patients on continuous subcutaneous insulin infusion (CSII) therapy use an insulin pump (e.g., *Spirit Combo*® [Accu-Check, 2013], *One Touch*® *Ping*® [Animas Corporation, 2013], *MiniMed*

[1] A1C glycated hemoglobin

[2] FPG fasting plasma glucose defined as no caloric intake for at least 8 h

[3] OGTT oral glucose tolerance test, with a glucose load containing the equivalent of 75 g anhydrous glucose dissolved in water

Pradigm® Revel™ [Medtronic, 2013b]) loaded with rapid-acting insulin, which provides a continuous infusion corresponding to the basal and can be programmed to deliver boluses as needed. The basal-bolus strategy comprises also testing of blood glucose levels at least prior to meals and snacks, occasionally postprandially, at bedtime, prior to exercise, when low blood glucose is suspected and after treating low blood glucose until normoglycemia is achieved [The American Diabetes Association, 2013]. Glucose monitoring is fundamental in that it allows patients to evaluate their individual response to therapy, adjust medications and assess whether glycemic targets are being attained. To this purpose, two primary techniques are available: self-monitoring of blood glucose (SMBG) and continuous glucose monitoring (CGM). In the first case, a small drop of blood is drawn from the fingertip and is analyzed in a test strip by the meter using enzymatically catalyzed-based electro-chemical or photometric methods with marketed device such as *HemoCue® Glucose Analyzer* [Hemocue, 2013]. In the second case, interstitial fluid measurements are taken by means of a subcutaneously inserted needle, and are converted to interstitial glucose assays. Examples of such devices include *Abbott FreeStyle Navigator™* [Abbott, 2013], *Dexcom Seven®Plus* [Dexcom, 2013], *Guardian®* [Medtronic, 2013a].

Intensive insulin therapy has been strongly promoted during the last decade, following the results of the major Diabetes Control and Complications Trial (DCCT) [The Diabetes Control and Complications Trial Research Group, 1993] and follow-up Epidemiology of Diabetes Interventions and Complications (EDIC) [The Diabetes Control and Complications Trial/Epidemiology of Diabetes Interventions and Complications Study Research Group, 2005] studies, in order to keep blood glucose levels as close to normal as possible. However, insulin therapy may induce potentially severe hypoglycemia, resulting from too high levels of insulin, leading to loss of consciousness, coma and, in rare severe cases, death. In current medical practice, the rough calculation of insulin doses and eventually extra carbohydrate intakes is based on empirical rules-of-thumbs. Many factors have to be considered in this decision process: health status, current blood glucose level, blood glucose target, foreseen activities, insulin sensitivity, expected future glycemia evolution and approximation of the estimated meal carbohydrate content effects as well as insulin impact on the subject own blood glucose, taking into account medical advice and patients previous experience of his/her own metabolism (Fig. 2.2). One common measure used in this regard is the carbohydrate-to-insulin ratio, which is an estimate of how many insulin units to administer to match the amount of digested carbohydrates. Actually, most patients are rather conservative in order to prevent insulin-induced hypoglycemia, remaining far from the optimal treatment.

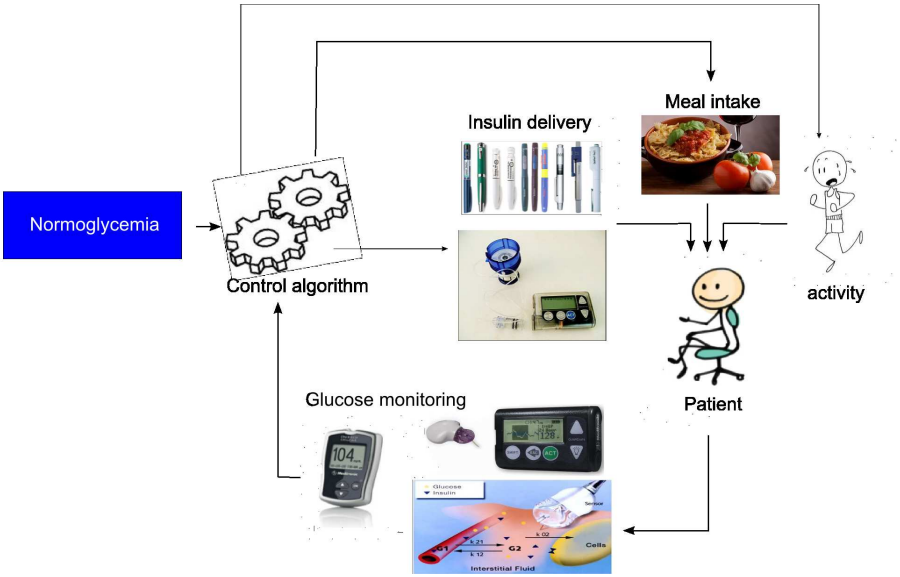

Figure 2.2 Schematic representation of diabetes management. Knowing the history of insulin doses, meals, activity, health status the patient assess current blood glucose measured via either a SMBG meter or a CGM device (bottom). Keeping therapy goals in mind in order to achieve normoglycemia, the patient calculate future control actions, either in the form of an insulin dose, a meal intake or some physical activity. The controller is the subject himself and the control algorithm is the set of rules-of-thumbs and estimation that are used to optimize therapy.

The task is non-trivial and demanding, although the standard tools in diabetes care improved significantly during the last decades. For this reason, the development of control tools aiming at assisting the patients in the management of their disease has been the focus of extensive research for almost 40 years [Cobelli et al., 2009] and is slowly progressing towards a fully automated closed-loop control artificial pancreas [AP, 2013; Cobelli et al., 2011; De Nicolao et al., 2011]. However, while such a system is expected to improve the quality of life reducing the time plasma glucose is outside the target range, it will be suitable only for pump and CGM users. In addition, closed-loop control introduces certain risks, the most dangerous being potentially severe and unavoidable hypoglycemia induced by overdelivery of insulin compensating for hyperglycemia following a meal [Cobelli et al., 2009].

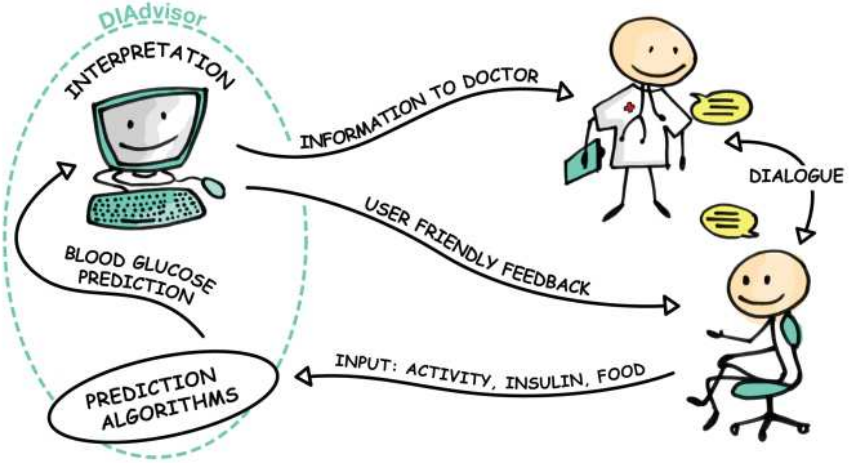

Figure 2.3 The DIAdvisor™ tool: a mobile short-term predictor and tretment advisor [DIAdvisor, 2012]

The DIAdvisor™ project

Against this background, the European FP7-IST research project DIAdvisor™ [DIAdvisor, 2012] during the quadrennium 2008-2012 pursued the development of a personalized blood glucose predicting system and an advisory control system, the DIAdvisor™ tool, to be used on the spot by the users in different daily situations, predicting glycemic excursions following meals, insulin intakes and exercise and giving them advices about how to adjust their treatments. Within this scenario the controller is expected to determine impulse-formed control inputs, namely insulin bolus doses and amount of carbohydrate of a meal, which are not automatically applied but rather recommended to the patient, thereby assuring safety. When a therapeutic action is suggested by the algorithm, the patient can accept or reject it, remaining firmly in the loop. The underlying concept of the system is illustrated in Fig. 2.3. The predictor system needs user inputs concerning patient condition (e.g., fasting, meal time, rest or physical activity), therapeutic mode (type of insulin delivery route, type of insulin preparations), time and size of meals, minimally invasive glucose sensors and wearable vital signs sensors measurements, and produces short-term, i.e., up to 120 minutes, blood glucose predictions to be graphically shown to the patients as well as suggestions to the user from a decision support module. The tool was realized as a joint

effort by a consortium of 14 partners, both academic institutions and commercial companies and can be defined as the first prototype of a mobile short-term blood glucose predictor and treatment advisor. The core of the system was represented by the patient's pocket computer which was able to collect sensor measurements, display predictions and actions to the user and send wirelessly all these information to a central database. Detailed information regarding the system components are to be found in Sec. 3.3. In-vivo tests on a population of 43 subjects following at least 70% of the DIAdvisor^{TM} recommendations showed an increase by 7.6% in the time spent in normo-glycemia and a reduction by 42% in the time spent in hypoglycemia [The DIAdvisor Consortium, 2012].

2.4 Models in diabetes

In diabetes research and therapy, modeling of the glucose-insulin control system has received significant attention for more than 50 years [Cobelli et al., 2009], [Cobelli et al., 2011]. Driving forces behind this endeavor have been the possibility for external blood glucose regulation and the consequent quest for an automated control of diabetic glycemia. Several types of models serving different purposes were proposed, most of these efforts being first-principles based descriptions of the physiological relationships associated with T1DM, and only to a lesser extent mathematical modeling by means of system identification.

Physiological models

The first pioneering work describing the relationships between insulin and glucose utilization was that of Bolie [1961], later modified by Ackerman and McGucking [1964] in order to provide a model of the glucose metabolism during an oral glucose tolerance test (OGTT). Greater attention was received by the so-called minimal model [Bergman et al., 1979], [Bergman et al., 1981], developed for the specific purpose of quantifying pancreatic responsiveness and insulin sensitivity during an intravenous glucose-tolerance test (IVGTT) in non-diabetic individuals. The model consists of three differential equations describing plasma glucose and plasma insulin in a remote compartment, accounting for neither the dynamics of subcutaneous insulin infusion nor the dynamics of gut glucose absorption from a carbohydrates meal. In [Lehmann and Deutch, 1992], a simulation model was presented, and later validated on a set of 24 subjects [Lehmann et al., 1994]. Glucose-insulin pharmacokinetics/pharmacodynamics in non-diabetic subjects was described by a 19-state model developed by Sorensen [1985], the major shortcoming of this model being the failure in capturing the hyperglycemic events characteristic of type 1

diabetes [Lynch and Bequette, 2002]. The nonlinear model proposed by Hovorka et al. [2004] describes glucose-insulin dynamics with several differential equations in three subsystems: a glucose subsystem, an insulin subsystem and an insulin action subsystem. Model inputs are the rate of subcutaneously infused fast acting insulin, meal carbohydrates amount and time of ingestion and its outputs are plasma glucose and insulin concentrations. The absorption kinetics associated with subcutaneous insulin delivery of the above mentioned model was later modified [Wilinska et al., 2005], the model replacing the original subcutaneous insulin subsystem consisting in two parallel fast and slow channels for insulin absorption as well as a degree of insulin degradation at the injection site, and integrated in a simulation environment dedicated to closed-loop evaluation of insulin delivery systems [Wilinska et al., 2010]. The efforts by Dalla Man and co-workers presented in [Dalla Man et al., 2002; Dalla Man et al., 2004; Dalla Man et al., 2005; Dalla Man et al., 2006] lead to the meal simulation model of the glucose-insulin system [Dalla Man et al., 2007] which has been accepted by the Food and Drug Administration (FDA) to be used as a substitute for animal trials in preclinical tests of closed-loop development [Kovatchev et al., 2008a], [Kovatchev et al., 2008b]. Dalla Man and co-workers [2007] used a sophisticated triple tracer method to estimate important meal-related quantities such as the rates of appearance of glucose in the blood from the meal, endogenous glucose production, utilization of glucose, and insulin secretion. Reviews of physiological diabetes models include that of Nucci and Cobelli [2000], who specifically examined several models of subcutaneous-to-intravenous insulin kinetics, Makroglou and co-workers [2006] presenting an overview of existing software packages specific to diabetes modeling and finally Cobelli and co-workers [2009], discussing the main contribution to both modeling and control in diabetes from the early 1960s.

Predictive models

Although seemingly simple in concept, the problem of glucose prediction in an active individual has to date proved intractable. Currently, continuous glucose monitoring (CGM) devices are the available technology able to provide high/low glucose alarms when certain user specified preset threshold levels have been crossed and to deliver warnings of events that are likely to occur if the current trend continues. However, patients will benefit more from an early alarm that predicts the hypoglycemic episode before it occures. A review of hypoglycemia prevention algorithms is reported in [Bequette, 2010]. To date many studies have investigated the possibility of predicting blood glucose concentration for the purpose of regulating glucose intervention, in order to enable individuals to take cor-

rective actions and avoid low or high glucose values. Bremer and Gough [1999] originally developed the idea of T1DM CGM time-series analysis using 10-minutes sampled data from ambulatory T1DM patients to identify autoregressive (AR) models. They explored 10, 20 and 30 minutes prediction horizons, and report that the 10-min predictions are accurate and the 20-min or 30-min predictions may also be acceptable for a limited set of data only. However, no quantification of the accuracy of the model predictions was provided. In [Reifman et al., 2007] tenth-order autoregressive models were identified from 5-days long glucose time-series belonging to a population of 5 in-hospital subjects. Performances of a single, cross-subject model compared with individual models were evaluated on 30- and 60 minutes prediction horizons. Gani et al. [2009] used a 30-th order AR model with a data smoothing and regularization procedure to minimize the changes in the glucose first-derivative, reducing the prediction lag for 60 and 90-min-ahead prediciton compared to [Reifman et al., 2007]. Sparacino et al. [2007] collected 48 h of continuous (3-min) glucose data from 28 T1DM subjects in ambulatory conditions. In their retrospective analysis, they recursively identified simple polynomial and AR models from the CGM time-series data, prefiltered to removed noise spikes. They investigated prediction horizons of 10 and 15 steps (i.e., 30 and 45 min) and concluded that hypoglycemia can be detected 25 minutes before the hypoglycemic threshold is passed. In [Palerm et al., 2005] a Kalman filter approach was proposed, which only used information on past CGM readings by assuming a double integrated random walk as prior for glucose dynamics and estimating the states corresponding to the interstitial glucose level, and the first and second derivative thereof, i.e., rate of glucose change and acceleration. The method was evaluated for 13 hypoglycemic clamp data sets in [Palerm and Bequette, 2007]. Using a hypoglycemic threshold of 70 [mg/dL], the sensitivity and specificity were 90 and 79%, respectively, with unknown alarm time. A tutorial overview of algorithms for CGM time series analysis to the purpose of alarm generation is provided in [Sparacino et al., 2008]. Eren-Oruklu et al. [2009] proposed a recursive second-order AR and ARMA model identification strategy with an adjustable forgetting factor for healthy and type II diabetics. Their models utilized only recent glucose history from a CGM device, achieving 3-5% error for 30-min ahead prediction. In [Naumova et al., 2012] a kernel-based regularization learning algortihm, in which the kernel and the regularization parameter are adaptively chosen on the basis of previous similar learning tasks, using past glucose information, was presented. The past few years witnessed the investigation of neural networks (NN) models for short-term glucose prediction proving it to be a competitive approach. Pappada et al. [2008] created NN models with variable predictive windows in the range 50-180 min, trained using 18 patients CGM

datasets and evaluated on patient data not included in the neural network formulation. They concluded that their models performed adequately in the normo- and hyperglycemic ranges, whereas hypoglycemic events were overestimated, a potential reason for that being due to the minimal occurences of hypoglycemia in the training data. In [Facchinetti et al., 2010] a feed forward NN whose inputs were CGM samples in the previous 20 min and the current time instant, and whose output was the glucose concentration 15, 30 and 45-minutes ahead was tested on 15 actual data sets. Root mean square error (RMSE) was 10, 18 and 27 [mg/dL] for the 15, 30 and 45-minute prediction, with a delay of around 4, 9, and 14 min for upward trends, and 5, 15, and 26 min for downward trends. Dassau and co-workers developed a real-time hypoglycemia prediction suite combining five individual algorithms, namely, linear prediction, Kalman filtering, hybrid impulse response (HIIR) filtering, statistical prediction and numerical logical into a voting-based system to predict hypoglycemia from 1-min sampled CGM data. A 35 min prediction horizon with an alarm threshold of 80 [mg/dL] and a voting threshold of three to five algorithms to predict hypoglycemia resulted in a 91% correct predictions. A short-coming of the methods listed above is the lack of exploitation of the dynamic interplay between previously injected insulin, meal intake and eventually exercise to the purpose of improving glucose prediction. Hovorka and his group [2004] performed experiments with ten T1DM patients under clinical conditions, using their physiological model to make predictions of glucose data up to 60 minutes into the future. The glucose was measured intravenously, but delayed by 30 min to mimic subcutaneous measurement. The model parameters were recursively estimated using a Bayesian method. The predictions of the resulting models had RMSE values of 8.6, 13.0, and 17.3 [mg/dL] for 2-step, 3-step, and 4-step (i.e., 30-min, 45-min, and 60-min) predictions, respectively. Finan et al. [2009a], where both batch-wise and recursively identified patient-specific ARX-models have been analysed for 9 patients with a mean 30-minute prediction error RMSE of 26 mg/dl. An ARX model with a nonlinear forgetting factor scaled according to the glucose range was considered in [Castillo-Estrada *et al.,* 2010a], [Castillo-Estrada *et al.,* 2010b], and a 45-minute prediction horizon showed good results. Finally, in [Gani et al., 2010] it was asserted that a universal data-driven modelidentified from a CGMS time-seris of a patient applying the algorithm previously published by the same authors in 2009 [Gani et al., 2009] could be used to make near-future glucose concentration predictions for other patients without any model customization procedure. They used regularization techniques to filter data from 34 subjects, then, using the filtered data, they develop auto-regressive models of order 30 to the purpose of making short-term, 30-min-ahead predictions. A feed-forward NN was also exploited in [Pap-

pada et al., 2011] and tested on 10 real datasets, incorporating, in addition to CGM data, other inputs such as SMBG readings, information on insulin, meal, hypo- and hyperglycemia symptoms, lifestyle, activity and emotions and predict glucose values up to 75 min. In [Zecchin et al., 2011; Zecchin et al., 2012; Zecchin et al., 2013], 30 min ahead prediction was performed with a feed-forward NN in cascade with the first-order polynomial model in [Sparacino et al., 2007]. The inputs to the linear predictor were the past CGM values weighted using a forgetting factor, while the inputs to the NN were current CGM and its trend, information on the past error committed by the polynomial model and information on meal, supplied as plasma glucose rate of appearance obtained from the physiological model of [Dalla Man et al., 2007]. Zhao et al. [2012] used a latent variable-based approach to predict future CGM values from past CGM and known carbohydrate and insulin boluses, transformed into time-smoothed inputs using second-order transfer functions. The method was applied to collected clinical data and simulated data generated by the model described in [Kovatchev et al., 2008a], [Kovatchev et al., 2008b]. They concluded that their LV-based method resulted in models whose prediction accuracy was as least as good as the accuracies of standard AR/ARX models. In [Eren-Oruklu et al., 2012] a multi-sensor body monitor providing seven signals related to activity and emotional conditions was used in addition to a CGM monitor to improve glucose prediction. A multivariate ARMAX model with weighted recursive least squares estimation of the unknown parameters using a variable forgetting factor was proposed. Results showed that the prediction error is significantly reduced with the addition of the vital signs measurements, as compared to an ARMA model based only on CGM signals.

Control-oriented models

To date control algorithms have been mainly based on physiological models such as [Hovorka et al., 2004; Dalla Man et al., 2007] and their linearized versions. Some studies identified models from simulated data and used those identified simpler models to controller design. In [Finan et al., 2006] ARX and Box-Jenkins (BJ) models of various orders have been identified from simulated patient data obtained with the Hovorka model and evaluated for their description of both calibration and validation data. Finan and co-workers concluded that in general, the high-order BJ models consistently explained more variability in the data than the ARX models [Finan et al., 2008]. This type of model has been considered in, e.g., [Finan et al., 2009a], where both batch-wise and recursively identified patient-specific ARX models have been analysed for 9 patients with a mean 30-minute prediction error RMSE of 26 mg/dl. In [Cescon, 2011] data-driven

black-box identification of ARX, ARMAX and state space models from actual T1DM data was investigated, the best performance was achieved with the ARX and the ARMAX models. The ARX model gave a standard deviation of the prediction error of 17, 34, 46 and 56 mg/dl on average for the 30-, 60-, 90- and 120-minute prediction, respectively. The corresponding results for the ARMAX model were 16, 30, 39 and 44 mg/dl. However, the idea of building models specifically for control purposes has not emerged in the field until very recently. Continuous-time first order integrating transfer function models with time delay were proposed in [Percival et al., 2010] to describe the magnitude and duration of effects of a carbohydrate intake and a subcutaneously administered insulin injection on blood glucose. Clinical data from 11 adult subjects with T1DM where the inputs were separated in time to allow unique identification of the unknown parameters were used. Heuristics and least-squares optimization were employed to estimate the model parameters. Percival and co-workers [2011] later exploited the same model structure in a control framework, where two cohorts of virtual subjects were generated by the Hovorka model [Hovorka et al., 2004; Wilinska et al., 2005] and University of Virginia/Padova type 1 diabetes simulator [Kovatchev et al., 2008a], [Kovatchev et al., 2008b]. A very similar model structure was proposed in [Kirchsteiger et al., 2011b; Kirchsteiger et al., 2011a], the difference being a time delay replaced by a time lag, targeting robust control design. The approach in [van Heudsen et al., 2012] consisted in identifying third-order models of the insulin-to-blood glucose dynamics from a population of ten virtual subjects from the UVa/Padova metabolic simulator [Kovatchev et al., 2008a], [Kovatchev et al., 2008b] for use in a zone model predictive controller. Such models were discrete-time third-order transfer functions, whose gain was personalized using the patient correction factor calculated with the 1800 rule [Walsh and Roberts, 2012] and a so-called "safety factor" chosen by a physician. The controllers based on the personalized models were tested in simulation on a cohort of 100 virtual subjects, and resulted to be robust.

2.5 Inherent challenges in T1DM modeling

Despite significant efforts devoted to the problem of blood glucose regulation in type 1 diabetic patients over the last several decades (see e.g. [Cobelli et al., 2009] for a comprehensive review), many inherent challenges that must be overcome still remain. At the most basic level, the disease can be viewed as a process having one output, namely, glucose concentration in plasma, and two inputs, namely, meal carbohydrates and administered insulin. The first and perhaps most crucial challenge to overcome in mod-

eling is that of poor data excitation: often the inputs are simultaneous and in the same ratio, the so-called insulin-to-carbohydrate ratio, precluding the possibility of distinguishing their relative effects. The system identification need for an experiment design with sufficient excitation and decorrelated input is often poorly understood. Second, the most widespread way of treating diabetes comprises a series of impulse-like control actions, i.e., insulin injections and food intakes, applied several times during the day at irregular sampling instants, typically at wake up, meal and bed times, the decisions being based on scarce assays of the controlled variable, i.e., blood glucose. This gives rise to the problem of non-uniformly sampled and infrequent data and, since the signals in play interact in the bloodstream, introduces assumptions on the subcutaneous-to-intravenous insulin absorption and gastro-intestinal carbohydrates absorption dynamics.

In the last ten years, advances in sensor technology saw the advent of continuous glucose monitors (CGM), systems capable of measuring glucose concentration frequently (e.g., every 5 minutes) for several days, providing the patient with well-sampled data in real time. However, it is important to stress that together with the benefits, they introduce yet another limitation. Indeed, those devices measure glucose concentration in the interstitium and not in plasma. Interstitial glucose (IG) fluctuations are related to BG presumably via diffusion process [Steil et al., 2005], [Keenan et al., 2009]. This leads to a number of issues, including distortion (which incorporates a time lag) and calibration errors, and necessitates the development of methods for their mitigation. In particular, it is necessary to consider that, since the BG-to-IG kinetics acts as a low-pass filter, the frequency content of interstitial glucose is different from that of blood glucose [Breton et al., 2008], [Miller and Strange, 2007].

As for the inputs, when taking into account the appearance of insulin in the bloodstream from subcutaneous delivery and that of glucose in plasma after a meal, new time-lags and dynamics are introduced; further, subcutaneous insulin infusion involves degradation at the site of delivery. In addition, meals must be recorded by the patients, and the actual amount of carbohydrates must be estimated, a process that is prone to errors. Also, in practice, the combination of simple and complex carbohydrates, fats and proteins can affect the glucose absorption in the digestive system. Unrepresented inputs, such as stress and illness constitute another challenge to diabetes modeling. Furthermore, it is a well known fact that physical activity, apart from having a glycemia-lowering effect due to utilization of glucose by the muscle cells, enhances insulin sensitivity, playing a substantial role in the picture, but the magnitude and duration of such effects are hard to consider. Another important aspect is the degree of variability of the overall system dynamics over the day (the so-called

"dawn phenomenon", for instance, is characterized by increased insulin resistance during the morning hours [Williams and Pickup, 1992]).

A priori knowledge of the diabetes process indicates two fundamental properties that should be satisfied by any model:

- the gain associated with the insulin input should be negative (i.e., an increase in insulin results in a decrease in glucose concentration);
- the gain associated with the meal input should be positive (i.e., a meal results in an increase in glucose concentration),

properties that a sound and valid model need to exhibit. However, the values of the above mentioned gains are related to age of the subject, disease duration, BMI, insulin sensitivity, β-cell responsiveness and probably many more unknown factors so that it is not clear how to take them into account in the modeling process.

3

Experimental Conditions and Clinical Data Acquisition

3.1 Introduction

In the framework of the DIAdvisor™ project [DIAdvisor, 2012], acquisition of bioclinical data linked or potentially involved in blood glucose control from insulin-treated diabetic subjects was accomplished in a series of experimental sessions. The investigations focused on a population of basal-bolus regimen treated subjects, either as combination of multiple daily insulin injections or as continuous insulin infusion from a pump. The clinical protocol for data acquisition was designed by the DIAdvisor™ Consortium and was reviewed and approved by the ethical committees of the Clinical Investigation Centers participating in the trials, namely, Montpellier University Hospital (CHU) in Montpellier, France, Padova University Clinics (UNIPD) in Padova, Italy and the Clinical Institute of Experimental Medicine (IKEM) in Prague, Czech Republic [DIAdvisor, 2012]. The subjects participating in the studies signed an informed and witnessed consent form prior to any study procedure. For the whole duration of the experiments, the participants were equipped with state-of-the-art devices provided by the DIAdvisor™ Consortium complying with the study protocol. Overall, collected data included: specific patient parameters (e.g., gender = male, age = 43 years old, BMI = 23.7, weight = 67 kg), characteristics related to diabetes (e.g., disease duration = 10 years, insulin delivery = external pump), associated health conditions and therapies, food intakes and administered insulin doses registered in a logbook, capillary glucose strips, interstitial glucose levels, plasma glucose and plasma insulin concentration from drawn blood samples as well as vital signs.

Three clinical studies were conducted: the data acquisition (DAQ) trial in 2008-2009 aiming at providing a large amount of data for algorithmic development of the DIAdvisor™ system components; the DIAdvisor I trial in 2010 with the purpose of testing the first prototype of the DIAdvisor™ system with respect to data collection, blood glucose prediction, therapy advices and the DIAdvisor II trial in 2011-2012 intended for final performances validation of un updated version of the DIAdvisor™ system against project endpoints. This thesis presents research undertaken utilizing data from all the three trials. The remainder of the chapter illustrates the study procedures in detail.

3.2 DAQ trial

Equipment

HemoCue® Glucose Analyzer

http://www.hemocue.com

The HemoCue® 201+ Glucose Analyzer [Hemocue, 2013] is a blood glucose meter based on a glucose dehydrogenase method and consists of a pocket size handheld analyzer and a unique disposable microcuvette. The analyzer was factory calibrated and no calibration was needed between cuvette batches. The device was used by each patient as a reference glucose meter, assessing plasma glucose levels from finger-stick samples.

Abbott FreeStyle Navigator™

https://www.
abbottdiabetescare.com

The Abbott FreeStyle Navigator™ [Abbott, 2013] is a Continuous Glucose Monitoring System (CGMS) consisting of an amperometric electrochemical sensor placed under the skin, a wireless transmitter connected to the sensor and a wireless receiver collecting the sensor signals. The subcutaneous sensor was inserted about 5 mm into the subcutaneous tissues and could be worn for up to five days before replacement. Calibration relative to capillary glucose was required at specific times, namely, 10, 12, 24 and 72 hours after insertion. Using the WIRED ENZYME™ technology, the sensor converted glucose concentration to electrical current. Once every minute the transmitter sent

the estimate of the intersitial glucose concentration to the receiver, which displayed the final values once every 10 minutes.

VivoMetrics Clinical LifeShirt®

The VivoMetrics Clinical LifeShirt® [Grossman, 2004] is a non-invasive and fully-integrated physiological data monitoring system consisting of a light-weight shirt with embedded vital signs sensors and a receiver/ transmitter. In this trial heart rate, respiration rate, skin temperature and body movements were recorded. To measure pulmonary function, sensors were worn around the chest and the abdomen. A three-lead single-channel ECG measured the heart rate and a three-axis accelerometer recorded the patient posture and activity level.

Clinical LifeShirt®

Biological sample collection

Blood samples were collected by medical personnel during the in-hospital visit to allow determination of blood glucose and blood insulin concentrations. An intra-venous (IV) catheter was placed in the patient's forearm on the antecubital vein and kept patent with a 0.9% saline infusion. The drawn samples were centrifuged for 10 minutes at 3500 [round/min] at 4 [°C]. Plasma was transferred in a secondary tube stored in a freezer at −20 [°C] until its analysis. Blood glucose was measured on plasma samples using the Yellow Spring Instrument *YSI 2300 STAT Plus™ Glucose Analyzer* [Yellow Spring Instruments, 2013] in the biochemical laboratory of the CHU in Montpellier. Insulin was dosed on serum samples using a radio-immunologic method. Analyses were carried out at the Nuclear Medicine laboratory of the CHU in Montpellier for lispro [*Humalog*® 2013] and glulisine [*Apidra*® 2013] and at Novo Nordisk central laboratory in Denmark, for aspart [*NovoLog*® 2013], detemir [*Levemir*® 2013] and glargine [*Lantus*® 2013] analogues.

Study protocol and experiments

The clinical study consisted of four visits: *visit 0* for patients screening, *visit 1* for sensors initialization, *visit 2* for 75-hours in-hospital tests, *visit 3* for 7-days ambulatory conditions. Figure A.1 in Appendix A gives the flow chart of the trial.

Visit 0

Prior to any study-related procedure, the subjects were scheduled for an outpatient screening visit, in order to evaluate his/her eligibility to the study participation. The investigator reviewed the subject's past medical files, performed a physical examination obtaining routine vital signs including height, weight, temperature, orthostatic blood pressure and pulse and analyzed biological analysis (blood cell-count, HbA1c, anti-insulin antibodies, creatinine, ASAT/ALAT, β-HCG for women of child-bearing age), the outcome of it being recorded in the clinician's sheet.

Visit 1

Within 4 weeks of *visit 0* the patient was admitted at the clinic to initialize the Abbott FreeStyle Navigator^{TM} device [Abbott, 2013]. The sensor was inserted subcutaneously and calibrated against capillary glucose from HemoCue® 201+ Glucose Analyzer [Hemocue, 2013] by a nurse. Although glucose sensing is available after a 10-hours initialization period following sensor calibration, optimal sensor signal stability and accuracy is obtained after 24 hours. For this reason, the subject was hospitalized 48 hours after sensor insertion, so to begin the tests with a well-calibrated device.

Visit 2

Visit 2 took place at the hospitals CHU, UNIPD and IKEM, respectively, for a duration of 75 hours. After patient admission at 7.00 am, a calibration of the Abbott Freestyle Navigator^{TM} [Abbott, 2013] against capillary glucose was performed. In case the CGM was not operating properly, it was replaced and the study investigations were postponed by 10 hours. Standard meals for breakfast (8.00 am), lunch (1.00 pm) and dinner (7.00 pm) were served, the amount of administered carbohydrates being 42, 70 and 70 grams, respectively. Blood samples were collected by nurses to measure plasma glucose and plasma insulin concentrations: every hour during day, every 2 hours during night, every 15 minutes after meals for 2 hours. A specific sampling scheduled was adopted after breakfasts: 30 min before, mealtime, 10, 20, 30, 60, 90, 120, 150, 180, 240, 300 min after, for a total of 37 blood samples per day. During the whole 3-days-long visit, the participant was permanently equipped with the Abbott Freestyle Navigator^{TM} [Abbott, 2013] and the VivoMetrics Clinical LifeShirt® [Grossman, 2004] devices. No specific

intervention on usual diabetes treatment was scheduled during the period. The patients decided their insulin needs according to the glucose measurements from the HemoCue® 201+ Glucose Analyzer [Hemocue, 2013] as usually in activities of daily life. As needed, particularly when hypo- or hyperglycemia occurred, support was provided by nurses and physicians. Table B.1 in Appendix B gives a summary of the data gathered during this phase.

Visit 3

At 10.00 am on the third day, the in-hospital phase ended, patients left the clinic and started a 7 days ambulatory period, continuing the study in normal-life conditions. The subjects kept the Abbott Freestyle Navigator™ [Abbott, 2013] and the VivoMetrics Clinical LifeShirt® [Grossman, 2004] devices, using the HemoCue® 201+ Glucose Analyzer [Hemocue, 2013] to perform blood glucose control tests and recording details about their diabetes management in their logbook. At the end of the ambulatory period, all the sensors were removed from the participants and returned back to the investigators together with the filled-in logbook, in order to close the study. At the end of the ambulatory period, all the sensors were removed from the partecipants and returned back to the investigators together with the filled-in logbook, in order to close the study.

Patients selection criteria

A total of 90 diabetic subjects, male and female adults, were included in the DAQ trial to allow availability of data from a wide spectrum of patients under basal-bolus regimen. Among these, a population of 14 patients was chosen (9 males and 5 females, age 45.8±12.7 [yr], disease duration 18±11.6 [yr], BMI 23.4±2.7 [kg/m^2], 10 MDI and 4 CSII, HbA1$_c$ 7.6±1 [%], total daily insulin 41.9±18.9 [IU]). The selection criteria were the quantity of data collected ($>$ 80% of the expected), no sensor failures, laboratory results all available and logbook correctly filled in. Table 3.1 reports the characteristics of the selected patients. Figures 3.1 and 3.2 display the data recorded during *Visit 2* for a representative MDI patient. Data belonging to a representative CSII patient may be found, instead, in Appendix D.

Modeling results obtained from DAQ trial *Visit 2* data will be dealt with throughout Chapters 4 and 6.

Table 3.1 DAQ Trial. Patient characteristics

Patient ID	*Gender*	*Age* [yr]	*Duration of disease* [yr]	*BMI* [kg/m^2]	HbA1$_c$[%]	*Therapy*	*Total Daily Insulin* [IU]
CHU102	M	41	19	26.5	6.5	MDI	43
CHU103	M	43	43	23.7	9.1	CSII	45.6
CHU104	M	44	12	20	7.6	MDI	42
CHU105	F	49	32	24.1	7.8	CSII	53.5
CHU106	F	58	9	21.2	7.8	CSII	18.4
CHU107	M	59	16	25.3	8.9	CSII	28.9
CHU108	M	37	2	23.7	5.7	MDI	23
CHU115	F	27	10	19.7	8.5	MDI	65
CHU118	M	32	7	24.1	7.4	MDI	54
CHU119	F	50	15	19.5	7.3	MDI	10
CHU120	F	31	22	22.4	9	MDI	51
CHU121	M	39	33	23.4	6.4	MDI	38
CHU128	M	64	24	24.3	6.7	MDI	42
CHU130	M	68	9	29.4	8.8	MDI	82
MEAN±SD		45.8±12.7	18±11.6	23.4±2.7	7.6±1		41.9±18.9

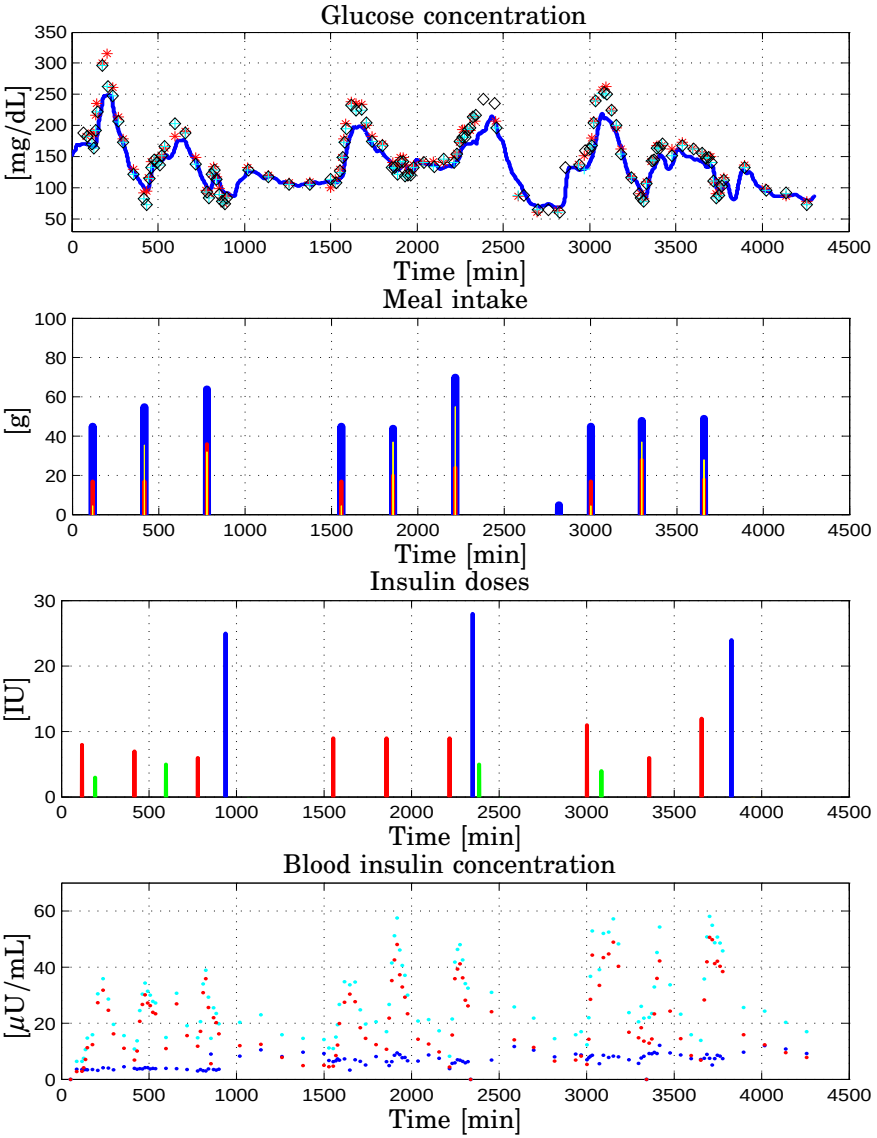

Figure 3.1 Patient CHU102. DAQ trial, *Visit 2*. *Top* Glucose concentration [mg/dL]: interstitial (blue), plasma (red), finger stick (cyan and black); *Upper Center* Meal intake [g]: carbohydrates (blue), lipids (red), proteins (yellow); *Lower Center* Insulin doses [IU]: basal (blue), bolus (red), correction (green); *Bottom* Blood insulin concentration [μU/mL]: basal (blue), bolus (red), total (cyan) vs. time [min]

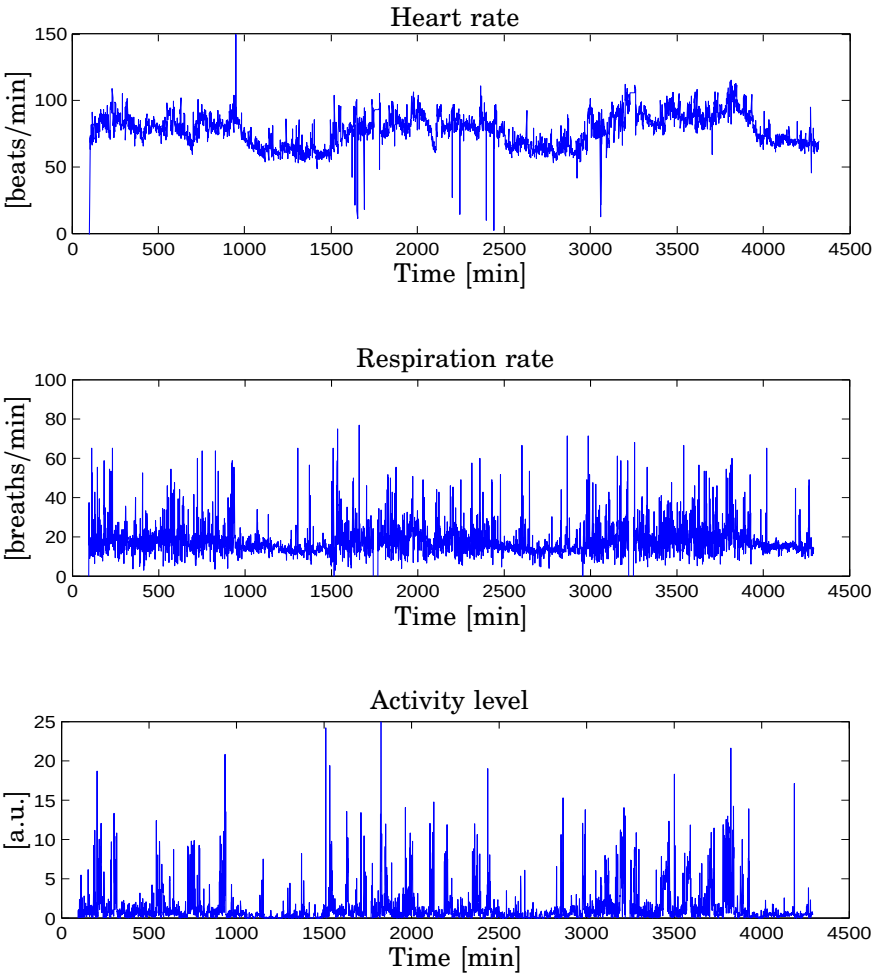

Figure 3.2 Patient CHU102. DAQ trial, *Visit 2*. *Top* Heart rate [beats/min]; *Center* Respiration rate [breaths/min]; *Bottom* Activity level [a.u.] vs. time [min]

3.3 DIAdvisor I trial

Equipment

DIAdvisor™ platform

The DIAdvisor™platform comprised a *viliv S5* ultra-mobile pocket computer (UMPC) [viliv, 2013] connected to a laptop through a wifi network, a CGM device, namely the Dexcom® SEVEN® PLUS Continuous Glucose Monitor [Dexcom, 2013] connected to the UMPC via USB and a vital signs monitor, the Sensium™ Life Pebble which streamed the collected data wirelessly to a dedicated USB network adapter plugged in to the *viliv S5*. Figure 3.5 reproduced the platform available to the patients. Meal and insulin informations were entered by the subject to the UMPC, thanks to the Man-Machine Interface (MMI) developed by the Consortium. Blood glucose predictions and therapy advices calculated by the system were shown to the patients only during dedicated experiments. Furthermore, all the stored data were sent to a laptop used by a clinician for supervision. Figures 3.3, 3.4 give examples of the user interface of the patient application.

Dexcom®SEVEN®PLUS [Dexcom, 2013]

http://www.dexcom.com

The Dexcom® SEVEN® PLUS is a CGM system consisting of a subcutaneous sensor, a transmitter fixed on the sensor and monitor which receives transmitter signal and provides real-time glucose values [Dexcom, 2013]. The sensor probe is 13 mm long and is positioned under the skin. It is placed with the help of an inserter and can be use for up to seven days. Using current measurements, the sensor utilizes a working electrode coated with a sensing element, the WIRED ENZYME™, that converts glucose concentration to electrical current. The transmitter snaps into the sensor and sends every 5 minutes glucose information to the receiver, using a secured wireless connection. The receiver has a large screen which displays glucose values and glucose trends. It has customizable alarms that can inform patient about potential hypo/hyperglycemia. The receiver stores up to 30 days of data. Once installed, the Seven®Plus system needs a 2-hour period of initialization before providing any continuous glucose data. The sensor has to be calibrated 2 hours after the insertion, and at least every 12 hours (2 calibrations per day). Calibration values are entered manually by the patient when performing a capillary glucose control. During this trial the receiver was connected to the UMPC to allow communication with the

DIAdvisor^{TM} platform for data storage and displaying of glucose trends to the patient.

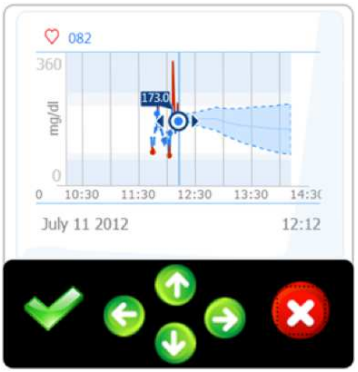

Figure 3.3 The DIAdvisor^{TM} tool patient application user interface. The display shows past glucose trends, the current glucose measurement and a projected future trajectory within specified uncertainty limits. On the upper left corner vital signs may be followed. The buttons on the bottom of the screen are used to operate the system.

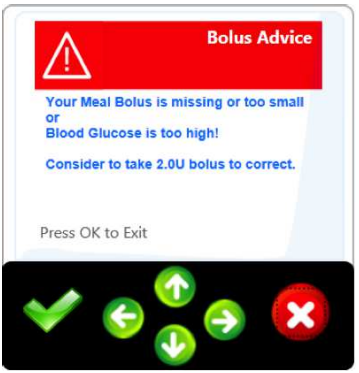

Figure 3.4 The DIAdvisor^{TM} tool patient application user interface. A bolus advice.

Sensium™ Life Pebble [*Sensium™ Life Pebble*]

The Sensium™ Life Pebble [*Sensium™ Life Pebble*] is an ultra small, ultra-low power device able to monitor continuously heart rate and physical activity thanks to a 3-axis accelerometer. In the trial it was attached to the body around the torso. It is mentioned here for completeness, even though data were not used for the thesis scope.

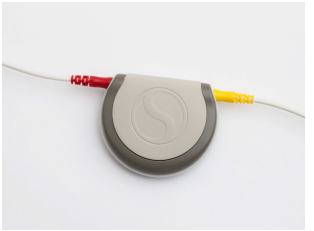

http://www.toumaz.com/

Biological sample collection

During this clinical study, blood sample collection was performed during *Visit 2* and *Visit 3*. Blood glucose reference value was measured on plasma samples using a *YSI 2300 STAT Plus™ Glucose Analyzer* [Yellow Spring Instruments, 2013]. Analysis were carried out in the biochemical laboratory of the CHU in Montpellier.

Study protocol and experiments

The clinical study consisted of four visits: *visit 0* for patients screening whereas *visit 1*, *visit 2* and *visit 3* for 52-hours and 76-hours, respectively, in-hospital visit. Figure A.2 in Appendix A gives the flow chart of the trial, while Table B.2, Appendix B summarizes the data collected.

Visit 0

Screening visit. The same procedure actuated in the DAQ trial was followed.

Visit 1 (data collection)

Visit 1 took place within 4 weeks of *visit 0* at the CHU in Montpellier where subjects were admitted for 52 hours, from 10.00 am on day 1 to 2.00 pm on day 3. Primary objective of this visit was to test data collection by the DIAdvisor UMPC. Upon arrival, at 10.00 am (±15 min) the Sensium™ Life Pebble electrodes were placed on the chest and connected to the wireless transmitter, the CGM device was inserted into the patient's skin and calibrated against fingerstick blood glucose assessed by the HemoCue™ meter. Thereafter, at 12.00 am (±15 min) data collection started for a 48 hour-period. Patients were served standardized meals for breakfast at 8.00 am, lunch at 1.00 pm and dinner at 7.00 pm, the amount of carbohydrate being 40, 70 and 70 [g], respectively. During the admission the subjects were asked to perform at least 6 blood glucose measurements per day using the HemoCue™ analyzer and to base their

decision on how to modulate insulin therapy on the results given by the fingerstick measure. At the end of the visit all the sensors were removed from the patients.

Visit 2 (testing of blood glucose prediction)

Patients were admitted at the CHU in Montpellier for a 76 hour-period starting from 10.00 am on day 1 to 2.00 pm on day 4. The same schedule followed for *visit 1* was applied, the only difference being blood sample collection in view of YSI measurements from 12.00 am on day 2 every hour all day and every 10 minutes during the 2 hours following meal intake. Objective of the visit was testing blood glucose prediction performed by the DIAdvisor^{TM} first prototype.

Visit 3 (testing of therapy advices)

Patients were admitted for a 76 hour-period starting from 10.00 am on day 1 to 2.00 pm on day 4. All the Consortium clinics participated in this phase, whose protocol is the same as the one for *visit 2*. However, objective of this trial was the testing of therapy advices suggested by the DIAdvisor^{TM} first prototype. On the last day at 2.00 pm (± 15 min), all the sensors were removed from the patient for closure of the study.

3.4 Patient selection criteria

A population of 8 patients was chosen (6 males and 2 females, age 33.7±15.2 [yr], BMI 24.3±3.7 [kg/m^2], all CSII). Table 3.2 reports their characteristic. The selection criterium was collection by the DIAdvisor platform of at least 85% of the expected Dexcom® samples. Results obtained from DIAdvisor 1 trial data will be shown in Chapter 4.

Table 3.2 DIAdvisor 1 Trial. Patient characteristics

Patient ID	*Gender*	*Age* [yr]	*BMI* [kg/m^2]	*Therapy*	*Visit*
CHU108	M	28	24.8	CSII	3
CHU112	M	24	28.3	CSII	2
CHU121	M	38	24.1	CSII	1
CHU130	M	69	31.2	CSII	2
IKEM305	F	34	20.2	CSII	3
IKEM308	M	31	24	CSII	3
IKEM320	M	22	21.8	CSII	3
IKEM327	F	24	20.7	CSII	3
MEAN±SD		33.7±15.2	24.3±3.7		

3.5 DIAdvisor II trial

Equipment

To the purpose of data collection during DIAdvisor II trial, the same devices used in DIAdvisor I trial were adopted.

Biological sample collection

Blood samples were collected by medical personnel during the in-hospital visits in view to *YSI 2300 STAT Plus™ Glucose Analyzer* [Yellow Spring Instruments, 2013] blood glucose assays. Analysis were carried out in the biochemical laboratory of the CHU in Montpellier.

Study protocol and experiments

The trial comprised a series of experimental sessions for a duration of up to 9 weeks per patient, involving CHU, UNIPD and IKEM clinics. In particular, to the purpose of separately estimating meal and insulin impact on blood glucose dynamics, overcoming therefore the lack of input excitation observed in almost all the data sets treated in the literature [Finan et al., 2009] a novel meal test was carried out as outlined in the following subsections. Figure A.3 in Appendix A gives the flow chart of the trial.

Visit 0

Screening visit. The same procedure actuated in the previous trials was followed.

Visit 1

Within 7 days of *Visit 0* an outpatient visit was scheduled for insertion of the Dexcom® SEVEN®PLUS [Dexcom, 2013] sensor, starting a 14 ± 3 days ambulatory period. Training on how to use the device, interpret its values to take appropriate decisions as well as assistance in performing the first calibration with the HemoCue®Glucose 201+ Analyzer [Hemocue, 2013] was provided by the study personnel during the visit. Patients were instructed to calibrate the sensor at least twice a day or when required by the system and in case of sensor failure or at the end of sensor life (around 7 days) they were asked to remove the sensor and to insert a new one in order to continue glucose monitoring. In addition, patients were requested to record on their logbook all self-measured glucose values, insulin doses, carbohydrate contents of meals, hypoglycemia treatments, sensor replacements, calibrations and any other event related to diabetes until the next visit.

Visit 2 (meal test)

Visit 2 took place at the clinical investigation center. Patients were admitted to the hospital for a 6.5 hours observation period, from 6.30 am to 1.00 pm, fasting from the midnight, equipped with a Dexcom® SEVEN® PLUS [Dexcom, 2013] continuous glucose monitoring sensor (CGMS) for interstitial glucose samples and a HemoCue®Glucose 201+ Analyzer [Hemocue, 2013] for capillary blood glucose measurements. After arrival, a recalibration of the CGM system was performed by the subjects using the HemoCue®meter, in order to be able to start data collection at 7.00 with a well calibrated glucose monitoring device. A standardized breakfast, the amount of carbohydrate being 40 [g], was served at 8.00 am and fully ingested within 20 minutes. The patients calculated and noted on their personal logbook the amount of insulin needed to cover this meal, based on the outcome of the HemoCue®glucose meter at the start of the meal. However, contrary to standard practice, the insulin bolus was administered 2 hours later. No other meals nor snacks were consumed until 1.00 pm. Blood samples were drawn every 10 minutes for the 3 hours following the meal intake and every 20 minutes otherwise from 7.00 am (±15 min) to 1.00 pm (± 15 min) to assess glucose concentration. Representative patients data are shown in Chapter 6, Figs. 8.4-8.6 and in Appendix D Figs. D.22, D.24, D.26. At the end of the meal test, patients kept the CGM device in place for continuous glucose monitoring.

Visit 3

Patients were admitted at the investigation center for a 76 hours period starting from 10.00 am on day 1 to 2.00 pm on day 4. At 10.00 am (± 15 min), the CGM device was connected to the UMPC platform, thereafter the Sensium^{TM} Life Pebble was placed on the patient's chest. Capillary blood glucose values, insulin delivery, meal contents and exercise details were entered in the UMPC application by the subjects throughout the whole admission period. Blood samples were drawn from 12.00 am (± 15 min) on day 1 to 12.00 (± 15 min) on day 4 at the rate of every hour during the day and every 15 minutes during the 2 hours following the start of a meal. During the 3 days of admission, patients were served standardized meals for breakfast at 8.00 am (± 15 min), lunch at 1:00 pm (± 15 min) and diner at 7.00 pm (± 15 min), the amount of carbohydrates administered being 40, 70 and 70 grams, respectively. During the visit, three situations were scheduled:

- On day 1 at 4:00 pm (± 15 min) patients performed a 30-minute exercise on a cyclo-ergometer followed by a one-hour rest period. Blood samples were collected every 5 minutes during the duration of the exercise and every 10 minutes during the hour rest.

- On day 2 at 1:00 pm (± 15 min), a 100 [g] carbohydrates content lunch was served.
- On day 3 a meal test as in *Visit 2* was performed. Blood samples were collected every 15 minutes during the 4 hours following the start of the meal to allow tight follow-up of blood glucose during this period.

In case of admission with disabled DIAdvisor algorithms, glucose predictions and therapy advices were not displayed. Patients decided their need of insulin according to the results given by the HemoCue®Glucose Analyzer [Hemocue, 2013] and the Dexcom® SEVEN® PLUS [Dexcom, 2013] CGM trends. In case of admission with activated DIAdvisor algorithms, glucose predictions and therapy advices were displayed to the patient. Hence, they were asked to follow the advices suggested by DIAdvisor^{TM}system according to their own judgement. In case of any doubt with the predictions displayed or the advices suggested, the patients were invited to ask study personal and/or the study physician for help. During the admission, CGM calibrations were performed in the morning before and 2 hours after the breakfast and in the evening around 2 hours after dinner. On the last day at 12.00 am, all the devices were disconnected.

Figure 3.5 DIAdvisor I and II trials equipment. The ultra mobile PC (*center*) is connected via USB to the Seven®Plus receiver (*left*) and the Sensium^{TM} Life Pebble (*bottom*) through its dedicated adapter.

Table 3.3 DIAdvisor II trial. Patient characteristics

Patient ID	*Gender*	*Age* [yr]	*Duration of disease* [yr]	*BMI* [kg/m^2]	HbA1$_c$[%]	*Therapy*	*Total Daily Insulin* [IU]
CHU101	M	25	15	23.7	9	MDI	50
CHU107	M	62	19	24.3	8.9	CSII	30.7
CHU117	M	61	42	31.1	8	CSII	53
CHU118	M	35	10	24.6	7.2	MDI	46
CHU125	F	69	25	28.7	7.6	MDI	25
CHU136	M	40	9	26.8	9.6	MDI	29
CHU138	M	46	33	22	7.5	CSII	28
CHU143	M	36	26	23.4	7.5	CSII	36.4
CHU144	F	38	31	22.6	7.2	CSII	30
CHU145	M	34	9	23	7.1	CSII	37
UNIPD201	M	28	7	21.7	7.1	MDI	55
UNIPD217	M	46	14	28.4	9.3	MDI	60
UNIPD219	M	48	36	21.1	7.6	MDI	40
UNIPD233	M	36	33	26.5	7.3	MDI	57
UNIPD234	M	24	11	21.7	7.1	MDI	55
IKEM302	M	29	10	23.5	5.7	CSII	60
IKEM306	M	35	7	21.8	5.9	CSII	31
IKEM309	F	51	11	23.5	7.4	MDI	31
IKEM311	M	44	38	24.5	6.8	MDI	48
IKEM324	F	28	16	21.5	6.4	CSII	36
IKEM326	F	50	12	23.9	8.2	CSII	29
IKEM330	M	64	18	25	5.4	MDI	48
MEAN±SD		42.2±13.1	18.36±11.5	24.2±2.6	7.4±1.12		41.5±11.7

3.6 Patients selection criteria

60 diabetic subjects, male and female adults, were recruited at this stage. A portion of them failed to comply with the protocol and were therefore disregarded for our purposes. Among those following the protocol, a total of 22 patients was selected on the basis of the Dexcom®SEVEN®PLUS correctness (17 males and 5 females, age 42.2±13.1 [yr], disease duration 18.4±11.5 [yr], BMI 24.2±2.6 [kg/m^2], 12 MDI and 10 CSII, HbA1$_c$7.4±1.1 [%], total daily insulin 41.5±11.7 [IU]). Patient informations are shown in Table 3.3. In this thesis the meal test data from *Visit 2* and from day 3 of *Visit 3* will be used in Chapter 8.

3.7 Blood glucose vs. interstitial glucose

Continuous glucose monitors assist the patients in the treatment of diabetes by providing frequently sampled blood glucose data. Studies have documented the benefits of CGM [Deiss et al., 2006], [Garg et al., 2006] and shown the potential to dramatically transform the control of the disease. However, it is important to remember that CGM devices measure glucose concentration in a different compartment–the interstitium, i.e., in between the body cells. A current, proportional to the interstitial glucose (IG) concentration is converted into a glucose level by a calibration step which exploits some blood glucose (BG) reference typically from self-monitored capillary glucose samples. Movements of nutrients, oxygen and glucose from the blood into the cells happen across the interstitium; therefore, during times of rapid change in blood glucose, e.g. after eating, dosing insulin, or exercising, differences in glucose measurement between interstitial fluid and blood measurements are expected to be observed. These deviations are physiological and reflect the time it takes for glucose to move between different compartments [Garg et al., 2010]. The BG-to-IG kinetics acts as a low-pass filter [Breton and Kovatchev, 2008], [Keenan et al., 2009] and introduces an attenuation in amplitude and a distortion in phase, which is usually well observable during dynamic phases. At other times, however, sensor measurements deviate form reference glucose because of inaccurate calibration, sensor misplacement and other artifacts. While the accuracy of CGM is increasing, it is still below the accuracy of direct BG readings [Clarke and Kovatchev, 2007], [Barry Keenan et al., 2009], [Garg et al., 2009], [Facchinetti et al., 2010], [Leelarathna et al., 2013].

Within the DIAdvisor^{TM} project interstitial measurements with the FreeStyle Navigator^{TM} and the DexCom®SEVEN®PLUS devices as well as capillary glucose samples with the HemoCue^{TM} and blood glucose

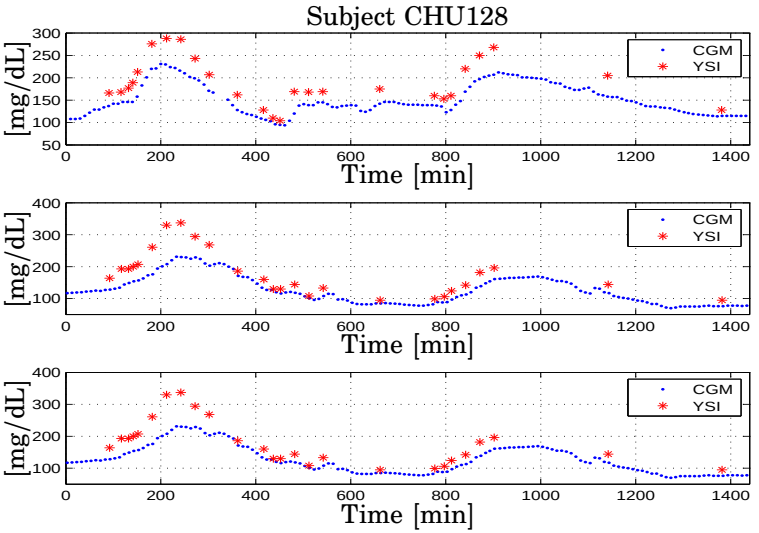

Figure 3.6 Patient CHU128. DAQ trial, *Visit 2*. Glucose concentration [mg/dL] vs. time [min]: interstitial CGM measurements (blue) vs. plasma YSI measurements (red). *Top* day 1; *Center* day 2; *Bottom* day 3

measurements assessed by a YSI [Yellow Spring Instruments, 2013] were collected. The availability of such records allowed comparison between the IG data and the corresponding BG. It was noted that in 40-50% of the FreeStyle Navigator™ traces gathered during the DAQ trial, the sensor was accurate at low glucose levels but inaccurate at high levels, a fact that cannot be explained by the plasma-to-interstitium dynamics only and may be explained by poor/difficult device calibration. An example of such situation is shown in Figure 3.6. Overall, the Dexcom®data seemed not to be affected by such an issue. The calibration problem with CGM devices is well known in the literature and some techniques have been proposed to correct the sensor signal provided by the device by exploiting information contained in the SMBG references which the patient collects during the day in parallel to CGM [King et al., 2007], [Facchinetti et al., 2007], [Bequette, 2010], [Perez-Gandia et al., 2010], [Facchinetti et al., 2013]. In this thesis we do not explicitly address the sensor model issue. Instead, we rely upon the Yellow Spring Instrument [Yellow Spring Instruments, 2013] assays when available and only in Chapter 6 we apply the offline recalibration method in [King et al., 2007] to the FreeStyle Navigator™ time series.

Accuracy of continuous glucose monitors

As already mentioned, continuous subcutaneous glucose monitors are less accurate than capillary glucose measurements. In this subsection we evaluate the mismatch between IG and BG for the data used in the thesis. Numerical accuracy was assessed pointwise by:

- absolute difference (AD) [mg/dL]: $\mathrm{AD}(k) = \mid y_{BG}(k) - y_{IG}(k) \mid$
- relative difference (RD): $\mathrm{RD}(k) = \dfrac{(y_{BG}(k) - y_{IG}(k))}{y_{BG}(k)}$
- International Organization for Standardization (ISO) [International Organization for Standardization (ISO), Publication 15197, 2003] criteria.

where $y_{BG}(\cdot)$ denote the YSI [Yellow Spring Instruments, 2013] blood glucose measurement and $y_{IG}(\cdot)$ stands for the interstitial glucose sensor measurement. Clinical accuracy was evaluated with Clarke error grid analysis [Kovatchev et al., 2004]. Numerical and clinical accuracy of the CGM devices with respect to the glucose time-series used in this thesis are given in Table 3.4, 3.5, 3.6 and 3.7.

Table 3.4 Numerical and Clinical Accuracy of CGMS measurements. DAQ trial, *Visit 2*.

Patient ID	*AD* [mg/dL]		*RD*		*ISO* [%]	*CG-pEGA* [%]		*CG-rEGA* [%]	
	Mean	Median	Mean	Median	∗	A	B	A	B
CHU102	19.81	15	0.07	0.07	82.07	81.65	16.51	83.33	9.25
CHU103	13.50	12.50	-0.07	-0.05	89.47	84.25	10.18	84.11	15.88
CHU104	18.96	17	-0.06	-0.06	80.76	77.98	19.26	79.62	14.81
CHU105	15.98	13	-0.05	-0.05	87.50	81.73	12.50	77.66	17.47
CHU106	32.79	33	-0.20	-0.20	46.93	44.95	47.70	75.92	12.96
CHU107	31.09	26.50	-0.03	-0.03	62.96	61.81	36.36	66.05	21.10
CHU108	13.25	9.50	-0.03	-0.03	83.83	81.48	14.81	81.30	14.01
CHU115	19.65	16.5	0.05	0.07	84.76	84.90	15.09	84.76	5.71
CHU118	21.98	17	0.01	0.04	74.22	69.09	22.72	81.65	12.84
CHU119	26.56	20	0.08	0.08	68.80	68.80	30.27	74.07	18.51
CHU120	26.72	25	-0.07	-0.01	73.26	69.15	26.16	76.41	18.86
CHU121	25.08	19	-0.05	0.05	72.72	68.18	24.54	77.98	14.67
CHU128	39.37	34	0.20	0.20	47.43	47.43	48.71	79.22	18.18
CHU130	25.39	19.50	-0.04	-0.05	81.69	78.20	14.10	77.92	16.88

∗ CGM readings within [20%] from reference y_{BG} when $y_{BG} \geq 75$[mg/dL]

Table 3.5 Numerical and Clinical Accuracy of CGMS measurements. DIAdvisor I trial

Patient ID	*AD* [mg/dL]		*RD*		*ISO* [%]	*CG-pEGA* [%]		*CG-rEGA* [%]	
	Mean	Median	Mean	Median	$*$	A	B	A	B
CHU108	14.50	10.46	0.13	0.09	76.19	82.35	17.64	96.96	3.03
CHU112	12.53	7.45	0.05	0.02	83.33	85.71	14.28	90	10
CHU121	26.23	19.93	0.15	0.13	58.62	66.66	33.33	100	0
CHU130	17.05	8.97	-0.05	-0.01	70.58	66.66	22.22	96.15	0
IKEM305	13.82	8.68	0.02	0.009	87.50	90.32	9.67	93.33	6.67
IKEM308	17.91	16.31	0.11	0.08	80	79.16	20.83	91.30	0
IKEM320	33.74	15.09	0.15	0.08	68.96	69.44	22.22	74.28	11.42
IKEM327	10.20	10.08	0.03	0.02	100	95.83	0	95.65	4.34

$*$ CGM readings within [20%] from reference y_{BG} when $y_{BG} \geq 75$[mg/dL]

Table 3.6 Numerical and Clinical Accuracy of CGMS measurements. DIAdvisor II trial, *Visit 2*, meal test.

Patient ID	*AD* [mg/dL]		*RD*		*ISO* [%]	*CG-pEGA* [%]		*CG-rEGA* [%]	
	Mean	Median	Mean	Median	∗	A	B	A	B
CHU101	18.59	18	0.06	0.07	100	100	0	96.15	3.84
CHU107	39.5	45.5	-0.20	-0.24	28.57	37.5	62.5	86.95	13.04
CHU117	20.48	21	0.10	0.09	100	96.29	3.70	96.15	3.84
CHU118	12.07	10.50	0.05	0.04	100	100	0	88	4
CHU125	8.29	7	-0.08	-0.08	100	95.83	4.16	60.86	39.13
CHU136	22.12	21	0.15	0.15	86.95	88	12	83.33	12.5
CHU138	12.32	13	-0.06	-0.06	96	96	4	100	0
CHU143	14.61	13	-0.05	-0.05	100	100	0	88	12
CHU144	17.20	17	0.10	0.08	96	96	4	91.66	4.16
CHU145	22.59	21	0.08	0.09	100	100	0	100	0
UNIPD201	26.44	33	-0.14	-0.16	84	85.18	14.81	88.46	11.53
UNIPD217	36.74	47	-0.16	-0.19	55.55	55.55	44.44	88.46	11.53
UNIPD219	50.25	44	-0.18	-0.17	48	51.85	48.14	57.69	26.92
UNIPD233	19.75	21.5	0.07	0.08	100	100	0	73.91	13.04
UNIPD234	18.12	14.5	0.04	0.03	100	100	0	73.91	13.04
IKEM302	21.29	21.89	-0.23	-0.18	72	53.84	30.76	100	0
IKEM306	9.25	7.5	-0.07	-0.08	100	100	0	100	0
IKEM309	11.06	10.55	0.01	-0.01	100	100	0	75	12.50
IKEM311	17.86	19.15	-0.08	-0.10	100	100	0	79.41	14.70
IKEM324	31.52	30	0.18	0.15	73.91	73.91	26.08	81.81	18.18
IKEM326	14.47	14	0.05	0.05	95.65	86.36	13.63	72.72	18.18
IKEM330	8.43	6.15	-0.03	0	100	100	0	86.36	13.63

∗ CGM readings within [20%] from reference y_{BG} when $y_{BG} \geq 75$[mg/dL]

Table 3.7 Numerical and Clinical Accuracy of CGMS measurements. DIAdvisor II trial, *Visit 3*, meal test.

Patient ID	*AD* [mg/dL]		*RD*		*ISO* [%]	*CG-pEGA* [%]		*CG-rEGA* [%]	
	Mean	Median	Mean	Median	$*$	A	B	A	B
CHU101	n/a	n/a	n/a	n/a	n/a	n/a	n/a	n/a	n/a
CHU107	n/a	n/a	n/a	n/a	n/a	n/a	n/a	n/a	n/a
CHU117	34.46	40	0.01	0.03	93.33	86.50	13.5	84	6
CHU118	43.31	42	0.01	0.07	56.25	85.18	14.81	65.38	26.92
CHU125	n/a	n/a	n/a	n/a	n/a	n/a	n/a	n/a	n/a
CHU136	n/a	n/a	n/a	n/a	n/a	n/a	n/a	n/a	n/a
CHU138	47.17	49		-0.19	-0.17	87.29	12.71	67.5	20.5
CHU143	36.17	33.91	-0.03	-0.06	78.12	82.75	17.24	32.14	35.71
CHU144	n/a	n/a	n/a	n/a	n/a	n/a	n/a	n/a	n/a
CHU145	n/a	n/a	n/a	n/a	n/a	n/a	n/a	n/a	n/a
UNIPD201	49.38	55.06	-0.15	-0.17	64.28	64.28	35.71	53.84	30.76
UNIPD217	26.19	18.49	-0.01	-0.1	92.85	92.85	7.14	74.07	18.51
UNIPD219	36.62	34.78	-0.06	-0.01	83.33	67.74	29.03	46.66	23.33
UNIPD233	25.14	26.5	-0.01	-0.01	92.85	75.24	24.76	92.3	0
UNIPD234	34.23	30	-0.06	-0.02	82.35	71.34	28.66	66.5	24.5
IKEM302	18.99	11.24	0.03	0.05	84.61	88.09	11.90	60.97	26.82
IKEM306	42.54	43.29	0.05	0.06	76.66	45.86	30.01	68.23	31.77
IKEM309	n/a	n/a	n/a	n/a	n/a	n/a	n/a	n/a	n/a
IKEM311	n/a	n/a	n/a	n/a	n/a	n/a	n/a	n/a	n/a
IKEM324	10.64	11	-0.08	-0.11	97.95	96.66	3.33	89.65	10.34
IKEM326	16.27	14.44	0.02	0.02	90.14	100	0	84.78	10.86
IKEM330	n/a	n/a	n/a	n/a	n/a	n/a	n/a	n/a	n/a

$*$ CGM readings within [20%] from reference y_{BG} when $y_{BG} \geq 75$[mg/dL]
n/a: not available data set

3.8 Discussion and conclusions

A wide range and large amount of bio-clinical information linked or potentially involved in blood glucose control were collected within the project DIAdvisor™ [DIAdvisor, 2012]. Data acquisition served different purposes suited to the project needs and were exploited accordingly. In particular, DAQ trial *Visit 2* data were used to build models and predictors for future integration in the first prototype of the tool (see Chapters 4 and 6 for results). Albeit being in a controlled environment, the subjects participating in the study experienced both hypo- and hyperglycemic events. However, data were not sufficiently excited. Indeed, as it is common practice, the majority of the subjects bolused just before being served the meal. Since meal intake and the insulin injections have opposite effects on the blood glucose level, each inputs contribution is difficult to distinguish when they are applied simultaneously. In order to overcome this limitation, data from the meal test in DIAdvisor II trial, *Visit 2* and *Visit 3* were chosen to improve the models (see Chapter 8).

Unfortunately, most of the collected data could not be represented, due to malfunctioning or failure of devices, patients not complying with the protocol (e.g., patient not wearing the vitals sign sensors as expected, patient taking insulin at the same time of breakfast in the meal test) too many missing meals and insulin injections in the subject diary.

4

Modeling of the Gluco-regulatory System

4.1 Introduction

The physiology of glucose metabolism in diabetes can be thought of as having one output, i.e., glucose level in the bloodstream y_{BG}, and two main inputs, i.e., carbohydrate intake u_{carb} and administered insulin I_{ir}. Further, given that physical activity has been proven to decrease plasma glucose levels due to increased glucose uptake by the exercising muscles [Williams and Pickup, 1992], the effect of exercise, i.e., increased heart rate, respiration rate and body movements, is therefore to be regarded as an additional input or load disturbance. Hence, for modeling purposes, based on current knowledge of the overall physiological model, four subsystems have to be considered (Fig. 4.1):

- the glucose subsystem (GS), describing glucose intestinal absorption following a food intake;
- the insulin subsystem (IS), accounting for the pharmacokinetics of the exogenously administered insulin;
- the physical activity and energy expenditure subsystem (EES), measuring the rate of physical activity intensity;
- the glucose-insulin interaction subsystem (GIIS).

In this chapter, compartment models from the literature are exploited to describe the GS and IS, while vital signs are used to account for the EES. Data-based system identification is used, instead, to model the GIIS.

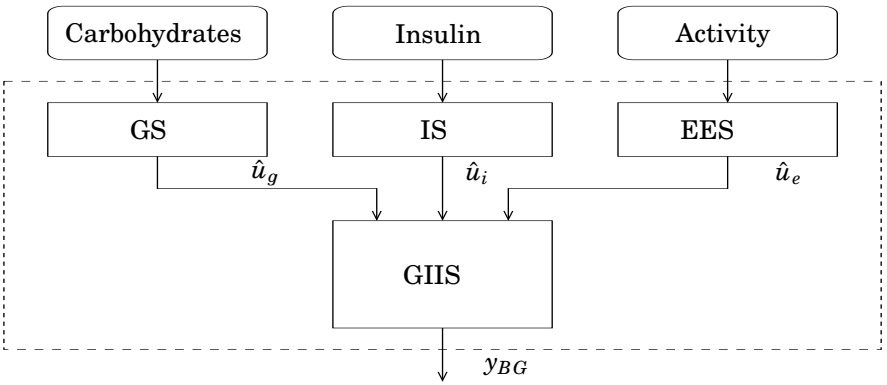

Figure 4.1 Physiological model describing diabetic blood glucose dynamics. Notation: GS glucose subsystem, IS insulin subsystem, EES energy expenditure subsystem, GIIS glucose insulin interaction subsystem; $\hat{u}_g$ glucose rate of appearance following a meal, $\hat{u}_i$ insulin in plasma after subcutaneous injection, $\hat{u}_e$ energy expenditure, y_{BG} blood glucose

4.2 Glucose subsystem

Glucose transit through the stomach and upper small intestine was described by a nonlinear chain of three compartments, where the first two compartments represent the stomach (solid and liquid phases) and the third one depicts the intestine. The left plot in Fig. 4.2 illustrates the model. Equations are [Dalla Man et al., 2006] :

$$\begin{aligned} q_{sto}(t) =& q_{sto1}(t) + q_{sto2}(t) & \\ \dot{q}_{sto1}(t) =& -k_{gri} \cdot q_{sto1}(t) + u_{carb} \cdot \delta(t), & q_{sto1}(0) = 0 \\ \dot{q}_{sto2}(t) =& -k_{empt} \cdot q_{sto2}(t) + k_{gri} \cdot q_{sto1}(t), & q_{sto2}(0) = 0 \\ \dot{q}_{gut}(t) =& -k_{abs} \cdot q_{gut}(t) + k_{empt} \cdot q_{sto2}(t), & q_{gut}(0) = 0 \\ \hat{u}_g(t) =& \frac{f \cdot k_{abs} \cdot q_{gut}(t)}{m_b}, & u_g(0) = 0 \end{aligned} \tag{4.1}$$

where $\hat{u}_g$ [mg/kg/min] denotes the rate of appearance of glucose in plasma, q_{sto1} $[mg]$ and q_{sto2} $[mg]$ are the amounts of carbohydrates in the stomach (solid and liquid phase, respectively), u_{carb} $[mg]$ is the amount of ingested carbohydrates, q_{gut} $[mg]$ is the carbohydrate mass in the intestine, k_{gri} is the rate of grinding, k_{empt} the rate of gastric emptying, m_b $[kg]$ the subject's body weight, k_{abs} the rate of absorption and f the fraction of intestinal absorption that actually appears in plasma. The rate of gastric emptying was a non-linear function of the amount of carbohydrates

in the stomach q_{sto} according to the following relationship:

$$k_{empt}(q_{sto}) = k_{min} + \frac{k_{max} - k_{min}}{2} \cdot \\ \cdot \{\tanh[\alpha(q_{sto} - b \cdot D)] - \tanh[\beta((q_{sto} - c \cdot D)] + 2\} \tag{4.2}$$

$$\alpha = \frac{5}{2 \cdot D \cdot (1-b)}, \qquad \beta = \frac{5}{2 \cdot D \cdot c} \tag{4.3}$$

Dalla Man and co-workers provided us with the mean population values for the parameters appearing in Eqs. 4.1, 4.2, 4.3 used thoughout the thesis. Table 4.1 reports such values.

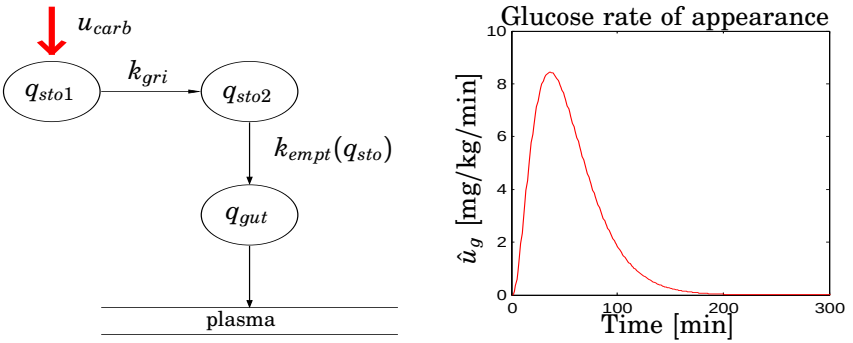

Figure 4.2 *Left* Glucose intestinal absorption model [Dalla Man et al., 2006]. *Right* Glucose rate of appearance $\hat{u}_g$ after ingestion of 40 [g] carbohydrate by a patient with m_b=65 [kg] at time t = 0, simulated with the model in Eq. (4.1) and parameters in Table 4.1

Table 4.1 Parameter values in the glucose intestinal absorption model

Parameter	Value	Measurement Unit
k_{gri}	0.0558	$[\text{min}^{-1}]$
k_{max}	0.0558	$[\text{min}^{-1}]$
k_{min}	0.0080	$[\text{min}^{-1}]$
k_{abs}	0.0568	$[\text{min}^{-1}]$
b	0.82	dimensionless
c	0.01	dimensionless
f	0.9	dimensionless

4.3 Insulin subsystem

The insulin flow $s(t)$ entering the bloodstream from the subcutaneous depots in the diabetic subject is described by a subcutaneous insulin infusion model, whose model equations are:

$$\begin{aligned} \dot{I}_{sc1}(t) &= -(k_d + k_{a_1})I_{sc1}(t) + I_{ir}(t), & I_{sc1}(0) &= I_{sc1b} \\ \dot{I}_{sc2}(t) &= k_d I_{sc1}(t) - k_{a_2} I_{sc2}(t), & I_{sc2}(0) &= I_{sc2b} \\ s(t) &= k_{a1} I_{sc1}(t) + k_{a_2} I_{sc2}(t) \end{aligned} \tag{4.4}$$

with I_{sc1}, I_{sc2} [pmol/kg] the amount of nonmonomeric and monomeric insulin in the subcutaneous space, respectively, k_d [min^{-1}] the rate constant of insulin dissociation, k_{a_1} [min^{-1}] and k_{a_2} [min^{-1}] the rate constants of nonmonomeric and monomeric insulin absorption, respectively, and I_{ir} [pmol/kg/min] the exogenous insulin infusion rate. The insulin flow $s(t)$ which entered the bloodstream is degraded in liver and periphery according to the model equations [Ferrannini and Cobelli, 1987]:

$$\begin{aligned} \dot{I}_p(t) &= -(m_2 + m_4)I_p(t) + m_1 I_l(t) + s(t), & I_p(0) &= I_{pb} \\ \dot{I}_l(t) &= -(m_1 + m_3)I_l(t) + m_2 I_p(t), & I_l(0) &= I_{lb} \\ \hat{u}_i(t) &= \frac{I_p(t)}{V_i} \end{aligned} \tag{4.5}$$

where I_p [pmol/kg] and I_l [pmol/kg] are insulin masses in plasma and liver, respectively, V_i [L/kg] is the distribution volume of insulin, while $\hat{u}_i$ [pmol/L] accounts for the total plasma insulin concentration. m_1 is the rate of hepatic clearance, m_2, m_3, m_4 [min^{-1}], instead, are rate parameters as follows:

$$\begin{aligned} m_2 &= \frac{3}{5}\frac{I_{CL}}{HE_b(V_i m_b)} \\ m_3 &= m_1 \frac{H_{E_b}}{1 - HE_b} \\ m_4 &= \frac{2}{5}\frac{I_{CL}}{V_i m_b} \end{aligned} \tag{4.6}$$

where HE_b [dimensionless] is the basal hepatic insulin extraction, while I_{CL} [L/min] is the insulin clearance. At steady-state

$$\begin{aligned} 0 &= -(k_d + k_{a_1})I_{sc1b} + I_{irb} \\ 0 &= k_d I_{sc1b} - k_{a_2} I_{sc2b} \\ s_b &= k_{a1} I_{sc1b} + k_{a_2} I_{sc2b} \end{aligned} \tag{4.7}$$

so that the basal value of insulin in the subcutaneous compartments, i.e., I_{sc1b} and I_{sc2b} is:

$$\begin{aligned} I_{sc1b} &= \frac{I_{ir_b}}{k_d + k_{a1}} \\ I_{sc2b} &= \frac{k_d}{k_{a2}} \cdot I_{sc1b} \end{aligned} \tag{4.8}$$

and $s_b = I_{irb}$. Further,

$$\begin{aligned} 0 &= -(m_2 + m_4) I_{pb} + m_1 I_{lb} + s_b \\ 0 &= -(m_1 + m_3) I_{lb} + m_2 I_{pb} \end{aligned} \tag{4.9}$$

leading to the expressions for the amount of insulin in the liver compartment at basal state:

$$I_{lb} = I_{pb} \frac{m_2}{m_1 + m_3} \tag{4.10}$$

and the amount of insulin in plasma at basal steady state:

$$I_{pb} = \frac{I_{irb}}{m_2 + m_4 - \frac{m_1 m_2}{m_1 + m_3}} \tag{4.11}$$

Model parameters used in the thesis were provided by Dalla Man and co-workers and are given in Table 4.2.

Figure 4.4 shows the filtered inputs for the representative patients.

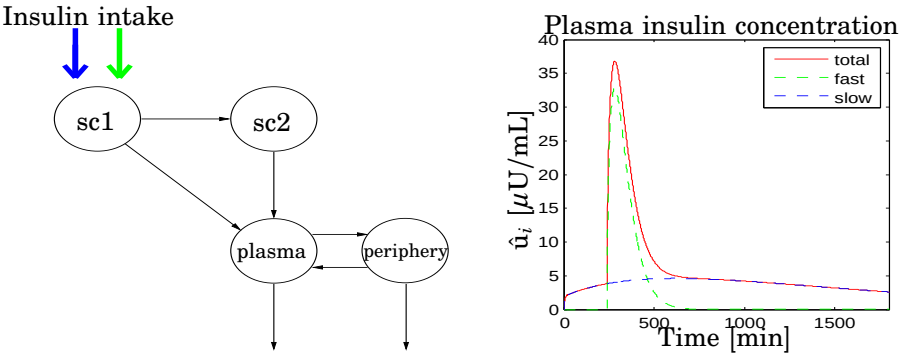

Figure 4.3 *Left* Insulin pharmacokinetics model [Kovatchev et al., 2008b]. It accounts for both slow- and fast-acting insulin. Compartments sc1 and sc2 represents the subcutaneous insulin infusion module. Plasma insulin concentration: total $\hat{u}_i$ [μU/mL] (red), slow-acting (blue) and fast-acting (green) resulting from a basal dose of 20 [IU] at t=0 and a bolus of 5 [IU] at t = 240 [min], taken by a patient with m_b= 65 [kg], simulated with the model in Eqs. (4.4)-(4.5) and parameters in Table 4.2

Table 4.2 Parameter values for the subcutaneous insulin infusion model

Parameter	Fast insulin	Slow insulin	Unit
k_{a1}	0.004	0.0002	$[\text{min}^{-1}]$
k_{a2}	0.0182	0.00091	$[\text{min}^{-1}]$
k_d	0.0164	0.00164	$[\text{min}^{-1}]$
m_1	0.1766	0.1766	$[\text{min}^{-1}]$
V_i	0.05	0.05	[L/kg]
I_{CL}	1.1069	1.1069	[L/min]
HE_b	0.6	0.6	dimensionless

4.4 Energy expenditure subsystem

Physical activity causes changes in the body, including altered blood tissue volumes, increased tissue blood flow [Chapman and Mitchell, 1965], increased heart rate and oxygen consumption [Robergs and Roberts, 2000], increased glucose uptake by the exercising muscles [Ahlborg et al., 1974], and increased glucose production by the liver [Wahren et al., 1971]. Incorporating such effects into a glucose metabolism model would therefore provide improvements in the description of glucose dynamics in patients during exercise. However, during daily life activities physical exercise is light or absent and the above mentioned effects may not be observed. A relevant question is, then, whether heart rate and respiration rate contribute in some way to the description of blood glucose dynamics during daily life. In order to address this question in the thesis, the heart rate and respiration rate data collected with the VivoMetrics Clinical LifeShirt® worn by the patients were used as additional input:

$$\hat{u}_e = [H_r \quad R_r]$$

where H_r denotes the heart rate and R_r the respiration rate.

4.5 Notation

In the following, let us denote with u_i plasma insulin concentration and with u_g plasma glucose rate of appearance following a carbohydrate intake, while with $\hat{u}_i$ and $\hat{u}_g$ the predicted plasma insulin and the predicted rate of appearance, respectively, obtained with models in Eqs. 4.1, 4.5.

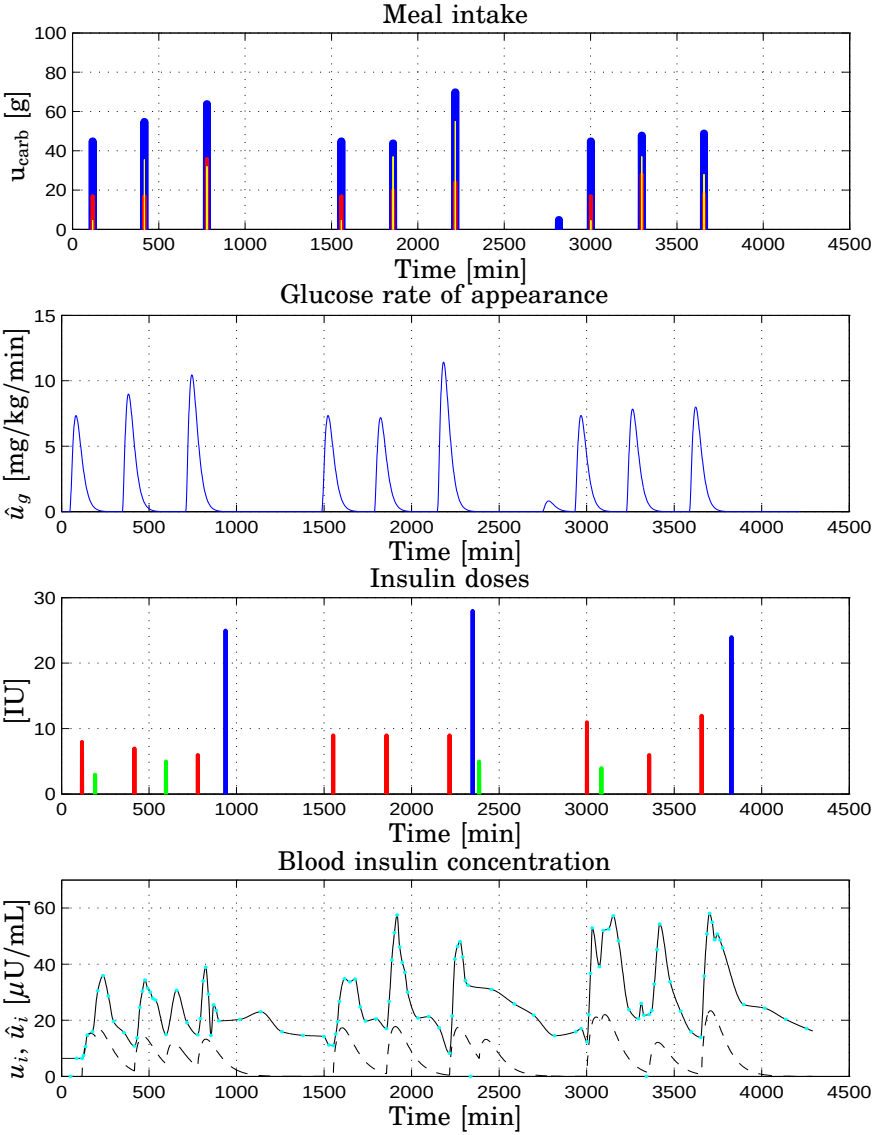

Figure 4.4 Patient CHU0102 data vs. time [min]. *Top* Meal intake: carbohydrates (blue), lipids (red), proteins (yellow); *Upper Center* Glucose Rate of appearance in plasma after a meal $\hat{u}_g$; *Lower Center* Insulin doses: basal (blue), bolus (red), correction (green); *Bottom* Total blood insulin concentration: interpolated u_i (solid black), blood samples (cyan), from physiological model $\hat{u}_i$ (dashed black)

4.6 Glucose-insulin interaction subsystem

Consider first modeling the dynamics of blood glucose concentration, y_{BG}, in response to plasma insulin concentration, u_i, and meal glucose rate of appearance in plasma, u_g.

Linear dynamic model structures for the GIIS were:

- autoregressive moving average with exogenous inputs (ARMAX) model on the form:

$$A(z^{-1})y_{BG}(k) = z^{-d_1}B_1(z^{-1})u_i(k) + z^{-d_2}B_2(z^{-1})u_g(k) + C(z^{-1})w(k) \quad (4.12)$$

where z^{-1} is the backward shift operator, d_1 and d_2 are time delays associated with the inputs, A, B_1, B_2, C are polynomials of order n_a, n_{b1}, n_{b2}, n_c, respectively

$$\begin{aligned} A(z^{-1}) &= 1 + a_1 z^{-1} + \cdots + a_{n_a} z^{-n_a} && (4.13)\\ B_1(z^{-1}) &= b_{0,1} + b_{1,1} z^{-1} + \cdots + b_{n_{b,1}} z^{-n_{b,1}} && (4.14)\\ B_2(z^{-1}) &= b_{0,2} + b_{1,2} z^{-1} + \cdots + b_{n_{b,2}} z^{-n_{b,2}} && (4.15)\\ C(z^{-1}) &= 1 + c_1 z^{-1} + \cdots + c_{n_c} z^{-n_c} && (4.16) \end{aligned}$$

and $w(k)$ is a white noise.

- autoregressive with exogenous inputs (ARX) model, which is a special case of the ARMAX model

$$A(z^{-1})y_{BG}(k) = z^{-d_1}B_1(z^{-1})u_i(k) + z^{-d_2}B_2(z^{-1})u_g(k) + w(k) \quad (4.17)$$

- state-space model in innovation form

$$\begin{cases} x(k+1) = \mathcal{A}x(k) + \mathcal{B}u(k) + \mathcal{K}e(k) \\ y_{BG}(k) = \mathcal{C}x(k) + e(k) \end{cases} \quad (4.18)$$

with $u(k) = [u_i(k) \quad u_g(k)]^\intercal$, $x(k) \in \mathbb{R}^n$ the state vector, $\mathcal{A} \in \mathbb{R}^{n\times n}$, $\mathcal{B} \in \mathbb{R}^{n\times 2}$, $\mathcal{C} \in \mathbb{R}^{1\times n}$, $\mathcal{K} \in \mathbb{R}^{n\times 1}$ and $\{e(k)\}$ the innovation process.

Deciding upon the model structure involves not only choosing which type of model to use in the identification, but also determining the model order and time delays. The following choices were made:

- $3 \leq n_a \leq 6$ for simplicity and low complexity
- $n_b, n_c \leq n_a$ in order to have proper transfer functions
- $d_1 = d_2 = 1$ because it is assumed that the signals in blood interact with no delay

4.7 Data

Data collected during the DAQ trial *Visit 2*, described in Section 3.2 were considered to the purposes of model identification. The carbohydrate content u_{carb} of the meals reported in the patient diary was used as input to the model in Eq. (4.1). Given the frequently drawn blood samples, it was decided to use the actual (interpolated and uniformly resampled) insulin assays for identification and validation purposes. The physiological insulin kinetics model in Eq. (4.4) was used at a later stage, to test the blood glucose response to 1 [IU] of fast acting insulin. It was decided to use blood glucose measurements from YSI [Yellow Spring Instruments, 2013] measurements instead of the CGM time-series because of the poor quality of the FreeStyle Navigator^{TM} (see Table 3.4 for accuracy evaluation and Section 3.8 for comments). Last, Montpellier patients were selected for bigger quantity of data collected with respect to the other sites participating.

4.8 Data analysis and pre-processing

Data analysis was performed in the following order [Johansson, 1993]:

- autospectrum of inputs

$$S_{uu}(i\omega) = \mathcal{F}\{\lim_{T\to\infty} \frac{1}{2T} \int_{-T}^{T} u(t)u^*(t-\tau)dt\}$$

- cross spectrum between inputs and output

$$S_{uy}(i\omega) = \mathcal{F}\{\lim_{T\to\infty} \frac{1}{2T} \int_{-T}^{T} u(t)y^*(t-\tau)dt\}$$

- quadratic coherence spectrum beween inputs and output

$$\gamma_{uy}^2(\omega) = \frac{\mid S_{uy}(i\omega) \mid^2}{S_{uu}(i\omega)S_{yy}(i\omega)}$$

The autospectra (power spectra) of inputs and output showing the frequency contents of the signals investigated are reported in Figure 4.6 for the representative patients CHU102. The coherence spectrum between the inputs and the controlled variable are shown in Figure 4.5.

For purposes of model identification, removal of the mean value of the data series u_i, $\hat{u}_g$, y_{BG} was done as part of standard data pre-processing [Ljung, 1999]. In addition, originally non-uniformly sampled, plasma glucose concentrations and plasma total insulin concentrations from laboratory results were linearly interpolated and uniformly resampled, the resampling period being 1 minute.

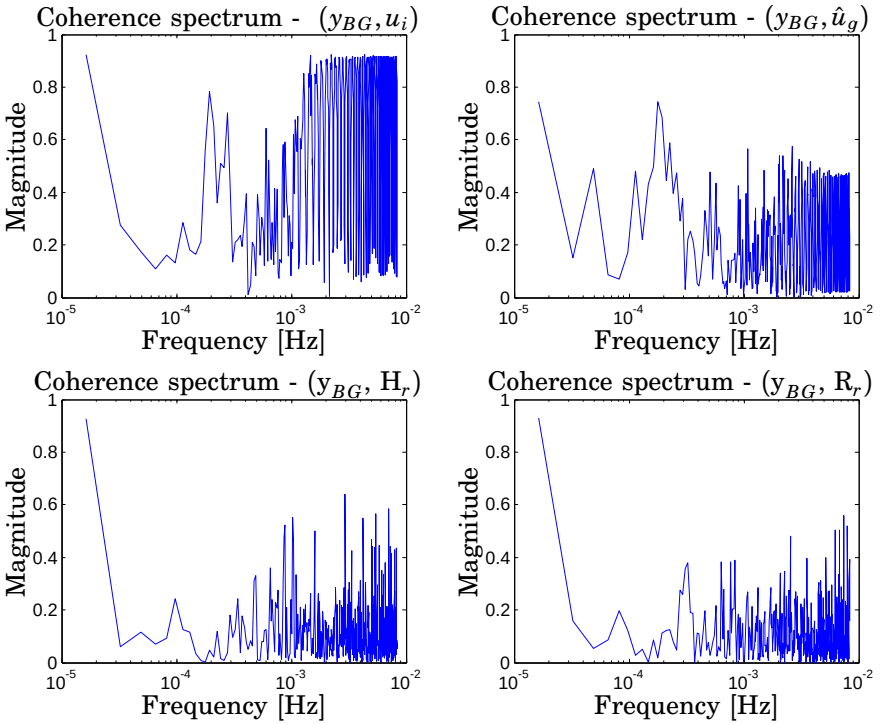

Figure 4.5 Patient CHU102. Coherence spectra between blood glucose and *Top Left* total plasma insulin; *Top Right* plasma glucose rate of appearance; *Bottom Left* Heart Rate; *Bottom Right* Respiration Rate. All the spectra vs. frequency [Hz]

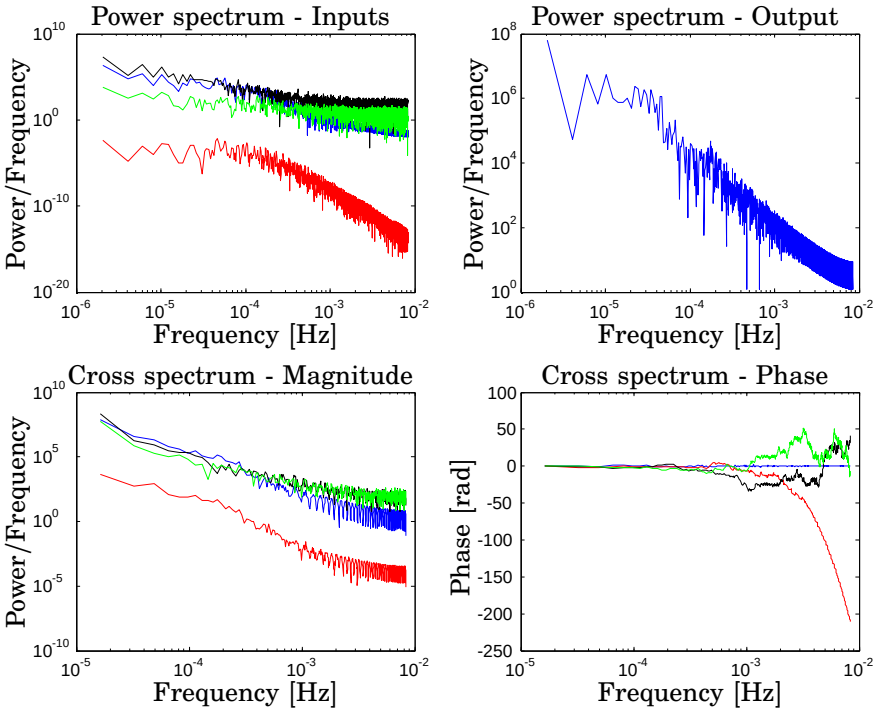

Figure 4.6 Patient CHU102. *Top Left* Magnitude of Power spectrum of inputs: total plasma insulin $[(\mu\text{U/mL})^2/(\text{Hz})]$ (blue), plasma glucose rate of appearance $[(\text{mg/kg/min})^2/(\text{Hz})]$ (red), heart rate $[(\text{beats/min})^2/(\text{Hz})]$ (black), respiration rate $[(\text{breaths/min})^2/(\text{Hz})]$ (green); *Top Right* Magnitude of Power spectrum of output: blood glucose $[(\text{mg/dL})^2/(\text{Hz})]$; *Bottom Left* Magnitude of cross spectrum: total plasma insulin, blood glucose $[(\mu\text{U/mL})^2(\text{mg/dL})^2/(\text{Hz})]$ (blue), plasma glucose rate of appearance, blood glucose $[(\text{mg/kg/min})^2(\text{mg/dL})^2/(\text{Hz})]$ (red), heart rate, blood glucose $[(\text{beats/min})^2(\text{mg/dL})^2/(\text{Hz})]$ (black), respiration rate, blood glucose $[(\text{breaths/min})^2(\text{mg/dL})^2$ (Hz)] (green); *Bottom Right* Phase of cross spectrum [rad]: total plasma insulin (blue), plasma glucose rate of appearance (red), heart rate (black), respiration rate (green). All the spectra vs. frequency [Hz]

4.9 Problem formulation

Given the inputs:

- interpolated total plasma insulin concentration from drawn blood samples u_i [μU/mL];
- plasma glucose rate of appearance after carbohydrate intestinal absorption $\hat{u}_g$ [mg/kg/min];

and the output:

- interpolated blood glucose y_{BG} [mg/dL] from drawn blood samples

the objective was to find an individual-specific and physiological relevant model of the glucose-insulin interaction for each of the subjects in the selected population.
Minimum requirements on the model were:

- stability;
- white residuals;
- qualitative correct blood glucose responses to
  - 1 [IU] fast-acting insulin;
  - 10 [g] carbohydrates;

Additional requirement on the model were:

- FIT $\geq$ 50% on 60-minutes-ahead model-based prediction on validation data;
- VAF $\geq$ 50% on 60-minutes-ahead model-based prediction on validation data.

4.10 Model estimation

The approach considered for modeling was system identification of the discrete-time, linear time-invariant models introduced in Sec 4.6 [Ljung, 1999]. The data belonging to each of the selected patients records was equally divided into two parts: the first one for the calibration procedure of obtaining the optimal model structure and model parameters, and the second one for validation of the chosen configuration.

For each of the calibration dataset different methods were used for the estimation of the model parameters:

- prediction-error identification methods (PEM) [Ljung, 1999] for identification of the ARX/ARMAX structures
- subspace-based methods, namely:
  - N4SID [Van Overschee and De Moor, 1994];
  - PO-MOESP [Verhaegen, 1994];
  - PBSID [Chiuso, 2007a], [Chiuso, 2007b];

  for the identification of the state-space model.

The identification procedure is outlined in Algorithm 4.1.

ALGORITHM 4.1—SYSTEM IDENTIFICATION PROCEDURE

1. ARX/ARMAX
   - for $3 \leq n_a \leq 6$
     - estimate model
     - compute Akaike Final Prediction Error
2. N4SID
   - choose the method for the estimation of the state-space
     - CVA [Larimore, 1990]
     - MOESP [Verhaegen, 1994]
   - set the past horizon $p = 120$ and the future horizon $f = 60$
   - set the model order $1 \leq n \leq 10$
   - select the model order $\bar{n}$ according to the singular values
   - estimate models with order $\bar{n} - 1$, $\bar{n}$, $\bar{n} + 1$
   - compute Akaike Final Prediction Error
3. MOESP
   - set the past and future horizons $p = f = 30$
   - select the model order $\bar{n}$ according to the singular values
   - estimate models with order $\bar{n} - 1$, $\bar{n}$, $\bar{n} + 1$
   - compute Akaike Final Prediction Error
4. PBSID
   - set the past horizon $p = 60$, and the future horizon $f = 20$

- select the model order $\bar{n}$ according to the singular values
- estimate models with order $\bar{n}-1$, $\bar{n}$, $\bar{n}+1$
- compute Akaike Final Prediction Error □

Throughout the work Matlab®System Identification Toolbox [MathWorks, 2013] and the SMI Toolbox [Haverkamp and Verhaegen, 1997] were used.

4.11 Model Evaluation and Selection Criteria

The system identification procedure provided a plethora of models for each of the subjects in the population. However, to the purpose of model-based controller design, it suffices to select one model per patient only. Necessary requirements on a model suitable for inclusion and exploitation in the DIAdvisor™ tool were:

- stability;
- white residuals;
- physiologically sensible responses to insulin and food intake, i.e., blood glucose concentration should decrease in response to insulin and increase in response to food intake.

In particular, in order to assess whether the model showed correct responses to inputs, the simulated blood glucose reactions to a

- 10 [g] carbohydrates intake
- 1 [IU] fast insulin injection

were compared. Glucose appearance in plasma resulting from 10 [g] carbohydrate ingestion was obtained with the model described in Sec. 4.2 and parameters in Table 4.1, while insulin appearing in plasma after subcutaneous injection of 1 [IU] was determined with the model in Sec. 4.3 and the parameters listed in Table 4.2.

Each of the estimated models was evaluated according to the diagram in Fig. 4.7. When a requirement was not fulfilled, the model was discarded. The models passing all the tests were ranked in increasing model order. Then, based on a tradeoff between accuracy as measured by the FPE and simplicity, one model per patient only was selected. Performances on short-term prediction, i.e., 30, 60, 90, 120 minutes ahead obtained with the Matlab® System Identification Toolbox [MathWorks, 2013] command *predict.m* were compared to those of the zero-order hold (ZOH) $\hat{y}_{BG}(k+\tau|k) = y_{BG}(k)$, with $\tau = 30, 60, 90, 120$ with respect to:

- Percentage FIT [%]

$$\text{FIT} = \left(1 - \frac{|| \, y_{BG} - \hat{y}_{BG} \, ||_2}{|| \, y_{BG} - \bar{y}_{BG} \, ||_2}\right) \times 100\%$$

- prediction error variance [$(\text{mg/dL})^2$]

$$\mathcal{E}[(y_{BG} - \hat{y}_{BG})(y_{BG} - \hat{y}_{BG})^\intercal]$$

- Percentage Variance Accounted For (VAF) [%]

$$VAF = 1 - \frac{\mathcal{E}[(y_{BG} - \hat{y}_{BG})(y_{BG} - \hat{y}_{BG})^\intercal]}{\mathcal{E}[y_{BG} y_{BG}^\intercal]} \times 100\%$$

with y_{BG} denoting actual blood glucose measurements, $\hat{y}_{BG}$ predicted blood glucose concentration, $\bar{y}_{BG}$ mean value of blood glucose concentration, $|| \cdot ||_2$ the 2-norm of a vector and $\mathcal{E}[\cdot]$ mathematical expectation. If $\hat{y}_{BG} = y_{BG}$, FIT and VAF are 100%, while the variance is zero. The more the prediction differ from the true value, the lower the FIT and VAF and the larger the variance. Notice that a negative FIT value is possible if $\hat{y}_{BG}$ differs from y_{BG} more than the mean value of y_{BG}, while a negative VAF value occurs if the variance of the prediction error $\hat{y}_{BG} - y_{BG}$ is larger than the variance of y_{BG}.

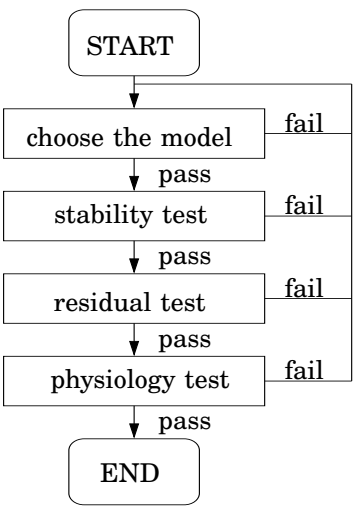

Figure 4.7 Diagram for model evaluation.

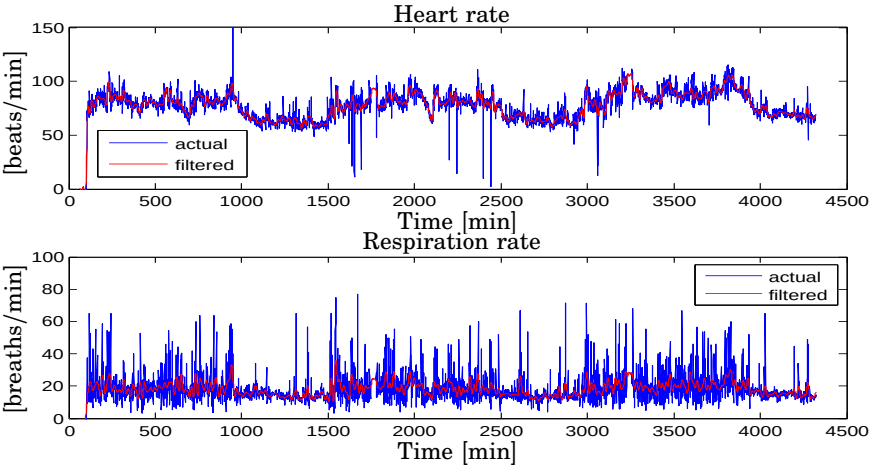

Figure 4.8 Patient CHU102. DAQ trial, *Visit 2*. *Top* Heart rate [beats/min]: actual (blue) vs. low-pass filtered (red); *Bottom* Respiration rate [breaths/min]: actual (blue) vs. low-pass filtered (red)

4.12 Incorporating Energy Expenditure

The model of each individual glucose metabolism passing all the requirements was expanded taking into account energy expenditure. The input $\hat{u}_e$ was added to the structure and a new model was identified.

Zero-phase distortion filtering was applied to the heart rate H_r and respiration rate R_r data in order to reduce the noise component from the signals. The filter used was a low-pass Butterworth filter of order 12 and 0.1 [π rad/sample] cutoff frequency for the point 3 dB below the passband value. The Bode diagram of the filter magnitude is shown in Fig. 4.9. Filtered data are depicted in Fig. 4.8.

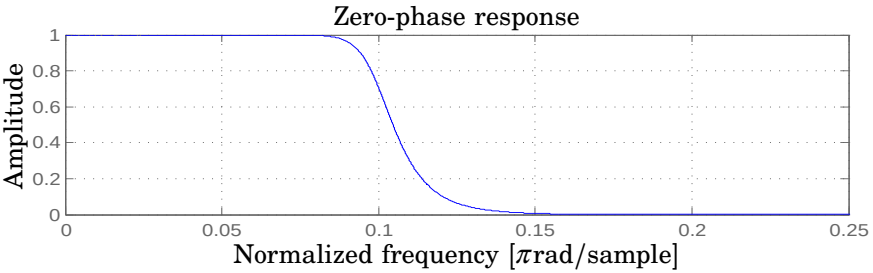

Figure 4.9 Low-pass Butterworth filter

4.13 Results

Models

Detailed results of the procedure outlined in Fig. 4.7 are given in Tables 4.3, 4.4 and 4.5. The methods failing to provide a model complying with the criteria in Sec. 4.11 are listed in the above mentioned tables along with the tests that were not met. The model for the representative patient CHU102 without the vital signs is the following:

$$\begin{aligned} &y(k) - 2.782y(k-1) + 2.579y(k-2) - 0.797y(k-3) = \\ &- 0.0004923u_i(k-1) + 2.397\hat{u}_g(k-1) + \\ &+ w(k) + 1.027w(k-1) + 0.1552w(k-2) + 0.06466w(k-3) \end{aligned} \tag{4.19}$$

scoring FPE = 0.000692238.

Figure 4.13 reports impulse responses of the model in Eq. (4.19). The output to 1 [IU] of insulin filtered with the insulin kinetics model in Eqs. (4.4)-(4.5) and to 10 [g] carbohydrates filtered with the carbohydrate intestinal absorption model in Eq. (4.1) are reported in the bottom diagram of Fig. 4.13.

Performances on short-term predictions, i.e., up to 120 minutes are displayed in Figure 4.11, while comparisons of the model-based predictors with the projection of the current glucose value in the future, i.e., the ZOH, are reported in Figure 4.12 and quantitatively in Tables 4.6, 4.7, 4.8. The boxplots in Figs. 4.14 show mean population performances.

Table 4.3 Model evaluation: fulfilled/ not fulfilled requirements for the discarded models. Patient 102

Patient ID	method	n	stability	residuals	physiological
102	N4SID	3	$\surd$	x	-
		4	$\surd$	x	-
		5	$\surd$	x	-
	PBSID	3	x	-	-
		4	x	-	-
		5	x	-	-
	MOESP	3	$\surd$	x	-
		4	$\surd$	x	-
		5	$\surd$	x	-

$\surd$ = pass; x= fail; - = not checked

Table 4.4 Model evaluation: fulfilled/ not fulfilled requirements for the discarded models. Patient 103, 104, 105, 106

Patient ID	method	n	stability	residuals	physiological
103	N4SID	2	√	x	-
		3	√	x	-
		4	√	√	x
	PBSID	4	x	-	-
		5	x	-	-
		6	x	-	-
	MOESP	3	√	x	-
		4	√	x	-
		5	√	x	-
104	N4SID	3	√	x	-
		4	√	√	x
		5	√	√	x
	PBSID	3	x	-	-
		4	√	x	-
		5	x	-	-
	MOESP	5	√	x	-
		6	x	-	-
		7	√	√	x
105	N4SID	2	√	√	x
		3	√	√	x
		4	√	√	x
	PBSID	2	x	-	-
		3	√	√	x
		4	√	√	x
	MOESP	3	√	x	-
		4	√	x	-
		5	√	x	-
106	N4SID	2	√	x	-
		3	√	x	-
		4	√	x	-
	PBSID	3	√	x	-
		4	x	-	-
		5	√	x	-
	MOESP	5	√	x	-
		6	√	x	-
		7	√	x	-

√ = pass; x= fail; - = not checked

Table 4.5 Model evaluation: fulfilled/ not fulfilled requirements for the discarded models. Patient 107, 115, 120, 130

Patient ID	method	n	stability	residuals	physiological
107	N4SID	2	√	x	-
		3	√	x	-
		4	√	√	x
	PBSID	2	√	x	-
		3	√	x	-
		4	x	-	-
	MOESP	4	√	x	-
		5	√	x	-
		6	√	x	-
115	N4SID	3	√	x	-
		4	√	x	-
		5	√	√	x
	PBSID	3	x	-	-
		4	x	-	-
		5	x	-	-
	MOESP	5	√	x	-
		6	√	x	-
		7	√	x	-
120	N4SID	2	√	√	x
		3	√	√	x
		4	√	√	x
	PBSID	2	√	x	-
		3	√	x	-
		4	√	x	-
	MOESP	5	√	x	-
		6	√	x	-
		7	√	x	-
130	N4SID	2	√	√	x
		3	√	√	x
		4	√	√	x
	PBSID	2	x	-	-
		3	x	-	-
		4	√	x	-
	MOESP	3	x	-	-
		4	√	√	x
		5	x	-	-

√ = pass; x= fail; - = not checked

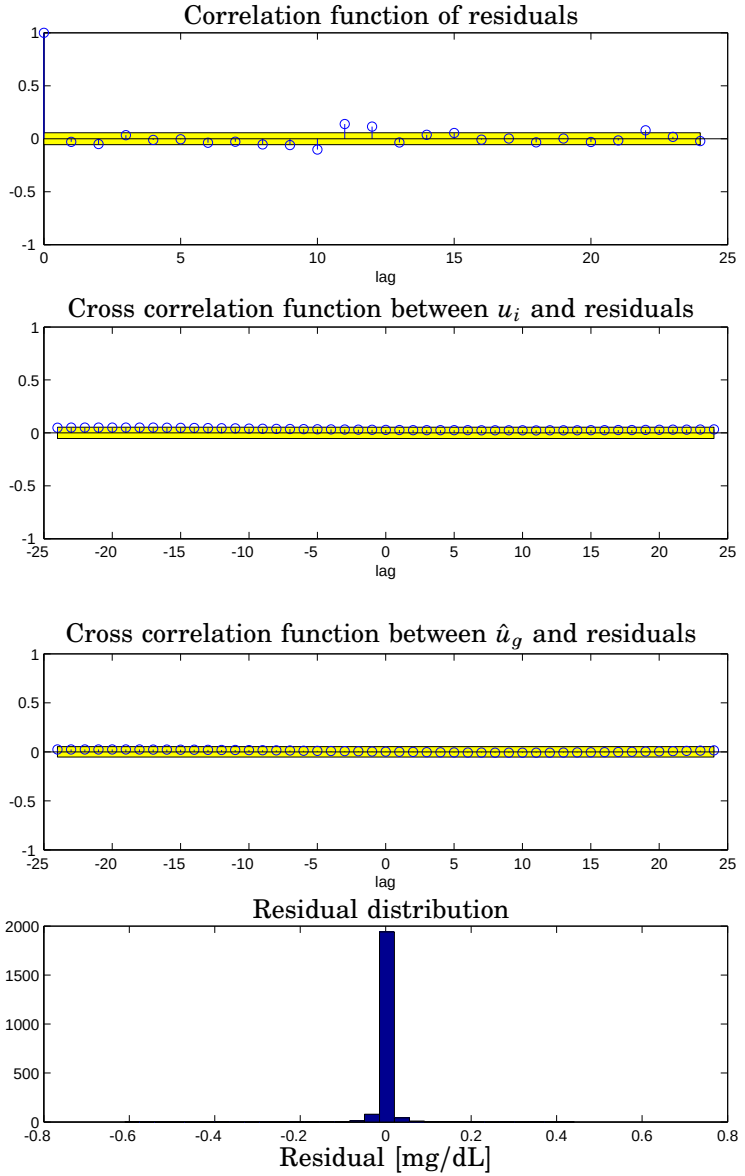

Figure 4.10 Patient 102. Residual analysis on validation data.

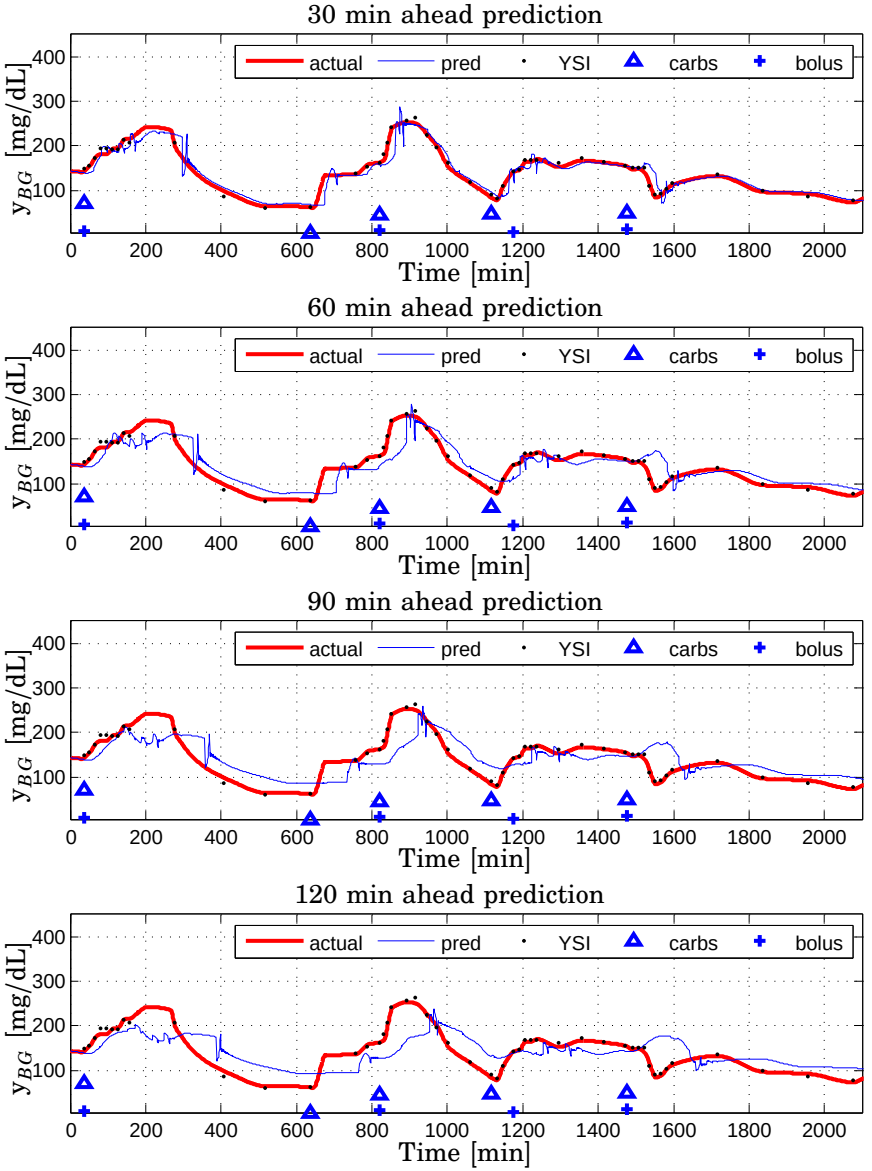

Figure 4.11 Patient CHU0102. Evaluation on validation data: 3rd-order ARMAX-based predictor (thin) and measured plasma glucose (thick) [mg/dL] vs. time [min].. *Top* 30-minutes ahead; *Top Center* 60-minutes ahead; *Bottom Center* 90-minutes ahead; *Bottom* 120-minutes-ahead prediction. DAQ Trial. Inputs: u_i, $\hat{u}_g$

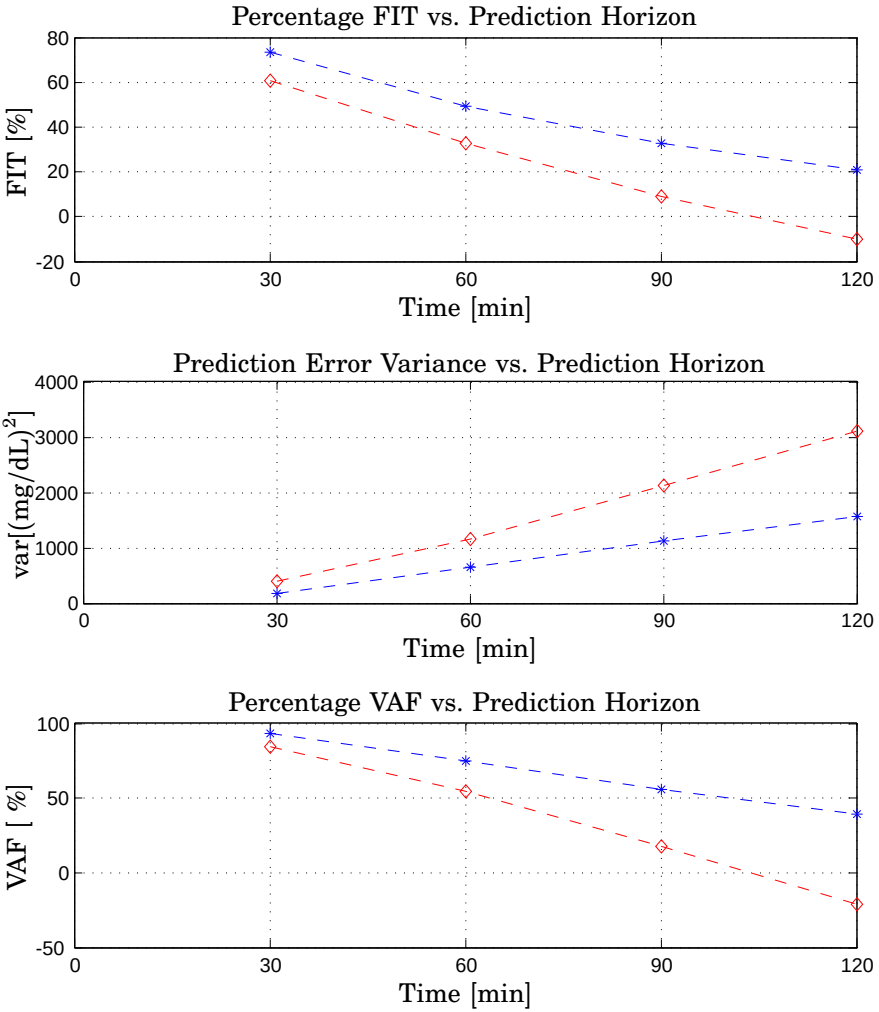

Figure 4.12 Patient CHU102. 3rd-order ARMAX-based predictor (star), ZOH (diamond). *Top* Percentage FIT [%]; *Center* Prediction Error Variance $[(\mathrm{mg/dL})^2]$; *Bottom* Percentage VAF [%]. All the metrics on validation data vs. Prediction Horizon [min]

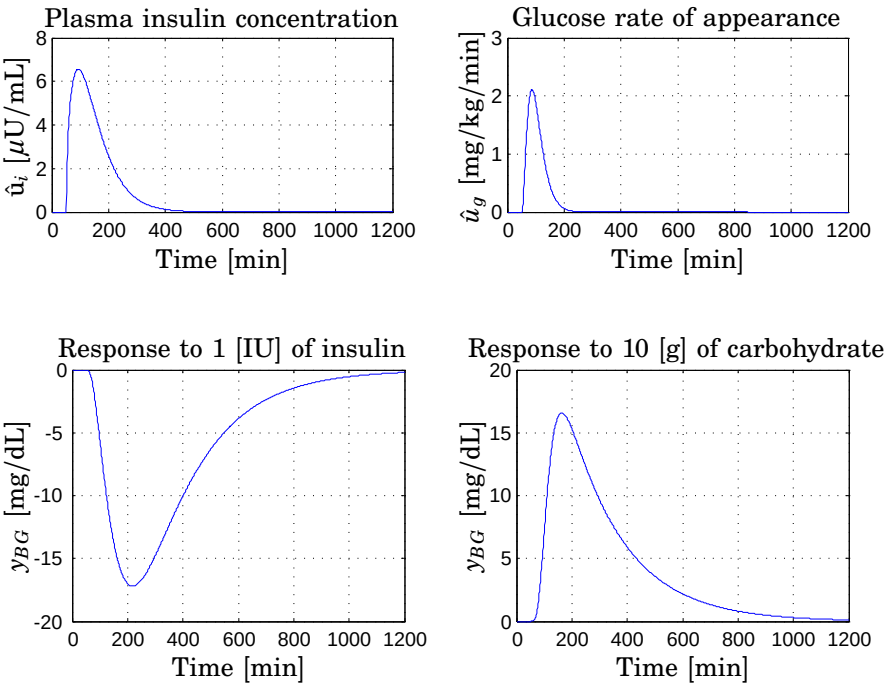

Figure 4.13 Patient CHU102. *Top Left* Insulin in plasma after injection of 1 [IU] at t = 50 [min] ; *Top Right* Glucose rate of appearance in plasma resulting from ingestion of 10 [g] carbohydrate at t = 50 [min]; *Bottom Left* Blood glucose response to 1 [IU] of fast-acting insulin; *Bottom Right* Blood glucose response to 10 [g] of carbohydrate

Table 4.6 Model-based predictor performance evaluation. Percentage FIT [%] vs. Prediction Horizon [min] on validation data. The best performing model is highlighted.

Patient ID	model	30[min]	60[min]	90[min]	120[min]
102	ARMAX	73.53	49.47	32.80	20.79
	ARMAX†	72.11	44.60	25.05	11.56
	ARX	72.07	45.25	23.01	1.36
	ZOH	60.64	32.57	9.01	-10.14
103	ARMAX	65.07	33.72	19.71	10.30
	ARMAX†	64.21	29.92	13.99	2.08
	ARX	62.80	26.17	3.95	-11.73
	ZOH	50.62	20.81	-1.37	-21.32
104	ARMAX	76.01	54.13	42.03	34.46
	ARMAX†	69.56	38.26	20.43	9.75
	ARX	76.52	45.54	21.27	4.21
	ZOH	52.14	19.16	-4.93	-22.71
105	ARMAX	57.16	27.79	13.45	7.26
	ARMAX†	57.35	25.49	7.52	-0.61
	ARX	52.32	10.31	-0.54	-19.01
	ZOH	47.21	14.58	-6.14	-18.
106	ARMAX	54.72	8.30	-25.15	-48.62
	ARMAX†	57.47	14.69	-10.23	-22.14
	ARX	58.95	14.46	-20.46	-40.14
	ZOH	44.06	9.70	-8.29	-15.45
107	ARMAX	68.29	48.32	34.00	26.57
	ARMAX†	63.86	30.80	5.19	-9.19
	ARX	63.51	31.36	3.42	-18.40
	ZOH	52.28	16.14	-10.62	-29.79
115	ARMAX	79.76	59.31	42.18	32.44
	ARMAX†	69.22	35.32	6.51	-15.97
	ARX	75.50	46.50	15.33	-9.32
	ZOH	63.65	34.72	12.38	-3.43
120	ARMAX	76.05	49.32	30.81	21.53
	ARMAX†	74.81	45.10	23.60	11.00
	ARX	73.92	42.33	17.77	2.53
	ZOH	58.48	27.03	4.31	-12.57
130	ARMAX	63.11	39.93	20.94	9.31
	ARMAX†	64.06	40.89	25.17	16.66
	ARX	64.76	34.36	8.68	-7.55
	ZOH	58.80	29.07	6.34	-9.56

† model with vital signs

Table 4.7 Model-based predictor performance evaluation. Prediction Error Variance [$(mg/dL)^2$] vs. Prediction Horizon [min] on validation data. The best performing model is highlighted.

Patient ID	model	30[min]	60[min]	90[min]	120[min]
102	ARMAX	178.8	646.2	1134.4	1564.1
	ARMAX†	199.7	786.0	1437.5	2000.5
	ARX	203.9	787.9	1572	2587.5
	ZOH	398.1	1167.6	2125.3	3113.9
103	ARMAX	165.4	589.6	847.4	1029.2
	ARMAX†	173.0	653.1	953.7	1189.4
	ARX	180.4	703.7	1195.3	1597.6
	ZOH	332.3	854.5	1398.8	2000.7
104	ARMAX	263.5	959.3	1529	1952.5
	ARMAX†	425.1	1748.2	2902.1	3732.7
	ARX	253.5	1356.5	2831.3	4175.4
	ZOH	1051.3	2997.6	5047	6894.9
105	ARMAX	284.2	802.8	1144.5	1299.5
	ARMAX†	280.0	849.9	1302.7	1532.2
	ARX	349.2	1241.8	1612.2	2287.8
	ZOH	430.6	1123.3	1724.5	2146.1
106	ARMAX	517.2	2110.3	3909.8	5479.1
	ARMAX†	461.1	1855.8	3098.7	3804.3
	ARX	415.5	1888.1	3820.3	5227
	ZOH	797.3	2076.3	2983.4	3386.2
107	ARMAX	243.3	639.1	1034.3	1271.5
	ARMAX†	315.2	1143	2131.2	2809
	ARX	323.8	1137.7	2236.9	3342.9
	ZOH	553.5	1708.8	2971.8	4088.5
115	ARMAX	73.13	283.4	555.9	729.4
	ARMAX†	175.8	775.3	1616.8	2482.1
	ARX	98.4	411.8	922.6	1415.3
	ZOH	242.3	778.6	1395.1	1932.1
120	ARMAX	202	895.2	1653.3	2106.9
	ARMAX†	225.8	1073.8	2079.3	2821.9
	ARX	245.8	1212.4	2479.7	3518.4
	ZOH	614.1	1896.8	3260.5	4509.9
130	ARMAX	710.8	1884.7	3264.8	4296.7
	ARMAX†	674.3	1822.2	2918.2	3616.6
	ARX	643.6	2152.9	4006.1	5410.5
	ZOH	886.8	2627.9	4582.5	6270.8

† model with vital signs

Table 4.8 Model-based predictor performance evaluation. Percentage VAF [%] vs. Prediction Horizon [min] on validation data. The best performing model is highlighted.

Patient ID	model	30[min]	60[min]	90[min]	120[min]
102	ARMAX	93.06	74.91	55.97	39.29
	ARMAX†	92.24	69.49	44.20	22.35
	ARX	92.20	70.26	40.95	2.74
	ZOH	84.54	54.68	17.51	-20.85
103	ARMAX	87.86	56.75	37.83	24.49
	ARMAX†	87.30	52.08	30.03	12.74
	ARX	86.86	49.48	14.88	-16.03
	ZOH	75.62	37.31	-2.61	-46.76
104	ARMAX	94.26	79.11	66.70	57.48
	ARMAX†	90.74	61.93	36.80	18.72
	ARX	94.53	70.89	39.93	11.74
	ZOH	77.10	34.72	-9.89	-50.13
105	ARMAX	81.69	48.30	26.29	16.31
	ARMAX†	81.96	45.26	16.10	1.32
	ARX	77.59	21.25	-0.75	-40.99
	ZOH	72.26	27.66	-11.05	-38.20
106	ARMAX	79.71	17.24	-53.31	-114.85
	ARMAX†	81.91	27.22	-21.51	-49.17
	ARX	83.94	27.72	-45.05	-95.55
	ZOH	68.73	18.58	-16.98	-32.78
107	ARMAX	90.00	73.74	57.51	47.76
	ARMAX†	87.05	53.04	12.45	-15.38
	ARX	86.70	53.44	8.95	-36.39
	ZOH	77.26	29.80	-22.08	-67.94
115	ARMAX	96.08	84.83	70.25	60.97
	ARMAX†	90.59	58.51	13.49	-32.80
	ARX	94.13	73.18	35.43	-2.43
	ZOH	87.03	58.33	25.36	-3.37
120	ARMAX	94.33	74.87	53.59	40.86
	ARMAX†	93.66	69.86	41.64	20.79
	ARX	93.20	66.75	32.42	5.25
	ZOH	82.76	46.76	8.49	-26.57
130	ARMAX	86.39	63.92	37.51	17.76
	ARMAX†	87.09	65.12	44.15	30.78
	ARX	87.71	58.28	21.83	-4.50
	ZOH	83.02	49.70	12.29	-20.01

† model with vital signs

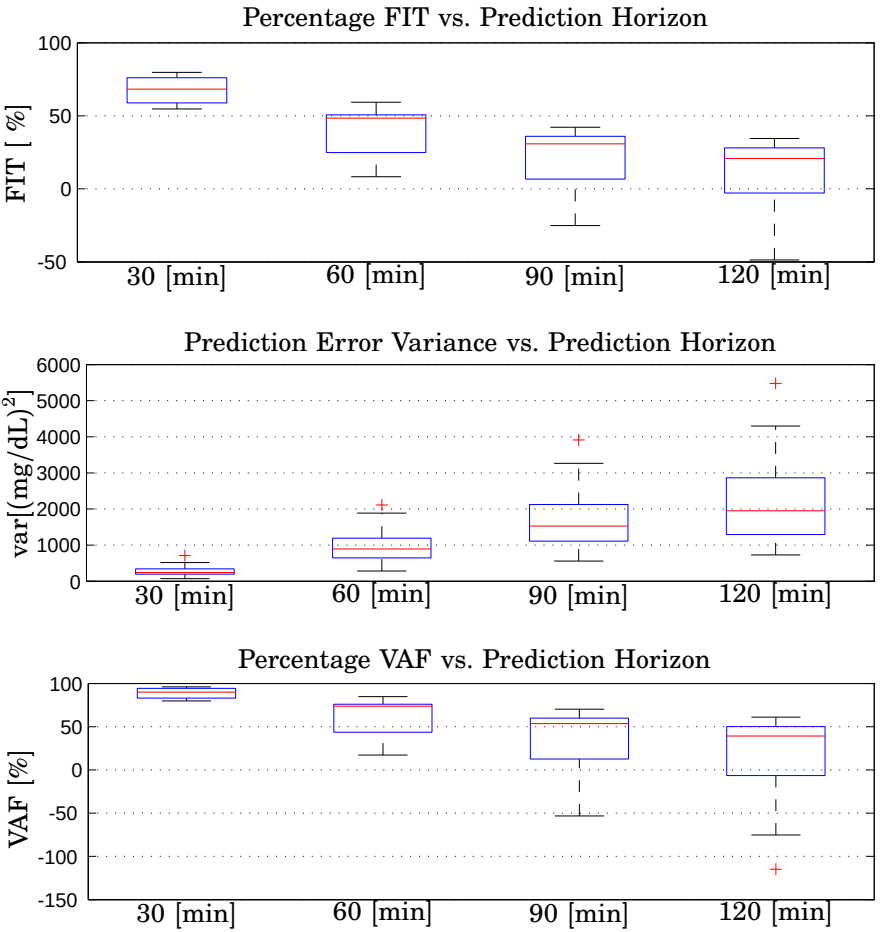

Figure 4.14 Model-based predictor performance evaluation. Population results on validation data. *Top* Percentage FIT vs. Prediction Horizon [min]; *Center* Prediction Error Variance [$(mg/dL)^2$] vs. Prediction Horizon [min]; *Bottom* Percentage VAF vs. Prediction Horizon [min]. Each box presents results over the population considered. The central mark is the median, the edges of the box are the 25th and the 75th percentiles.

Table 4.9 Numerical and clinical accuracy of predictions. 30 [min] prediction

Patient	*AD* [mg/dL]		*RD*		*ISO* [%]	*CG-pEGA* [%]		*CG-rEGA* [%]	
	Mean	Median	Mean	Median	$*$	A	B	A	B
CHU102	13.03	9.64	0.01	0.01	85.10	85.71	12.24	79.16	10.41
CHU103	15.04	12.45	-0.02	-0.02	78.04	79.16	18.75	72.34	14.89
CHU104	15.93	13.37	0	0	86.95	84	14	79.59	6.12
CHU105	18.49	13.73	0	-0.04	85.36	82.22	13.33	72.72	11.36
CHU106	44.61	32.09	-0.09	0.06	53.65	48.88	44.44	65.90	20.45
CHU107	15.79	11.53	-0.03	-0.04	83.33	81.63	18.36	77.08	8.33
CHU115	15.09	11.06	-0.04	-0.04	85.10	85.41	14.58	76.59	10.63
CHU120	21.64	17.50	0.05	0.07	89.58	89.58	8.33	61.70	27.65
CHU130	96.08	104.37	-0.01	0.25	14.58	14.58	56.25	59.57	12.76

$*$ prediction within [20%] from reference y_{BG} when $y_{BG} \geq 75$[mg/dL]

Table 4.10 Numerical and clinical accuracy of predictions. 60 [min] prediction

Patient	*AD* [mg/dL]		*RD*		*ISO* [%]	*CG-pEGA* [%]		*CG-rEGA* [%]	
	Mean	Median	Mean	Median	$*$	A	B	A	B
CHU102	20.36	13.88	-0.01	0.02	74.46	71.42	20.40	77.08	10.41
CHU103	23.57	20.11	-0.10	-0.06	58.53	56.25	37.50	63.82	23.40
CHU104	27.11	21.67	-0.08	-0.04	69.56	64	28	65.30	24.48
CHU105	28.90	25.20	-0.03	-0.08	60.97	55.55	35.55	65.90	18.18
CHU106	53.94	46.82	-0.13	0	39.02	35.55	48.88	61.36	18.18
CHU107	22.30	18.94	-0.08	-0.06	66.67	65.30	34.69	79.16	8.33
CHU115	26.41	21.21	-0.07	-0.08	61.70	60.41	37.50	70.21	23.40
CHU120	35.69	21.71	0.09	0.08	64.58	64.58	31.25	70.21	10.63
CHU130	105.18	98.69	0.03	0.24	16.67	16.67	47.91	36.17	40.42

$*$ prediction within [20%] from reference y_{BG} when $y_{BG} \geq 75$[mg/dL]

Table 4.11 Numerical and clinical accuracy of predictions. 90 [min] prediction

Patient	*AD* [mg/dL]		*RD*		*ISO* [%]	*CG-pEGA* [%]		*CG-rEGA* [%]	
	Mean	Median	Mean	Median	$*$	A	B	A	B
CHU102	26.75	21.17	-0.03	0.01	68.08	65.30	24.48	77.08	14.58
CHU103	27.85	24.55	-0.17	-0.16	53.65	45.83	43.75	74.46	14.89
CHU104	33.85	27.76	-0.10	-0.06	54.34	52	42	79.59	16.32
CHU105	33.43	30.21	-0.07	-0.11	51.21	46.66	42.22	68.18	22.72
CHU106	59.65	40.41	-0.16	-0.01	43.90	40	44.44	54.54	18.18
CHU107	27.98	23.43	-0.12	-0.05	56.25	55.10	42.85	68.75	16.66
CHU115	33.12	29.24	-0.09	-0.09	48.93	47.91	50	70.21	21.27
CHU120	41.74	27.32	0.09	0.13	54.16	54.16	37.50	65.95	19.14
CHU130	115.73	100.04	0.03	0.24	16.67	16.67	39.58	36.17	36.17

$*$ prediction within [20%] from reference y_{BG} when $y_{BG} \geq 75$[mg/dL]

Table 4.12 Numerical and clinical accuracy of predictions. 120 [min] prediction

Patient	*AD* [mg/dL]		*RD*		*ISO* [%]	*CG-pEGA* [%]		*CG-rEGA* [%]	
	Mean	Median	Mean	Median	$*$	A	B	A	B
CHU102	31.54	26.12	-0.03	0.01	59.57	57.14	32.65	77.08	16.66
CHU103	30.53	26.03	-0.23	-0.11	56.09	47.91	41.66	70.21	21.27
CHU104	38.37	30.78	-0.13	-0.09	50	46	48	73.46	22.44
CHU105	33.96	33.93	-0.11	-0.09	53.65	48.88	40	70.45	18.18
CHU106	59.90	39.79	-0.22	-0.07	48.78	44.44	37.77	59.09	22.72
CHU107	31.61	28.25	-0.14	-0.09	52.08	51.02	44.89	70.83	16.67
CHU115	36.66	38.22	-0.10	-0.10	36.17	35.41	62.50	72.34	19.14
CHU120	44.71	33.94	0.10	0.16	43.75	43.75	43.75	63.82	63.82
CHU130	122.03	91.84	0.01	0.19	16.67	16.67	39.58	36.17	38.29

$*$ prediction within [20%] from reference y_{BG} when $y_{BG} \geq 75$[mg/dL]

4.14 Discussion

Data

The autospectra (power spectra) showing the frequency contents of the signals investigated and the coherence spectra between the inputs and the controlled variable were calculated to perform spectral analysis [Johansson,1993]. Recall that a coherence spectrum can be interpreted as a correlation analysis (or signal-to-noise analysis) made for each frequency. A large absolute value close to 1 indicates that the input and output are correlated. A coherence value of 0.5 denotes that half of the output variation may be explained by variations in the stimulus input. As predictable, the data collected offered poor model input excitation despite the careful selection of the subjects, because of the correlation between food intake and consequent insulin injection.

Modeling

Throughout the work, estimation of the glucose flux in the blood stream after intestinal absorption and the total insulin flux in the blood stream from subcutaneous injection of slow-acting and fast-acting analogues were considered as input variables. A limitation arose from the required physiological models as input generating components. Such physiological models, indeed, were not tailored to the study participants. Population mean values were used for the parameters, thus disregarding the inter-personal variability. Tuning such models to the individual would need specific tracer-to-tracee data (see e.g., [Dalla Man et al., 2004]), which are difficult to obtain and require costly experiments. It is important to underline, moreover, that the model parameters were time-invariant and did not account for circadian variation of patient metabolism. As far as the glucose absorption modeling is concerned, it is a well known fact that not only the size of the meal but also the composition of the meal affects the digestion dynamics (see e.g. [Brouns et al., 2005]). Unfortunately, detailed quantitative information on meal composition was not available in the data set considered for this thesis. In absence of such information, all sources of carbohydrates were assumed to be equal.

The transport of insulin from the subcutaneous injection site to the blood stream has been described by several insulin pharmacokinetics model (see, e.g., [Nucci and Cobelli, 2000] and [Wilinska et al., 2005] for reviews). Among these, the compartment model in [Kovatchev et al., 2008b] was adopted. Actually, insulin absorption is a complex process influenced by many factors, including type of insulin, injected volume, concentration, site of injection and blood flow in the tissues [Galloway et al., 1981], [Binder et al., 1984]. Furthermore, a model describing in

detail the processes of subcutaneous absorption for the commercially available insulin used in the DIAdvisor^{TM}trials was not available. These reasons may explain the mismatch between the actual plasma insulin concentration profile and that obtained with the simulation model (Eqs. 4.4, 4.5, 4.8).

Individual-specific models of low-complexity were identified from the collected data. Estimated model structures included ARX/ARMAX models and state-space models. As far as the ARX/ARMAX structure is concerned, identification of the model parameters was accomplished by minimization of a quadratic prediction error criterion using the Matlab®System Identification Toolbox routines *arx.m* and *armax.m*, respectively. The range of the orders n_a, n_b, n_c was empirically set to $3 \leq n_a \leq 6$, $n_b \leq n_a$, $n_c \leq n_a$ while the inputs-output delays were chosen as $d_1 = d_2 = 1$. The Akaike Information Criterion (AIC) was calculated for each of the configurations and used subsequently to rank the models according to their increasing AIC [Ljung, 1999]. Regarding the subspace-based techniques, the Matlab® function *n4sid.m* and the SMI Toolbox [Haverkamp and Verhaegen, 1997] were used. Two parameters having substantial influence on the quality of the resulting model needed to be chosen, namely the lengths of past and future horizons, representing the dimension of certain Hankel matrices constructed with the data. There are no simple rules for choosing them [Ljung, 2003], [Chiuso, 2008], [Chiuso, 2007a]. However, the knowledge of the application, that is blood glucose prediction up to 120-minutes ahead, provided an initial guess. The parameters were then tuned empirically: $p = f = 120$ in the N4SID algorithm [Van Overschee and De Moor, 1994], s=30 in the PO-MOESP algorithm [Verhaegen, 1994] and p=60, f=20 in PBSID [Chiuso, 2007b].

The estimated models were tested according to various criteria. Stability was the first requirement that a model needed to fulfill. Residual tests with the purpose of finding remaining correlations which indicate whether the model order is adequate were carried out. With adequate model order, the residual process is white only and of sufficiently small magnitude. The residual autocorrelation and cross correlation between the prediction errors and the input tests needed to give significant (99% confidence) validation with respect to changes of sign, independence of residuals, normality, and independence between residuals and input in order for the test to be passed. Finally, qualitatively correct responses to inputs were attained by the selected models. From a quantitative point of view, according to clinicians and their experience gained from clinical trials, the average lowering effect of 1IU of fast insulin falls within 25-60 [mg/dL], with peak time $60 - -240$ [min], depending upon the subject's resistance or sensitivity to insulin, whereas an ingestion of 10 [g] pure dextrose makes the blood glucose rising 15 [mg/dL], in 20 minutes at

best. However, these requirements seemed hard to achieve and were not fulfilled by all models.

Another problem was that impulse responses from a carbohydrate or insulin input to a blood glucose output were not compatible with physiology and clinical practice in all the cases, either in the magnitude or in the time scale.

Tables 4.3, 4.4 and 4.5 report for each of the patients the identification methods leading to models not meeting one or more of the requirements in Sec. 4.11. When a criterion was not satisfied, the corresponding model was disregarded. Overall, from the tables it emerges that the main difficulties encountered while carrying out the modeling task were assuring white residuals and estimating physiologically correct inputs to output transfer functions.

Last, as far as physical activity is concerned, given the results shown in this work and summarized in Tables 4.6–4.8, it may be concluded that it does not improve the predictions obtained without using vital signs. One explanation could be that during the in-hospital tests, the intensity of such exercise was very low, so that heart rate and respiration rate didn't contribute to blood glucose dynamics. Further, the data were very noisy and the low-pass filtering carried out prior to modeling might not have been appropriate, removing together with the noise also some of the information content of the signals.

Prediction

The quality of the predictors developed was assessed by mathematical metrics in order to quantify the error between the predicted blood glucose profile vs. the actual ones. Specifically, predictions were evaluated with respect to

- FIT [%]
- prediction error variance $[(\mathrm{mg/dL})^2]$
- VAF [%]

and qualitative assessments by eye inspection concerning glucose trends detection. Indeed, in diabetes management, the perhaps most important feature for a predictor is the ability of capturing hypoglycemias and hyperglycemias, rather than being correct in the normo-glycemic range. The performances of the third-order ARX/ARMAX based predictors were compared to those achieved with the zero-order-hold. Results on this comparison are presented in Tables 4.6–4.8. The highlighted rows correspond to the model achieving the best performances. In all the cases the ARMAX structure outperformed the other.

4.15 Conclusions

This chapter dealt with linear modeling and short-term prediction in diabetes physiology. Specifically, data-driven techniques were investigated to the purpose of the DIAdvisor^{TM} tool application [DIAdvisor, 2012] and evaluated for type 1 diabetes mellitus records belonging to a population of 9 subjects in hospital conditions.

Modeling

An individual-specific, physiologically relevant model of the glucose-insulin interaction subsystem was identified from each of the subjects data using prediction error methods and subspace-based methods. Inputs to the models were:

- interpolated total plasma insulin concentration from drawn blood samples u_i [μU/mL];
- plasma glucose rate of appearance after carbohydrate intestinal absorption u_g [mg/kg/min];

and the output was:

- interpolated blood glucose y_{BG} [mg/dL] from drawn blood samples

ARMAX models of order in the range [3:6] satisfied all the criteria required, specifically:

- stability;
- white residuals;
- physiologically sensible responses to 1 [IU] of insulin and 10 [g] of carbohydrates

and were therefore selected for inclusion in the advisory tool. However, the additional requirements on model-based predictor performances were met only partially. Indeed, whereas a value of VAF $\geq$ 50% on 60-minutes-ahead model-based prediction on validation data was achieved by all the models except the 5th-order ARMAX model for patient 105 and the 6th-order ARMAX model for patient 106, a value of FIT $\geq$ 50% on 60-minutes-ahead model-based prediction on validation data was achieved by the 3rd-order ARMAX model identified from patient 104 data and the 6th-order ARMAX model identified from patient 115 data, only.

Prediction

Individual-specific short-term blood glucose predictors were identified from Type 1 Diabetes Mellitus subject data. Predictors coefficients were directly identified from the input-output data, without the intermediate model identification step. Inputs to the models were:

- interpolated total plasma insulin concentration from drawn blood samples u_i [μU/mL];
- plasma glucose rate of appearance after carbohydrate intestinal absorption u_g [mg/kg/min];

and the output was:

- interpolated blood glucose y_{BG} [mg/dL] from drawn blood samples

The structures investigated were third-order ARX-based predictors and their regularized version, and subspace-based multivariate predictors. Across the population, the performances of the proposed predictors were superior to those achieved by projecting the last blood glucose value into the future, i.e., ZOH. However, the goal of a FIT value $\geq$ 50% on 60-minutes-ahead prediction on validation data was not accomplished, while a VAF value $\geq$ 50% on 60-minutes-ahead prediction on validation data was reached.

Appendix to Chapter 4

This appendix presents a small population study using patient data from DIAdvisor I trial described in Sec. 3.3. The characteristics of the subjects included are reported in Table 3.2. The goal was to identify individualized models having as inputs $\hat{u}_i$, $\hat{u}_g$ from the physiological models in Sections 4.2–4.3, respectively, and as output y_{IG} measured by the Dexcom®device [Dexcom, 2013]. The methodology outlined in Sections 4.10–4.11 was followed. Tables 4.13–4.15 compare the predictor performances achieved with third-order ARMAX models to those of the ZOH.

Table 4.13 Model-based predictor performance evaluation. Percentage FIT [%] vs. Prediction Horizon [min] on validation data.

Patient ID	model	30[min]	60[min]	90[min]	120[min]
108	ARMAX	61.95	41.20	32.65	29.72
	ZOH	41.11	0.95	-22.63	-33.76
112	ARMAX	64.45	37.80	21.42	11.37
	ZOH	61.77	37.56	17.54	-1.59
121	ARMAX	57.61	33.33	19.07	10.28
	ZOH	50.09	21.09	0.43	-12.88
130	ARMAX	46.25	11.12	-12.47	-29.09
	ZOH	44.54	8.97	-15.17	-32.01
305	ARMAX	68.00	40.00	21.46	11.71
	ZOH	51.86	9.91	-23.74	-48.26
308	ARMAX	52.64	30.87	15.31	7.75
	ZOH	41.58	7.05	-19.28	-36.95
320	ARMAX	47.20	25.37	11.50	3.46
	ZOH	41.47	11.15	-11.50	-26.48
327	ARMAX	55.88	27.34	8.11	-2.53
	ZOH	49.27	14.91	-12.21	-32.72

Table 4.14 Model-based predictor performance evaluation. Prediction Error Variance $[(mg/dL)^2]$ vs. Prediction Horizon [min] on validation data.

Patient ID	model	30[min]	60[min]	90[min]	120[min]
108	ARMAX	387.15	923.38	1209.3	1315.4
	ZOH	929.28	2628.2	4025.0	4777.6
112	ARMAX	270.09	822.34	1306.5	1657.5
	ZOH	312.35	833.95	1456.3	2210.5
121	ARMAX	1148.3	2839.0	4178.0	5127.3
	ZOH	1590.5	3976.6	6335.5	8147.1
130	ARMAX	291.97	794.68	1267.1	1662.9
	ZOH	314.07	845.52	1352.1	1774.2
305	ARMAX	427.29	1495.8	2547.8	3199.3
	ZOH	980.96	3435.0	6479.3	9296.3
308	ARMAX	862.32	1837.4	2758.0	3271.4
	ZOH	1311.4	3319.2	5466.4	7207.0
320	ARMAX	1536.9	3064.9	4298.5	5103.1
	ZOH	1889.5	4354.5	6860.8	8829.7
327	ARMAX	240.91	625.14	969.18	1177.1
	ZOH	349.11	982.48	1709.6	2391.9

Table 4.15 Model-based predictor performance evaluation. Percentage VAF [%] vs. Prediction Horizon [min] on validation data.

Patient ID	model	30[min]	60[min]	90[min]	120[min]
108	ARMAX	85.55	65.55	54.88	50.92
	ZOH	65.33	1.94	-50.16	-78.24
112	ARMAX	87.42	61.70	39.15	22.80
	ZOH	85.45	61.16	32.17	-2.94
121	ARMAX	82.04	55.59	34.65	19.80
	ZOH	75.12	37.80	0.91	-27.42
130	ARMAX	71.45	22.31	-23.86	-62.56
	ZOH	69.29	17.34	-32.17	-73.43
305	ARMAX	89.90	64.66	39.82	24.43
	ZOH	76.82	18.86	-53.03	-119.57
308	ARMAX	77.57	52.21	28.27	14.93
	ZOH	65.89	13.68	-42.15	-87.41
320	ARMAX	72.17	44.51	22.18	7.61
	ZOH	65.79	21.16	-24.20	-59.84
327	ARMAX	82.25	53.96	28.62	13.30
	ZOH	74.28	27.64	-25.90	-76.15

5

Linear Multi-step Predictors for Predictive Control

5.1 Introduction

Time series filtering and prediction theory based on linear systems has a long history dating back to the 1940s and the works of Kolmogorov [Kolmogorov, 1939b], [Kolmogorov, 1939a] and Wiener [Wiener, 1949]. From the Wiener-Kolmogorov theory of stochastic processes, the Kalman filter [Kalman, 1960] and the ARMAX-based predictor [Åström, 1970] could be formulated, representing solutions suitable for a digital implementation. Thorough descriptions of a variety of predictor structures can be found in [Anderson and Moore, 1979], [Hannan and Deistler, 1988], [Caines, 1988], [Hamilton, 1994], [Kailath and Hassibi, 2000]. Usually, the predictors are formulated for one-step-ahead prediction horizon and are based on a known model. Many practical cases, however, face the problem of simultaneously forecasting the time-series of interest for multiple look ahead. This prediction scheme is called a multi-step predictor [Holst, 1977], [Stoica and Nehorai, 1989]. Efforts in this direction towards adaptive control were made by Mosca et. al. [Menga and Mosca, 1980], [Mosca et al., 1989]. An alternative solution to the prediction problem for multi-input multi-output systems is offered by the so-called subspace identification methods (SIMs) [Katayama, 2005], [Van Overschee and De Moor, 1994], [Van Overschee and De Moor, 1996], [Verhaegen, 1994], [Ljung and McKelvey, 1996], [Jansson, 2003], [Chiuso and Picci, 2005b]. In the SIM framework, indeed, the first step for the construction of a state-space model from observed input-output data involves the estimation of the output predictor. The algorithmic step was exploited in the past by several authors in receding horizon type of control strategies [Di Ruscio, 1997], [Favoreel et al., 1999], [Woodley et al., 2001], [Kadali et al., 2003], [Dong et al., 2008], [Dong and Verhaegen, 2008a], [Dong and Verhaegen, 2008b]. The *N4SID*

algorithm [Van Overschee and De Moor, 1994] was applied in [Di Ruscio, 1997], [Favoreel et al., 1999], [Woodley et al., 2001], [Kadali et al., 2003], while the VARX (vector autoregressive with exogenous inputs) developed in [Chiuso, 2007a], [Chiuso, 2007b] was exploited in [Dong et al., 2008], [Hallouzi, 2008].

Based on subspace-based identification methods for linear systems this chapter formulates short-term multi-step-ahead predictors for application in predictive control.

Model description

Consider a discrete-time linear time-invariant system $\mathcal{S}_n(A,B,C,K)$ in innovation form

$$\begin{aligned} x_{k+1} &= Ax_k + Bu_k + Ke_k \\ y_k &= Cx_k + e_k \end{aligned} \tag{5.1}$$

where $u_k \in \mathbb{R}^m$ is the input, $y_k \in \mathbb{R}^l$ the output, $x_k \in \mathbb{R}^n$ the state, $e_k \in \mathbb{R}^l$ the zero-mean white noise innovation process uncorrelated with u_k and $A \in \mathbb{R}^{n\times n}$, $B \in \mathbb{R}^{n\times m}$, $C \in \mathbb{R}^{l\times n}$, $K \in \mathbb{R}^{l\times n}$ are constant matrices. In the following, assume that (A,B) is reachable and (C,A) is observable. The joint input-output process denoted by $z_k = [u_k^T y_k^T]$ is assumed purely non-deterministic. In addition, the determinant of the spectral density matrix $S_{zz}(e^{j\omega})$ should have no zero on the unit circle [Chiuso, 2007b], [Katayama and Picci, 1999], [Hannan and Poskitt, 1988]. This last condition guarantees persistency of excitation (PE) of the data of sufficiently high order. Further, assume that no linear feedback from the states to the input is present, i.e., input-output data are obtained from an open loop experiment.
Transfer function relationships using z-transform are:

$$Y(z) = G(z)U(z) + H(z)E(z) \tag{5.2}$$

$$G(z) = C(zI - A)^{-1}B \tag{5.3}$$

$$H(z) = I + C(zI - A)^{-1}K \tag{5.4}$$

$$H^{-1}(z) = I - C(zI - A + KC)^{-1}K \tag{5.5}$$

Reconstruction of $\{e_k\}$ from input-output data may be accomplished by means of the inverse transfer function relationship

$$E(z) = H^{-1}(z)(Y(z) - G(z)U(z)) \tag{5.6}$$

and state-space realization of estimator

$$\hat{x}_{k+1|k} = A\hat{x}_{k|k-1} + Bu_k + K\hat{e}_k \tag{5.7}$$
$$\hat{y}_{k|k-1} = C\hat{x}_{k|k-1} \tag{5.8}$$
$$\hat{e}_k = y_k - \hat{y}_k = y_k - C\hat{x}_k \tag{5.9}$$

Considering the innovation model (5.1) in predictor form, with $\bar{A} = A - KC$, the one-step-ahead predictor can be formulated

$$\begin{aligned} \hat{x}_{k+1} &= \bar{A}\hat{x}_k + Bu_k + Ky_k \\ \hat{y}_{k|k-1} &= Cx_k + e_k \end{aligned} \tag{5.10}$$

with state error dynamics

$$\tilde{x}_k = x_k - \hat{x}_k \tag{5.11}$$
$$\tilde{x}_{k+1} = A\hat{x}_{k|k-1} + Bu_k + Ke_k\hat{x}_k \tag{5.12}$$
$$= -((A - KC)\hat{x}_k + Ky_k + Bu_k) = (A - KC)\tilde{x} = \bar{A}\tilde{x} \tag{5.13}$$

and covariance

$$P_k = \mathcal{E}\{\tilde{x}_k\tilde{x}_k^\mathsf{T}\} \tag{5.14}$$
$$P_{k+1} = \mathcal{E}\{\tilde{x}_{k+1}\tilde{x}_{k+1}^\mathsf{T}\} = \mathcal{E}\{\bar{A}\tilde{x}_k\tilde{x}_k^\mathsf{T}\bar{A}^\mathsf{T}\} = \bar{A}\mathcal{E}\{\tilde{x}_k\tilde{x}_k^\mathsf{T}\}\bar{A}^\mathsf{T} = \bar{A}P_k\bar{A}^\mathsf{T} \tag{5.15}$$

Notation

The available data sequences $\{u_k\}$, $\{y_k\}$, the state $\{x_k\}$ and the innovation process $\{e_k\}$ will be organized in Hankel matrices denoted by uppercase letters. Subscript indices $[\alpha, \beta]$ of a Hankel matrix will be used to indicate the argument of the upper-left and the lower-left element, respectively, e.g., $U_{[t_1,t_2]}$ will contain in the first column the input history between instants t_1 and t_2. Accordingly, data records of finite length N will be represented by the block rows of the Hankel data matrices and will be denoted by uppercase letters, the subscript indicating the first time instants of the time series:

$$U_{[t_1,t_2]} = \begin{bmatrix} U_{t_1} \\ U_{t_1+1} \\ \vdots \\ U_{t_2} \end{bmatrix} = \begin{bmatrix} u_{t_1} & u_{t_1+1} & \cdots & u_{t_1+N-1} \\ u_{t_1+1} & u_{t_1+2} & \cdots & u_{t_1+N} \\ \vdots & \vdots & \cdots & \vdots \\ u_{t_2} & u_{t_2+1} & \cdots & u_{t_2+N-1} \end{bmatrix}$$

The orthogonal projection of the rows of a given matrix A onto the row space of a given matrix B will be denoted by $\hat{E}\{A \mid B\}$, whereas the symbol $\hat{E}_{\|C}\{A \mid B\}$ will denote the oblique projection of the row space of A

onto the row space of B along the row space of C, the projection operator being $\hat{E}\{\cdot\}$. Throughout the chapter k will be the discrete-time index, t shall denote the current time instance in the identification problem, t_0 shall be the initial time from which the data are collected, so that $t - t_0 = p$ is the past horizon in the identification problem, T shall be such that $T - t + 1 = f$ represents the future horizon. The two integers p and f are such that $p \geq \max(f, n)$, n model order. Last, the number of steps in the look ahead that one wishes to investigate will be denoted by τ, where $\tau \leq f$.

Statement of the Problem

Let the finite sequences $\{u_k\}_{k=t-p}^{t+f-1}$ and $\{y_k\}_{k=t-p}^{t+f-1}$ be the measured input and the corresponding output, respectively, of the system (5.1). Our aim is to find a multi-step estimator of the output sequence $\{y_k\}_{k=t}^{t+f-1}$ by means of linear combinations of the past joint input-output $\{z_k\}_{k=t-p}^{t-1}$ and future input $\{u_k\}_{k=t}^{t+f-1}$.

5.2 Subspace-based linear multi-step predictors

Suppose ideally that we have observations of the processes $\{u_k\}$, $\{y_k\}$, $\{x_k\}$, $\{e_k\}$, $k \in [t-p, t+f-1]$. In addition, suppose the finite length N of the interval be large. Since the finite length observed data sequences are realization of the underlying stochastic processes in Eq. (5.1), the following holds:

$$\begin{aligned} X_{k+1} &= AX_k + BU_k + KE_k \\ Y_k &= CX_k + E_k \end{aligned} \tag{5.16}$$

Furthermore, from the observed samples construct the following block Hankel matrices:

$$U^p = U_{[t-p,t-1]} \in \mathbb{R}^{p\cdot m \times N} \tag{5.17}$$

$$U^f = U_{[t,t+f-1]} \in \mathbb{R}^{f\cdot m \times N} \tag{5.18}$$

called the past and future input data matrices, respectively, and

$$Y^p = Y_{[t-p,t-1]} \in \mathbb{R}^{p\cdot l \times N} \tag{5.19}$$

$$Y^f = Y_{[t,t+f-1]} \in \mathbb{R}^{f\cdot l \times N} \tag{5.20}$$

called the past and future output data matrices, respectively.

Construction of the projection-based predictors

Define the extended observability matrix

$$O_f = \begin{bmatrix} C \\ CA \\ CA^2 \\ \vdots \\ CA^{f-1} \end{bmatrix} \tag{5.21}$$

and the Toeplitz matrices containing the impulse responses of the system due to the input u_k and the innovation process e_k, respectively

$$\mathcal{H}_f = \begin{bmatrix} 0 & 0 & \cdots & 0 \\ CB & 0 & \cdots & 0 \\ \vdots & \vdots & \ddots & \vdots \\ CA^{f-2}B & CA^{f-3}B & \cdots & 0 \end{bmatrix}, \mathcal{W}_f = \begin{bmatrix} I & 0 & \cdots & 0 \\ CK & I & \cdots & 0 \\ \vdots & \vdots & \ddots & \vdots \\ CA^{f-2}K & CA^{f-3}K & \cdots & 0 \end{bmatrix} \tag{5.22}$$

Then, by iteration of the system equations in Eq. (5.1), the following matrix input-output relations may be written to express the future output matrix:

$$Y^f = O_f X_f + \mathcal{H}_f U^f + \mathcal{W}_f E^f \tag{5.23}$$

In the practical scenario the state sequence X_f is not known, so future outputs cannot be computed. An estimator of future output can be found, however, from the available data as a linear combination of the joint input-output past and the future input (see Appendix A.6 in [Van Overschee and De Moor, 1996] for a proof), provided that u_k and e_k are uncorrelated:

$$\hat{Y}^f = \hat{\Gamma} Z^p + \hat{\Lambda} U^f \tag{5.24}$$

where we have introduced the short-hand notation

$$Z^p = \begin{bmatrix} U^p \\ Y^p \end{bmatrix} = Z_{[t-p,t-1]} \in \mathbb{R}^{p\cdot(m+l)\times N} \tag{5.25}$$

to denote the past joint input-output data matrix. Now, the problem of finding an optimal output predictor can mathematically be formulated as a least-squares problem:

$$\hat{\Gamma}, \hat{\Lambda} = \arg \min_{\substack{\Gamma \in \mathbb{R}^{lp\times(l+m)p} \\ \Lambda \in \mathbb{R}^{lp\times mf}}} \left|\left| Y^f - \begin{bmatrix} \Gamma & \Lambda \end{bmatrix} \begin{bmatrix} Z^p \\ U^f \end{bmatrix} \right|\right|_F^2 \tag{5.26}$$

where $||\cdot||_F$ stands for the Frobenius norm of a matrix. Note that in this way f prediction problems are solved simultaneously row-wise. Each

problem consists in estimating $\hat{Y}_{t+\tau}$, $\tau \in [0, f-1]$:

$$\hat{Y}^f = \begin{bmatrix} \hat{Y}_t \\ \hat{Y}_{t+1} \\ \vdots \\ \hat{Y}_{t+f-1} \end{bmatrix} = \begin{bmatrix} \hat{y}_t & \hat{y}_{t+1} & \cdots & \hat{y}_{t+N-1} \\ \hat{y}_{t+1} & \hat{y}_{t+2} & \cdots & \hat{y}_{t+N} \\ \vdots & \vdots & \vdots & \vdots \\ \hat{y}_{t+f-1} & \hat{y}_{t+f} & \cdots & \hat{y}_{t+f+N-2} \end{bmatrix} \tag{5.27}$$

A geometric interpretation can be given to the least-squares problem as the orthogonal projection of Y^f onto $\begin{bmatrix} Z^p & U^f \end{bmatrix}^T$, i.e.,

$$\hat{Y}^f = \hat{E}\left\{ Y^f \mid \begin{bmatrix} Z^p \\ U^f \end{bmatrix} \right\} \tag{5.28}$$

Actually, the orthogonal projection (5.28) corresponds to the sum of two oblique projections ([Katayama and Picci, 1999, lemma 1]) under the assumption $span(Z^p) \cap span(U^f) = \{0\}$, with $span(\cdot)$ standing for the space spanned by the raw vectors of a matrix:

$$\hat{Y}^f = \hat{E}_{\|U^f}\{Y^f \mid Z^p\} + \hat{E}_{\|Z^p}\{Y^f \mid U^f\} \tag{5.29}$$

$$= \hat{\Gamma} Z^p + \hat{\Lambda} U^f \tag{5.30}$$

Once the operator $\hat{\Gamma}$ and $\hat{\Lambda}$ have been estimated, they can be applied to new data generated by the same underlying mechanisms, to forecast the output τ steps ahead. In particular, note that matrix relation (5.28) can be expressed vector-by-vector in the following way:

$$\begin{bmatrix} \hat{y}_t \\ \hat{y}_{t+1} \\ \hat{y}_{t+2} \\ \vdots \\ \hat{y}_{t+f-1} \end{bmatrix} = \hat{\Gamma} \begin{bmatrix} z_{t-p} \\ z_{t-p+1} \\ z_{t-p+2} \\ \vdots \\ z_{t-1} \end{bmatrix} + \hat{\Lambda} \begin{bmatrix} u_t \\ u_{t+1} \\ u_{t+2} \\ \vdots \\ u_{t+f-1} \end{bmatrix} \tag{5.31}$$

Computing projections

As just pointed out in Sec. 5.2, linear regression problems have a geometric interpretation which involves appropriate projection operations. Recall Eq. (5.28). The orthogonal projection is:

$$\hat{Y}^f = \hat{E}\left\{ Y^f \mid \begin{bmatrix} Z^p \\ U^f \end{bmatrix} \right\} \tag{5.32}$$

$$= Y^f \begin{bmatrix} Z^p \\ U^f \end{bmatrix}^\intercal \left(\begin{bmatrix} Z^p \\ U^f \end{bmatrix} \begin{bmatrix} Z^p \\ U^f \end{bmatrix}^\intercal \right)^\dagger \begin{bmatrix} Z^p \\ U^f \end{bmatrix} \tag{5.33}$$

$$= Y^f \begin{bmatrix} Z^{p\intercal} & U^{f\intercal} \end{bmatrix} \begin{bmatrix} Z^p Z^{p\intercal} & Z^p U^{f\intercal} \\ U^f Z^{p\intercal} & U^f U^{f\intercal} \end{bmatrix}^\dagger \begin{bmatrix} Z^p \\ U^f \end{bmatrix} \tag{5.34}$$

Under the no feedback assumption, the orthogonal projection (5.28) can be decomposed as the sum of two oblique projections:

$$\begin{aligned}\hat{Y^f} &= \hat{E}_{\|U^f}\{Y^f \mid Z^p\} + \hat{E}_{\|Z^p}\{Y^f \mid U^f\} \\ &= Y^f \begin{bmatrix} Z^{p\intercal} & U^{f\intercal} \end{bmatrix} \begin{bmatrix} Z^p Z^{p\intercal} & Z^p U^{f\intercal} \\ U^f Z^{p\intercal} & U^f U^{f\intercal} \end{bmatrix}^{\dagger}_{p\cdot(m+l)\text{ columns}} Z^p \\ &+ Y^f \begin{bmatrix} Z^{p\intercal} & U^{f\intercal} \end{bmatrix} \begin{bmatrix} Z^p Z^{p\intercal} & Z^p U^{f\intercal} \\ U^f Z^{p\intercal} & U^f U^{f\intercal} \end{bmatrix}^{\dagger}_{f\cdot m\text{ columns}} U^f\end{aligned} \tag{5.35}$$

Numerically, the efficient implementation of such projection operations relies upon LQ decompositions (i.e., transpose of the QR decomposition) [Golub and Van Loan, 1996]. As a matter of fact, LQ decompositions have also a system theoretic interpretation (see, e.g., [Katayama, 2006]). Two algorithms are outlined.

ALGORITHM 5.1—[VERHAEGEN, 1994], [VAN OVERSCHEE AND DE MOOR, 1996]

1. Consider the following

$$\begin{bmatrix} U^f \\ Z^p \\ Y^f \end{bmatrix} = \begin{bmatrix} L_{11} & 0 & 0 \\ L_{21} & L_{22} & 0 \\ L_{31} & L_{32} & L_{33} \end{bmatrix} \begin{bmatrix} {Q_1}^T \\ {Q_2}^T \\ {Q_3}^T \end{bmatrix} \tag{5.36}$$

   where $L_{11} \in \mathbb{R}^{fm\times fm}$, $L_{22} \in \mathbb{R}^{p(m+l)\times p(m+l)}$, $L_{33} \in \mathbb{R}^{fl\times fl}$ and Q_i, $i = 1,\cdots,3$ are orthogonal.

2. Define

$$\hat{\Gamma} = L_{32}{L_{22}}^{\dagger} \tag{5.37}$$

$$\hat{\Lambda} = (L_{31} - L_{32}{L_{22}}^{\dagger}L_{21}){L_{11}}^{-1} \tag{5.38}$$

3. Use Eq. (5.24) to calculate the future outputs as $Y^f = \hat{\Gamma}Z^p + \hat{\Lambda}U^f$

□

ALGORITHM 5.2—[FAVOREEL ET AL., 1999]

1. Set

$$W^p = \begin{bmatrix} Y^p & U^p \end{bmatrix}^{\intercal} \tag{5.39}$$

2. Let the LQ decomposition be defined by

$$\begin{bmatrix} W^p \\ U^f \\ Y^f \end{bmatrix} = \begin{bmatrix} \mathcal{L}_{11} & 0 & 0 \\ \mathcal{L}_{21} & \mathcal{L}_{22} & 0 \\ \mathcal{L}_{31} & \mathcal{L}_{32} & \mathcal{L}_{33} \end{bmatrix} \begin{bmatrix} {Q_1}^T \\ {Q_2}^T \\ {Q_3}^T \end{bmatrix} \tag{5.40}$$

   where $\mathcal{L}_{11} \in \mathbb{R}^{p(m+l)\times p(m+l)}$, $\mathcal{L}_{22} \in \mathbb{R}^{fm\times fm}$, $\mathcal{L}_{33} \in \mathbb{R}^{fl\times fl}$ and Q_i, $i = 1,\cdots,3$ are orthogonal.

3. Define

$$\hat{\Upsilon} = (\mathcal{L}_{31} - \mathcal{L}_{32}\mathcal{L}_{22}^{-1}\mathcal{L}_{21})\mathcal{L}_{11}^{\dagger} \tag{5.41}$$

$$\hat{\Lambda} = \mathcal{L}_{32}\mathcal{L}_{22}^{-1} \tag{5.42}$$

4. The output predictor is finally retrieved as $Y^f = \hat{\Upsilon}W^p + \hat{\Lambda}U^f$. □

A proof of algorithm 5.1 is given in Appendix C.

5.3 Construction of the VARX-based predictors

Let us now consider the innovation model (5.1) in predictor form, i.e., Eq. (5.10). Recall that by iteration of Eq. (5.10) it is possible to express the output data sequence $Y_{k+\tau}$, $0 \leq \tau \leq f-1$ according to:

$$\begin{aligned} Y_{k+\tau} &= C\bar{A}^{\tau}X_k + \sum_{h=1}^{\tau} C\bar{A}^{h-1}(BU_{k+\tau-h} + KY_{k+\tau-h}) + E_{k+\tau} \\ &= C\bar{A}^{\tau}x_{k-p} + \Xi_{\tau}Z^p + \sum_{h=1}^{\tau} C\bar{A}^{h-1}(BU_{k+\tau-h} + KY_{k+\tau-h}) + E_{k+\tau} \end{aligned} \tag{5.43}$$

From the point of view of the current time instant t:

$$Y_{t+\tau} = C\bar{A}^{\tau}x_{t-p} + \Xi_{\tau}Z^p + \sum_{h=1}^{\tau} C\bar{A}^{h-1}(BU_{t+\tau-h} + KY_{t+\tau-h}) + E_{t+\tau} \tag{5.44}$$

where in (5.3) the first term depends on the initial conditions of the state, the second term depends upon past input-output data and the third on future input-output data. Stacking all the future data sequences on top of each other and discarding the effects of the unknown initial states for sufficiently large p (see Appendix B in [Chiuso, 2007a] for a formal proof), we obtain the matrix relation:

$$Y^f = \Xi Z^p + \Psi Z^f + E^f \tag{5.45}$$

Matrices Ψ and Ξ are given in (5.46) and (5.47), respectively.

$$\Psi = \begin{bmatrix} 0 & \cdots & \cdots & \cdots & 0 \\ C\Phi & 0 & \cdots & \cdots & 0 \\ C\bar{A}\Phi & C\Phi & 0 & \cdots & 0 \\ \vdots & \ddots & \ddots & \ddots & 0 \\ C\bar{A}^{f-2}\Phi & \cdots & \cdots & C\Phi & 0 \end{bmatrix}, \quad \Phi = [B \quad K] \tag{5.46}$$

$$\Xi = \begin{bmatrix} \Xi_0 \\ \Xi_1 \\ \vdots \\ \Xi_{f-1} \end{bmatrix} = \begin{bmatrix} C\bar{A}^{p-1}\Phi & C\bar{A}^{p-2}\Phi & \cdots & \cdots & \cdots & C\Phi \\ 0 & C\bar{A}^{p-1}\Phi & \cdots & \cdots & \cdots & C\bar{A}\Phi \\ \vdots & \ddots & \ddots & \ddots & \ddots & \vdots \\ 0 & \cdots & 0 & C\bar{A}^{p-1}\Phi & \cdots & C\bar{A}^{f-1}\Phi \end{bmatrix} \tag{5.47}$$

Observe the Toeplitz structure of matrices Ψ and Ξ. Now, the first block-row expressing the output sequence Y_t does not depend upon future data sequences, that is Y_t can be expressed as

$$Y_t = \Xi_0 Z^p + E_t \tag{5.48}$$

Solving the least-squares problem

$$\hat{\Xi}_0 = \arg\min_{\Xi_0} || \, Y_t - \Xi_0 Z^p \, ||_F^2 \tag{5.49}$$

corresponding, geometrically, to the projection

$$\hat{Y}_t = \hat{E}\{Y_t \mid Z^p\} \tag{5.50}$$

the Markov parameters of the system (5.1) are obtained [Chiuso, 2007b; Dong et al., 2008]. The following algorithm is delineated:

ALGORITHM 5.3—[CHIUSO, 2007B; DONG ET AL., 2008]

1. Perform an LQ-decomposition

$$\begin{bmatrix} Z^p \\ Y_t \end{bmatrix} = \begin{bmatrix} \mathscr{L}_{11} & 0 \\ \mathscr{L}_{21} & \mathscr{L}_{22} \end{bmatrix} \begin{bmatrix} \mathscr{Q}_1{}^T \\ \mathscr{Q}_2{}^T \end{bmatrix} \tag{5.51}$$

where $\mathscr{L}_{11} \in \mathbb{R}^{p(m+l)\times p(m+l)}$, $\mathscr{L}_{22} \in \mathbb{R}^{l\times l}$ to get the estimate $\hat{\Xi}_0$

$$\hat{\Xi}_0 = \mathscr{L}_{21}\mathscr{L}_{11}^{-1} \tag{5.52}$$

2. Use the estimated coefficients from

$$\hat{\Xi}_0 = \begin{bmatrix} \hat{C}\hat{\bar{A}}^{p-1}\hat{\Phi} & \hat{C}\hat{\bar{A}}^{p-2}\hat{\Phi} & \cdots & \cdots & \hat{C}\hat{\Phi} \end{bmatrix} \tag{5.53}$$

3. Calculate

$$\gamma_\iota = \hat{\Xi}_\iota + \sum_{j=0}^{\iota-1} \hat{C}\hat{\tilde{A}}^{\iota-j-1}\hat{K}\gamma_j \tag{5.54}$$

$$\lambda_\iota = \hat{C}\hat{\tilde{A}}^{\iota-1}\hat{B} + \sum_{j=1}^{\iota-1} \hat{C}\hat{\tilde{A}}^{\iota-j-1}\hat{K}\lambda_j, \quad \iota \in [1, f-1] \tag{5.55}$$

with $\gamma_0 = \hat{\Xi}_0$, $\lambda_1 = \hat{C}\hat{B}$ and $\hat{\Xi}_\iota$ shifted versions of $\hat{\Xi}_0$ constructed according to Eq. (7.31)

4. The multi-step predictors are now given by

$$\hat{Y}^f = \begin{bmatrix} \gamma_0 \\ \gamma_1 \\ \gamma_2 \\ \vdots \\ \gamma_{f-1} \end{bmatrix} Z^p + \begin{bmatrix} 0 & 0 & \cdots & 0 \\ \lambda_1 & 0 & \cdots & 0 \\ \lambda_2 & \lambda_1 & \ddots & \vdots \\ \vdots & \vdots & \ddots & 0 \\ \lambda_{f-1} & \lambda_{f-2} & \cdots & \lambda_1 \end{bmatrix} = \hat{\bar{\Gamma}} Z^p + \hat{\bar{\Lambda}} U^f \tag{5.56}$$

□

5.4 Examples

The behaviour of the subspace predictors was evaluated with simulation examples. The experimental set-up is depicted in Fig. 5.1. The processes n_k and e_k were uncorrelated, zero mean, white gaussian noises with strandard deviations $\sigma_n = 1$ and $\sigma_e = 10^4$, respectively. Throughout the experiments, the input to the algorithms was u_k whereas the output was y_k. The transfer functions $\Phi(z)$, $G(z)$, $T(z)$ and $H(z)$ are given in Table 5.4 and were taken from [Chiuso and Picci, 2005a]. We tested the predictors both in the open loop and in the closed loop scenario. In many practical cases, indeed, feedback is present also if one cannot directly recognize physical controllers which "close the loop"; therefore it is of interest to test the limitations of the subspace predictors also in the presence of feedback. Sampling period was $T_s = 1$ [sec]. In all experiments the past and future horizons were chosen to be $p = f = 25$, while the prediction horizon τ was in the range $[1, 25]$. 100 Monte Carlo runs were repeated with 1000 data points each for n_k and e_k. Each of the Monte Carlo runs consisted of two steps: the first for the identification of the predictor matrices according to Eqs. (5.37), (5.38), (5.41), (5.42), (5.54) and (5.55), respectively, using the first half of the data records, and the second for the calculation of the predictions exploiting the remaining

Table 5.1 Transfer functions in the examples

#	$G(z)$	$H(z)$	$\Phi(z)$	$T(z)$
1	$\frac{0.3}{z-0.7}$	0	1	0
2	$\frac{0.3}{z-0.7}$	$\frac{z+0.5}{z}$	1	0
3	$\frac{0.3}{z-0.7}$	$\frac{z+0.5}{z}$	1	-1
4	$\frac{2.5}{z-3}$	$\frac{z+0.5}{z}$	1	-1
5	$\frac{2.5}{z-3}$	$\frac{z+0.999}{z}$	$\frac{0.2(z+0.999)}{z-0.99}$	-1
6	$\frac{2.5}{z-3}$	$\frac{z+0.999}{z}$	1	-1

data previously saved for validation. Prediction error properties over the 100 simulations were characterized by means of boxplots of prediction error variance vs. prediction horizon. On each box, which refers to a specific prediction horizon, the central mark is the median, the edges of the box are the 25th and 75th percentiles, the whiskers extend to the most extreme datapoints the algorithm considers to be not outliers, and the outliers are plotted individually. Figures 5.2-5.7 show boxplots of prediction errors on validation data. For comparison, Figs. D.6-D.11 in Appendix D show boxplots of prediction errors on identification data.

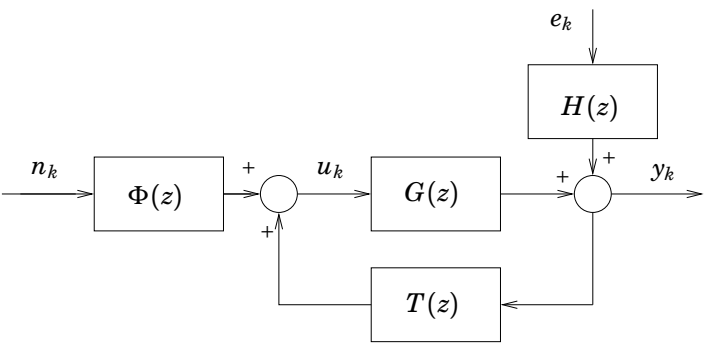

Figure 5.1 System used in the examples

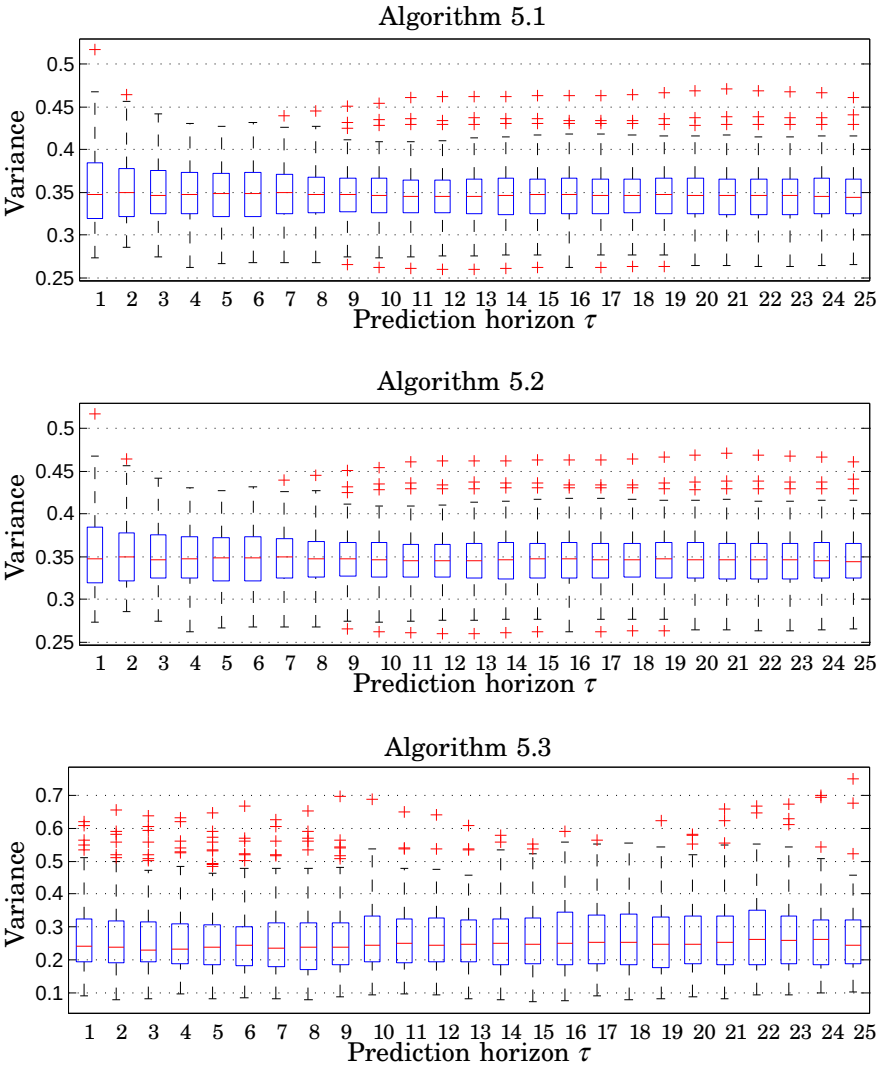

Figure 5.2 Example 1. Open loop. Multi-step predictors performances on validation data. Prediction error variance vs. prediction horizon. Top Algorithm 5.1, Center Algorithm 5.2, Bottom Algorithm 5.3

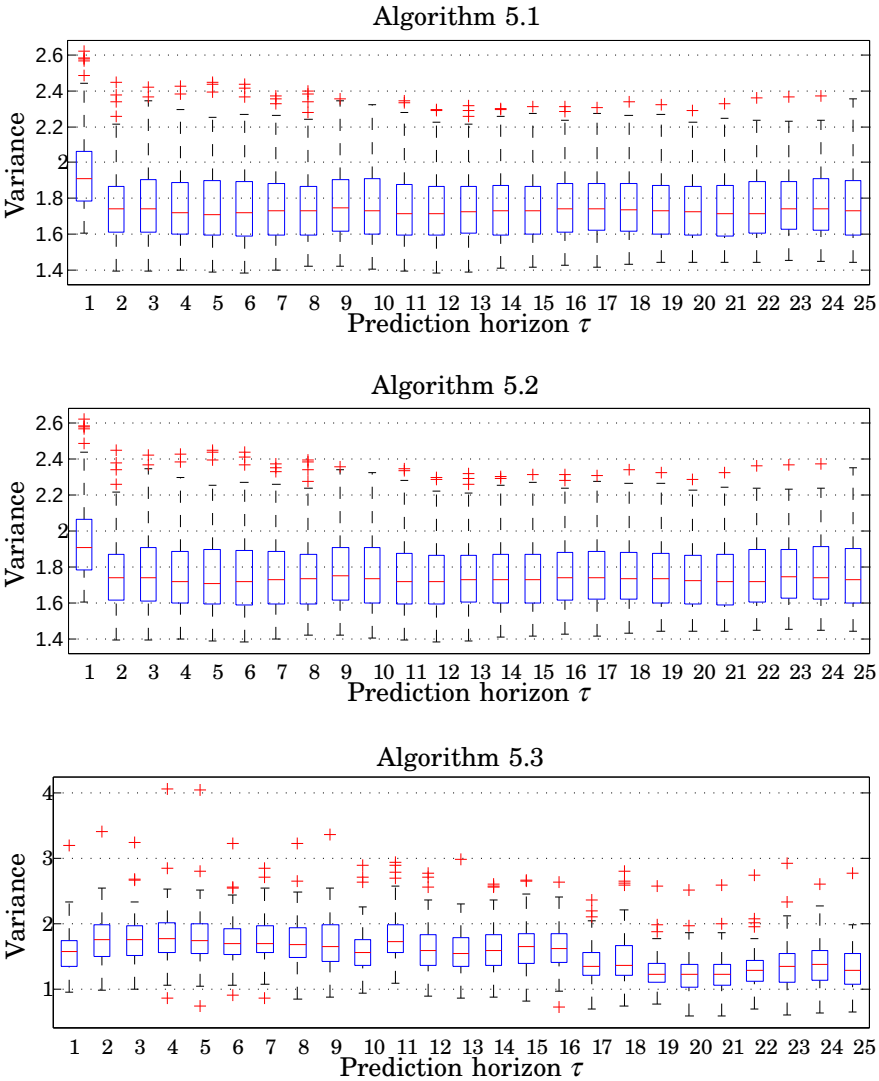

Figure 5.3 Example 2. Open Loop. Multi-step predictors performances on validation data. Prediction error variance vs. prediction horizon. Top Algorithm 5.1, Center Algorithm 5.2, Bottom Algorithm 5.3

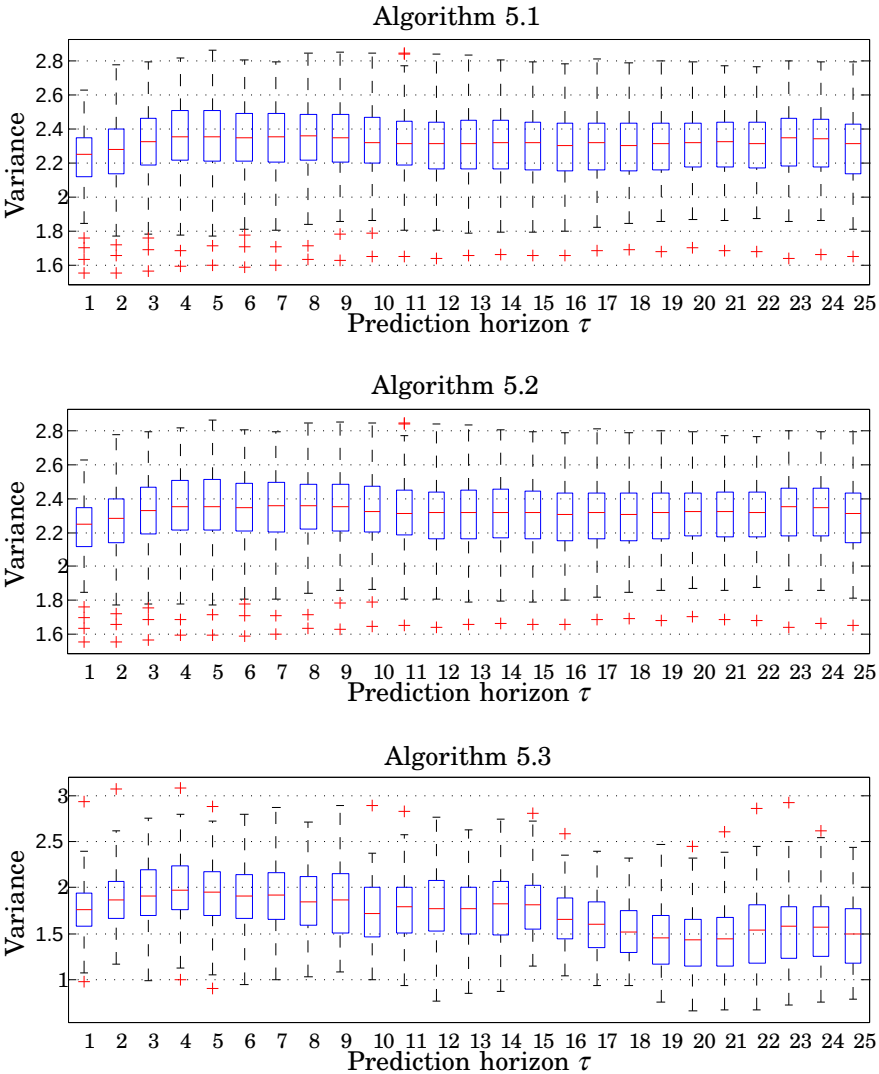

Figure 5.4 Example 3. Closed-loop. Multi-step predictors performances on validation data. Prediction error variance vs. prediction horizon. Top Algorithm 5.1, Center Algorithm 5.2, Bottom Algorithm 5.3

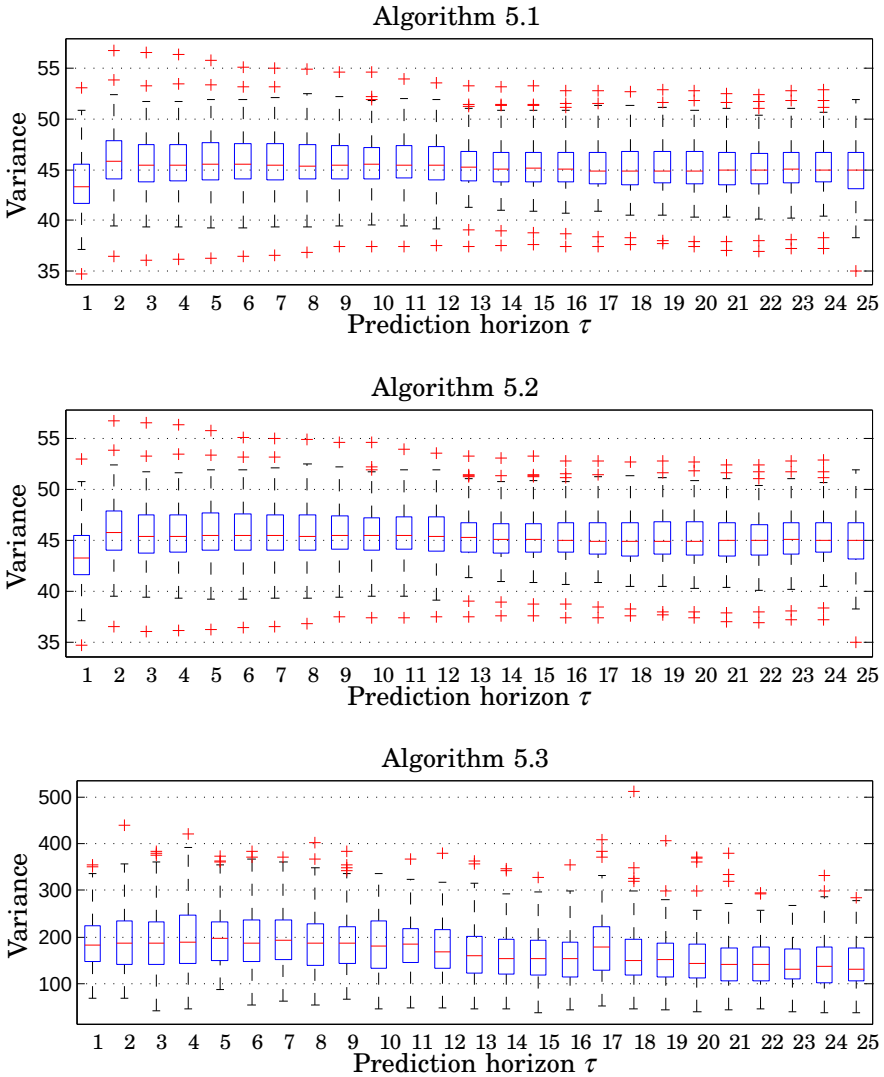

Figure 5.5 Example 4. Closed-loop. Multi-step predictors performances on validation data. Prediction error variance vs. prediction horizon. Top Algorithm 5.1, Center Algorithm 5.2, Bottom Algorithm 5.3

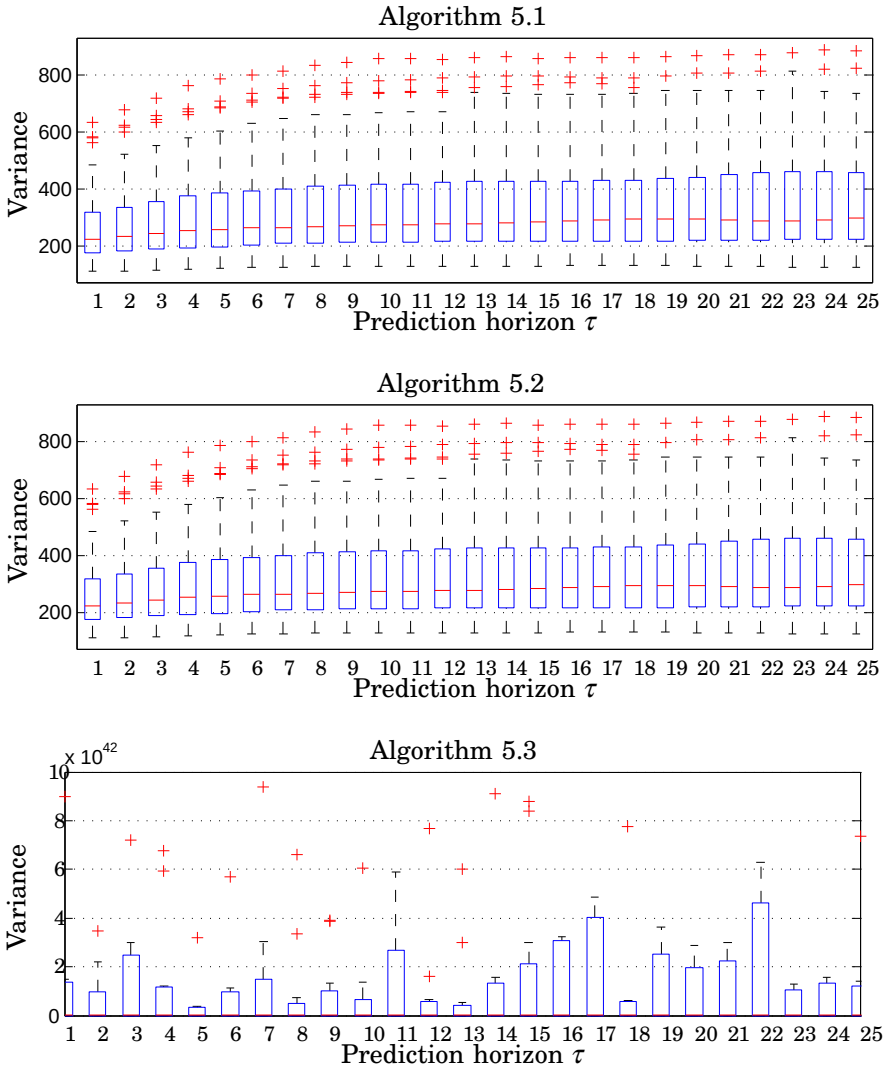

Figure 5.6 Example 5. Closed-loop. Multi-step predictors performances on validation data. Prediction error variance vs. prediction horizon. Top Algorithm 5.1, Center Algorithm 5.2, Bottom Algorithm 5.3

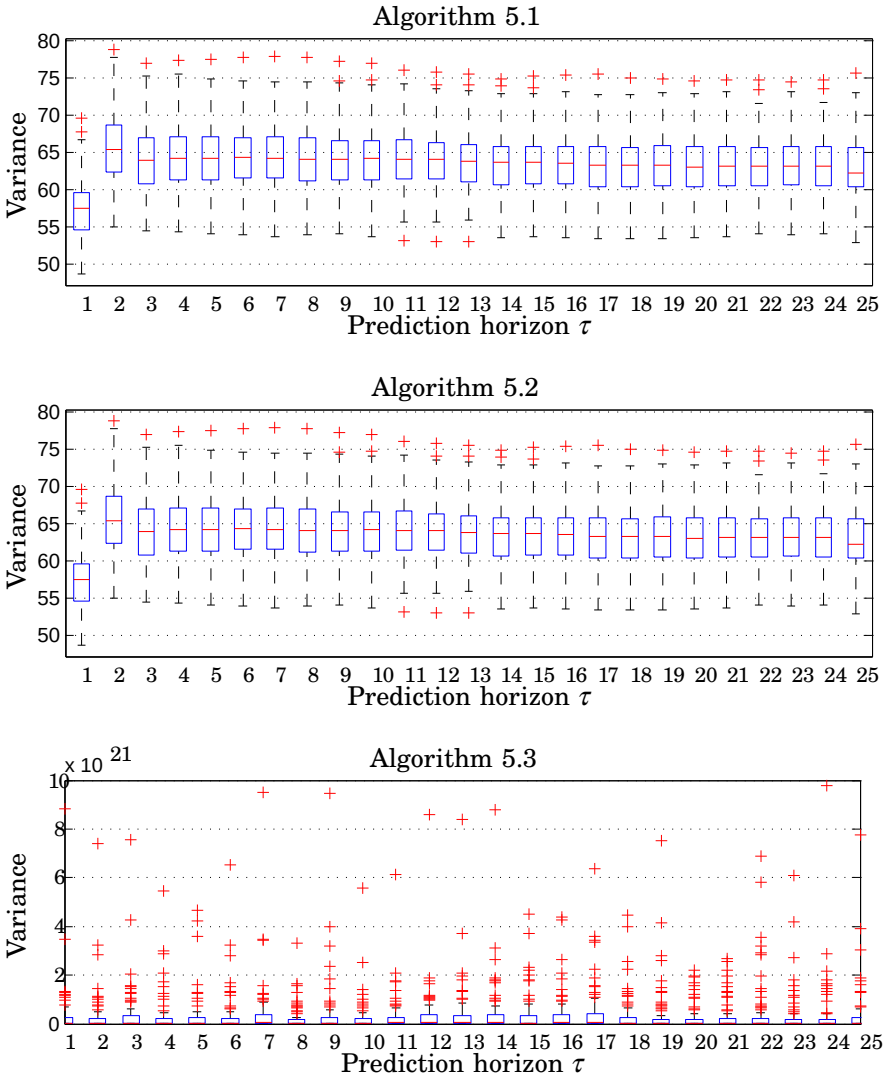

Figure 5.7 Example 6. Closed-loop. Multi-step predictors performances on validation data. Prediction error variance vs. prediction horizon. Top Algorithm 5.1, Center Algorithm 5.2, Bottom Algorithm 5.3

5.5 Discussion and conclusions

In this chapter subspace-based data-driven linear multi-step predictors have been presented. Resorting to geometric operations on appropriate subspaces spanned by the measured input-output data sequences, predictor coefficients were estimated directly from the collected data without any prior knowledge of the system generating the data. No model structure selection nor model order determination were, therefore, required at this stage. The strategy appears to be quite appealing for those real life application in which a reliable model of the system is not available or hard to obtain. Actually, Chapter 6 will give such an example.

Some conditions need to be fulfilled in order to have unbiased predictors. Specifically, for the projection-based approach of Algorithms 5.1, 5.2

- input data should be "rich" enough, that is, the persistency of excitation of the data should be of sufficiently high order
- the space spanned by the row vectors of matrix Z_p and the space spanned by the row vectors of matrix U_f should have zero intersection: $\text{span}(Z_p) \cap \text{span}(U_f) = \{0\}$. This corresponds to no feedback interconnection

whereas for the VARX-based approach of Algorithm 5.3

- input-output data should be PE of sufficiently high order
- p should be sufficiently large

The first and the third conditions are related to the LQ-decompositions required to solve the problems in Eq. (5.26) and (5.49), respectively. Matrix inversion in Eqs. (5.37), (5.42) and (5.52) is possible if and only if L_{11}, $\mathcal{L}_{22}$, $\mathscr{L}_{11}$ are full rank matrices. This is guaranteed when the input signal u is PE of order at least $f \cdot m$ in for the projection-based approach, and z is PE of order at least $p(m+l)$ for the VARX-based approach.

The second condition is necessary for the orthogonal projection to split uniquely into the sum of two oblique projections (Eq. (5.29)). When data are generated in closed loop this condition is no longer satisfied.

Last, the fourth condition on the integer p permitted to disregard the effect of the unknown initial states in Eq. (5.3). Actually, a lower bound on p was given in [Bauer and Ljung, 2001] and was exploited in [Chiuso, 2007a], Appendix B, to prove the statement.

Throughout the chapter, p was chosen so to satisfy the following condition:

$$p \geq \max\{n, \tau\}$$

in order for the system (5.1) to be observable (condition $p \geq n$) and to guarantee predictions up to the largest future horizon we wish to investigate (condition $p \geq \tau$). The parameter has strong connections with model order, and to optimize results it should be given by the user from knowledge or intuitions on the system dynamics. Indeed, requesting to predict with a look-ahead $\tau >> n$ implies to choose also $p >> n$, which lead to overparametrization of the model and suboptimal performances.

Examples 1 and 2 examined the open loop scenario. The system generating the data was stable and was fed with white noise which is PE of any order. All the algorithms performed similarly, with Alg. 5.3 having a slight edge over the others. Predictions were more accurate in the noise-free case (Ex. 1), as predictable (Figs. 5.2-5.3). In case 3 a unit negative feedback was added to the loop. Algorithm 5.3 outperformed the others. However, the performances were not uniform over the prediction horizons (Figure 5.4).

The remaining 3 examples presented an unstable system in closed-loop. The bias is no longer negligible, as expected (Figs. 5.5, 5.6, 5.7).

Based on the above mention analysis, we may expect satisfactory prediction performances in those real-life application falling within the first 3 cases.

6

Subspace-based Linear Multi-step Predictors in Diabetes

6.1 Introduction

As seen in Chapter 2, a major challenge for a person with diabetes is to adapt insulin dosage regimens, food intake and exercise to keep blood glucose within tolerable limits during daily life activities. The diabetic subject has usually inadequate understanding and overview of the actual physiological state at any time and would therefore benefit from accurate predictions of blood glucose levels. The early knowledge about the effects of inputs on glycemia would, indeed, provide the patients with invaluable informations for appropriate on-the-spot decision making concerning the management of the disease. Against this background, data-driven predictors may be used to overcome the limitations arising from the lack of the underlying physiological system model.

An overview of the existing methods for blood glucose prediction was presented in Sec. 2.4. Results of model-based prediction achieved with third order ARX/ARMAX models identified from actual patient data were summarized in Chapter 4. In this chapter we show how the data-driven predictors presented in Chapter 5 may be exploited to the purpose of predicting blood glucose multiple steps ahead in the future.

6.2 Materials and methods

The population participating in the 3 days in-hospital DAQ trial shown in Table 3.1 and used for modeling purposes in Chapter 4 was considered. In accordance with Chapter 4, the glucoregulatory system was assumed to

have two input channels, i.e., carbohydrate intake and insulin injections, respectively, and one output, i.e., glycemia levels in blood. Two scenarios were outlined. In the first, the physiological models described in Secs. 4.2 and 4.3 exploiting mean population values for the parameters appearing therein were used to filter the raw informations on meals and insulin collected by the study participants in their diaries. This allowed to retrieve the glucose rate of appearance in plasma after a meal, $\hat{u}_g$, and the insulin appearing in plasma after subcutaneous injection, $\hat{u}_i$, which were used as input signals. The Abbott FreeStyle Navigator™ [Abbott, 2013] CGM records were taken as assessment of glycemia, the main reason being that in standard diabetes care, extensive analysis on blood samples are not available. As noticed in Section 3.8, the Navigator^{TM} system did not provide reliable blood glucose measurements. A retrospective recalibration against the collected HemoCue [Hemocue, 2013] samples was, thus, performed offline. The algorithm proposed by King et al. (2007), later evaluated by Facchinetti et al. in [Facchinetti et al., 2007], was used. For each patient a recalibration parameter α^r was found by least-squares estimation:

$$\alpha^r = \arg\min_{\alpha} ||y_{BG} - \alpha y_{IG}||^2$$

with y_{BG} and y_{IG} denoting the HemoCue and the CGM samples, respectively. The recalibrated traces $y^r_{IG} = \alpha^r y_{IG}$ were provided by Facchinetti and co-workers within the DIAdvisor™ project and were used as output signals. In Chapter 4, models were identified from the interpolated insulin assessments from laboratory results u_i, glucose rate of appearance $\hat{u}_g$ and glycemia levels from YSI assays [Yellow Spring Instruments, 2013] y_{BG}. In the second scenario, therefore, to allow comparison with the results shown therein, we used the same signals for multi-step predictions.

We were interested in predictions up to 120 [min] ahead. Actually, for each scenario, we distinguished two simulation set-ups: Case A where we wanted to optimize predictions up to 30 [min] ahead, i.e., $\tau_{max} = 30$ and Case B with focus on predictions up to 120 [min], i.e., $\tau_{max} = 120$ where τ_{max} [min] denotes the maximum prediction horizon we take into consideration.

Algorithm 5.1 was adopted. Below the scheme used for calculation of multi-step predictions is reported.

ALGORITHM 6.1—MULTI-STEP PREDICTION

1. Choose the maximum prediction horizon τ_{max}
2. Set $p = f = \tau_{max}$

3. Estimate $\hat{\Gamma}$ and $\hat{\Lambda}$ from Eqs. 5.37, 5.38 applying Algorithm 5.1 to the first half of the data

4. Let t denote the current time step. Form the predictions $\hat{y}$ of the second half of the data (validation) using the relation

$$\begin{bmatrix} \hat{y}_t \\ \hat{y}_{t+1} \\ \hat{y}_{t+2} \\ \vdots \\ \hat{y}_{t+f-1} \end{bmatrix} = \hat{\Gamma} \begin{bmatrix} z_{t-p} \\ z_{t-p+1} \\ z_{t-p+2} \\ \vdots \\ z_{t-1} \end{bmatrix} + \hat{\Lambda} \begin{bmatrix} \hat{u}_t \\ \hat{u}_{t+1} \\ \hat{u}_{t+2} \\ \vdots \\ \hat{u}_{t+f-1} \end{bmatrix} \tag{6.1}$$

where $\begin{bmatrix} z_{t-p} & z_{t-p+1} & \cdots & z_{t-1} \end{bmatrix}^\intercal$ are the joint input-output data up to time $t-1$ and $\begin{bmatrix} \hat{u}_t & \hat{u}_{t+1} & \cdots & \hat{u}_{t+f-1} \end{bmatrix}^\intercal$ are the future inputs. In the first scenario $\hat{u} = \begin{bmatrix} \hat{u}_i & \hat{u}_g \end{bmatrix}$ and $y = y_{IG}^r$ while in the second $\hat{u} = \begin{bmatrix} u_i & \hat{u}_g \end{bmatrix}$ and $y = y_{BG}$ □

6.3 Results

The predictors *per se* were evaluated with respect to prediction performances on validation data, on the basis of the prediction error variance, i.e., $\mathcal{E}[(y-\hat{y})(y-\hat{y})^\intercal]$, with y, $\hat{y}$ indicating either the recalibrated interstitial glucose y_{IG}^r or blood glucose y_{BG}, depending on the scenario examined and its prediction, respectively. In addition, given the importance of ultimately predict glucose levels in blood, the accuracy of the overall predictions in scenario 1, i.e., $\hat{y}_{IG}^r$, was evaluated according to the metrics presented in Section 3.7.

Performances were assessed for the prediction horizons

- Case A: $\tau = 10, 20, 30$ [min]
- Case B: $\tau = 30, 60, 90, 120$ [min]

Tables 6.1 and 6.2 present assessment of prediction *per se* relative to scenario 1, case A and B, respectively, while tables 6.3 and 6.4 summarize the results for scenario 2, case A and B, respectively. Prediction performances with respect to y_{BG} starting from y_{IG} are given in Tables 6.5–6.8. Figure 6.1 show predictions for one representative subject, relative to scenario 1, case B, whereas Fig. 6.2 reproduces predictions for the same subject in scenario 2, case B. For comparison, Fig. D.12 in the Appendix gives prediction obtained using as output the non-recalibrated interstitial glucose y_{IG}. For completeness, figures dealing with other subjects than CHU102 are reported in Appendix D.

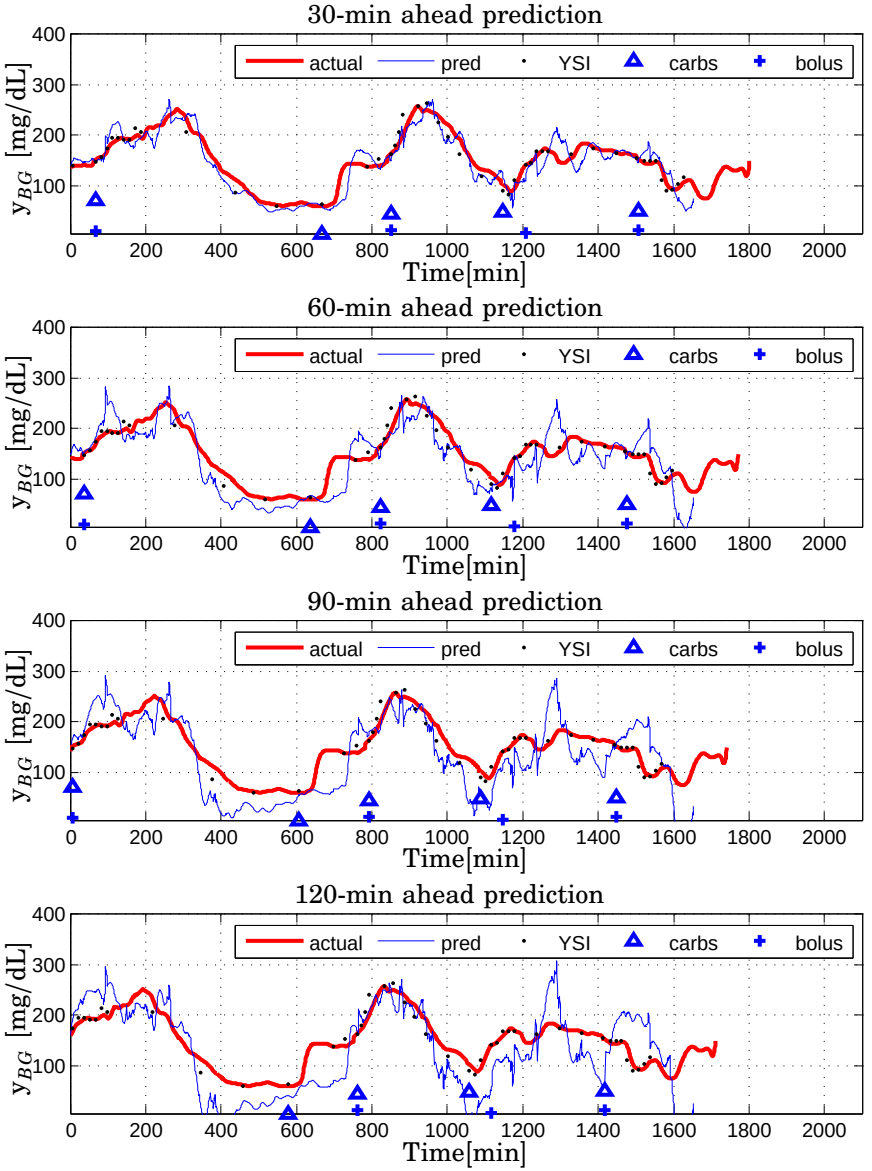

Figure 6.1 Patient CHU102. Multi-step predictions. Scenario 1, Case B, p=f=120. Evaluation on validation data. Predictor (thin) and recalibrated interstitial glucose $\hat{y}_{IG}$ (thick) [mg/dL] vs. time [min]. *Top* 30-minutes ahead; *Top Center* 60-minutes ahead; *Bottom Center* 90-minutes ahead; *Bottom* 120-minutes-ahead prediction. Meals and injections are indicated with triangles and pluses, respectively.

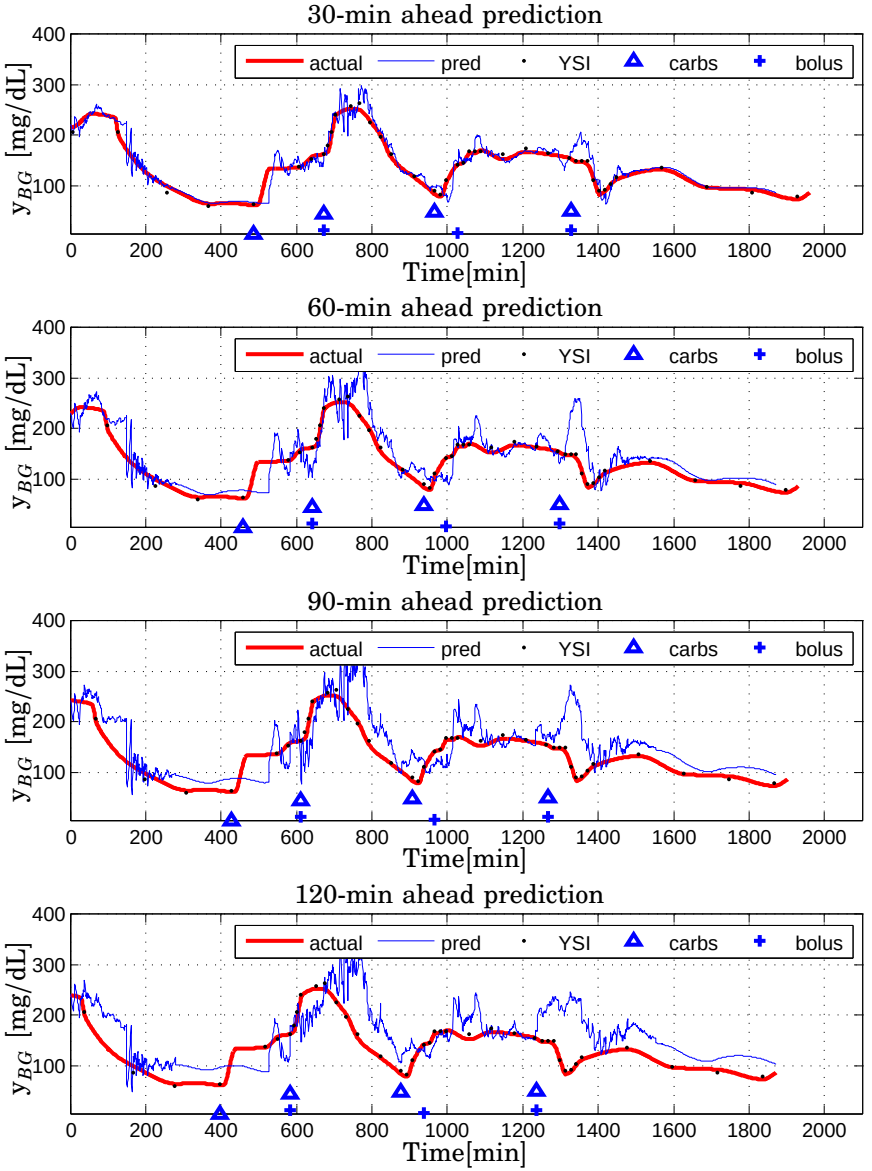

Figure 6.2 Patient CHU102. Multi-step predictions. Scenario 2, Case B, $p{=}f{=}120$. Evaluation on validation data. Predictor (thin) and measured plasma glucose y_{BG} (thick) [mg/dL] vs. time [min]. *Top* 30-minutes ahead; *Top Center* 60-minutes ahead; *Bottom Center* 90-minutes ahead; *Bottom* 120-minutes-ahead prediction. Meals and injections are indicated with triangles and pluses, respectively.

Table 6.1 Multi-step short-term predictors performance evaluation. Scenario 1, Case A. Prediction Error Variance $[(\text{mg/dL})^2]$ vs. Prediction Horizon [min] on validation data.

Patient ID	10[min]	20[min]	30[min]
102	7.41	47.31	119.34
103	20.08	107.65	247.32
104	18.31	157.28	495.43
105	13.17	91.54	243.34
106	20.49	129.38	341.73
107	11.99	69.48	174.09
108	7.28	54.56	158.25
115	6.77	38.83	96.32
119	19.92	212.34	714.18
120	5.50	44.79	147.20
121	12.06	72.03	180.02
128	9.39	49.71	114.12
130	13.28	93.56	276.08

Table 6.2 Multi-step short-term predictors performance evaluation. Scenario 1, Case B. Prediction Error Variance $[(\text{mg/dL})^2]$ vs. Prediction Horizon [min] on validation data.

Patient ID	30[min]	60[min]	90[min]	120[min]
102	136.79	482.88	772.60	952.69
103	530.97	1448.3	2336.1	2644.8
104	605.97	2914.4	6277.8	9574.6
105	307.96	946.07	1316.5	1488.3
106	549.67	2492.6	5032.0	7642.2
107	252.2019	964.6733	1781.7	2181.5
108	364.3953	1453.2	1772.7	1202.3
115	131.3680	467.64	966.32	1544
119	1498.1	6013.8	9100.3	10287
120	244.8146	1472.8	3364.6	5043.8
121	210.82	805.47	1500.7	2338.7
128	154.78	442.87	814.99	1383.4
130	449.51	1864.3	3548	4916.2

Table 6.3 Multi-step short-term predictors performance evaluation. Scenario 2, Case A. Prediction Error Variance [$(mg/dL)^2$] vs. Prediction Horizon [min] on validation data.

Patient ID	10[min]	20[min]	30[min]
102	13.18	84.13	223.68
103	8.66	68.81	200.44
104	13.06	134.51	420.29
105	512.16	3406.00	5726.10
106	34.36	232.19	626.34
107	24.14	190.59	422.75
108	11.45	82.47	221.16
115	5.65	44.49	110.38
119	14.98	86.20	203.27
120	16.37	102.75	273.10
121	14.13	137.81	435.29
128	6.55	62.99	213.85
130	116.29	451.48	741.11

Table 6.4 Multi-step short-term predictor performance evaluation. Scenario 2, Case B. Prediction Error Variance [$(mg/dL)^2$] vs. Prediction Horizon [min] on validation data.

Patient ID	30[min]	60[min]	90[min]	120[min]
102	209.73	802.81	1417.90	1784.70
103	216.32	818.88	1202.60	1422.80
104	618.95	3247.10	5941.90	6561.00
105	2478.30	1226.40	1899.60	12325.00
106	634.08	2502.40	4818.00	7038.60
107	254.86	1186.70	2067.80	2668.40
108	342.41	1133.30	1617.70	1540.60
115	141.41	613.02	1405.30	2107.70
119	246.95	913.31	1680.90	2329.00
120	331.12	1680.20	3993.20	6807.90
121	498.07	2483.30	5256.70	7491.50
128	327.01	1789.20	3472.80	4898.60
130	1102.60	2052.40	3524.90	4785.80

Table 6.5 Numerical and clinical accuracy of predictions. Scenario 1, case B, 30 [min] prediction

Patient	*AD* [mg/dL]		*RD*		*ISO* [%]	*CG-pEGA* [%]		*CG-rEGA* [%]	
	Mean	Median	Mean	Median	$*$	A	B	A	B
CHU102	18.56	13.40	.2365e-4	0.01	77.27	78.26	21.73	60.00	28.88
CHU103	27.61	23.39	-0.12	-0.16	43.58	45.65	52.17	60.00	24.44
CHU104	35.41	29.67	-0.05	-0.0071	50	48.93	42.55	52.17	26.08
CHU105	33.42	22.56	-0.04	-0.05	56.09	55.55	37.77	54.54	11.36
CHU106	29.49	24.45	-0.09	-0.12	58.13	56.52	39.13	64.44	15.55
CHU107	31.83	29.26	-0.11	-0.03	52.17	51.06	46.80	54.34	26.08
CHU108	26.27	16.86	-0.01	0.02	55.55	54.34	41.30	57.77	20.00
CHU115	20.94	14.56	-0.01	-0.01	78.26	78.26	21.73	68.88	15.55
CHU118	21.61	16.43	0.01	0.0042	65.85	63.82	31.91	58.69	19.56
CHU119	58.30	36.35	-0.02	0.05	46.80	46.80	38.29	41.30	34.78
CHU120	37.96	28.12	-0.10	-0.01	58.69	58.69	41.30	48.88	26.66
CHU121	30.30	25.27	-0.05	-0.02	52.38	55.31	42.55	58.69	17.39
CHU128	25.30	20.41	0.04	0.008	68.75	68.75	31.25	61.29	19.35
CHU130	39.61	32.76	-0.01	-0.01	60	62.50	31.25	54.83	19.35

$*$ prediction within [20%] from reference y_{BG} when $y_{BG} \geq 75$[mg/dL]

Table 6.6 Numerical and clinical accuracy of predictions. Scenario 1, case B, 60 [min] prediction

Patient	*AD* [mg/dL]		*RD*		*ISO* [%]	*CG-pEGA* [%]		*CG-rEGA* [%]	
	Mean	Median	Mean	Median	$*$	A	B	A	B
CHU102	28.62	24.29	-0.01	0.0079	65.11	66.66	33.33	45.45	34.09
CHU103	42.34	39.67	-0.19	-0.28	31.57	31.11	62.22	52.27	36.36
CHU104	64.03	46.76	-0.06	-0.01	66.66	43.47	28.26	46.66	24.44
CHU105	51.54	33.36	-0.06	-0.12	37.50	36.36	47.72	39.53	13.95
CHU106	50.85	45.56	-0.16	-0.12	35.71	35.55	60.00	56.81	27.27
CHU107	44.05	32.67	-0.22	-0.08	53.33	52.17	39.13	46.66	13.33
CHU108	47.62	29.48	0.01	0.04	43.18	42.22	46.66	47.72	20.45
CHU115	27.11	21.27	-0.04	-0.01	60	60	37.77	50	18.18
CHU118	49.74	44.15	0.08	0.04	37.50	36.95	54.34	55.55	24.44
CHU119	76.71	46.17	0.01	0.08	43.47	43.47	36.95	33.33	33.33
CHU120	68.03	43.18	-0.22	0.02	37.77	37.77	51.11	43.18	27.27
CHU121	44.69	35.22	-0.04	0.09	43.90	47.82	43.47	44.44	28.88
CHU128	30.44	27.46	0.08	0.08	59.37	59.37	37.50	64.51	19.35
CHU130	58.96	54.99	-0.0084	0.07	33.33	37.50	56.25	48.38	22.58

$*$ prediction within [20%] from reference y_{BG} when $y_{BG} \geq 75$[mg/dL]

Table 6.7 Numerical and clinical accuracy of predictions. Scenario 1, case B, 90 [min] prediction

Patient	*AD* [mg/dL]		*RD*		*ISO* [%]	*CG-pEGA* [%]		*CG-rEGA* [%]	
	Mean	Median	Mean	Median	$*$	A	B	A	B
CHU102	37.77	33.69	-0.01	-0.02	48.83	51.11	48.88	63.63	18.18
CHU103	48.87	37.49	-0.19	-0.11	40.54	36.36	52.27	55.81	25.58
CHU104	86.46	65.39	-0.09	0.03	33.33	32.60	36.95	35.55	35.55
CHU105	51.04	38.16	-0.14	-0.16	30	29.54	61.36	53.48	20.93
CHU106	69.20	51.80	-0.13	-0.14	29.26	29.54	52.27	37.20	30.23
CHU107	52.60	42.39	-0.19	-0.11	40.90	40.00	51.11	45.45	22.72
CHU108	47.19	33.75	0.01	0.09	34.09	33.33	55.55	47.72	29.54
CHU115	29.16	21.43	-0.04	-0.05	65.90	65.90	34.09	48.83	32.55
CHU118	64.22	58.67	0.19	0.22	22.50	26.08	58.69	55.55	26.66
CHU119	86.04	52.44	0.07	0.11	37.77	37.77	37.77	34.09	31.81
CHU120	88.84	62.76	-0.28	-0.03	26.66	26.66	55.55	47.72	20.45
CHU121	49.05	37.15	0.0029	0.06	37.50	40.00	51.11	54.54	15.90
CHU128	47.59	39.35	0.13	0.18	45.16	45.16	48.38	53.33	26.66
CHU130	61.08	63.03	-0.01	0.01	33.33	35.48	58.06	43.33	16.66

$*$ prediction within [20%] from reference y_{BG} when $y_{BG} \geq 75$[mg/dL]

Table 6.8 Numerical and clinical accuracy of predictions. Scenario 1, case B, 120 [min] prediction

Patient	*AD* [mg/dL]		*RD*		*ISO* [%]	*CG-pEGA* [%]		*CG-rEGA* [%]	
	Mean	Median	Mean	Median	$*$	A	B	A	B
CHU102	49.33	42.67	0.05	0.04	39.02	41.86	58.13	59.52	19.04
CHU103	51.09	43.87	-0.25	-0.12	32.43	27.27	61.36	53.48	20.93
CHU104	98.97	63.47	-0.14	0.09	26.82	27.27	36.36	23.25	30.23
CHU105	54.57	49.65	-0.27	-0.28	31.57	28.57	66.66	58.53	24.39
CHU106	78.62	60.58	-0.15	-0.09	36.58	34.09	36.36	37.20	27.90
CHU107	62.77	69.62	-0.17	-0.08	25	24.44	68.88	43.18	34.09
CHU108	38.05	30.37	0.01	0.07	40.47	39.53	55.81	42.80	30.95
CHU115	37.77	30.40	-0.06	-0.01	51.16	51.16	46.51	52.38	23.80
CHU118	73.38	56.88	0.23	0.25	26.31	27.27	52.27	37.20	32.55
CHU119	91.51	58.52	0.09	0.11	40	40.00	35.55	43.18	27.27
CHU120	113.98	98.49	-0.30	0.13	9.30	9.30	55.81	47.61	19.04
CHU121	60.08	35.0	-0.18	0.07	42.50	42.22	37.77	47.72	20.45
CHU128	59.04	44.16	0.18	0.16	43.33	43.33	40	31.03	41.37
CHU130	75.17	58.84	0.05	0.11	26.66	26.66	60	48.27	17.24

$*$ prediction within [20%] from reference y_{BG} when $y_{BG} \geq 75$[mg/dL]

6.4 Discussion and conclusions

Subspace-based multi-step data-driven predictors were applied to the problem of short-term T1DM glycemia prediction. Among the algorithms proposed in Chapter 5, Algorithm 5.1 was used. The choice was based on the analysis of the results reported for the open-loop cases in Chapter 5. In such examples, indeed, Alg. 5.1 performed consistently over all the prediction horizons, in all the cases. Moreover, from an implementation point of view, the approach was attractive, amounting only to an LQ decomposition of appropriately organized input-output Hankel matrices.

The user was required to choose one parameter: the length of the past horizon, p. It represents the size of the past Hankel data matrices and has strong connections with the underlying model order. A too large prediction horizon may lead to overparametrization and hence poor performances. On the other hand, p is lower-bounded by the maximum prediction horizon τ_{max} one wishes to investigate. Actually, as noted in Section 5.5, the parameter p should be given by the user so to optimize performances. In other words, if the objective is to predict τ =30 [min] ahead p should not be given >> 30. Inspection of Tables 6.1–6.4 confirmed this statement. The highlighted columns refer to the same prediction horizon, i.e., τ =30 [min], and showed better performances in the case where $p = \tau$ (Case A). An exception was represented by patient CHU105 and CHU107 in Scenario 2 and might be due to some artifacts in the data caused by the interpolation of either the YSI samples or the insulin in blood samples.

Tables 6.1–6.4 evaluated the predictors *per se*. The performances varied not only among the population, as it could be expected as some patients are easier to describe than others, but also between the scenarios. The results appearing in Table 6.2 can be compared to those shown in Table 4.7. From this analysis it may, then, be concluded that the strategy presented in Chapter 4 was more successful. However, from a clinical diabetes point of view, a different conclusion is drawn. Let us examine Tables 6.5–6.8 and Tables 4.9–4.12. The absolute prediction error in the multi-step predictors case was somewhat larger, nevertheless, the percentage of points falling in the A+B regions in the CG-EGA, hence considered safe predictions, was almost the same in both cases.

7

Continuous-time State-Space Identification

7.1 Introduction

Prior to the mid 1960s, early research on system identification for automatic control and system analysis focused on continuous-time models obtained by reference to either frequency response data or transient response data, as most control system implementations at the time employed analogue techniques [Truxal, 1955]. Subsequently however, developments in digital data acquisition and computing technology led to an emphasis on the use of discrete-time system models and discrete-time control designs, most of the system identification research being, thus, concerned with the estimation of parameters in discrete-time models from sampled data [Åström and Eykhoff, 1971; Ljung, 1999; Söderström and Stoica, 1989; Johansson, 1993]. Nevertheless, in areas such as biology, medicine and physiology the accurate knowledge of the natural continuous-time transfer function is still a prerequisite to many methods in physical modelling and control system design. Actually, glucose metabolism modeling in diabetes is no exception to this case. Comprehensive descriptions of the glucose-insulin control system attempting to fully implement the knowledge about metabolic regulation into a typically nonlinear model of high order, with a large number of parameters are available in the literature [Hovorka et al., 2004], [Dalla Man et al., 2006], [Wilinska et al., 2010]. Generally, such models are difficult to personalize, the identification of all the unknown parameters appearing therein requiring costly and complicated massive experimental investigation on a single individual [Dalla Man et al., 2002], [Dalla Man et al., 2004], [Dalla Man et al., 2005], [Dalla Man et al., 2006], [Cobelli et al., 2009] and may lack structural identifiability. Overall, these aspects make them unsuitable to the purposes of prediction and

control while their utility is in the possibility for simulation studies. An alternative practical scenario was illustrated in Chapter 4, where simpler discrete-time models of the signals and systems involved in diabetes were identified from blood glucose concentration, insulin doses and quantities of carbohydrate in a meal. Yet, there is no undisputed algorithm for parameter translation from discrete-time parameters to a continuous-time description. Problems in this context are associated with translation of the system zeros from the discrete-time model to the continuous-time model whereas the system poles are mapped by means of complex exponentials [Åström et al., 1984]. As a result, a poor parameter translation tends to affect both the frequency response such as the Bode diagram and the transient response such as the impulse response. Hence, another particularly interesting and appealing option is represented by the direct continuous-time glucose-insulin metabolism system identification from discrete-time collected data.

The main obstacle in handling continuous time (CT) models is associated with the need of the normally unmeasured time-derivative terms of the input-output signals. In early contributions, this difficulty was removed by processing the signals with state variable filters (SVF) acting on the inputs and outputs of the continuous-time process [Young, 1964], in order to provide approximate derivatives which might be exploited for linear regression and other identification methods. However, several alternatives to the use of SVFs were proposed, each being characterized by specific advantages such as mathematical benefit, handling the effect of initial conditions, accuracy, computation simplicity and others [Garnier et al., 2003; Sinha and Rao, 1991; Unbehauen and Rao, 1987a; Young, 1981b; Young and Garnier, 2006]. Johansson [1986] interestingly suggested an algebraic reformulation of transfer function models exploiting the operator λ as substitute of the Laplace operator to represent differentiations. This approach was taken later on by the same author to identify continuous-time models from sampled data by means of subspace model identification (SMI) algorithms [Johansson et al., 1999]. Bergamasco and Lovera [2010, 2011] building on the framework introduced in [Haverkamp, 2001] and exploting Laguerre filtering and Laguerre projections as in [Ohta and Kawai, 2004] derived a closed-loop predictor-based SMI scheme.

This chapter is concerned with state-space model identification algorithms that fits CT models to discrete time (DT) (possibly non-uniformly) sampled data. The underlying motivation to this work is obtaining personalized continuous-time data-driven models of T1DM glucose dynamics from actual patients sampled input-output data. Two approaches are presented: one subspace-based as in [Bergamasco and Lovera, 2010], [Bergamasco and Lovera, 2011] and one realization-based [Johansson et al.,

2013].

Altogether, there are a number of advantages of such a strategy:

1. Continuous-time models provide good physical insight into the glucose metabolism system properties

    - The estimated parameters have clinically relevant meaning, e.g., static gains and time constants for glucose and insulin. While these parameters are directly linked to the CT model, the parameters of DT models are a function of the sampling interval and do not normally have any physical interpretation [Garnier et al., 2008];

2. Ability of handling non-uniformly sampled data

    - meal and insulin intakes appear at sparse discrete time instants, non equidistantly spaced and not synchronized with blood glucose self-monitoring. In addition, in the situation of a subcutaneous glucose sensor often samples are missed every now and then, due to loss of connection between transmitter and receiver and sensor misplacement. Hence, the standard DT LTI model will not be applicable because the assumption of a uniformly sampled environment no longer holds. The coefficients of CT models, instead, are assumed to be independent of the sampling period, the measurements are considered as points on a continuous line which do not need to be equidistantly spaced [Åström et al., 1984];

3. Transformation between CT and DT models

    - when a CT model is transformed into its DT counterpart, the DT parameters are functions of the CT parameters and the sample time, and in general there is no unique retransformation. One source of error in many existing algorithms is that computation of the system zeros is affected by the assumed and actual inter-sample behavior (e.g., ZOH) of the control variables.

4. Use of linear algebra tools in the algorithms (subspace based) [Golub and Van Loan, 1996]

    - robust implementation and overcome being trapped into local minima (subspace based)

7.2 A model transformation

The strategies presented in this chapter introduce an algebraic reformulation of transfer function models. The idea is to find a causal, stable, realizable linear operator that may replace the differential operator while keeping an exact transfer function. This shall be done in such a way that a linear model for estimation of the original transfer function parameters is obtained. Actually, there is always a linear one-to-one transformation which relates the continuous-time parameters and the convergence points for each choice of operator [Johansson, 1994].

Consider a linear nth order transfer operator formulated with a differential operator $\sigma = d/dt$ and unknown coefficients a_i, b_i.

$$G_0(\sigma) = \frac{b_1\sigma^{n-1} + \cdots + b_n}{\sigma^n + a_1\sigma^{n-1} + \cdots + a_n} = \frac{B(\sigma)}{A(\sigma)} \tag{7.1}$$

where it is assumed that $A(\cdot)$ and $B(\cdot)$ are coprime. It is supposed that the usual isomorphism between transfer operators and transfer functions, i.e., the corresponding functions of a complex variable s, is valid. Because of this isomorphism, G_0 will sometimes be regarded as a transfer function and sometimes as a transfer operator. A notational difference will be made with σ denoting the differential operator and s denoting the complex frequency variable of the Laplace transform.

On any transfer function describing a physically realizable continuous-time system, it is a necessary requirement that the transfer function be proper because pure derivatives of the input cannot be implemented. This requirement is fulfilled as $\lim_{s\to\infty} G_0(s)$ is finite, i.e., $G_0(s)$ has no poles at infinity. An algebraic approach to system analysis may be suggested. Let a be point on the positive real axis and define the mapping

$$f(s) = \frac{a}{s+a}, \qquad s \in \mathbb{C}$$

Let $\bar{\mathbb{C}} = \mathbb{C} \cup \infty$ be the complex plane extended with the 'infinity point'. Then f is a bijective mapping from $\bar{\mathbb{C}}$ to $\bar{\mathbb{C}}$ and it maps the 'infinity point' to the origin and $-a$ to the 'infinity point'. The unstable region—i.e., the right half plane ($\mathrm{Re}\, s > 0$)—is mapped onto a region which does not contain the 'infinity point'. Introduction of the operator

$$\lambda = f(\sigma) = \frac{a}{\sigma+a} = \frac{1}{1+\sigma\tau}, \qquad \tau = 1/a \tag{7.2}$$

allows us to make the following transformation

$$G_0(\sigma)_{|\sigma=\frac{1-\lambda}{\tau\lambda}} = G_0^*(\lambda) = \frac{B^*(\lambda)}{A^*(\lambda)}$$

with

$$A^*(\lambda) = 1 + \alpha_1\lambda + \alpha_2\lambda^2 + \cdots + \alpha_n\lambda^n \tag{7.3}$$

$$B^*(\lambda) = \beta_1\lambda + \beta_2\lambda^2 + \cdots + \beta_n\lambda^n \tag{7.4}$$

An input-output model is easily formulated as

$$A^*(\lambda)y(t) = B^*(\lambda)u(t) \tag{7.5}$$

or on regression form

$$y(t) = -\alpha_1[\lambda y](t) - \cdots - \alpha_n[\lambda^n y](t) + \beta_1[\lambda u](t) + \cdots + \beta_n[\lambda^n u](t) \tag{7.6}$$

This is now a linear model of a dynamical system at all points of time. Notice that $[\lambda u], [\lambda y]$ etc. denote filtered inputs and outputs. The parameters α_i, β_i may now be estimated by any suitable method for estimation of parameters of a linear model. A reformulation of the model Eq. (7.6) to a linear regression form is

$$\begin{aligned} y(t) &= \varphi_\tau^T(t)\theta_\tau, \\ \theta_\tau &= \begin{pmatrix} \alpha_1 & \alpha_2 \ldots \alpha_n & \beta_1 & \beta_2 \ldots \beta_n \end{pmatrix}^T \\ \varphi_\tau(t) &= \left(-[\lambda y](t), \ldots - [\lambda^n y](t), [\lambda u](t), \ldots [\lambda^n u](t)\right)^T \end{aligned} \tag{7.7}$$

with parameter vector θ_τ and the regressor vector φ_τ.

Parameter transformations

Before proceeding, we should make clear the relationship between the parameters α_i, β_i of (7.3)–(7.4) and the original parameters a_i, b_i of the transfer function (7.1). Let the vector of original parameters be denoted by

$$\theta = \begin{pmatrix} -a_1 & -a_2 & \ldots & -a_n & b_1 & \ldots & b_n \end{pmatrix}^T \tag{7.8}$$

Using the definition of λ of Eq. (7.2), it is straightforward to show that the relationship between the operator-transformed parameters of Eq. (7.7) and the original parameters of Eq. (7.8) is

$$\theta_\tau = F_\tau\theta + G_\tau \tag{7.9}$$

where the $2n \times 2n-$matrix F_τ is

$$F_\tau = \begin{pmatrix} M_\tau & 0_{n\times n} \\ 0_{n\times n} & M_\tau \end{pmatrix} \tag{7.10}$$

and where M_τ is the Pascal matrix

$$M_\tau = \begin{pmatrix} m_{11} & 0 & \cdots & 0 \\ m_{12} & m_{22} & \ddots & \vdots \\ \vdots & & \ddots & 0 \\ m_{n1} & m_{n2} & \cdots & m_{nn} \end{pmatrix}, \tag{7.11}$$

$$m_{ij} = (-1)^{i-j}\binom{n-j}{i-j}\tau^j \tag{7.12}$$

Furthermore, the $2n \times 1-$vector G_τ is given by

$$G_\tau = \begin{pmatrix} g_1 \dots g_n & 0 \dots 0 \end{pmatrix}^T; \quad g_i = \binom{n}{i}(-1)^i \tag{7.13}$$

The matrix F_τ is invertible when M_τ is invertible, i.e. for all $\tau > 0$. The parameter transformation is then one-to-one and

$$\theta = F_\tau^{-1}(\theta_\tau - G_\tau) \tag{7.14}$$

We may then conclude that the parameters a_i, b_i of the continuous-time transfer function G_0 may be reconstructed from the parameters α_i, β_i of θ_τ by means of basic matrix calculations. As an alternative we may estimate the original parameters a_i, b_i of θ from the linear relation

$$y(t) = \theta_\tau^T \varphi_\tau(t) = (F_\tau \theta + G_\tau)^T \varphi_\tau(t) \tag{7.15}$$

where F_τ and G_τ are known matrices for each τ. Moreover, orthogonal linear combinations of the regressor vector components by means of some transformation matrix T could be accommodated by modification of Eq. (7.15) to

$$y(t) = (T\varphi_\tau(t))^T T^{-T} F_\tau \theta + (T\varphi_\tau(t))^T T^{-T} G_\tau$$

Hence, the parameter vectors θ_τ and θ are related via known and simple linear relationships so that translation between the two parameter vectors can be made without any problem arising. Moreover, identification can be made with respect to either θ or θ_τ.

7.3 Predictor-based state-space model identification

Consider a continuous-time time-invariant system $\Sigma_n(A, B, C)$ described by the differential equations:

$$\begin{cases} dx(t) = Ax(t)dt + Bu(t)dt + dw(t) \\ dz(t) = Cx(t)dt + dv(t) \\ y(t)dt = dz \end{cases} \tag{7.16}$$

with input $u \in \mathbb{R}^m$, output $y \in \mathbb{R}^l$, state vector $x \in \mathbb{R}^n$. The noise $w(t) \in \mathbb{R}^n$ and $v(t) \in \mathbb{R}^l$ acting on the state dynamics and the output, respectively, are Wiener processes with incremental covariance given by (ignoring terms dependent on $(dt)^2$):

$$\mathcal{E}\{\begin{bmatrix} w(t)dt \\ v(t)dt \end{bmatrix} \begin{bmatrix} w(t)dt \\ v(t)dt \end{bmatrix}^{\mathsf{T}}\} = \begin{bmatrix} Q & S \\ S^{\mathsf{T}} & R \end{bmatrix} dt \tag{7.17}$$

The initial state, $w(t)$, $v(t)$ and $u(t)$ are assumed to be mutually independent. The system matrices $A \in \mathbb{R}^{n\times n}$, $B \in \mathbb{R}^{n\times m}$, $C \in \mathbb{R}^{p\times n}$ are such that (A, C) is observable, $(A, [B, Q^{\frac{1}{2}}])$ is controllable and the system is stable. The input-output data sequences of system (7.16) are observed at the sample times not necessarily equidistantly spaced $\{t_k\}_{k=0}^N$, $t_{k+1} \geq t_k$ for all k and are denoted as $\{u(t_k)\}_{k=0}^N$, $\{y(t_k)\}_{k=0}^N$. The continuous-time model identification problem, thus, consists in identifying the system parameters A, B, C up to a similarity transformation or equivalently the (system invariant) transfer function $F(s) = C(sI - A)^{-1}B$ starting from $\{u(t_k)\}_{k=0}^N$, $\{y(t_k)\}_{k=0}^N$.

Remark: As computation and statistical validation tests deal with discrete-time data, we assume the original sampled stochastic disturbance sequences to be uncorrelated with a uniform spectrum up to the Nyquist frequency, thereby avoiding the mathematical problems associated with Brownian motion [Johansson, 1994].

Continuous-Time State-Space Linear System

From the set of first-order differential equations, we have in the Laplace domain notation:

$$\begin{aligned} sX(s) &= AX(s) + BU(s) + W(s) + sx_0, \qquad x_0 = x(t_0) \\ Y(s) &= CX(s) + V(s) \end{aligned} \tag{7.18}$$

Introduction of the complex variable transform

$$\lambda(s) = \frac{1}{1 + s\tau} \tag{7.19}$$

corresponding to a stable, causal operator in order to replace the Laplace domain differentiation as represented by s, mapping the left-half plane into the disc Ω centered in 0.5, permits an algebraic transformation of the model [Johansson et al., 1999]

$$\begin{aligned} X &= (I + \tau A)[\lambda X] + \tau B[\lambda U] + \tau[\lambda W] + (1 - \lambda)x_0 \\ Y &= CX + V \end{aligned} \tag{7.20}$$

Reformulation while disregarding the initial conditions to linear system equations gives:

$$\begin{aligned}\begin{bmatrix}\xi\\ y\end{bmatrix} &= \begin{bmatrix}(I+\tau A) & \tau B\\ C & 0\end{bmatrix}\begin{bmatrix}x\\ u\end{bmatrix} + \begin{bmatrix}\tau v\\ e\end{bmatrix}, \quad x(t) = [\lambda\xi](t)\\ &= \begin{bmatrix}A_\lambda & B_\lambda\\ C & 0\end{bmatrix}\begin{bmatrix}x\\ u\end{bmatrix} + \begin{bmatrix}\tau v\\ e\end{bmatrix}\end{aligned} \tag{7.21}$$

where

$$\begin{cases}A_\lambda = I + \tau A\\ B_\lambda = \tau B\end{cases} \tag{7.22}$$

the mapping between (A, B) and (A_λ, B_λ) being bijective. Provided that a standard positive semi-definiteness condition of Q is fulfilled so that the Riccati equation has a solution

$$\begin{aligned}P_\lambda &= A_\lambda P_\lambda A_\lambda^\intercal + Q_\lambda - (A_\lambda P_\lambda C_\lambda^\intercal + S_\lambda^\intercal)(C_\lambda P_\lambda C_\lambda^\intercal + R_\lambda)^{-1}(C_\lambda P_\lambda A_\lambda^\intercal + S_\lambda)\\ K_\lambda &= (A_\lambda P_\lambda C_\lambda^\intercal + S_\lambda^\intercal)(C_\lambda P_\lambda C_\lambda^\intercal + R_\lambda)^{-1}\end{aligned} \tag{7.23}$$

$$\mathcal{E}\{\begin{bmatrix}\tau v(t)dt\\ e(t)dt\end{bmatrix}\begin{bmatrix}\tau v(t)dt\\ e(t)dt\end{bmatrix}^\intercal\} = \begin{bmatrix}Q_\lambda & S_\lambda\\ S_\lambda^\intercal & R_\lambda\end{bmatrix} dt \tag{7.24}$$

it is possible to replace the linear model of Eq. (7.21) by the innovations model

$$\begin{bmatrix}\xi\\ y\end{bmatrix} = \begin{bmatrix}A_\lambda & B_\lambda\\ C & 0\end{bmatrix}\begin{bmatrix}x\\ u\end{bmatrix} + \begin{bmatrix}K_\lambda\\ I\end{bmatrix} w \tag{7.25}$$

$$K_\lambda = \tau K \tag{7.26}$$

Taking the innovations model inverse (predictor form), we have

$$\begin{aligned}\begin{bmatrix}\xi\\ w\end{bmatrix} &= \begin{bmatrix}A_\lambda - K_\lambda C & B_\lambda\\ -C & 0\end{bmatrix}\begin{bmatrix}x\\ u\end{bmatrix} + \begin{bmatrix}K_\lambda\\ I\end{bmatrix} y\\ &= \begin{bmatrix}\bar{A}_\lambda & B_\lambda\\ -C & 0\end{bmatrix}\begin{bmatrix}x\\ u\end{bmatrix} + \begin{bmatrix}K_\lambda\\ I\end{bmatrix} y, \quad \bar{A}_\lambda = A_\lambda - K_\lambda C\\ y &= Cx + w\end{aligned} \tag{7.27}$$

Further, all the eigenvalues of $\bar{A}_\lambda$ are assumed to be inside the disc Ω. By recursion it is found that [Johansson et al., 1999]

$$\begin{aligned}
[\lambda^p y](t) &= C\bar{A}_\lambda^p \xi(t) + \\
&\quad + \sum_{h=1}^{p} C\bar{A}_\lambda^{h-1}(B_\lambda[\lambda^{p-h}u](t) + K_\lambda[\lambda^{p-h}y](t)) + [\lambda^p w](t) \\
[\lambda^{p+1} y](t) &= C\bar{A}_\lambda^{p+1} \xi(t) + \\
&\quad + \sum_{h=1}^{p+1} C\bar{A}_\lambda^{h-1}(B_\lambda[\lambda^{p+1-h}u](t) + K_\lambda[\lambda^{p+1-h}y](t)) + [\lambda^{p+1} w](t) \\
&\vdots \\
[\lambda^{p+f} y](t) &= C\bar{A}_\lambda^{p+f} \xi(t) + \\
&\quad + \sum_{h=1}^{p+f} C\bar{A}_\lambda^{h-1}(B_\lambda[\lambda^{p+f-h}u](t) + K_\lambda[\lambda^{p+f-h}y](t)) + [\lambda^{p+f} w](t)
\end{aligned} \tag{7.28}$$

To the purpose of predictor-based subspace model identification [Chiuso, 2007a], [Chiuso, 2007b], [Bergamasco and Lovera, 2010], it is straightforward to formulate extended linear models for the original models and its innovations form

$$\mathcal{Y}_{[p,p+f]}(t) = \bar{O}_{[p,p+f]}\xi(t) + \Xi_0 \mathcal{Z}_{[p-1,p+f-1]}(t) + \mathcal{W}_{[p,p+f]}(t) \tag{7.29}$$

with

$$\begin{aligned}
\mathcal{Y}_{[p,p+f]}(t) &= \begin{bmatrix} [\lambda^p y](t) & [\lambda^{p+1} y](t) & \cdots & [\lambda^{p+f} y](t) \end{bmatrix} \\
\mathcal{U}_{[p,p+f]}(t) &= \begin{bmatrix} [\lambda^p u](t) & [\lambda^{p+1} u](t) & \cdots & [\lambda^{p+f} u](t) \end{bmatrix} \\
\mathcal{W}_{[p,p+f]}(t) &= \begin{bmatrix} [\lambda^p w](t) & [\lambda^{p+1} w](t) & \cdots & [\lambda^{p+f} w](t) \end{bmatrix} \\
\mathcal{Z}_{[p-1,p+f-1]}(t) &= \begin{bmatrix} [\lambda^{p-1} z](t) & [\lambda^p z](t) & \cdots & [\lambda^{p+f-1} z](t) \\ \vdots & \vdots & \cdots & \vdots \\ [\lambda^0 z](t) & [\lambda z](t) & \cdots & [\lambda^{f-1} z](t) \end{bmatrix}
\end{aligned} \tag{7.30}$$

where

$$z(t) = \begin{bmatrix} u(t) \\ y(t) \end{bmatrix}$$

and parameter matrices

$$\begin{aligned}
\Xi_0 &= \begin{bmatrix} C\bar{A}_\lambda^{p-1}[B_\lambda \quad K_\lambda] & C\bar{A}_\lambda^{p-2}[B_\lambda \quad K_\lambda] & \cdots & \cdots & C[\bar{B}_\lambda \quad K_\lambda] \end{bmatrix} \\
\bar{O}_{[p,p+f]} &= \begin{bmatrix} C\bar{A}_\lambda^{p} & C\bar{A}_\lambda^{p+1} & \cdots & C\bar{A}_\lambda^{p+f} \end{bmatrix}^\mathsf{T}
\end{aligned} \tag{7.31}$$

System identification algorithm

The framework provided permits the reformulation of the PBSID algorithm which was originally developed in discrete-time [Chiuso, 2007a], [Chiuso, 2007b], though with application to continuous-time modeling and identification [Bergamasco and Lovera, 2010]. To this end, consider the finite sequences of (possibly non-uniformly) sampled input-output data $\{u(t_k)\}_0^N, \{y(t_k)\}_0^N$ at sample times $\{t_k\}_0^N$, $t_{k+1} \geq t_k$, $\forall k$. As the regression model of Eq. (7.29) is valid for all times, it is also a valid regression model at sample times $\{t_k\}_0^N$

$$\mathcal{Y}_{[p,p+f]}(t_k) = \bar{O}_{[p,p+f]}\xi(t_k) + \Xi_0 \mathcal{Z}_{[p-1,p+f-1]}(t_k) + \mathcal{W}_{[p,p+f]}(t_k) \tag{7.32}$$

The first term on the right hand-side of Eq. (7.32) contains the sequence of the unknown initial states, which induces a bias to the identification of Ξ_0, the matrix containing the system parameters. Due to the scaling by $\bar{A}_\lambda^p$ this bias can be made arbitrarily small by choosing p sufficiently large as compared to the eigenvalues of $\bar{A}_\lambda$. Actually, this statement holds true because the eigenvalues of $\bar{A}_\lambda$ are inside the disc Ω. Then, the effect of the unknown initial states can be neglected, i.e., $\bar{A}_\lambda^j \in o(1/\sqrt{N})$, $\forall j \geq p$, N number of available samples [Chiuso, 2007a], [Chiuso, 2007b], so that finally we obtain

$$\mathcal{Y}^N_{[p,p+f]} = \Xi_0 \mathcal{Z}^N_{[p-1,p+f-1]} + \mathcal{W}^N_{[p,p+f]} + o(1/\sqrt{N}) \tag{7.33}$$

where

$$\mathcal{Y}^N_{[p,p+f]} = \begin{bmatrix}[\lambda^p y](t_0) & \cdots & [\lambda^p y](t_N) & \cdots & [\lambda^{p+f} y](t_0) & \cdots & [\lambda^{p+f} y](t_N)\end{bmatrix} \tag{7.34}$$

and similarly for $\mathcal{U}^N_{[p,p+f]}, \mathcal{Z}^N_{[p-1,p+f-1]}, \mathcal{W}^N_{[p,p+f]}$. The matrix Ξ_0 is estimated solving the least-squares problem

$$\hat{\Xi}_0 = \arg\min_{\Xi_0, D} || \mathcal{Y}^N_{[p,p+f]} - \Xi_0 \mathcal{Z}^N_{[p-1,p+f-1]} ||_F^2 \tag{7.35}$$

where $|| \cdot ||_F$ stands for the Frobenius norm of a matrix [Golub and Van Loan, 1996]. For finite p the solution of this linear problem will be biased due the approximation made disregarding the initial states. In the LTI literature a number of papers appeared that studied the effect of the window size and although they proved the asymptotic properties of the algorithms (if $p \to \infty$ the bias disappears) it is hard to quantify the effect for finite p [Knudsen, 2001; Chiuso, 2007a; Chiuso, 2007b]. Once the Markov parameters of the system are found in Ξ_0 estimated solving Eq. (7.35), the next step consists in estimating the state sequence. To this

end, consider the following matrix

$$\begin{aligned}\Xi &= \begin{bmatrix} \Xi_0 \\ \Xi_1 \\ \vdots \\ \Xi_{f-1} \end{bmatrix} =, \qquad [B_\lambda \quad K_\lambda] = \bar{B}_\lambda \\ &= \begin{bmatrix} C\bar{A}_\lambda^{p-1}\bar{B}_\lambda & C\bar{A}_\lambda^{p-2}\bar{B}_\lambda & \cdots & \cdots & \cdots & C\bar{B}_\lambda \\ 0 & C\bar{A}_\lambda^{p-1}\bar{B}_\lambda & \cdots & \cdots & \cdots & C\bar{A}_\lambda\bar{B}_\lambda \\ \vdots & \ddots & \ddots & \ddots & \ddots & \vdots \\ 0 & \cdots & 0 & C\bar{A}_\lambda^{p-1}\bar{B}_\lambda & \cdots & C\bar{A}_\lambda^{f-1}\bar{B}_\lambda \end{bmatrix}\end{aligned} \tag{7.36}$$

and

$$\bar{O}_{[0,p-1]} = \begin{bmatrix} C \\ C\bar{A}_\lambda \\ C\bar{A}_\lambda^2 \\ \vdots \\ C\bar{A}_\lambda^{p-1} \end{bmatrix} \tag{7.37}$$

It holds

$$\bar{O}_{[0,p-1]}\mathcal{X}^N_{[p,p]} = \Xi\mathcal{Z}^N_{[p-1,p-1]} \tag{7.38}$$

By singular value decomposition

$$\Xi\mathcal{Z}^N_{[p-1,p-1]} = \begin{bmatrix} U & U_\perp \end{bmatrix} \begin{bmatrix} \Sigma_n & 0 \\ 0 & \Sigma \end{bmatrix} \begin{bmatrix} V \\ V_\perp \end{bmatrix} \tag{7.39}$$

the state can be estimated:

$$\mathcal{X}^{\hat{N}}_{[p,p]} = \Sigma_n V \tag{7.40}$$

From the output equation in Eq.(7.27) an estimate of C can be obtained by means of least-squares estimation, i.e.,

$$\hat{C} = \arg\min_C \| \mathcal{Y}^N_{[p,p]} - C\mathcal{X}^N_{[p,p]} \|^2_F \tag{7.41}$$

as well as the innovation sequence

$$\mathcal{W}^N_{[p,p]} = \mathcal{Y}^N_{[p,p]} - \hat{C}\hat{\mathcal{X}}^N_{[p,p]} \tag{7.42}$$

Finally, the matrices $A_\lambda, B_\lambda, K_\lambda$ are found solving the least-squares problem

$$\hat{A}_\lambda, \hat{B}_\lambda, \hat{K}_\lambda = \arg\min_{A_\lambda, B_\lambda, K_\lambda} \| \hat{\mathcal{X}}^N_{p+1,p} - A_\lambda\hat{\mathcal{X}}^N_{p,p-1} - B_\lambda\mathcal{U}^N_{p,p-1} - K_\lambda\mathcal{W}^N_{p,p-1} \|^2_F \tag{7.43}$$

A summary of the steps carried out in the identification procedure is reported in Algorithm 7.1.

ALGORITHM 7.1—PBSID [CHIUSO, 2007A], [CHIUSO, 2007B], [BERGAMASCO AND LOVERA, 2010]

1. Construct the matrices $\mathcal{U}^N_{[p,p+f]}, \mathcal{Y}^N_{[p,p+f]}, \mathcal{Z}^N_{[p-1,p+f-1]}$ according to Eq. (7.34)
2. Solve Eq.(7.35) for $\hat{\Xi}_0$
3. Compute the SVD in Eq.(7.39)
4. Choose the model order by inspecting the singular values from step (3)
5. Get the estimated state-sequence $\hat{\mathcal{X}}^N_{[p,p]}$ using Eq.(7.40)
6. With $\hat{\mathcal{X}}^N_{[p,p]}$ solve Eq.(7.41)
7. Compute the innovation sequence from Eq.(7.42)
8. Obtain $A_\lambda, B_\lambda, K_\lambda$ solving the least-squares in Eq.(7.43)
9. Calculate the state-space matrices A, B, K by means of the relations in Eq.(7.22,7.26) □

7.4 System realization

ALGORITHM 7.2—SYSTEM REALIZATION [HO AND KALMAN, 1966; JOHANSSON ET AL., 1999; JOHANSSON, 2010]

1. Use linear regression to find a truncated multivariable transfer function

$$G^m(\lambda(s)) = \sum_{k=0}^{m} G^m_k \lambda^k \tag{7.44}$$

where the prediction error

$$\varepsilon(t,\theta) = y(t) - \underbrace{\begin{pmatrix} G^m_1 & \dots & G^m_m \end{pmatrix}}_{\theta} \begin{pmatrix} [\lambda^1 u](t) \\ \vdots \\ [\lambda^m u](t) \end{pmatrix}$$

be minimized at the set of sample times $\{t_k\}_{k=1}^N$ by least-squares estimation of θ or $\{G^m_k\}_{k=1}^m$.

2. For suitable numbers q, r, s such that $r+s \leq N$ arrange the Markov parameters in the Hankel matrix

$$G_{r,s}^{(q)} = \begin{bmatrix} G_{q+1} & G_{q+2} & \cdots & G_{q+s} \\ G_{q+2} & G_{q+3} & \cdots & G_{q+s+1} \\ \vdots & \vdots & \ddots & \vdots \\ G_{q+r} & G_{q+r+1} & \cdots & G_{q+r+s-1} \end{bmatrix} \tag{7.45}$$

3. Determine rank n and resultant system matrices

$$G_{r,s}^{(0)} = U\Sigma V^T \text{ (SVD)} \tag{7.46}$$

$$E_y^T = [I_{p\times p} \quad 0_{p\times(r-1)p}] \tag{7.47}$$

$$E_u^T = [I_{m\times m} \quad 0_{m\times(s-1)m}] \tag{7.48}$$

$$\Sigma_n = \text{diag}\,\{\sigma_1, \sigma_2, \ldots, \sigma_n\} \tag{7.49}$$

$$U_n = \text{matrix of first } n \text{ columns of } U \tag{7.50}$$

$$V_n = \text{matrix of first } n \text{ columns of } V \tag{7.51}$$

Finally, calculate the state-space matrices

$$A_n = \Sigma_n^{-1/2} U_n^T G_{r,s}^{(1)} V_n \Sigma_n^{-1/2}, \quad \widehat{A} = \frac{1}{\tau}(A_n - I) \tag{7.52}$$

$$B_n = \Sigma_n^{1/2} V_n^T E_u, \quad \widehat{B} = \frac{1}{\tau} B_n \tag{7.53}$$

$$C_n = E_y^T U_n \Sigma_n^{1/2}, \quad \widehat{C} = C_n \tag{7.54}$$

$$D_n = G_0, \quad \widehat{D} = D_n \tag{7.55}$$

which yields the nth-order state-space realization

$$\begin{aligned} \dot{x}(t) &= \widehat{A}x(t) + \widehat{B}u(t) \\ y(t) &= \widehat{C}x(t) + \widehat{D}u(t) \end{aligned} \tag{7.56}$$

□

Remark: A similar algorithm is obtained by replacing Steps 3-4 by balanced model reduction of the system

$$\tau \dot{x}_u = A_\lambda x_u + B_\lambda u, \tag{7.57}$$

$$y = \widehat{C}x_u, \quad \widehat{C} = \begin{pmatrix} G_1^m \ldots G_2^m & 0 \ldots 0 \end{pmatrix} \tag{7.58}$$

with the regressor-state vector

$$x_u = \begin{pmatrix} [\lambda^1 u] \\ [\lambda^2 u] \\ \vdots \\ [\lambda^n u] \end{pmatrix} \tag{7.59}$$

and A_λ, B_λ according to Eq. (7.22).

7.5 Discussion and conclusions

This chapter considered identification methods for continuous-time state-space models using discrete-time data. The transformation by means of λ allows an exact reparametrization of a continuous-time transfer function. High-frequency dynamics and low-frequency dynamics thus appear without distortion in the mapping from input to output. The low-pass filters implemented for the estimation model have a filtering effect in producing regressor variables for identification. In this context, other filtering approaches such as the Poisson moment functional (PMF) or the Laguerre polynomials may be used [Unbehauen and Rao, 1990; Young, 1969; Young, 1981a]. Implementation of the operator λ may be done as continuous-time filters, discrete-time filters or by means of numerical integration methods [Johansson, 1994].

In the PBSID approach, four parameters have to be chosen : (i) the low-pass filter pole location $1/\tau$, (ii) the system order n, (iii) the length of the past horizon p and (iv) the length of the future horizon f. The parameter τ is related to the expected bandwidth ω_b of the system to identify, and should be chosen $1/\tau \geq \omega_b$ so that the input-output signals are not attenuated within ω_b. As far as the model order n is concerned, it is selected by inspection of the singular values form the SVD of $\Xi \mathcal{Z}^N_{[p-1,p-1]}$. The length of the past horizon p, $p \geq n$ has to be estimated from data, e.g., using standard criterions for VARX model order estimation [Peternell, 1995; Chiuso, 2007b]. A suitable future horizon f can be taken $f \leq p$, as suggested in [Chiuso, 2010]. Statistical consistency analysis is left to future work. Application of the methods presented in this chapter to the diabetes metabolism modeling will be dealt with in Chapter 8.

8

Impact of Meal and Insulin Intakes on Glycemia

8.1 Introduction

One of the main limiting factors in improving glucose control for T1DM subjects is the lack of a precise description of meal and insulin intake effects on blood glucose. The knowledge of magnitude and duration of such effects would be useful not only for patients and physicians when deciding upon the most suitable therapy, but also for the development of a controller targeting glycemia regulation (Chapter 2). In current medical practice, indeed, the calculation of insulin doses and eventually extra carbohydrate intakes needed to maintain normoglycemia is roughly based on empirical rules-of-thumbs taking into account patients personal knowledge of his/her own metabolism, expected future glycemia evolution and approximation of the estimated meal carbohydrate content effects as well as insulin impact on the subject own blood glucose. Actually, there is the need of a mathematical model able to describe blood glucose evolution in response to the main driving sources, i.e., a meal intake and an insulin dose. To date several types of glucose metabolism models, both first principle- and data-based, have been proposed to this purpose (see Chapter 2 for a review). However, as pointed out in Chapter 4, less attention has been dedicated to the fundamental aspects of estimating physiologically plausible and qualitatively correct signs and time constants of the identified models impulse responses. In addition, desirable features of a glucose metabolism model would include a clinician-friendly structure and few tunable parameters with physiological meaning.

Therefore, in this chapter we focus on estimating low-complexity yet physiologically sound and individualized multi-input single-output (MISO) models of the glucose metabolism in T1DM able to reflect the basic dy-

namical features of the glucose-insulin metabolic system in response to a meal intake or an insulin injection. The models are continuous-time second-order transfer functions relating the amount of carbohydrate of a meal and the insulin units of the accordingly administered dose (inputs) to plasma glucose evolution (output) and consist of few parameters clinically relevant to be estimated.

The estimation strategy was continuous-time data-driven system identification and exploited a database in which meals and insulin boluses are separated in time, allowing the unique identification of the model parameters.

8.2 Data

In order to separately estimating meal and insulin impacts on blood glucose dynamics, the lack of input excitation observed in almost all the data-sets treated in the literature [Finan et al., 2009] must be overcome. Suitable data were collected in the framework of DIAdvisor ™ [DIAdvisor, 2012] during DIAdvisor II trial, *Visit 2* and day 3 in *Visit 3* (see Chapter 3 for details). We recall here in passing that the appealing feature of such data was due to the scheduled 2-hours time split between carbohydrate and insulin intakes. The CGMS data were used as measurements of glycemia, because the sensor measurements were more numerous than the blood samples and compared well with the YSI [Yellow Spring Instruments, 2013] measurements (see Table 3.7 for accuracy analysis). Figures 8.4-8.6 show representative patients records, the remaining patients in the population behaved similarly. Data collected during *Visit 2* were used for identification of the model parameters, whereas cross validation was performed on those gathered in *Visit 3*.

8.3 Model structure

Second-order linear transfer function models with time delays were proposed to approximate the behaviour of glucose in response to inputs, namely meal and insulin intakes. The choice was based on the analysis of the data collected and was motivated by physiology as follows. During the night hours, up until breakfast, the blood glucose levels were almost constant (see Fig. 8.1), due to the overnight fast and the sleep. The glucoregulatory system could be considered, therefore, at steady state. At 8.00 am a 40 [g] carbohydrate input was applied to the system, corresponding to breakfast. As a consequence, glucose concentration raised (Fig. 8.1, 8.4, 8.6). During the next two hours following breakfast, no other actions

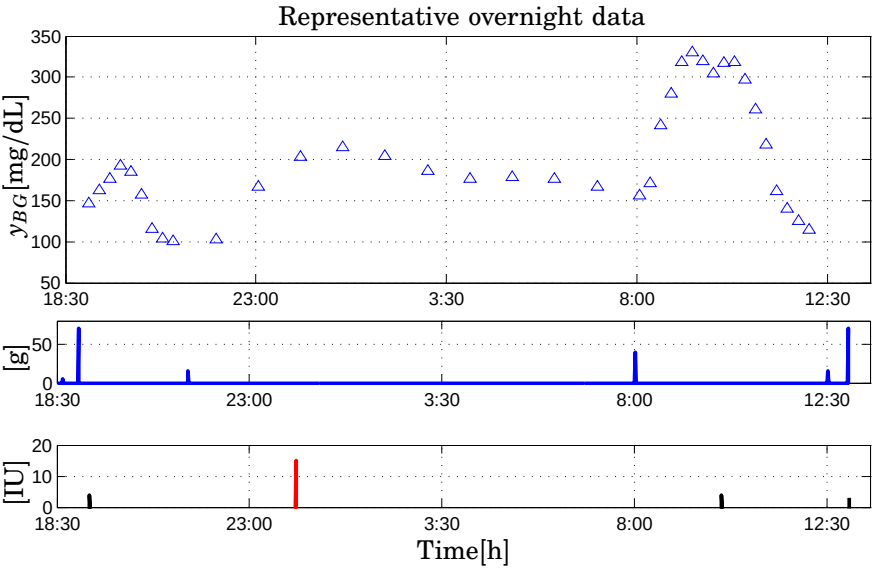

Figure 8.1 Patient UNIPD219. DIAdvisor II trial, *Visit 3*. *Top* Actual YSI (triangle) [mg/dL]; *Center* Carbohydrate intake [g]; *Bottom* Insulin [IU]: bolus (blue), basal (red). All the measurements vs. time of the day [h]

were taken, allowing to characterize the effects of carbohydrate on blood glucose. For some patients plasma glucose concentration began to fall after about 90 minutes from carbohydrate ingestion (e.g., patient UNIPD219 in Figs. 8.4, 8.10) suggesting the presence of 2 poles in the transfer function from carbohydrate to blood glucose, one faster than the other. For other patients, plasma glucose didn't fall during the time interval 8.00 am to 10.00 am (e.g., patient IKEM326 in Figs. 8.6, 8.10) leading to the assumption of an integrator term in the transfer function as glucose storage term. At 10.00 am, the second input, i.e., the insulin dose–which was previously calculated by the patient, was administered, making glucose concentration to clearly fall for both the previously described type of subjects with an integrator-like behaviour (Figs. 8.4, 8.6, 8.10). Further, a time delay associated with both inputs was observed in each of the data series and incorporated in the model structure. It is well known from physiology, indeed, that there are time delays accounting for glucose intestinal absorption dynamics and insulin pharmacokinetics/pharmacodynamics. In contrast to most of the existing models in the literature (see Section 2.4 for an overview), we did not use

any compartment model for the description of the rate of appearance in plasma following a food intake, nor for the subcutaneous depots-to-plasma insulin dynamics, as we did in Chapter 4. By doing this, the limitations introduced by the nonlinear nature of such models [Dalla Man et al., 2007] could be overcome and most importantly the issues related to the complex tracer experiments needed to collect the appropriate data required to fit the unknown parameters of those models to the individuals didn't require attention any longer. Rather, the meal input was represented by a pulse of the duration of 15 minutes (since the food was completely ingested by the patients within 20 minutes at maximum to comply with the clinical protocol), applied at the time instant $t_{carb} = 8.00$ am, while the insulin injection was considered an impulse-formed input applied at time instant $t_{ins} = 10.00$ am. All these facts, led us to the formulation of the following model structure:

$$Y_{BG}(s) = G_{carb}(s)u_{carb}(s) + G_{ins}(s)u_{ins}(s) \tag{8.1}$$

where $Y_{BG}(s)$ is the Laplace transform of the output blood glucose concentration, $u_{carb}, u_{ins} \in \mathbb{Z}_+$ are the inputs carbohydrate amount and insulin doses, respectively, while the transfer functions from carbohydrate to blood glucose $G_{carb}(s)$ and from insulin to blood glucose $G_{ins}(s)$ are given in Eqs. 8.2 and 8.3, respectively:

$$G_{carb}(s) = e^{-s\tau_{carb}} \frac{K_{carb}}{(1 + sT_{carb,1})(1 + sT_{carb,2})} \tag{8.2}$$

$$G_{ins}(s) = e^{-s\tau_{ins}} \frac{K_{ins}}{s(1 + sT_{ins})} \tag{8.3}$$

Further, K_{carb} [mg/dL/g] and K_{ins} [mg/dL/IU] are the gains and $T_{carb,1}$, $T_{carb,2}$, T_{ins} [min] the time constants governing rise and fall, respectively, of plasma glucose, while τ_{carb}, τ_{ins} [min] are the time delays associated with carbohydrate and insulin appearance in plasma, respectively. Actually, for the type of patients depicted in Figure 8.6, $T_{carb,2} = \infty$ and the transfer function becomes:

$$G_{carb}(s) = e^{-s\tau_{carb}} \frac{K_{carb}}{s(1 + sT_{carb,1})} \tag{8.4}$$

The proposed model structure has some interesting properties. First of all it is simple, containing only a few parameters to be identified from data. $K_{carb}, T_{carb,1}, T_{carb,2}$ can be related to glucose tolerance, i.e., how the body metabolizes glucose, K_{ins}, T_{ins} can be related to insulin sensitivity or resistance, i.e., how effective is insulin in lowering blood sugar levels. Moreover, τ_{carb}, τ_{ins} account for food transportation and

absorption along the gastro-intestinal tract and insulin transit from the subcutaneous tissues to plasma, respectively. All these factors are of uttermost importance in diabetes treatment and failure to estimate them correctly leads to unsuccessful glucose control. We believe this type of model is easy to understand by practitioners, since all the parameters can be given a clinical interpretation. In particular, it would be straightforward for a physician to assess whether a model is physiologically plausible or not.

Identification of the parameters

Our objective was to estimate the unknown parameter vector

$$\hat{\theta} = \begin{bmatrix} \hat{K}_{carb} & \hat{K}_{ins} & \hat{T}_{carb,1} & \hat{T}_{carb,2} & \hat{T}_{ins} & \hat{\tau}_{carb} & \hat{\tau}_{ins} \end{bmatrix} \tag{8.5}$$

so that the estimation error between the actual blood glucose data $y_{BG}(t)$ and the simulated model data $\hat{y}_{BG}(t)$ was minimized in a least-squares sense:

$$\hat{\theta} = \arg\min_{\theta} \int_0^T (y_{BG}(t) - \hat{y}_{BG}(t,\theta))^2 dt \tag{8.6}$$

where t is the continuous-time index and $T = 5$ [h], i.e., time interval 8.00 am-1.00 pm, subject to some constraints on θ, namely $\hat{K}_{carb} > 0$, $\hat{K}_{ins} < 0$ to guarantee qualitatively correct responses to inputs (blood glucose increases after a meal intake and decreases after an insulin shot) and $\hat{T}_{carb,1}, \hat{T}_{carb,2}, \hat{T}_{ins} > 0$ to guarantee stability. The equilibrium glycemia level, i.e., the value of blood glucose just before breakfast was administered, was subtracted from the data series. Subsequently, the meal test data sequences were splitted into 2 parts: the interval $[8.00 + \tau_{carb}, 10.00 + \tau_{ins})$ for the estimation of $G_{carb}(s)$ and the interval $[10.00 + \tau_{ins}, 13.00]$ for that of $G_{ins}(s)$, the time delays being determined empirically. The continuous-time predictor-based identification algorithm $\text{PBSID}_{\text{cont}}$ shown in Chapter 7 was applied to the first portion of the data and the parameters K_{carb}, $T_{carb,1}, T_{carb,2}$ were estimated. Next, the effect of such carbohydrate intake predicted by the identified model if no insulin would have been taken at 10.00 am was removed (black dotted curve in Figs. 8.4, 8.6) and the PBSID_{cont} algorithm applied to the resulting data in order to get an estimate of K_{ins}, T_{ins}.

Up to 6% missing CGMS data points for one single subject was reported; however, this didn't play a major role as the continuous-time set-up for the identification can handle non-uniformly sampled records.

The user parameters were chosen as follows:

- $\tau = 10$ was selected at first, then refined by trial and error
- $n = 2$

- $p = 3$
- $f = 3$

8.4 Results

Figures 8.2 and 8.3 show the Bode diagrams for the estimated transfer functions. Table 8.1 summarizes the estimated parameters for all the patients, while the distribution of the parameters can be seen in Fig. 8.12. Figures 8.4 and 8.6 presents simulation results on identification data for the representative patients. In particular, the actual CGMS data used for model parameters identification is compared with the glycemia level predicted by the meal model when no insulin is taken and the estimated glycemia level resulting from the application of both meal and insulin model. Figures 8.5 and 8.7 show the response to 10 [g] of carbohydrate and to 1 [IU] predicted by the models for the representative patients. Notice that, without loss of generality, the equilibrium level at the start of the simulation was chosen as the actual CGMS value at the beginning of the breakfast as far as the carbohydrate response is concerned, and as the highest glucose peak for insulin response.

Validation was performed on the second admission set of data. The YSI measurements were taken as glycemia assessment, due to poorer CGM data (see Chapter 3). We recall in passing that *Visit 3* in the DIAdvisor II trial took place 14 ± 3 days after *Visit 2* and that in the days prior to the test the subjects glucoregulatory system were challenged by an exercise test and a big lunch containing 100 [g] carbohydrate. Validation results are shown in Fig. 8.10 for the representative patients. In the above mentioned figures, the simulated glycemia is compared to both the actual CGMS data and YSI data. Additional figures reproducing simulation results for patients UNIPD201 and IKEM306 are given in Appendix D.

As for performance assessment, the following metrics were considered:

- Percentage Variance Accounted For (VAF):

$$\text{VAF} = \left(1 - \frac{\mathcal{E}[(y_{BG}(t) - \hat{y}_{BG}(t))(y(t) - \hat{y}_{BG}(t))^\intercal]}{\mathcal{E}[y_{BG}(t)y^\intercal(t)]}\right) \times 100\%$$

  where $\mathcal{E}[\cdot]$ denotes mathematical expectation.

- Root Mean Square Error (RMSE) [mg/dL]:

$$\text{RMSE} = \sqrt{\frac{(y_{BG}(t) - \hat{y}_{BG}(t))(y_{BG}(t) - \hat{y}_{BG}(t))^\intercal}{N}}$$

  where N denotes the number of samples.

Results of performance statistics compared across the population are presented in Tables 8.2 and 8.3 and in Figs. 8.8 and 8.9.

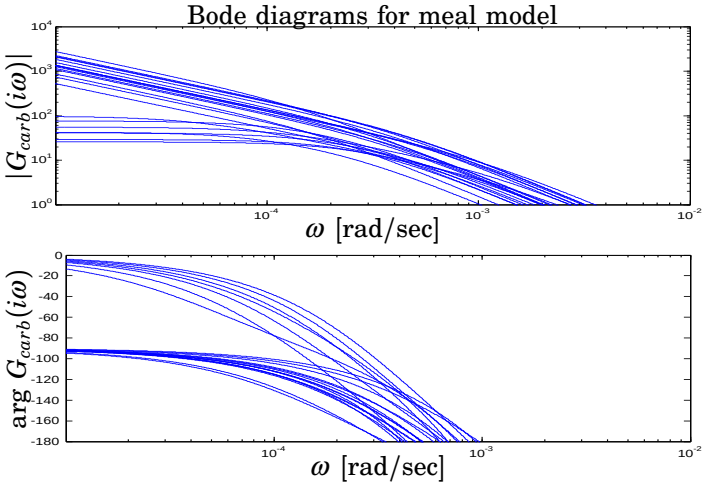

Figure 8.2 Bode diagrams of the estimated transfer functions for all the subjects participating in the trial, from meal carbohydrate [g] to blood glucose [mg/dL]: *Top* Magnitude *Bottom* Phase

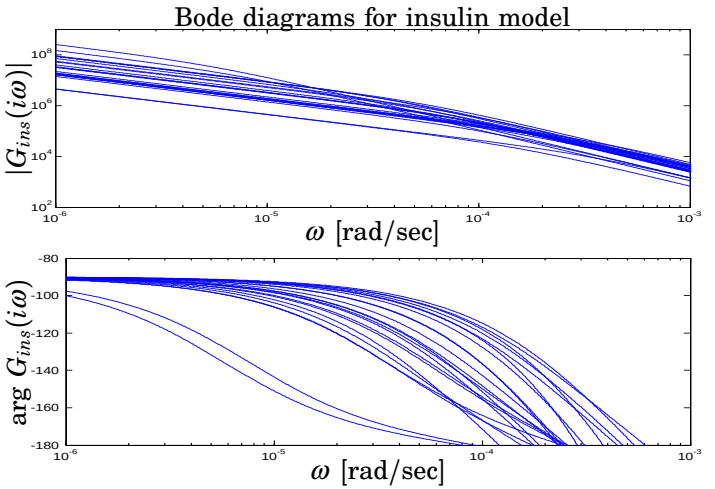

Figure 8.3 Bode diagrams of the estimated transfer functions for all the subjects participating in the trial, from insulin dose [IU] to blood glucose [mg/dL]: *Top* Magnitude *Bottom* Phase

Table 8.1 Estimated model parameters

Patient ID	τ_{carb}	K_{carb}	$T_{carb,1}$	$T_{carb,2}$	τ_{ins}	K_{ins}	T_{ins}
CHU101	30	42.78	58.85	185.85	10	-16.35	72.40
CHU107	20	6.27	34.1	∞	30	-85.46	380.5
CHU117	15	29.23	55.05	62.5	20	-90.09	45.65
CHU118	15	25.81	37.5	63.10	30	-17.58	85.95
CHU125	20	3.96	54.25	∞	20	-55.27	220.75
CHU136	25	40.94	33.10	99.40	15	-21.88	88.70
CHU138	25	2.58	92.75	∞	50	-4.50	500
CHU143	20	4.07	22.85	∞	10	-70.51	474.75
CHU144	20	8.29	111.70	∞	15	-85.41	294.1
CHU145	25	2.21	53.35	∞	40	-4.40	107.15
UNIPD201	15	75.91	60.05	132.25	40	-33.56	209.20
UNIPD217	15	3.79	16	∞	15	-254.38	2942
UNIPD219	30	55.20	13.7	138.1	15	-18.45	77.65
UNIPD233	25	97.83	11.90	357.1	15	-146.38	2172
UNIPD234	10	4.09	26.4	∞	30	-19.05	53.4
IKEM302	35	3.44	38.6	∞	15	-16.76	59.3
IKEM306	20	6.74	44.95	∞	15	-39.63	277.75
IKEM309	25	6.45	34.40	∞	60	-51.99	298.15
IKEM311	15	5.53	42.05	∞	25	-31.47	196.05
IKEM324	20	3.23	45.9	∞	40	-32.43	182.25
IKEM326	20	4.69	55.55	∞	45	-16.05	100.1
IKEM330	45	1.57	20.2	∞	25	-13.90	161.45

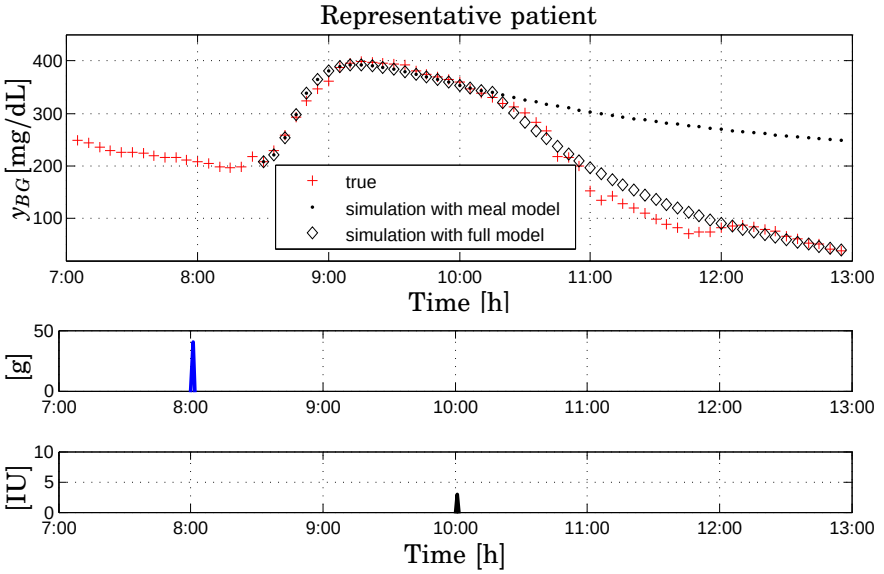

Figure 8.4 Patient UNIPD219. DIAdvisor II trial, *Visit 2*, meal test. *Top* Actual CGMS (star) vs. simulated breakfast impact (dot) and simulated joint meal and insulin intakes (diamond) [mg/dL]; *Center* Carbohydrate intake [g]; *Bottom* Insulin bolus [IU]. All the measurements vs. time of the day [h]

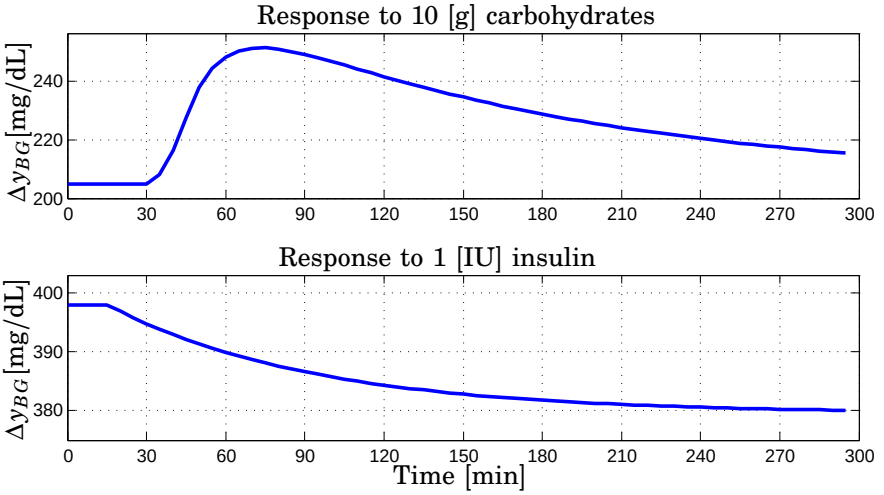

Figure 8.5 Patient UNIPD219. Response to *Top* 10 [g] of carbohydrate *Bottom* 1 [IU] of insulin. Blood glucose excursion [mg/dL] vs. time [min]

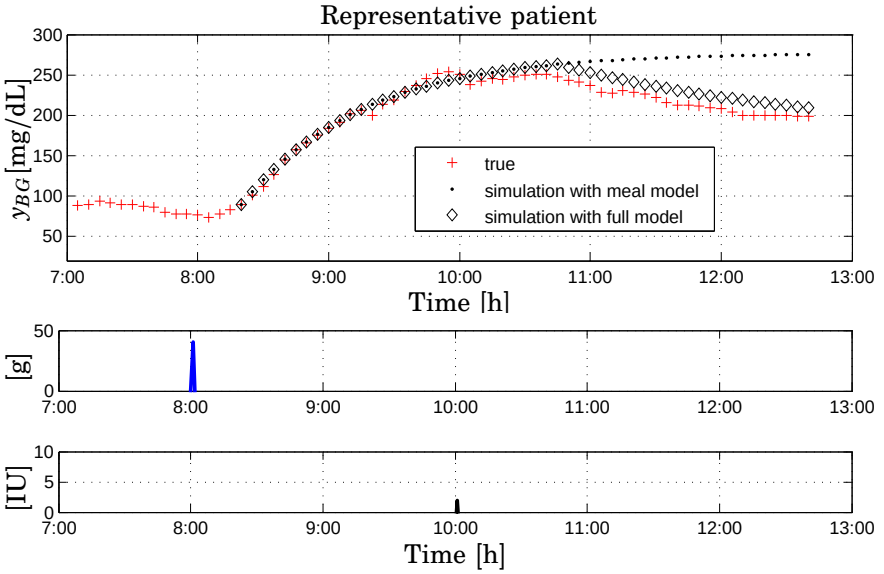

Figure 8.6 Patient IKEM326. DIAdvisor II trial, *Visit 2*, meal test. *Top* Actual CGMS (star) vs. simulated breakfast impact (dot) and simulated joint meal and insulin intakes (diamond) [mg/dL]; *Center* Carbohydrate intake [g]; *Bottom* Insulin bolus [IU]. All the measurements vs. time of the day [h]

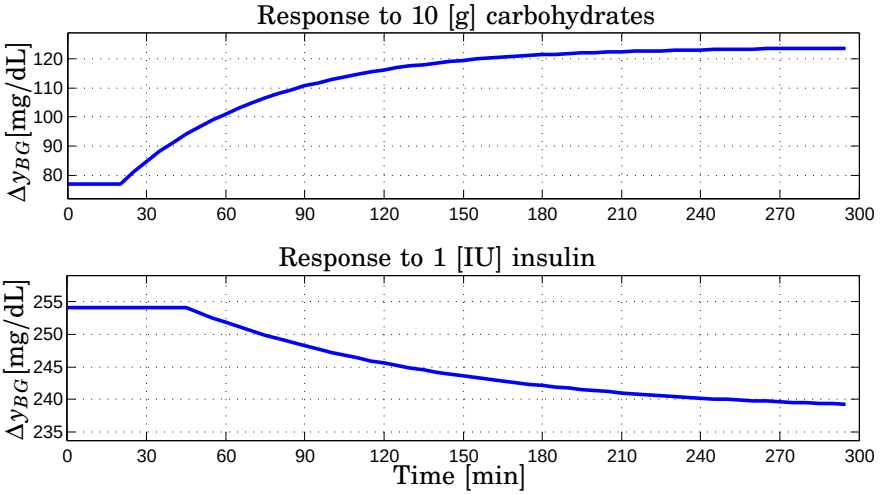

Figure 8.7 Patient IKEM326. Response to *Top* 10 [g] of carbohydrate *Bottom* 1 [IU] of insulin. Blood glucose excursion [mg/dL] vs. time [min]

Table 8.2 Carbohydrate impact modeling: performance evaluation. Infinite horizon prediction

	On estimation data		On validation data	
Patient ID	VAF [%]	RMSE [mg/dL]	VAF [%]	RMSE [mg/dL]
CHU101	96.05	4.99	n/a	n/a
CHU107	96.30	22.81	n/a	n/a
CHU117	91.35	10.81	81.84	35.90
CHU118	91.71	13.42	39.37	42.56
CHU125	97.08	11.38	n/a	n/a
CHU136	92.90	16.03	n/a	n/a
CHU138	96.59	6.19	79.58	24.30
CHU143	92.27	21.75	78.09	51.57
CHU144	99.81	6.60	n/a	n/a
CHU145	97.83	5.62	n/a	n/a
UNIPD201	98.97	6.40	94.81	16.63
UNIPD217	92.21	14.67	86.84	25.99
UNIPD219	97.62	8.61	69.11	151.33
UNIPD233	95.92	9.94	69.46	42.74
UNIPD234	93.19	22.18	73.96	36.94
IKEM302	95.48	12.64	71.39	53.50
IKEM306	99.17	11.25	67.74	21.20
IKEM309	92.38	19.98	82	79.49
IKEM311	93.98	28.16	n/a	n/a
IKEM324	98.09	6.79	70.37	52.35
IKEM326	98	7.98	77.97	127.82
IKEM330	94.49	5.64	n/a	n/a
MEAN	95.51	12.44	74.46	54.45

n/a: not available data set

Table 8.3 Insulin impact modeling: performance evaluation. Infinite horizon prediction.

	On estimation data		On validation data	
Patient ID	VAF [%]	RMSE [mg/dL]	VAF [%]	RMSE [mg/dL]
CHU101	95.63	18.08	n/a	n/a
CHU107	99.75	1.65	n/a	n/a
CHU117	98.52	6.58	73.09	168.34
CHU118	98.96	3.90	53.89	176.58
CHU125	99.35	2.64	n/a	n/a
CHU136	97.27	6.69	n/a	n/a
CHU138	98.71	3.01	42.19	48.45
CHU143	98.88	4.36	71.87	91.22
CHU144	98.98	12.48	n/a	n/a
CHU145	97.17	2.88	n/a	n/a
UNIPD201	99.49	5.88	22.88	141.93
UNIPD217	99.30	7.38	64.71	116.17
UNIPD219	89.79	20.90	62.75	99.71
UNIPD233	97.70	10.47	57.61	202.78
UNIPD234	96.17	14.16	11.57	98.11
IKEM302	97.39	15.35	86.93	182.47
IKEM306	99.81	2.58	63.67	57.71
IKEM309	94.40	8.63	71.34	56.68
IKEM311	97.89	10.47	n/a	n/a
IKEM324	98.16	4.44	20.58	134.16
IKEM326	98.47	2.71	74.45	46.67
IKEM330	98.44	2.96	n/a	n/a
MEAN	97.73	7.64	62.67	115.78

n/a: not available data set

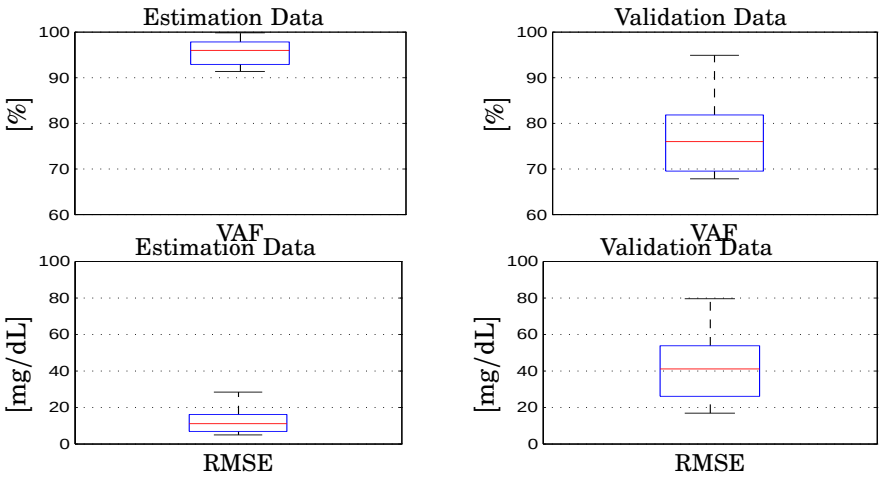

Figure 8.8 Population results. Carbohydrate impact modeling. Infinite horizon prediction. *Top Panels* VAF [%]; *Bottom Panels* RMSE [mg/dL]. *Left* Performances evaluated on *Visit 2* meal test (estimation) data; *Right* Performances evaluated on *Visit 3* meal test (validation) data. Each box presents results achieved over the population. The central mark is the median, the edges of the box are the 25th and 75th percentiles.

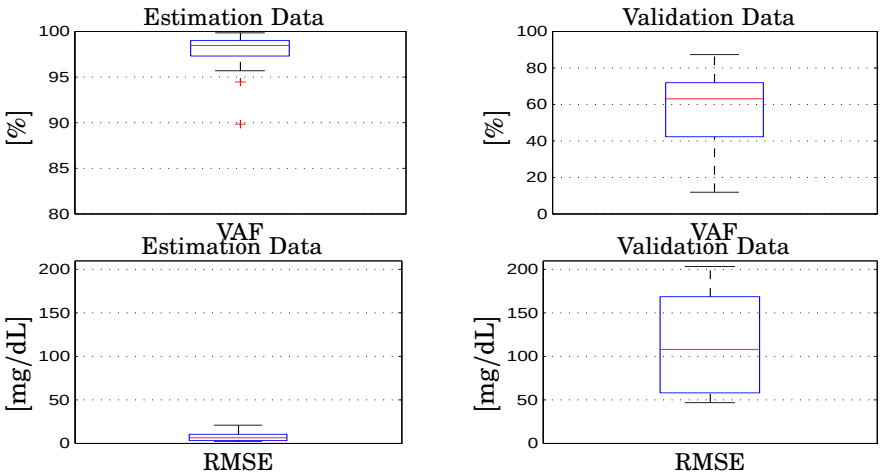

Figure 8.9 Population results. Insulin impact modeling. Infinite horizon prediction. *Top Panels* VAF [%]; *Bottom Panels* RMSE [mg/dL]. *Left* Performances evaluated on *Visit 2* meal test (estimation) data; *Right* Performances evaluated on *Visit 3* meal test (validation) data. Each box presents results achieved over the considered population. The central mark is the median, the edges of the box are the 25th and 75th percentiles.

Table 8.4 Meal model. Time required to reach 95% of maximum peak.

Patient ID	$\tau_{carb} + 3T_{carb}$ [min]
CHU107	122
CHU125	183
CHU138	303
CHU143	88
CHU144	355
CHU145	185
UNIPD217	63
UNIPD234	89
IKEM302	151
IKEM306	155
IKEM309	128
IKEM311	141
IKEM324	158
IKEM326	187
IKEM330	106
MEAN±SD	160.9±78.3

Table 8.5 Meal model. Time required to reach the maximum peak.

Patient ID	[min]
CHU101	110
CHU117	70
CHU118	60
CHU136	65
UNIPD201	100
UNIPD219	50
UNIPD233	55
MEAN±SD	72.85±23.06

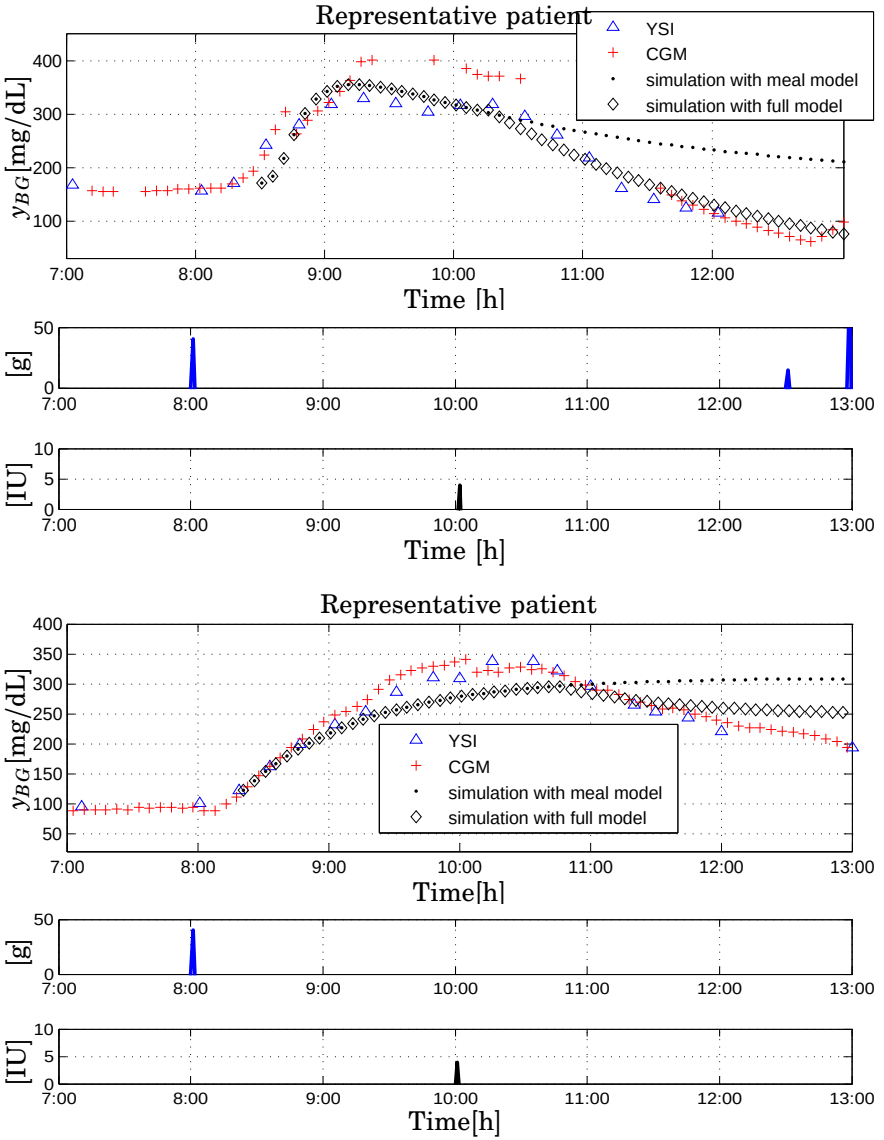

Figure 8.10 Cross validation. DIAdvisor II trial, *Visit 3*, meal test. *Top panels* Patient UNIPD219; *Bottom panels* Patient IKEM326. *Top* Actual CGMS (cross) and actual YSI (triangle) vs. simulated breakfast impact (dot) and simulated joint meal and insulin intakes (diamond) [mg/dL]; *Center* Carbohydrate intake [g]; *Bottom* Insulin bolus [IU]. All the measurements vs. time of the day [h]

Table 8.6 Insulin model. Time required to reach 95% of maximum peak.

Patient ID	$\tau_{ins} + 3T_{ins}$ [min]
CHU101	227
CHU107	1171
CHU117	157
CHU118	288
CHU125	682
CHU136	281
CHU138	1550
CHU143	1434
CHU144	897
CHU145	361
UNIPD201	668
UNIPD217	8843
UNIPD219	248
UNIPD233	6666
UNIPD234	190
IKEM302	193
IKEM306	848
IKEM309	954
IKEM311	613
IKEM324	588
IKEM326	345
IKEM330	510
MEAN±SD	1259.7±2165.8

8.5 Realization-based identification

Application of Algorithm 2 derived in Chapter 7 was successful in accurate modeling of the blood glucose concentration response to meals and insulin. Figure 8.11 shows an example of non-uniformly sampled diabetic blood glucose concentration $y_{BG}(t)$, continuous-time model output $\widehat{y}_{BG}(t)$ and model error $y_{BG}(t) - \widehat{y}_{BG}(t)$, in response to food input u_{carb}, insulin input u_{ins} with regressors for $\tau = 10$ [min], $n = 4$ and $m = 10$. The error $\mathcal{L}_2$ norm of the open-loop model response to inputs was less than 1% of the output $\mathcal{L}_2$ norm for model order $n = 4$. A good result is that a model with good fit for both inputs is found with a short experiment and few data. Whereas the inputs are separated in time and thus not correlated, however, excitation is barely acceptable and the few input-output data points available limit the statistical accuracy.

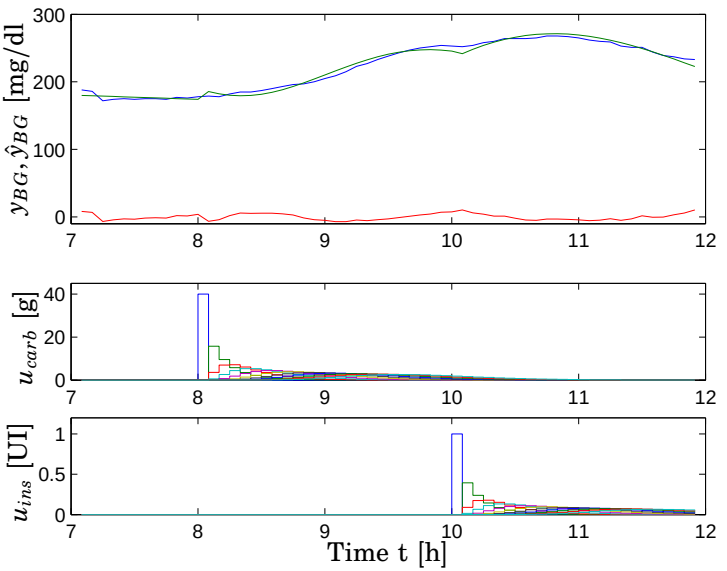

Figure 8.11 Non-uniformly sampled diabetic blood glucose concentration $y_{BG}(t)$ (*upper, blue*), continuous-time model output $\hat{y}_{BG}(t)$ (*upper, green*), model error $y_{BG}(t) - \widehat{y}_{BG}(t)$ (*upper, red*), in response to food input u_{carb} (*middle*), insulin input u_{ins} (*lower*) with regressors for $\tau = 10$ [min], $n = 4$ and $m = 10$.

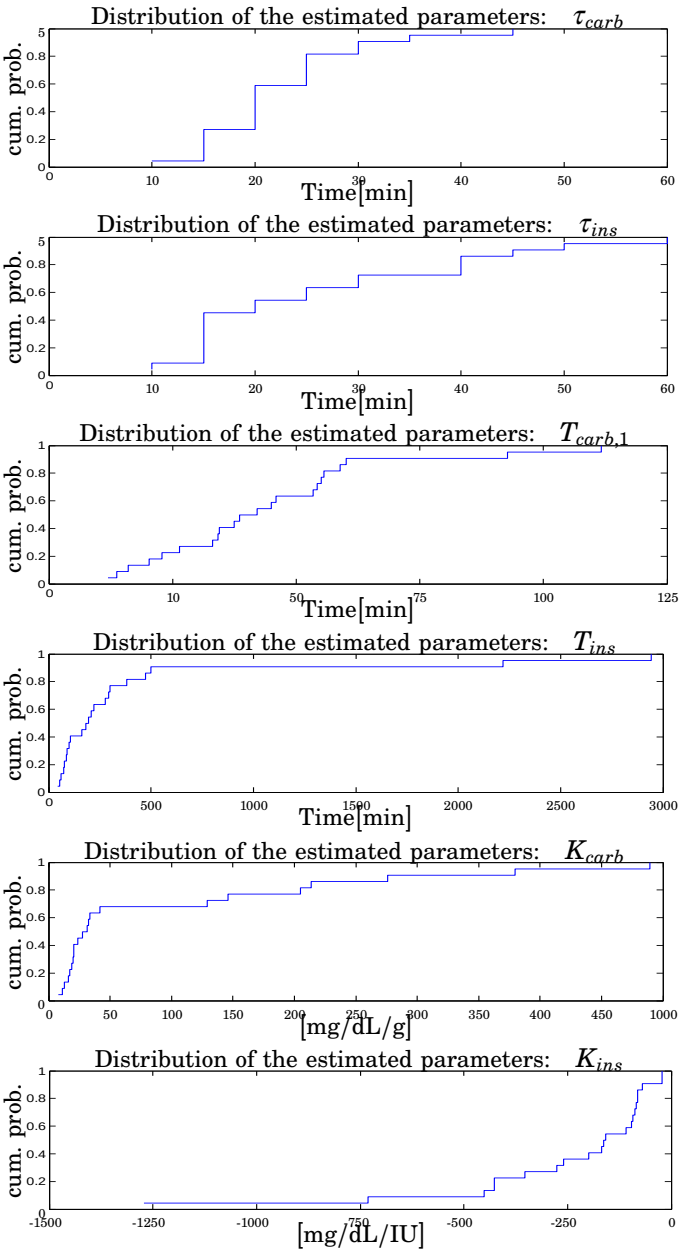

Figure 8.12 Empirical distribution of the parameters. *Top panel* τ_{carb} and τ_{ins}; *Center panel* $T_{carb,1}$ and T_{ins}; *Bottom panel* K_{carb} and K_{ins}. Notation: cum. prob. stands for cumulative probability.

8.6 Discussion

Continuous-time transfer function models of second order with time delays were proposed to quantify the impact of a carbohydrate intake and an insulin injection on blood glucose dynamics. The choice of the model structure was motivated by inspection of the data series for the available 6 hours test with a physiologically sound interpretation. The glucoregulatory system was considered at steady-state during the overnight fast up until breakfast (see Fig. 8.1 for overnight data). Actually, small fluctuations around the blood glucose equilibrium level were noticed but were not considered significant nor affecting the estimation procedure. The so-called dawn-phenomenon [Williams and Pickup, 1992] was disregarded as well. The parameters in the models are linked to clinical variables. In particular, K_{carb}, T_{carb} can be related to glucose tolerance, i.e., how the body metabolizes glucose, whereas K_{ins}, T_{ins} are connected to insulin sensitivity or resistance, i.e., how effective is insulin in lowering blood glucose. Time delays accounting for food transportation along the gastro-intestinal tract as well as insulin kinetics from the subcutaneous tissues to plasma have been incorporated in the models as in [Percival et al., 2010]. Further, the long delays between subcutaneous insulin administration and insulin action in the identified transfer functions reflected what already known from clinical practice. Model responses to 10 [g] of carbohydrate and 1 [IU] of insulin were considered physiologically plausible, resulting compatible with experimental evidence. Indeed, the empirical observations recently published by Elleri and co-workers [Elleri et al., 2013a] and by Schmidt and co-workers [Schmidt et al., 2012] strengthened the achieved results. Specifically, Elleri and co-workers studied the effects of a low-glycemic-load (LG) meal and a high-glycemic-load (HG) meal [Brouns et al., 2005] matched for carbohydrates (121 [g]) on T1DM children. The outcome was a sustained, slowly declining plasma glucose profile which continued beyond the 8 hours of observations with an unpronounced peak of 210.6±36 [mg/dL] within 153±104 [min] after the intake of the LG meal, and a distinct earlier peak of 248.4±63 [mg/dL] at 98±29 [min] in the case of the HG meal. The first is similar to the absorption profile in Figure 8.7, while the second to that in Figure 8.5. Similar experimental evidences were presented in [Schmidt et al., 2012], where solid meals and a liquid snack were compared, the first behaving like a LG meal, while the second like a HG meal. According to our models, the time required to reach 95% of maximum peak for patients of the first type resulted to be 160.9±78.3 [min] (see Table 8.4). Further, by inspection of Table 8.1 it can be noticed that their value for K_{carb} is much smaller as compared to that of patients CHU101, CHU117, CHU118, CHU136, UNIPD201, UNIPD219 and UNIPD233. Patients of the second type, i.e., those with a glycemic

profile like that of patient UNIPD219, exhibited a blood glucose peak at 72.85±23.06 [min] (Table 8.5). As for insulin response, the experiments in [Schmidt et al., 2012] showed a larger decrease in glycemia per insulin unit than that predicted by the proposed models, the reason being attributable to the different initial conditions of the subjects metabolism. From the analysis of the time constant of maximum decrease in blood glucose due to insulin (see Table 8.6) it turned out that a few patients, i.e., CHU107, CHU138, CHU143, UNIPD217, UNIPD233 presented a very slow action. Unfortunately we did not have any data collected after 1.00 pm, preventing us from the possibility of verifying the duration of insulin action predicted by the identified models.

Prior information could be incorporated in the tuning procedure, taking into account the patient personal history of the disease and the experience gained in its regulation. It is a well known fact, indeed, that the subjects learn by trial-and-error how their glycemia reacts to different sources of carbohydrate and different insulin analogues. However, as yet, it is not clear how this can be realized.

The inputs were considered impulse-formed, the only information required by the identification method being the size of the meal and of the insulin intake, retrieved from the patient's logbook. The approach resembles standard clinical practice, it is personalized and it takes into account the high inter-subject variability. The strategy is particularly appealing as it amounts to estimating only 7 parameters. Contrary to previous contributions dealing with simulated data obtained with in-silico ad-hoc experiments, e.g. [van Heudsen et al., 2012], [Boiroux et al., 2012], we have employed actual T1DM patient data collected within DIAdvisor ™ [DIAdvisor, 2012]. Moreover, estimation and validation were performed on separate sets of data, collected at least two weeks apart. To the best of the author's knowledge this is the first time that such a validation methodology is followed in diabetic blood glucose dynamics modeling. Intra-patient variability was observed by cross-validation, as highlighted by the poor performances reported in Tables 8.2 and 8.3 and may suggest the need of a model parameters updating scheme. Experiment design turned out to be of crucial importance, not only being tightly connected to the intended use of the model but also being constrained due to safety issues when dealing with patients harm. Despite the simple structure the models are able to sufficiently describe the main dynamics of the gluco-regulatory system. The proposed models have been obtained from breakfast data only and may, hence, turn out not to be accurate in modeling lunch and dinner. In order to assess whether or not this is the case, a clinical meal test similar to that used in this contribution should be carried out, provided a 4-hours at least period of steady state

prior to the test so to be able to apply the same method to the new set of data. In addition to this, it would be appropriate to administer a high-glycaemic-load and a low-glycaemic-load [Brouns et al., 2005] meals containing the same type of food to different groups of subjects, in order to verify whether the dynamic behaviour of blood glucose in response to a meal intake is due to patients or food characteristics. In an ideal protocol, insulin administration should be postponed by at least 3 hours and patient monitoring should continue for at least 6-8 hours after insulin intake, in order to model the effects of the inputs accurately. In the actual setting glycemia levels were assessed by a subcutaneous continuous glucose monitoring sensor calibrated against a self-monitoring finger-stick glucose meter (accuracy is reported in Tables 3.6, 3.7). This introduces issues such as sensor noise, device recalibration, sensor time delays just to mention a few, requiring additional components to the control system, i.e., a sensor model [Breton and Kovatchev, 2008], [Perez-Gandia et al., 2010], which was disregarded.

In order to identify the unknown parameters in the transfer functions, a continuous time-domain identification approach was taken, specifically, the predictor based subspace identification method using low-pass filters presented in Chapter 7. The algorithm requires a few user parameters to be tuned. The pole of the low-pass filter was chosen larger than the expected bandwidth of the system and refined by trial and error; the length of the past and the future window size p and f, respectively, was chosen to be 3 according to standard criteria for model-order estimations [Ljung, 1999].

Implication for control design

Although simple second-order linear transfer function models are not a fine representation of the glucose-insulin dynamic interactions, they are useful tools when designing a model-based controller [Percival et al., 2011], [Kirchsteiger et al., 2011b]. A representative scenario would be that of basal-bolus therapy, involving impulsive control variables, namely insulin injections and meal carbohydrates, administered several times over the course of the day at irregularly spaced time instants. A possible controller, then, would consider the effects of a meal or an insulin intake on blood glucose concentration predicted by the proposed models, in order to determine the appropriate control moves, the objective being the maintainance of blood glucose in the normoglycemic range. Such a strategy was proposed in [Cescon et al., 2012], [Stemmann, 2013]. In addition to this, the second order with time delay (SOTD) structure is especially suitable for PID control design [Åström and Hägglund, 2005]. However, in this specific application, the long time delays between

subcutaneous insulin administration and insulin action could be a major difficulty in the realization of the controller.

Figures 8.2 and 8.3 show the Bode diagrams of the estimated transfer function for the population. In the frequency range of interest which is around $6 \cdot 10^{-3}$ [rad/sec] for the meal model, the amplitude curves are far from each other. This feature reflect the variability of the parameters across the population. However, in the case of the insulin model, in the frequency range around $5 \cdot 10^{-4}$ [rad/sec] the amplitude curves are very similar to each other. The variability in the phase curves reflects the significant dispersion of τ_{ins}. Obviously, the benefit of an individualized model over a nominal model for model-based prediction would be significant in this case.

8.7 Conclusions and future work

The chapter presented a successful application of continuous-time identification methods to T1DM blood glucose dynamics modeling. Low-order continuous-time transfer function models were identified from actual T1DM patients data collected adhering to a unique protocol for a meal test and validated on a separate set of data collected 14 ± 3 days apart. The strategy is appealing as it amounts to estimating only 7 parameters. The model structure is simple and the parameters have intuitive meaning that can be linked to clinical practice. The estimated models are straightforward and can be easily interpreted by health-care professionals and may guide development of clinical decision support systems or automated closed-loop insulin delivery. The work considered breakfast data only. Thus, it would be interesting to perform the same type of modeling for other meals or snacks, possibly administering both a high-glycaemic-load and a low-glycaemic-load meal to the same subject. Further, future work will be carried out to extend the study on a larger population. By doing so, it will become apparent whether or not it is possible to classify subjects based on their clinical characteristics so to build appropriate nominal models, suitable as instruments for therapy, for each of the category. Last, control design based on the presented model will be pursued.

9

Conclusions

Without treatment, people with type 1 diabetes experience persistently elevated blood glucose concentrations, which can lead to serious long-term health damages. Controlling the increased prandial glycemia by exogenous insulin replacement becomes then a key factor in order to avoid the complications caused by the disesase.

Conventional therapy relies upon the patient decisions concerning the appropriate treatment to be administered. Many factors must be taken into account: current glucose levels, estimated meal composition, personal knowledge on his/her own glucose metabolism and information on foreseen activity. Failure in the management of the treatments can result in postprandial hyper- or hypoglycemia. Clearly, supporting the individual on the spot in the decision making task would relieve the already heavy load of daily interventions in the life of a diabetic individual.

In this context, this dissertation presented modeling and prediction techniques developed and evaluated for type 1 diabetes, investigated for possible use in an advisory tool, i.e., the DIAdvisor^{TM} device.

The contributions of the thesis may now be summarized.

In Chapter 4 linear dynamic models of glucose metabolism were identified from actual patient data. Inputs to the models were the interpolated plasma insulin assays, the glucose rate of appearance in blood obtained from a glucose intestinal absorption model, while the output was the interpolated blood glucose concentration from laboratory analysis. The estimated models were thereafter used for prediction of blood glucose. The model structure that outperformed the others with respect to physiologically plausible responses to inputs and prediction capability on new data was the ARMAX model structure. The model order able to guarantee a good tradeoff between simplicity and accuracy turned out to be $n = 3$. The approach was competitive with respect to previously published results. Vital signs, i.e., heart rate and respiration rate data, were afterward included in the model structure as additional inputs. From

the analysis presented in Chapter 4 it was concluded that their use did not provide any significant additional information to the purpose of glucose prediction during activities of daily life. This negative result somewhat limits the scope for minimally invasive sensing in blood glucose prediction strategies.

One of the main difficulties encountered in model identification of blood glucose dynamics in diabetes lied in the fact that the two main inputs, i.e., meal and insulin, were applied to the system almost simultaneously and in a proportional factor, the so-called, insulin-to carbohydrate ratio. As a result, it became hard to estimate correctly each input contribution to blood glucose dynamics. A remedy to this problem was proposed in Chapter 8.

When the only goal is predicting the future evolution of time-series for multiple look ahead, the modeling step can actually be omitted and the predictor coefficients can be directly identified from input-output data. Chapter 5 dealt with this problem. Linear multi-step predictors were developed exploiting the state-space construction step in subspace-based identification algorithms. The advantages of this type of predictors are manifold. First, they inherit the appealing features of the subspace-based methods, namely, the use of LQ decompositions of appropriately organized Hankel data matrices and the possibility of a system-theoretic interpretation of the involved procedures. Second, there is no need for canonical parametrizations and choice of model structure. Chapter 5 showed that under open-loop operating conditions and input signals with sufficient excitation, the strategy is successful.

Prompted by the quest for short-term diabetes blood glucose prediction, one of the algorithms treated in Chapter 5 was applied to the actual T1DM patients data of the population studied in Chapter 4. Predictions up to 120 minutes ahead in the future were explored and presented in Chapter 6. One practical scenario considered as input signals the appearances of insulin in plasma from subcutaneous injection and of glucose after food intestinal absorption predicted by physiological models and as output the recalibrated interstitial glucose. From a clinical diabetes point of view the glucose predictions obtained within this case compared favourably with those attained in Chapter 4.

Models and predictors examined so far assumed a zero-order-hold inter-sample behaviour. Moreover, the discrete-time nature of the identified black-box models precluded the interpretation of the parameters from a clinically relevant viewpoint. Therefore, in order to tackle this points, in Chapter 7 the problem of continuous-time model identification from discrete-time data was covered.

Chapter 8 exploited a unique database collected under the aegis of DIAdvisor^{TM} [DIAdvisor, 2012]. The interesting feature of such data set was the time split of two hours between the inputs which allowed to identify the impacts of meal and insulin intakes on T1DM glycemia separately. The model structure was a second-order transfer function with time delay whose parameters were estimated by means of a continuous-time system identification strategy presented in Chapter 7. Despite the simple structure, the estimated models were able to capture the main dynamics of the glucose-insulin system. The dominating time constants in the transfer functions were in agreement with recently published clinical studies [Elleri et al., 2013b].

The individualized short-term model and predictors satisfied the accuracy requirement stated by the DIAdvisor^{TM} project.

Whereas the requirements on prediction accuracy based on a nominal model are not fulfilled, the prediction accuracy can be achieved using individualized models. Not surprisingly, the robustness requirement that prediction accuracy be maintained also for incorrectly declared inputs—e.g., snacks, forgotten insulin injections—can not always be achieved. Note that also a 'perfect' model will exhibit output divergence if deprived of input data.

Open questions

Some fundamental open research topics are recognized.

Meal model

The correct characterization of meal absorption dynamics is fundamental in diabetes management. Actually, post-prandial blood glucose fluctuations in type 1 diabetes depend on a number of factors: these include preprandial glycemia, glucose tolerance, meal size and composition, intestinal absorption of nutrients and rate of gastric emptying. The relative contribution of each of these factors remains unclear and is expected to vary with time [Horowitz et al., 2002]. The glycemic index (GI) methodology [Brouns et al., 2005] is used to categorize nutrients on the basis of their glycemia raising effect, relative to consumption of pure glucose (GI = 100). A low GI meal is characterized by a slow absorption profile that results in an prolongued blood glucose increase with a relatively low peak, while for a high GI meal the peak is more pronounced and appears earlier (see e.g., [Elleri et al., 2013a] and Sec. 8.6). Food absorption dynamics is determined also by its fat and protein content. A higher percentage of fat and protein tends to slow down the rate of glucose absorption, which produces a delayed and reduced blood glucose peak compared to low-fat

and low-protein meals containing the same amount of carbohydrates [Normand et al., 2001]. To date, there is no undisputed model able to account for food absorption dynamics. Research in this direction is, thus, worth pursuing.

Time-varying glucose metabolism dynamics

An important aspect of glucose metabolism is its time-variability. Circadian variations are observed in hormones secretion and action, including insulin sensitivity, which in turn impact glucose dynamics. For instance, the dawn phenomenon is a transient increase in insulin requirements induced by nocturnal release of growth hormone which may occur in the early morning hours, i.e., between 4.00 and 8.00 am [Perriello et al., 1991]. In T1DM subjects if the increase in insulin requirement is not met, hyperglycemia develops. Still, pre-breakfast near- normoglycemia is highly desirable, therefore being able to accurately capture the dawn phenomenon would permit to schedule an adequate overnight insulin therapy.

To the best of the author's knowledge a comprehensive description of time-variability of the glucose metabolism is still lacking. One reason for that may be the scarcity of long, not flawed, data sequences. Within DIAdvisor^{TM} acquisition of clinical data up to 7 consecutive days was accomplished and may be exploited in the future to shed some light on the topic. Segmentation into models whose parameters are piecewise constant in time (e.g., [Ohlsson and Ljung, 2011], [Ohlsson and Ljung, 2013]) seems a promising technique to be exploited in diabetes modeling as well as linear-parameter-varying (LPV) strategies [Bamieh and Giarre, 2002], [Verdult and Verhaegen, 2002].

Patients clustering

Every patient is different, as the intuition would suggest, therefore a personalized approach to diabetes management should be preferred to nominal strategies. However, the extent of the interpatient variability is yet unknown and would be interesting to analyze. Clustering the diabetic population into smaller cohorts of patients may, hence, result to be possible. In such a case, the development of successful therapies for the target groups would lighter the design procedure.

A

Flow Charts Trials

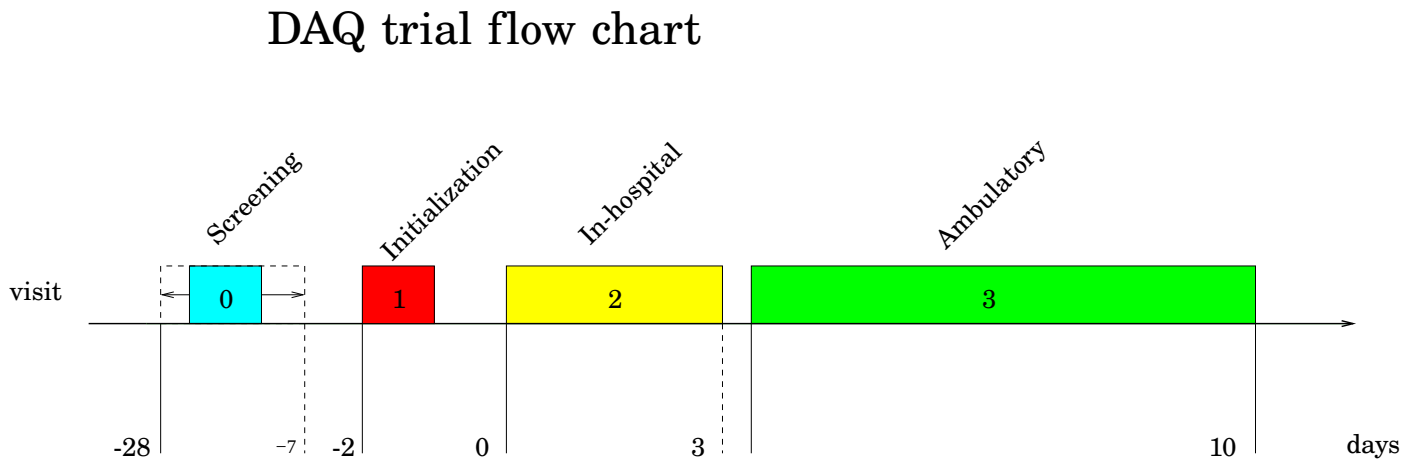

Figure A.1 DAQ trial. *visit 0* Screening visit (light bule box), *visit 1* sensor initialization visit (red box), *visit 2* in-hospital tests (yellow box), *visit 3* ambulatory tests (green box)

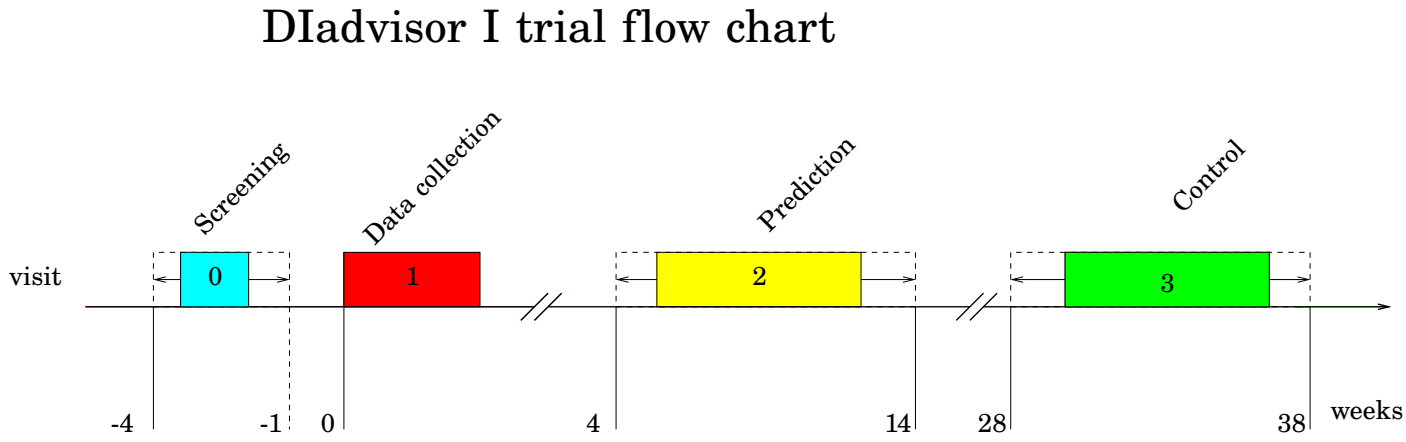

Figure A.2 DIAdvisor I trial. *visit 0* Screening visit (light bule box), *visit 1* testing of data collection (red box), *visit 2* testing of blood glucose prediction (yellow box), *visit 3* testing of controller (green box)

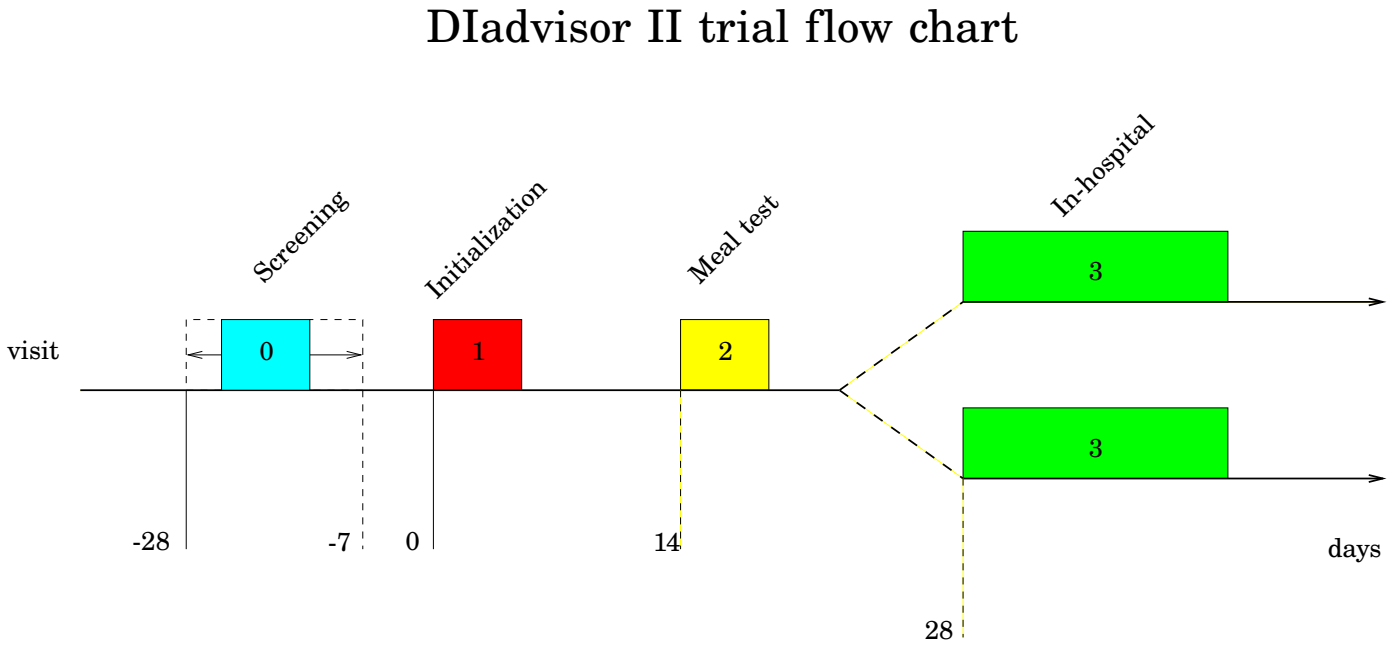

Figure A.3 DIAdvisor II trial. *visit 0* Screening visit (light bule box), *visit 1* sensor initialization (red box), *visit 2* meal test (yellow box), *visit 3* in-hospital admission (green box)

B

List of collected data per trial

Table B.1 DAQ trial,*Visit 2*. List of collected data samples and description

Data Description	Units	Device
Patient parameters	-	Clinician's sheet
Insulin Therapy	-	Clinician's sheet
Interstitial glucose	[mg/dL]	Navigator^{TM}
Carbohydrates	[g]	Patient's logbook
Lipids	[g]	Patient's logbook
Proteins	[g]	Patient's logbook
Fast-acting insulin	[IU]	Patient's logbook
Slow-acting insulin	[IU]	Patient's logbook
Hyperglycemia-correction	[IU]	Patient's logbook
Plasma glucose	[mg/dL]	*YSI 2300 STAT Plus*^{TM}
Capillary glucose	[mg/dL]	HemoCue^{TM}
Basal plasma insulin	[μU/mL]	Blood sample
Bolus plasma insulin	[μU/mL]	Blood sample
Total plasma insulin	[μU/mL]	Blood sample
Heart rate	[beats/min]	LifeShirt®
Respiration rate	[breaths/min]	LifeShirt®
Activity level	[a.u.]	LifeShirt®
Skin temperature	[°C]	LifeShirt®

[a.u.] arbitrary units

Table B.2 DIAdvisor I trial. List of collected data samples and description

Data Description	Units	Device
Patient parameters	-	Clinician's sheet
Insulin Therapy	-	Clinician's sheet
Interstitial glucose	[mg/dL]	Dexcom® Seven®Plus
Carbohydrates	[g]	*viliv S5*
Fast-acting insulin	[IU]	*viliv S5*
Slow-acting insulin	[IU]	*viliv S5*
Hyperglycemia-correction	[IU]	*viliv S5*
Plasma glucose	[mg/dL]	*YSI 2300 STAT Plus*^{TM}
Capillary glucose	[mg/dL]	HemoCue^{TM}
Heart rate	[beats/min]	Pebble®

Table B.3 DIadvisor II trial,*Visit 2* & *3*. List of collected data samples and description

Data Description	Units	Device
Patient parameters	-	Clinician's sheet
Insulin Therapy	-	Clinician's sheet
Interstitial glucose	[mg/dL]	Dexcom® Seven®Plus
Carbohydrates	[g]	*viliv S5*
Fast-acting insulin	[IU]	*viliv S5*
Plasma glucose	[mg/dL]	*YSI 2300 STAT Plus*^{TM}
Capillary glucose	[mg/dL]	HemoCue^{TM}

C

Proofs

C.1 Proof of algorithm (5.1)

For convenience set $p = f$. Let us rewrite Eq. (5.36) as

$$\begin{bmatrix} U^f \\ U^p \\ Y^p \\ Y^f \end{bmatrix} = \begin{bmatrix} L_{11}^{'} & 0 & 0 & 0 \\ L_{21}^{'} & L_{22}^{'} & 0 & 0 \\ L_{31}^{'} & L_{32}^{'} & L_{33}^{'} & 0 \\ L_{41}^{'} & L_{42}^{'} & L_{43}^{'} & L_{44}^{'} \end{bmatrix} \begin{bmatrix} Q_1^{'T} \\ Q_2^{'T} \\ Q_3^{'T} \\ Q_4^{'T} \end{bmatrix} \tag{C.1}$$

where $L_{11}^{'}$, $L_{22}^{'} \in \mathbb{R}^{pm \times pm}$, $L_{33}^{'}$, $L_{44}^{'} \in \mathbb{R}^{pl \times pl}$ and Q_1, $Q_2 \in \mathbb{R}^{N \times pm}$, Q_3, $Q_4 \in \mathbb{R}^{N \times pl}$ are orthogonal. Further, assume that the following conditions are statisfied:

1. the system in Eq. (5.1) is reachable
2. there is no linear feedback from the states to the inputs
3. the input is sufficiently PE

Then, $\text{rank}(L_{22}) = \text{rank} \begin{bmatrix} L_{22}^{'} & 0 \\ L_{32}^{'} & L_{33}^{'} \end{bmatrix} = pm + n \leq p(m+l)$, so that L_{22} is rank deficient. Now, from Eq. (5.36)row-wise we have

$$Q_1^T = L_{11}^{-1} U^f \tag{C.2}$$

$$Q_2^T = L_{22}^{\dagger}(Z^p - L_{21} Q_1^T) \tag{C.3}$$

$$Y^f = L_{31} Q_1^T + L_{32} Q_2^T \tag{C.4}$$

Using (C.2) and (C.3) in (C.4) we obtain

$$Y^f = (L_{31} - L_{32} L_{22}{}^{\dagger} L_{21}) L_{11}{}^{-1} U^f + L_{32} L_{22}{}^{\dagger} Z^p \tag{C.5}$$

Defining

$$\hat{\Gamma} = L_{32}{L_{22}}^{\dagger} \tag{C.6}$$

$$\hat{\Lambda} = (L_{31} - L_{32}{L_{22}}^{\dagger}L_{21}){L_{11}}^{-1} \tag{C.7}$$

the algorithm is proved.

D

Additional results

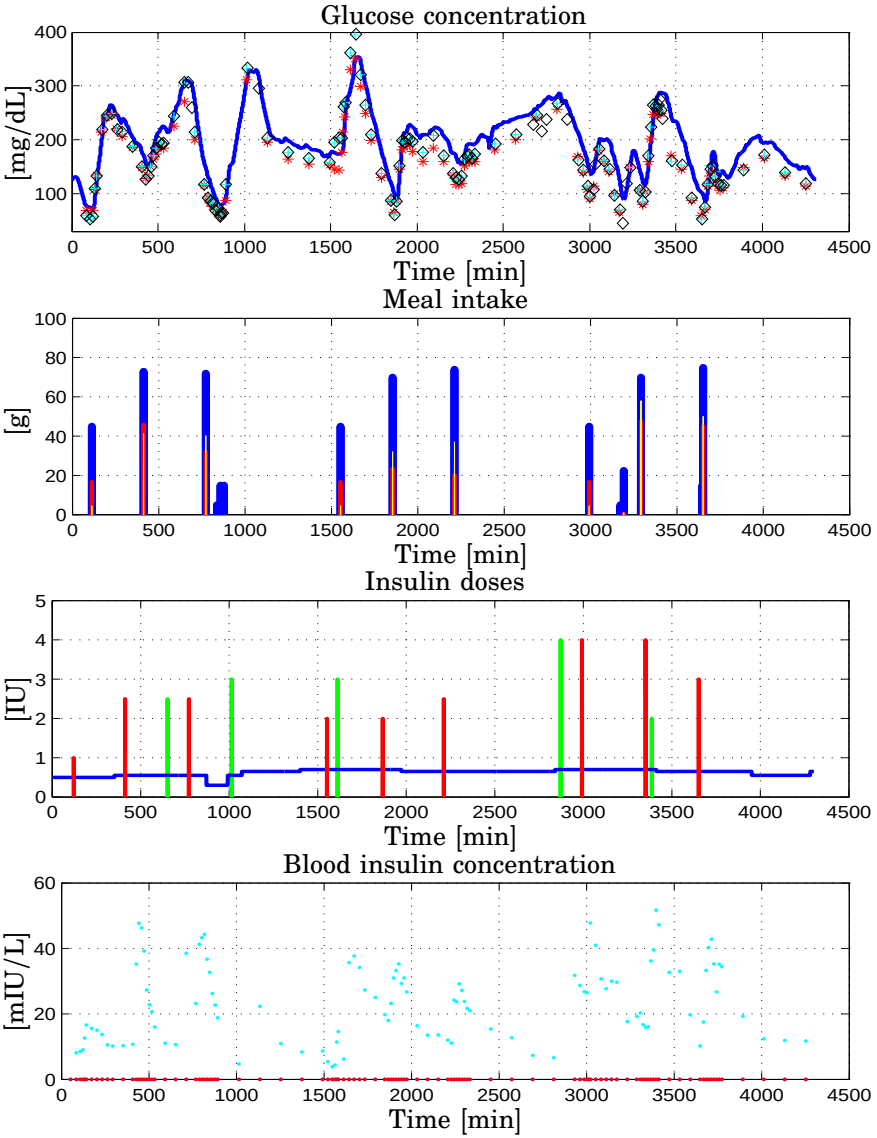

Figure D.1 Patient CHU106. DAQ trial, *Visit 2*. *Top* Glucose concentration [mg/dL]: interstitial (blue), plasma (red), finger stick (cyan and black); *Upper Center* Meal intake [g]: carbohydrates (blue), lipids (red), proteins (yellow); *Lower Center* Insulin doses [IU]: basal (blue), bolus (red), correction (green); *Bottom* Blood insulin concentration [mIU/L]: basal (blue), bolus (red), total (cyan) vs. time [min]

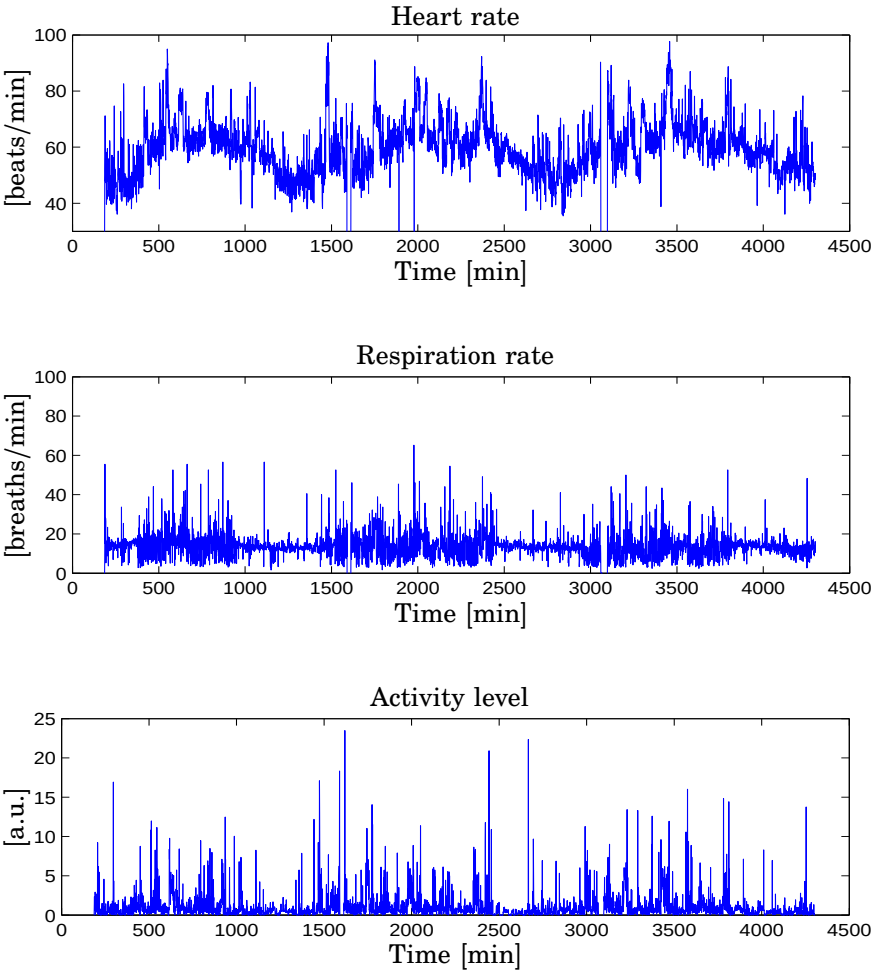

Figure D.2 Patient CHU106. DAQ trial, *Visit 2*. *Top* Heart rate [beats/min]; *Center* Respiration rate [breaths/min]; *Bottom* Activity level [a.u.] vs. time [min]

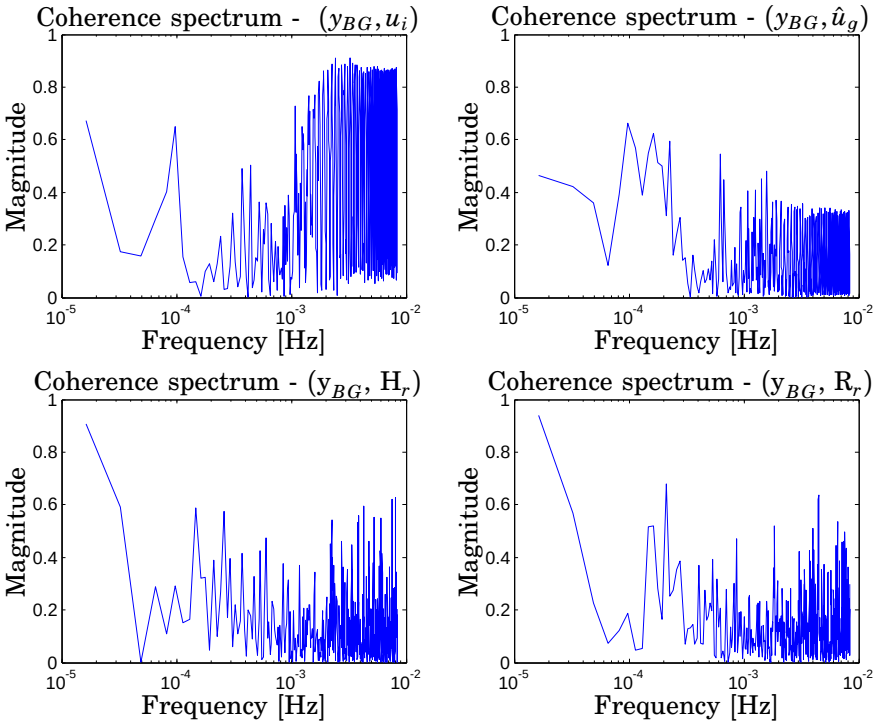

Figure D.3 Patient CHU106. Coherence spectra between blood glucose and *Top Left* total plasma insulin; *Top Right* plasma glucose rate of appearance; *Bottom Left* Heart Rate; *Bottom Right* Respiration Rate. All the spectra vs. frequency [Hz]

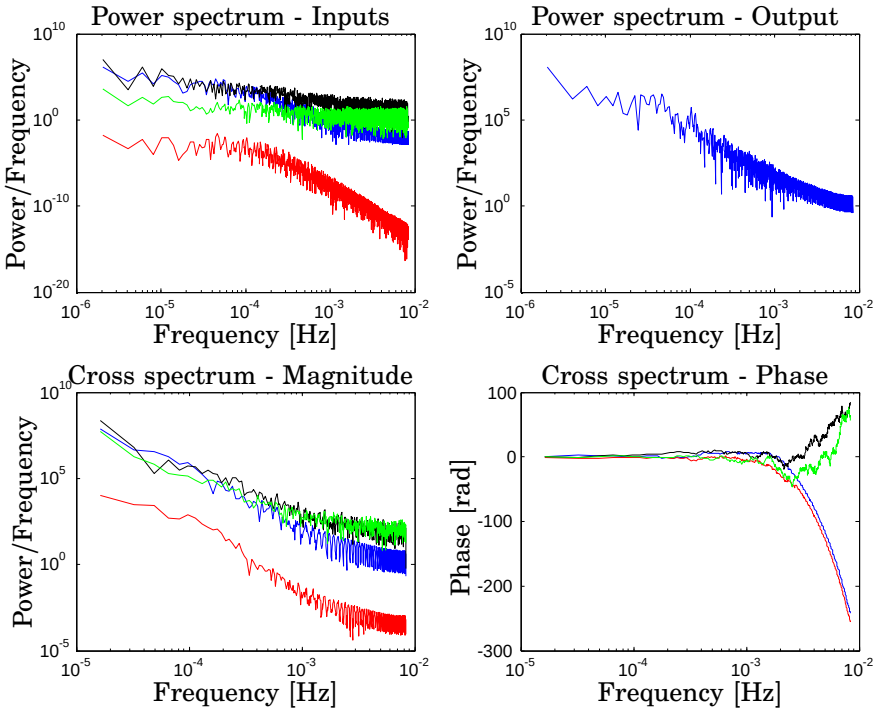

Figure D.4 Patient CHU106. *Top Left* Magnitude of Power spectrum of inputs: total plasma insulin $[(\mu U/mL)^2/(Hz)]$ (blue), plasma glucose rate of appearance $[(mg/kg/min)^2/(Hz)]$ (red), heart rate $[(beats/min)^2/(Hz)]$ (black), respiration rate $[(breaths/min)^2/(Hz)]$ (green); *Top Right* Magnitude of Power spectrum of output: blood glucose $[(mg/dL)^2/(Hz)]$; *Bottom Left* Magnitude of cross spectrum: total plasma insulin, blood glucose $[(\mu U/mL)^2(mg/dL)^2/(Hz)]$ (blue), plasma glucose rate of appearance, blood glucose $[(mg/kg/min)^2(mg/dL)^2/(Hz)]$ (red), heart rate, blood glucose $[(beats/min)^2(mg/dL)^2/(Hz)]$ (black), respiration rate, blood glucose $[(breaths/min)^2(mg/dL)^2$ $(Hz)]$ (green); *Bottom Right* Phase of cross spectrum [rad]: total plasma insulin (blue), plasma glucose rate of appearance (red), heart rate (black), respiration rate (green). All the spectra vs. frequency [Hz]

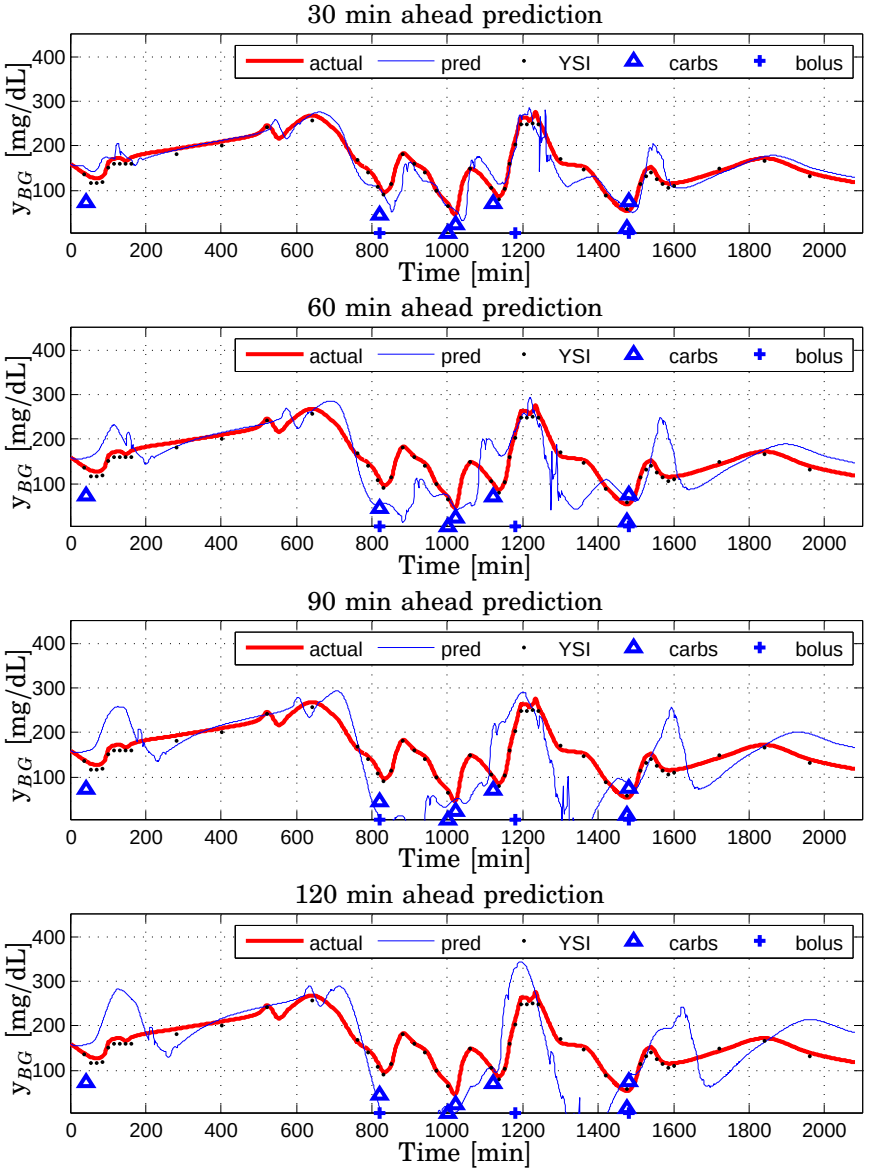

Figure D.5 Patient CHU0106. Evaluation on validation data: 3rd-order ARMAX-based predictor (thin) and measured plasma glucose (thick) [mg/dL] vs. time [min]. *Top* 30-minutes ahead; *Top Center* 60-minutes ahead; *Bottom Center* 90-minutes ahead; *Bottom* 120-minutes-ahead prediction. DAQ Trial. Inputs: u_i, $\hat{u}_g$

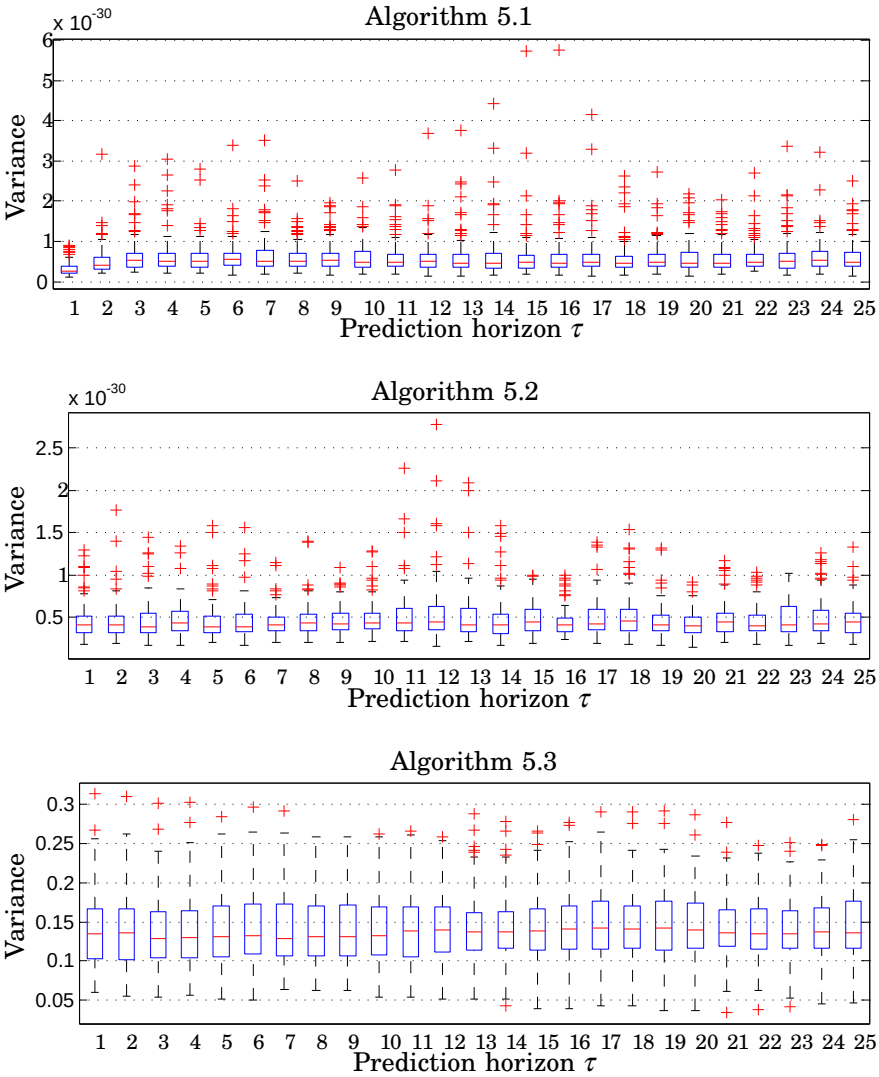

Figure D.6 Example 1. Open loop. Multi-step predictors performances on identification data. Prediction error variance vs. prediction horizon. Top Algorithm 5.1, Center Algorithm 5.2, Bottom Algorithm 5.3

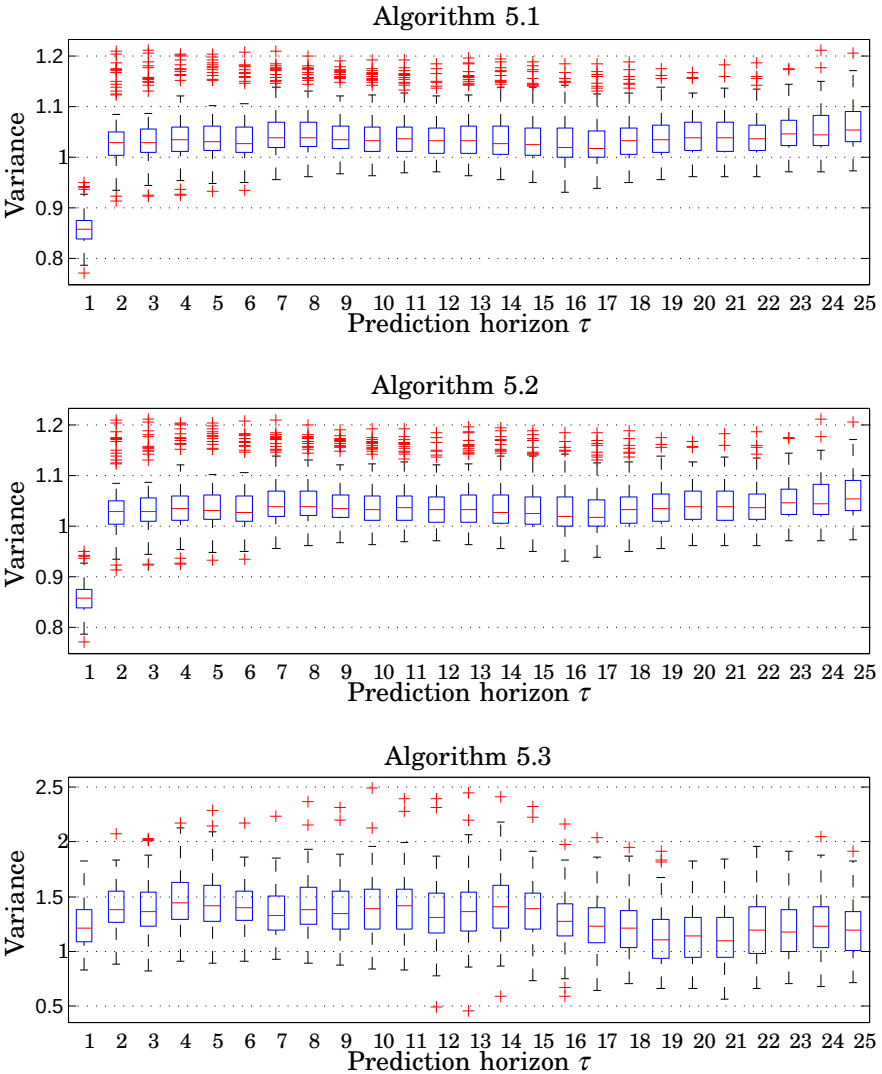

Figure D.7 Example 2. Open loop. Multi-step predictors performances on identification data. Prediction error variance vs. prediction horizon. Top Algorithm 5.1, Center Algorithm 5.2, Bottom Algorithm 5.3

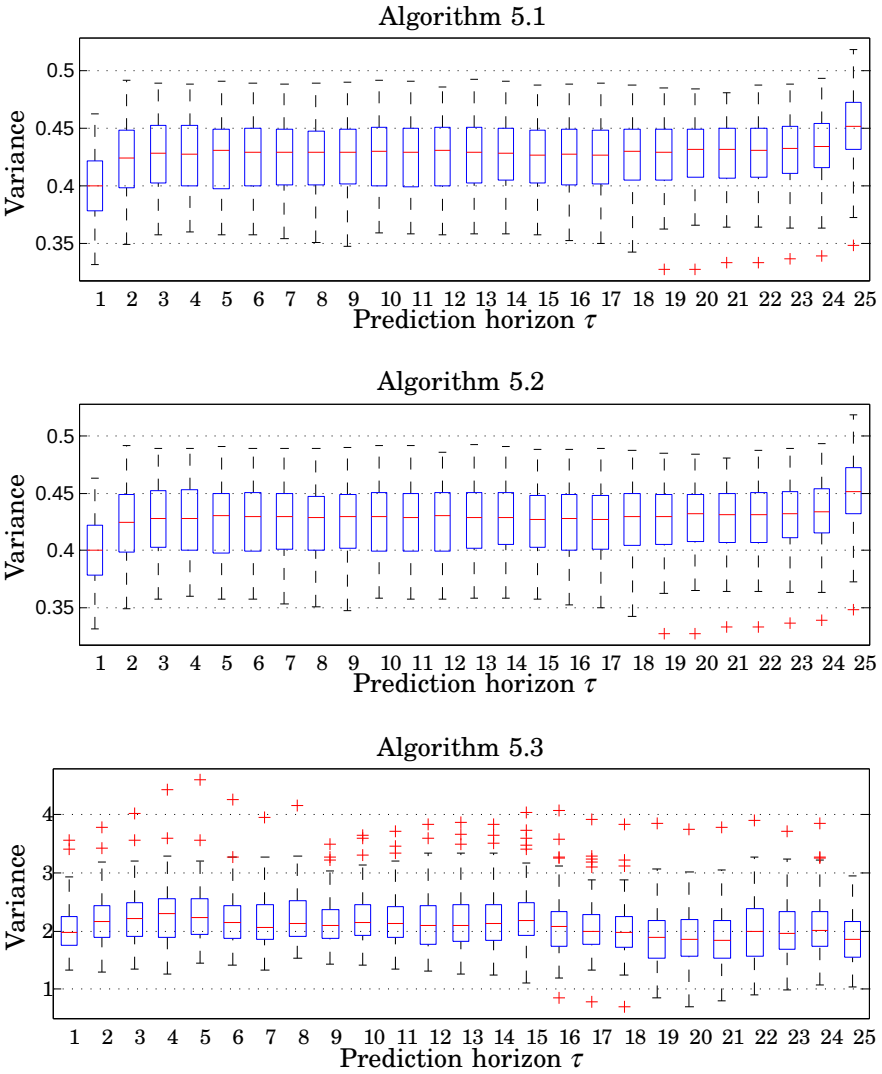

Figure D.8 Example 3. Closed loop. Multi-step predictors performances on identification data. Prediction error variance vs. prediction horizon. Top Algorithm 5.1, Center Algorithm 5.2, Bottom Algorithm 5.3

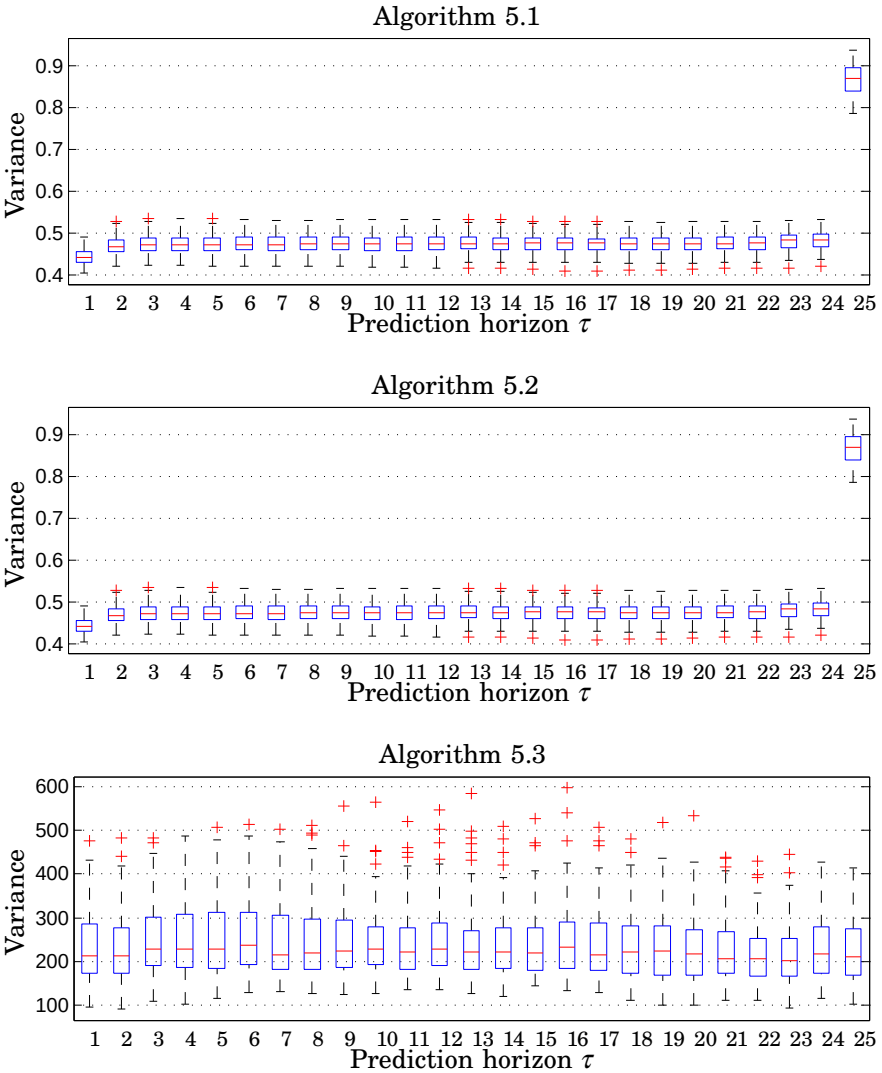

Figure D.9 Example 4. Closed loop. Multi-step predictors performances on identification data. Prediction error variance vs. prediction horizon. Top Algorithm 5.1, Center Algorithm 5.2, Bottom Algorithm 5.3

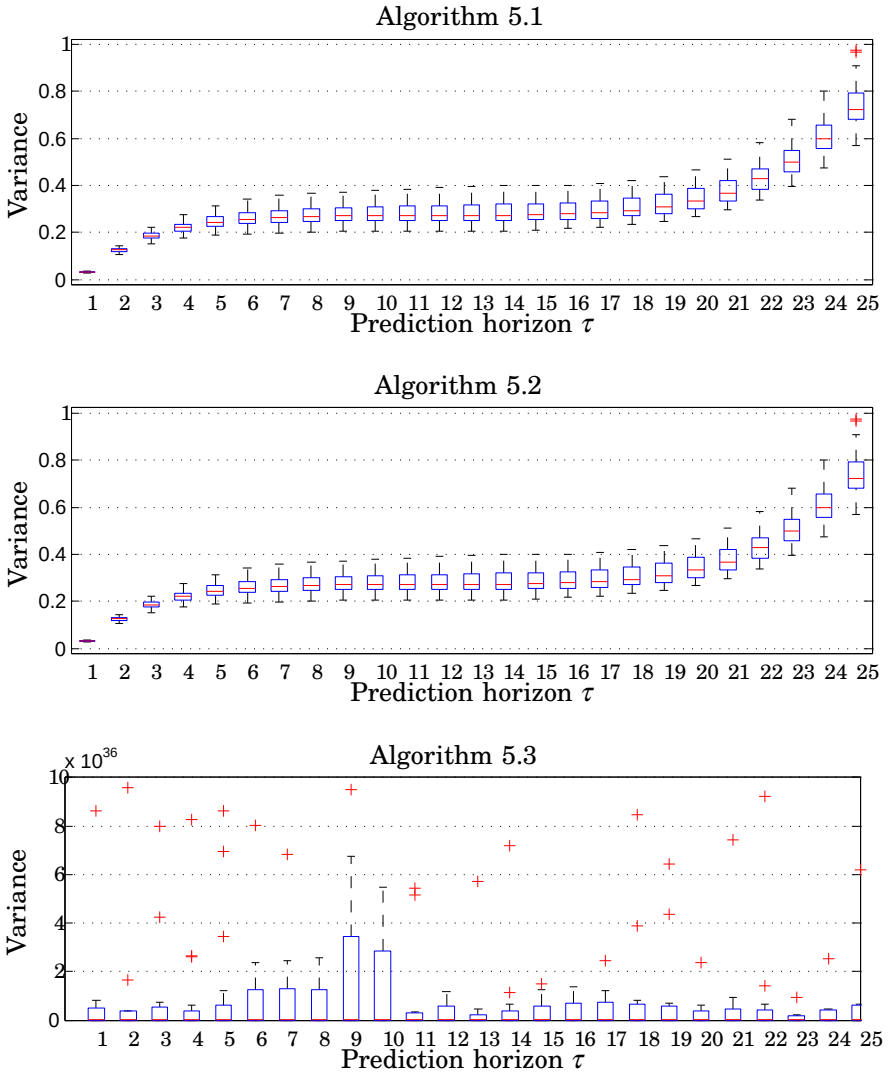

Figure D.10 Example 5. Closed loop. Multi-step predictors performances on identification data. Prediction error variance vs. prediction horizon. Top Algorithm 5.1, Center Algorithm 5.2, Bottom Algorithm 5.3

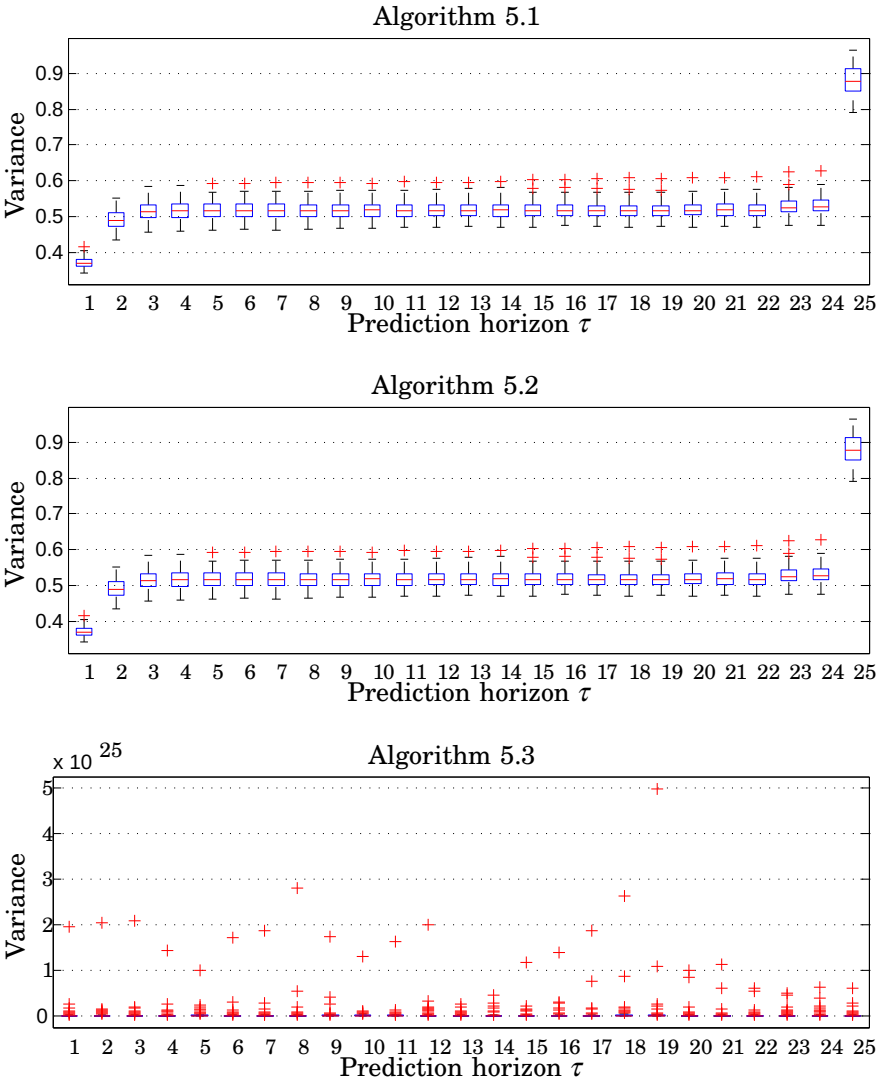

Figure D.11 Example 6. Closed loop. Multi-step predictors performances on identification data. Prediction error variance vs. prediction horizon. Top Algorithm 5.1, Center Algorithm 5.2, Bottom Algorithm 5.3

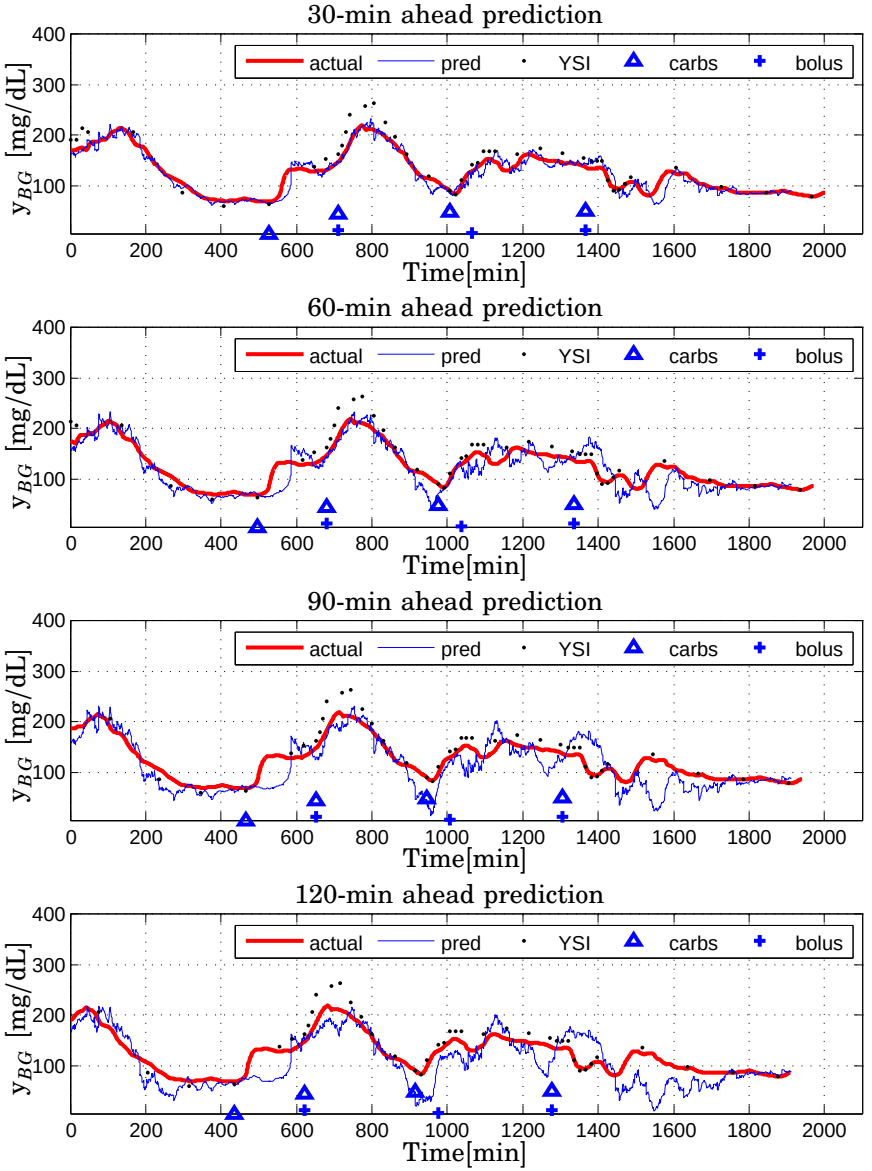

Figure D.12 Patient CHU102. Multi-step predictions. Case B, p=f=120. Evaluation on validation data. Predictor (thin) and measured interstitial glucose y_{IG} (thick) [mg/dL] vs. time [min]. *Top* 30-minutes ahead; *Top Center* 60-minutes ahead; *Bottom Center* 90-minutes ahead; *Bottom* 120-minutes-ahead prediction. CGM data case. Meals and injections are indicated with triangles and pluses, respectively.

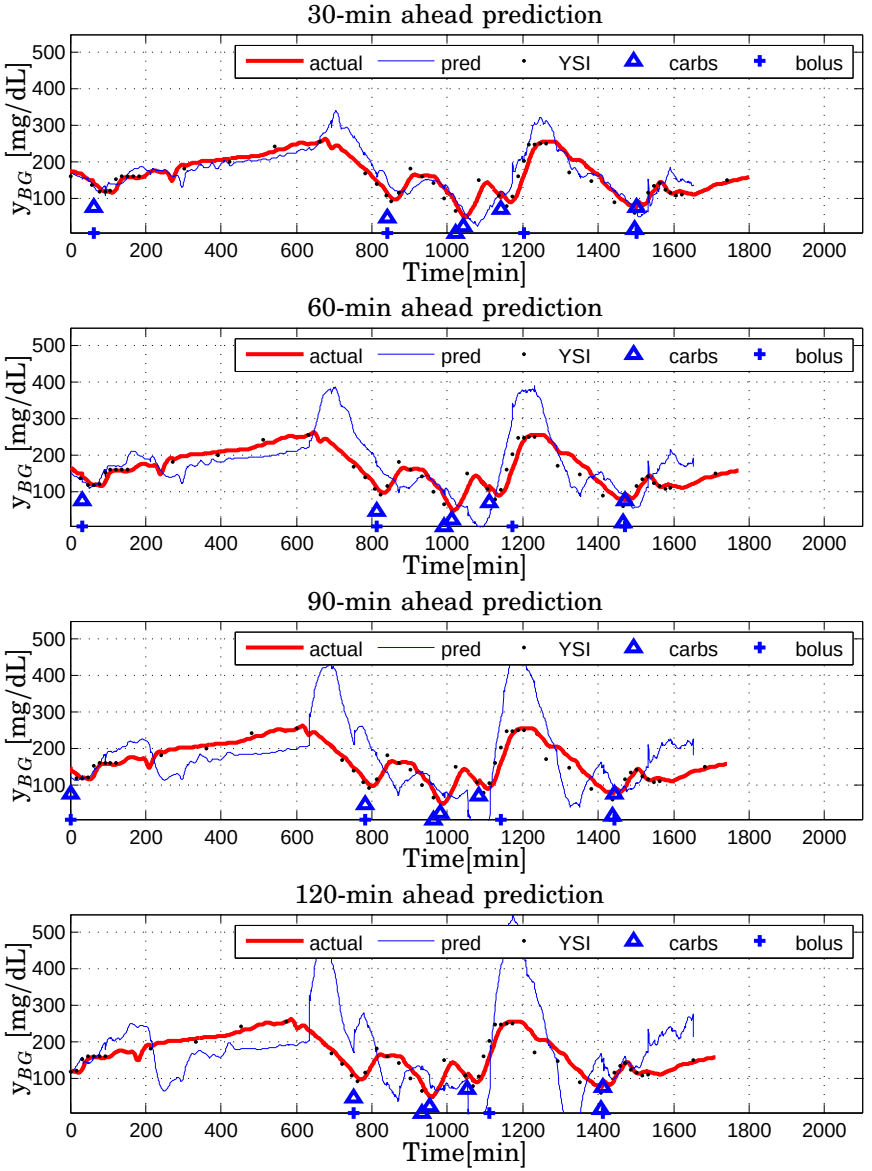

Figure D.13 Patient CHU106. Multi-step predictions. Scenario 1, Case B, p=f=120. Evaluation on validation data. Predictor (thin) and measured plasma glucose y_{BG} (thick) [mg/dL] vs. time [min]. *Top* 30-minutes ahead; *Top Center* 60-minutes ahead; *Bottom Center* 90-minutes ahead; *Bottom* 120-minutes-ahead prediction. Meals and injections are indicated with triangles and pluses, respectively.

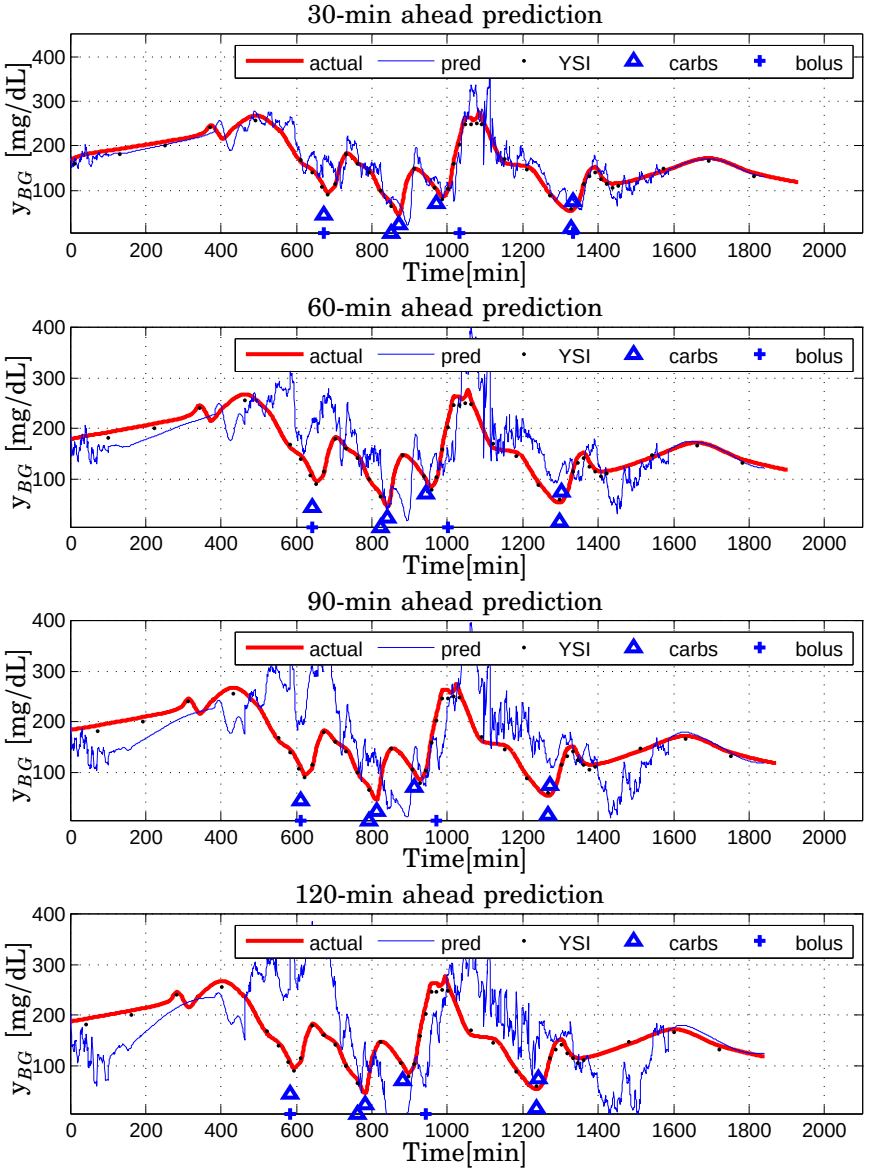

Figure D.14 Patient CHU106. Multi-step predictions. Scenario 2, Case B, p=f=120. Evaluation on validation data. Predictor (thin) and measured plasma glucose y_{BG} (thick) [mg/dL] vs. time [min]. *Top* 30-minutes ahead; *Top Center* 60-minutes ahead; *Bottom Center* 90-minutes ahead; *Bottom* 120-minutes-ahead prediction. Meals and injections are indicated with triangles and pluses, respectively.

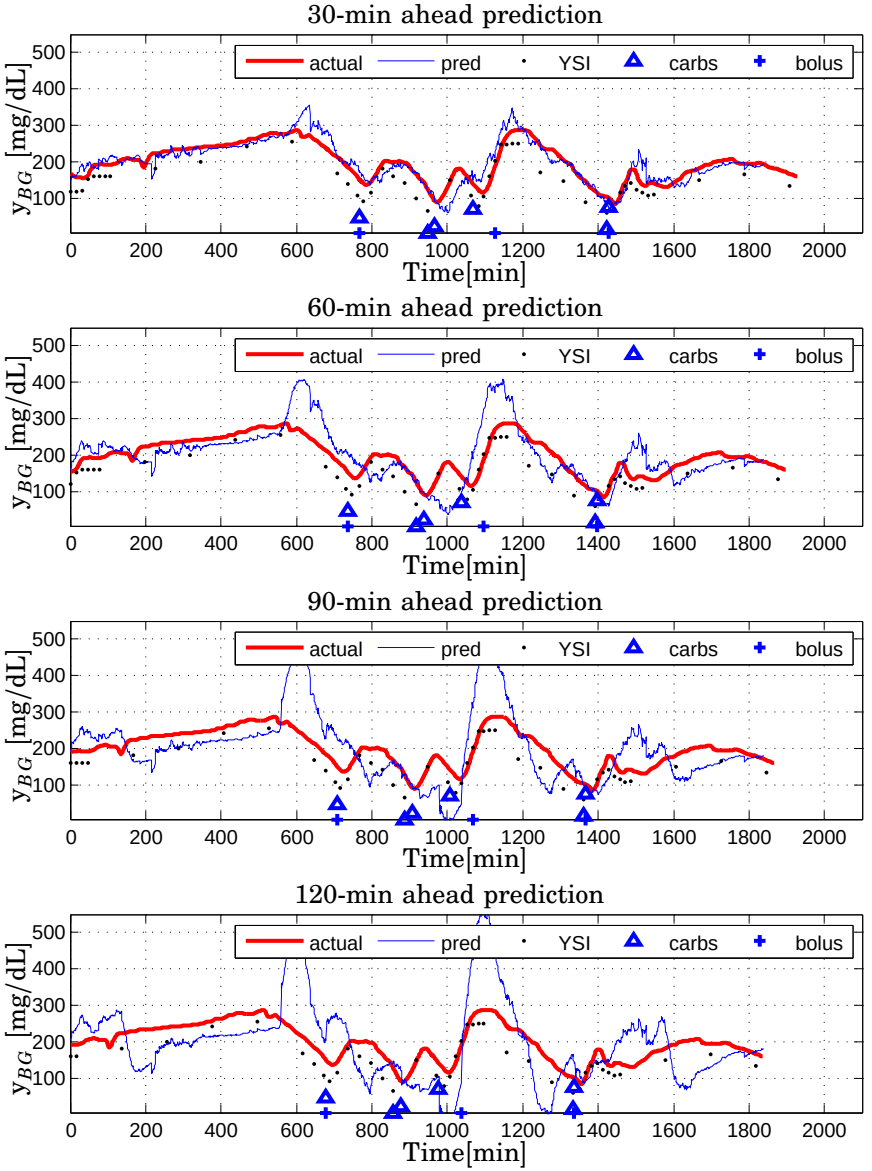

Figure D.15 Patient CHU106. Multi-step predictions. Case B, $p = f = 120$. Evaluation on validation data. Predictor (thin) and measured plasma glucose y_{BG} (thick) [mg/dL] vs. time [min]. *Top* 30-minutes ahead; *Top Center* 60-minutes ahead; *Bottom Center* 90-minutes ahead; *Bottom* 120-minutes-ahead prediction. CGM data case. Meals and injections are indicated with triangles and pluses, respectively.

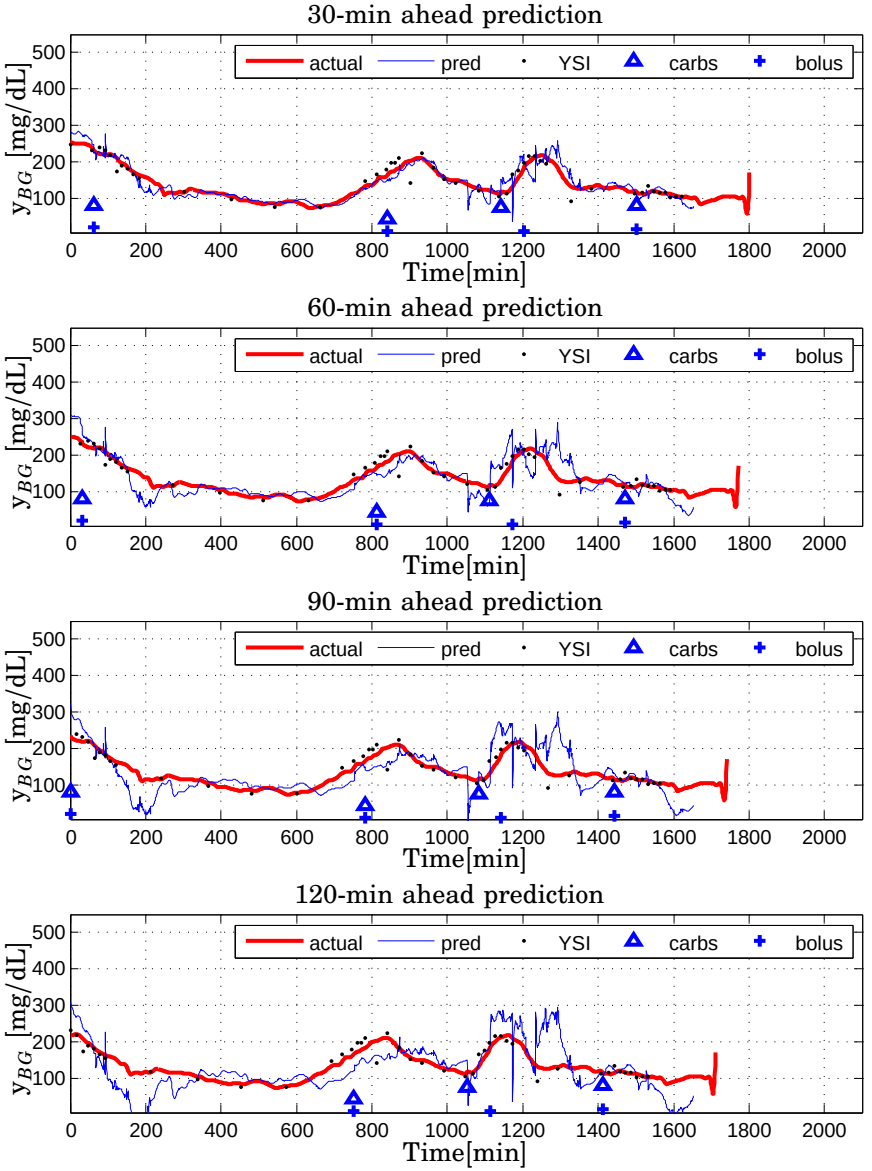

Figure D.16 Patient CHU115. Multi-step predictions. Scenario 1, Case B, p=f=120. Evaluation on validation data. Predictor (thin) and measured plasma glucose y_{BG} (thick) [mg/dL] vs. time [min]. *Top* 30-minutes ahead; *Top Center* 60-minutes ahead; *Bottom Center* 90-minutes ahead; *Bottom* 120-minutes-ahead prediction. Meals and injections are indicated with triangles and pluses, respectively.

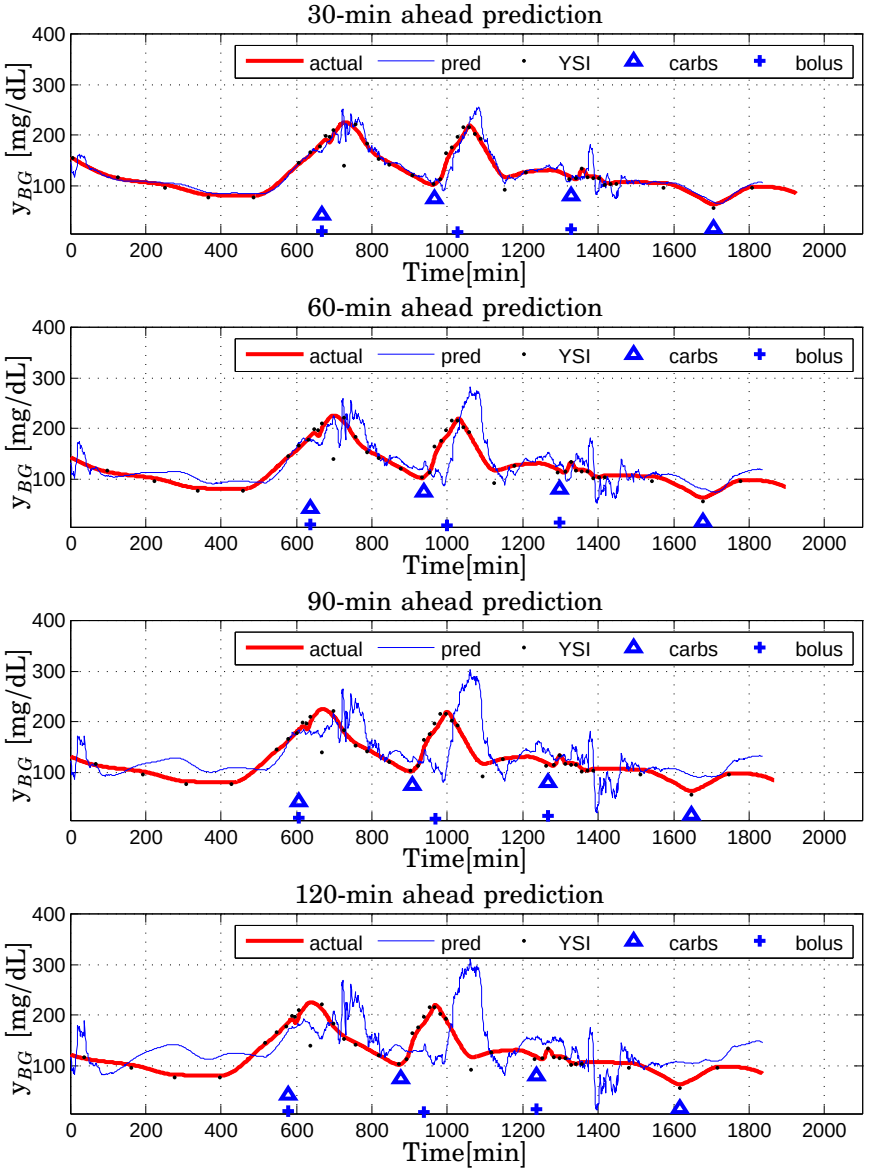

Figure D.17 Patient CHU115. Multi-step predictions. Scenario 2, Case B, p=f=120. Evaluation on validation data. Predictor (thin) and measured plasma glucose y_{BG} (thick) [mg/dL] vs. time [min]. *Top* 30-minutes ahead; *Top Center* 60-minutes ahead; *Bottom Center* 90-minutes ahead; *Bottom* 120-minutes-ahead prediction. Meals and injections are indicated with triangles and pluses, respectively.

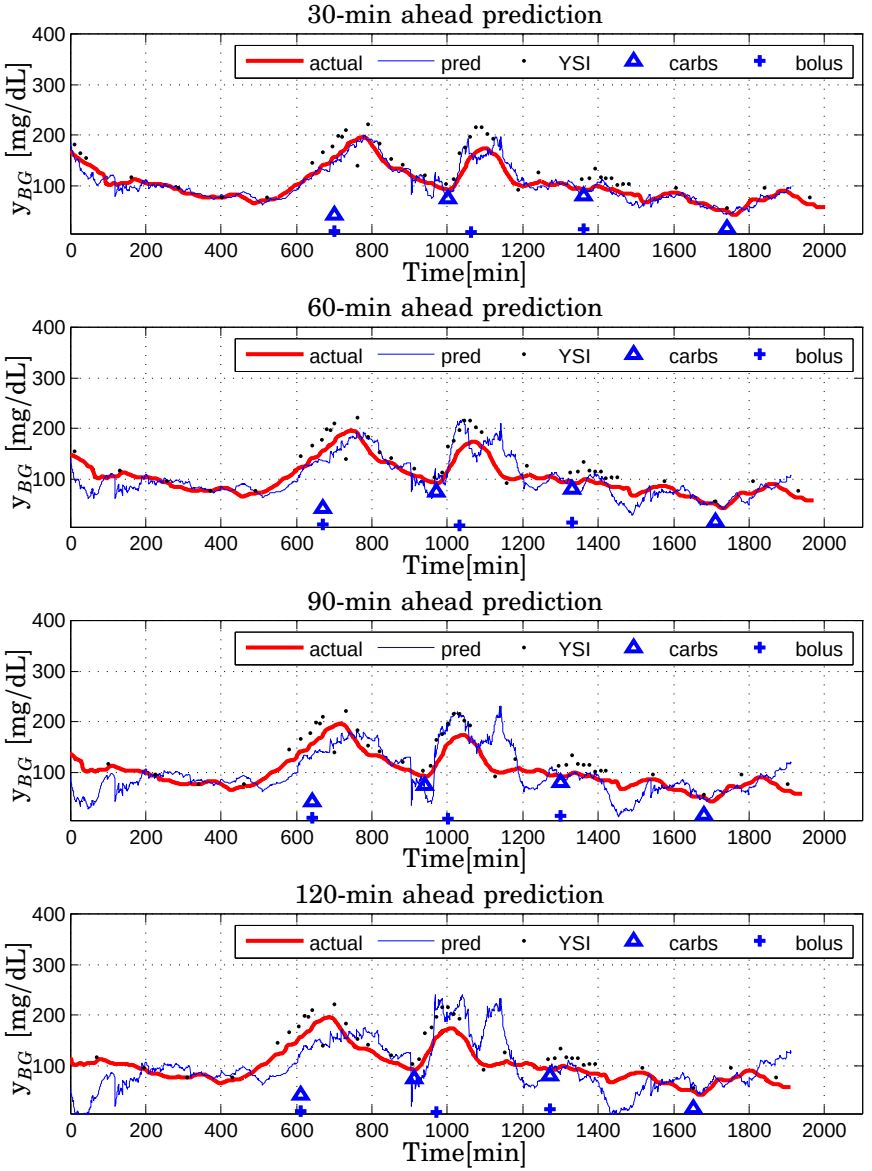

Figure D.18 Patient CHU115. Multi-step predictions. Case B, $p = f = 120$. Evaluation on validation data. Predictor (thin) and measured plasma glucose y_{BG} (thick) [mg/dL] vs. time [min]. *Top* 30-minutes ahead; *Top Center* 60-minutes ahead; *Bottom Center* 90-minutes ahead; *Bottom* 120-minutes-ahead prediction. CGM data case. Meals and injections are indicated with triangles and pluses, respectively.

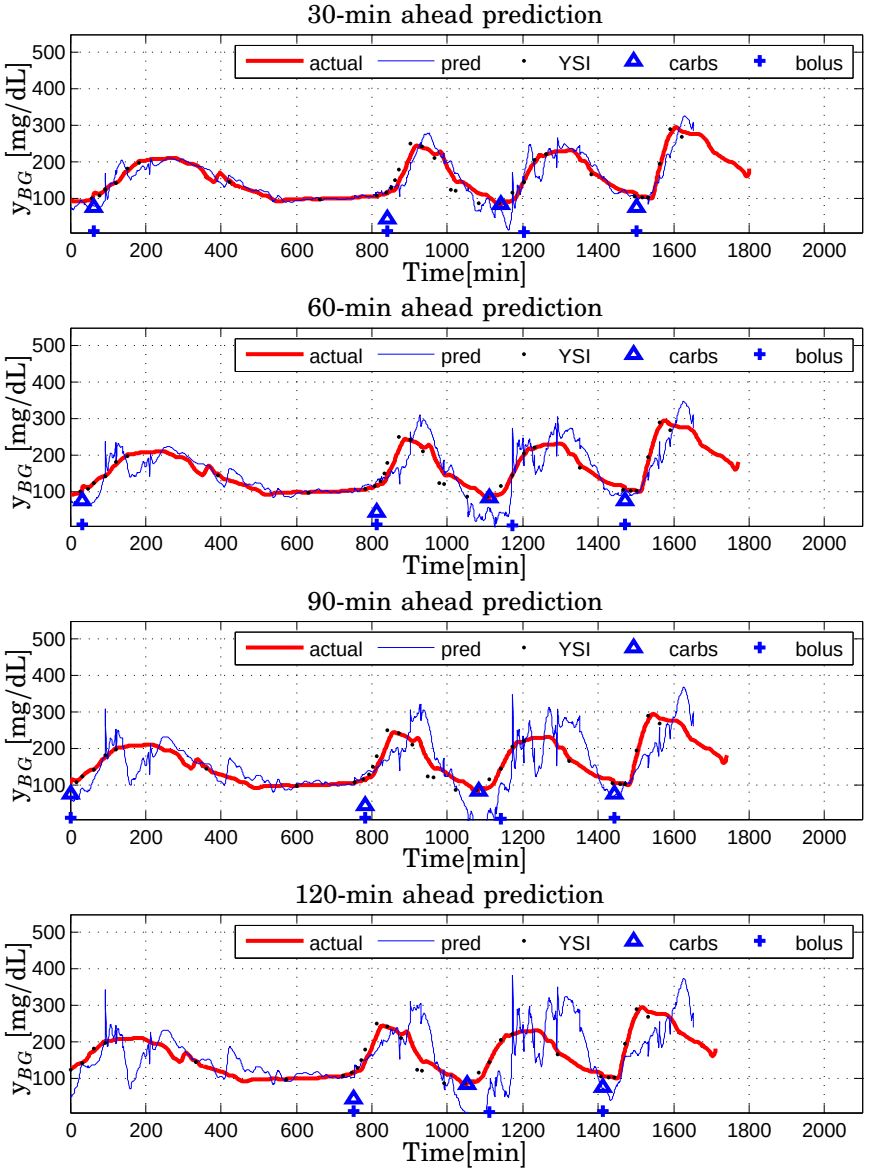

Figure D.19 Patient CHU128. Multi-step predictions. Scenario 1, Case B, p=f=120. Evaluation on validation data. Predictor (thin) and measured plasma glucose y_{BG} (thick) [mg/dL] vs. time [min]. *Top* 30-minutes ahead; *Top Center* 60-minutes ahead; *Bottom Center* 90-minutes ahead; *Bottom* 120-minutes-ahead prediction. Meals and injections are indicated with triangles and pluses, respectively.

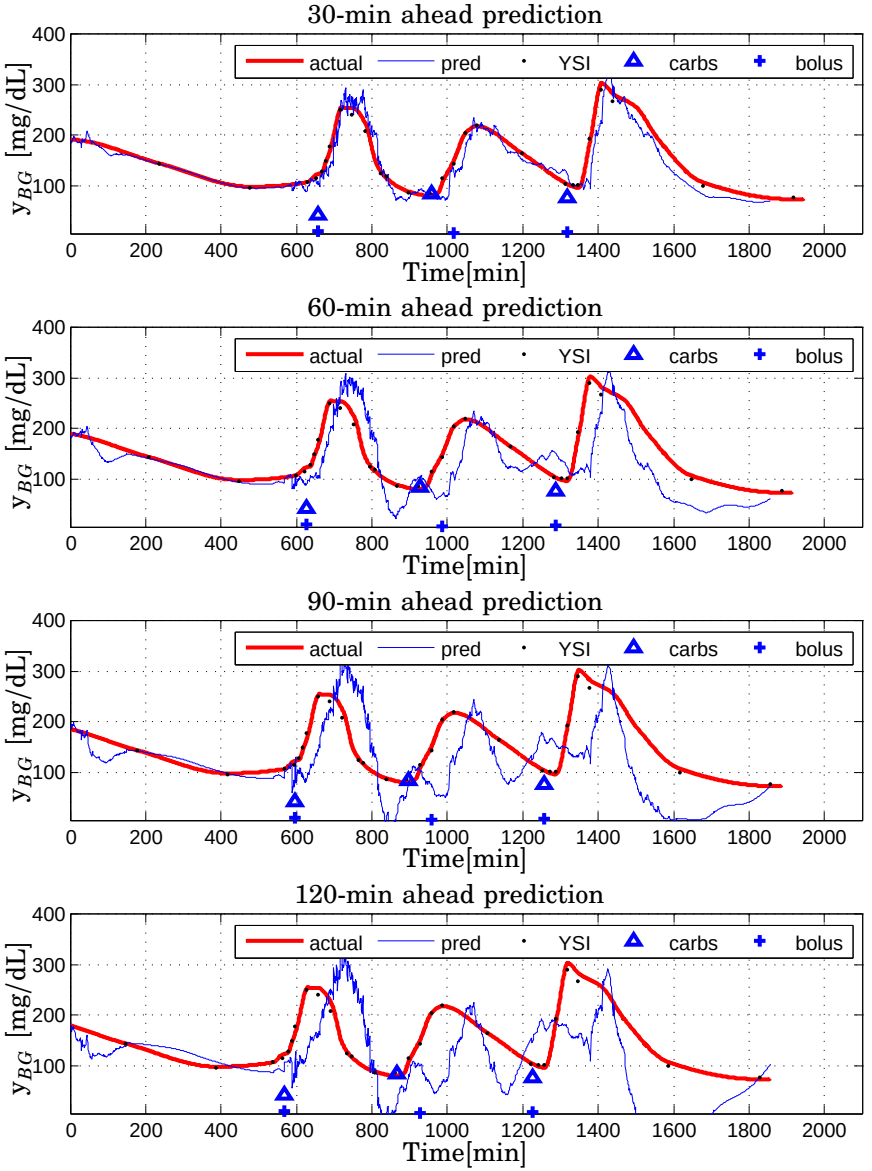

Figure D.20 Patient CHU0128. Multi-step predictions. Scenario 2, Case B, p=f=120. Evaluation on validation data. Predictor (thin) and measured plasma glucose y_{BG} (thick) [mg/dL] vs. time [min]. *Top* 30-minutes ahead; *Top Center* 60-minutes ahead; *Bottom Center* 90-minutes ahead; *Bottom* 120-minutes-ahead prediction. Meals and injections are indicated with triangles and pluses, respectively.

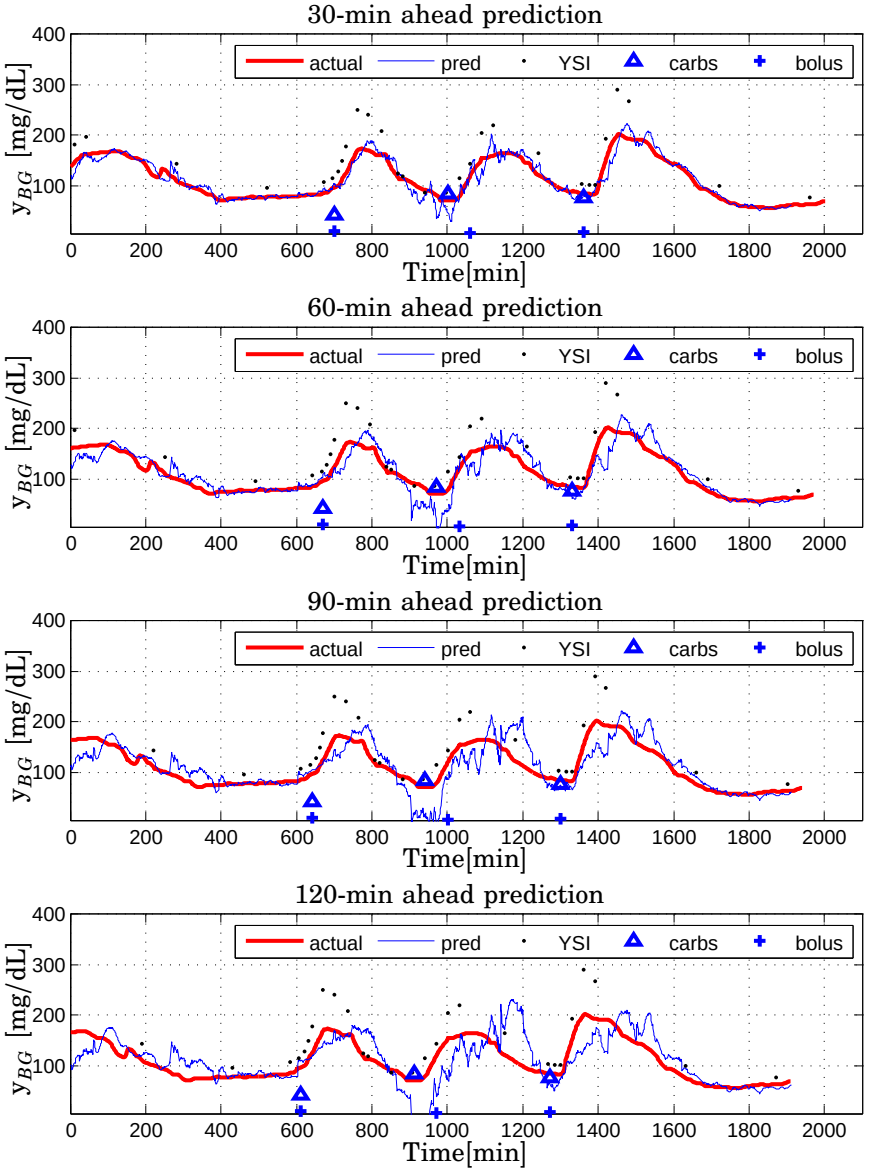

Figure D.21 Patient CHU0128. Multi-step predictions. Case B, $p = f = 120$. Evaluation on validation data. Predictor (thin) and measured plasma glucose y_{BG} (thick) [mg/dL] vs. time [min]. *Top* 30-minutes ahead; *Top Center* 60-minutes ahead; *Bottom Center* 90-minutes ahead; *Bottom* 120-minutes-ahead prediction. CGM data case. Meals and injections are indicated with triangles and pluses, respectively.

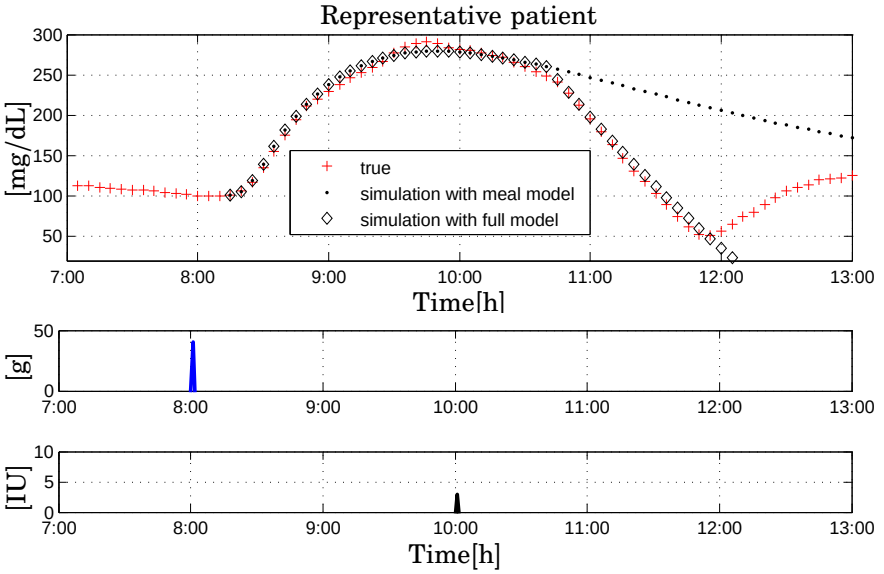

Figure D.22 Patient UNIPD201. DIAdvisor II trial, *Visit 2*, meal test. *Top* Actual CGMS (star) vs. simulated breakfast impact (dot) and simulated joint meal and insulin intakes (diamond) [mg/dL]; *Center* Carbohydrate intake [g]; *Bottom* Insulin bolus [IU]. All the measurements vs. time of the day [h]

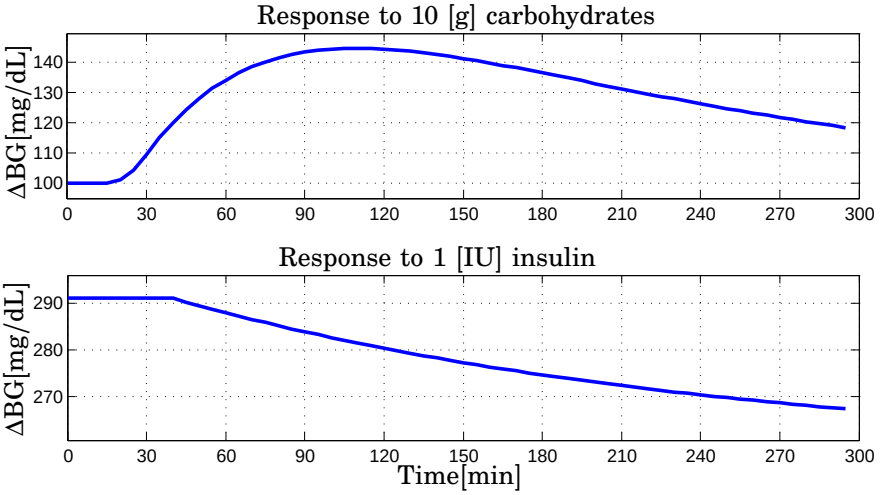

Figure D.23 Patient UNIPD201. Response to *Top* 10 [g] of carbohydrate *Bottom* 1 [IU] of insulin. Blood glucose excursion [mg/dL] vs. time [min]

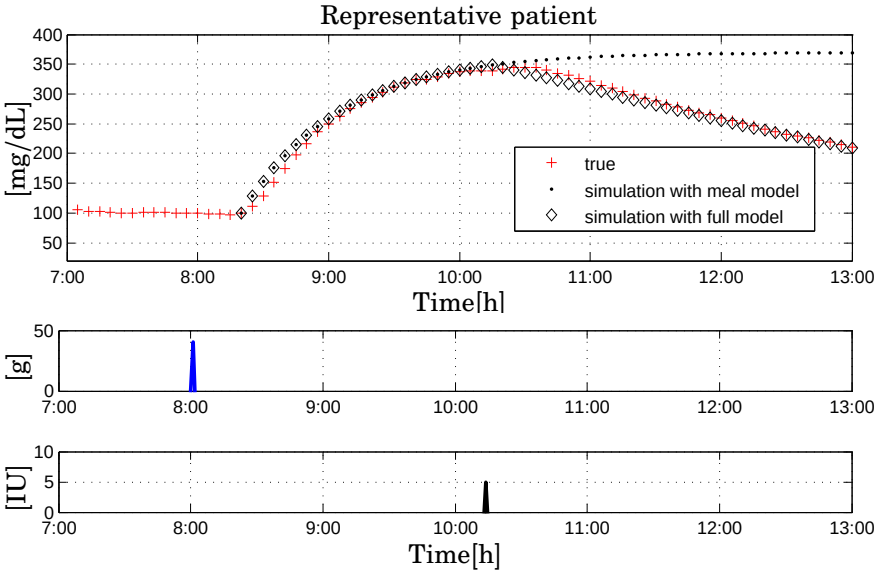

Figure D.24 Patient IKEM306. DIAdvisor II trial, *Visit 2*, meal test. *Top* Actual CGMS (star) vs. simulated breakfast impact (dot) and simulated joint meal and insulin intakes (diamond) [mg/dL]; *Center* Carbohydrate intake [g]; *Bottom* Insulin bolus [IU]. All the measurements vs. time of the day [h]

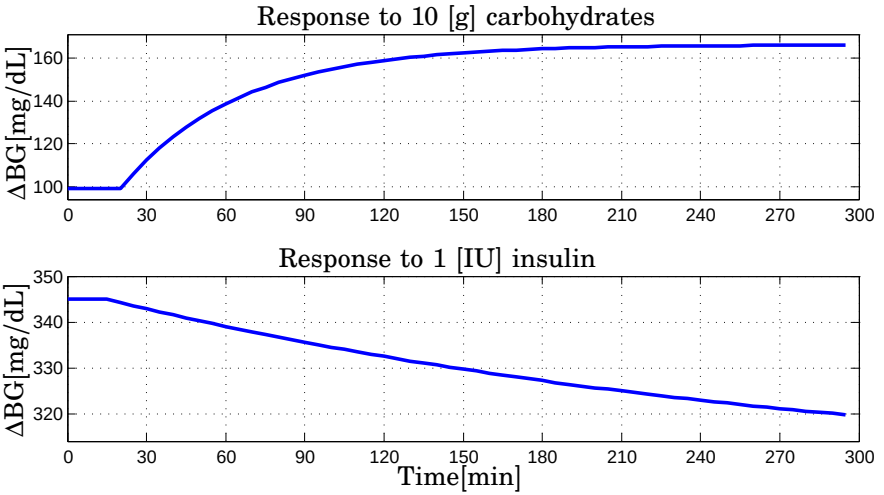

Figure D.25 Patient IKEM306. Response to *Top* 10 [g] of carbohydrate *Bottom* 1 [IU] of insulin. Blood glucose excursion [mg/dL] vs. time [min]

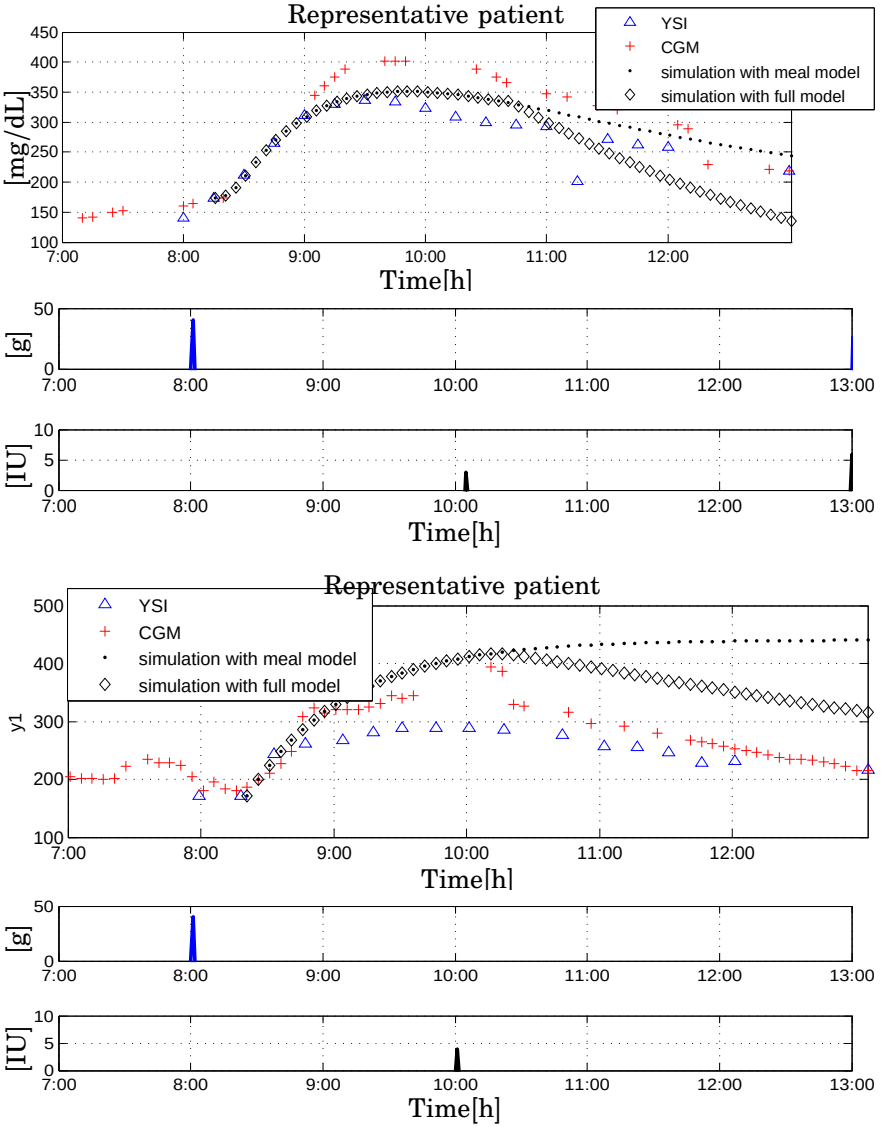

Figure D.26 Cross validation. DIAdvisor II trial, *Visit 3*, meal test. *Top panels* Patient UNIPD201; *Bottom panels* Patient IKEM306. *Top* Actual CGMS (cross) and actual YSI (triangle) vs. simulated breakfast impact (dot) and simulated joint meal and insulin intakes (diamond) [mg/dL]; *Center* Carbohydrate intake [g]; *Bottom* Insulin bolus [IU]. All the measurements vs. time of the day [h]

Bibliography

Abbott (2013). *FreeStyle Navigator^{TM}*. http://www.abbottdiabetescare.co.uk/your-products/freestyle-navigator. Page retrieved September 2013.

Accu-Check (2013). *Spirit Combo®*. https://www.accu-chekinsulinpumps.com/ipus/products/insulinpumps/combo.html. Page retrieved September 2013.

Ackerman, J. and W. McGucking (1964). "A mathematical model of the glucose tolerance test". *Phys. Medicine Biol.* **9**, pp. 203–213.

Ahlborg, G., P. Felig, L. Hagenfeldt, R. Hendler, and J. Wahren (1974). "Substrate turnover during prolonged exercise in man. splanchnic and leg metabolism of glucose, free fatty acids and amico acids". *J. Clin. Invest.* **53**, pp. 1080–1090.

Anderson, B. and J. Moore (1979). *Optimal Filtering*. Ed. by T. Kailath. Prentice-Hall, Englewood Cliffs, NJ.

Animas Corporation (2013). *One Touch® Ping®*. http://www.animas.com/animas-insulin-pumps/onetouch-ping. Page retrieved September 2013.

AP (2013). *The artificial pancreas project*. http://www.artificialpancreasproject.com/. Page retrieved May 2013.

Apidra® (2013). http://www.apidra.com. Page retrieved September 2013.

Åström, K. J. (1970). *Introduction to Stochastic Control Theory*. Academic Press, New York.

Åström, K. J. and T. Hägglund (2005). *Advanced PID Control*. ISA - The Instrumentation, Systems, and Automation Society, Research Triangle Park, NC 27709.

Åström, K. J., P. Hagander, and J. Sternby (1984). "Zeros of sampled systems". *Automatica* **20**, pp. 31–38.

Åström, K. (1980). "Maximum likelihood and prediction error methods". *Automatica* **16**, pp. 551–574.

Åström, K. and P. Eykhoff (1971). "System identification–a survey". *Automatica* **7**:2, pp. 123–162.

Bamieh, B. and L. Giarre (2002). "Identification of linear parameter varying models". *Int. Journal of Robust and Nonlinear Control* **12**:9, pp. 841–853.

Barry Keenan, D., J. Mastrototaro, G. Voskanyan, and G. Steil (2009). "Delays in minimally invasive continuous glucose monitoring devices: a review of current technology". *Journal of Diabetes Science and Technology* **3**:5, pp. 1207–1214.

Bauer, D. and L. Ljung (2001). "Some facts about the choice of the weighting matrices in Larimore type of subspace algorithm". *Automatica* **36**, pp. 763–773.

Bequette, B. (2010). "Continuous glucose monitoring: real-time algorithms for calibration, filtering and alarms". *Journal of Diabetes Science and Technology* **4**:2, pp. 404–418.

Bergamasco, M. and M. Lovera (2010). "Continuous-time subspace identification in closed-loop". In: *Proc. of the 19th International Symposium on Mathematical Theory of Networks and Systems MTNS2010*. Budapest, Hungary, pp. 1359–1365.

Bergamasco, M. and M. Lovera (2011). "Continuous-time predictor-based subspace identification using Laguerre filters". *IET Control Theory and Applications* **5**:7, pp. 856–867.

Bergman, R., Y. Ziya Ider, C. Bowden, and C. Cobelli (1979). "Quantitative estimation of insulin sensitivity". *American Journal of Physiology* **236**:6, E667–E677.

Bergman, R., L. Phillips, and C. Cobelli (1981). "Physiologic evaluation of factors controlling glucose tolerance in man: measurement of insulin sensitivity and beta-cell sensitivity from the response to intravenous glucose". *Journal Clinical Investigation* **68**, pp. 1456–1467.

Binder, C., T. Lauritzen, O. Faber, and S. Pramming (1984). "Insulin pharmacokinetics". *Diabetes* **7**, pp. 188–199.

Boiroux, D., A. Duun-Henriksen, S. Schmidt, K. Norgaard, S. Madsbad, O. Skyggebjerg, P. Jensen, N. Poulsen, H. Madsen, and J. Jørgensen (2012). "Overnight control of blood glucose in people with type 1 diabetes". In: *Proc. of the 8th IFAC Symposium on Biological and Medical Systems (IFAC BMS2012)*. Budapest, Hungary, pp. 73–78.

Boiroux, D., D. Finan, J. Jørgensen, N. Poulsen, and H. Madsen (2011). "Strategies for glucose control in people with type 1 diabetes". In: *Proceedings of the 18th World Congress of the International Federation of Automatic Control (IFAC2011)*. Milan, Italy.

Bolie, V. (1961). "Coefficients of normal blood glucose regulation". *J. Appl. Physiol.* **16**, pp. 783–788.

Bremer, T. and D. A. Gough (1999). "Is blood glucose predictable from previous values?" *Diabetes* **48**, pp. 445–451.

Breton, M and B. Kovatchev (2008). "Analysis, modeling and simulation of the accuracy of continuous glucose sensors". **2**:5. Journal of Diabetes Science and Technology, pp. 853–862.

Breton, M., D. Shields, and B. Kovatchev (2008). "Optimum subcutaneous glucose sampling and Fourier analysis of continuous glucose monitors". *Journal of Diabetes Science and Technology* **2**, pp. 495–500.

Brouns, F., I. Bjork, K. Frayn, A. Gibbs, V. Lang, G. Slama, and T. Wolever (2005). "Glycaemic index methodology". *Nutrition Research Review* **18**, pp. 145–171.

Caines, P. (1988). *Linear Stochastic Systems*. John Wiley, New York.

Cameron, F., G. Niemayer, K. Gundy-Burlet, and B. Buckingham (2008). "Statistical hypoglycemia prediction". *Journal of Diabetes Science and Technology* **2**:4, pp. 612–621.

Cameron, F., G. Niemeyer, and B. Buckingham (2009). "Probabilistic evolving meal detection and estimation of meal total glucose appearance". *Journal of Diabetes Science and Technology* **3**:5, pp. 1022–1030.

Castillo-Estrada, G., H. Kirchsteiger, L. Del Re, and E. Renard (2009). "Model based validation of meal inputs in diabetes therapy". In: *Proc. of 15th IFAC Symposium on System Identificaiton SYSID2009*. Saint-Malo, France, pp. 239–244.

Castillo-Estrada, G., H. Kirchsteiger, L. Del Re, and E. Renard (2010a). "Innovative approach for online prediction of blood glucose profile in type 1 diabetes patients". In: *Proc. American Control Conference ACC2010*. Baltimore, MD, USA, pp. 2015–2020.

Castillo-Estrada, G., L. Del Re, and E. Renard (2010b). "Nonlinear gain in online prediction of blood glucose profile in type 1 diabetic patients". In: *Proc. 49th IEEE Conference on Decision and Control (CDC2009)*. Atlanta, GA, USA, pp. 1668–1673.

Cescon, M. (2011). *Linear Modeling and Prediction in Diabetes Physiology*. Licentiate Thesis TFRT--3250--SE. Department of Automatic Control, Lund University, Sweden.

Cescon, M., F. Ståhl, R. Johansson, and M. Landin-Olsson (2009a). "Short-term diabetes blood glucose prediction based on blood glucose measurements". In: *Proc. 2nd International Conference on Advanced Technologies and Treatments for Diabetes (ATTD2009)*. Athens, Greece.

Cescon, M., F. Ståhl, M. Landin-Olsson, and R. Johansson (2009b). "Subspace-based model identification of diabetic blood glucose dynamics". In: *Proc. 15th IFAC Symposium on System Identification (SYSID2009)*. Saint-Malo, France, pp. 233–238.

Cescon, M., M. Stemmann, and R. Johansson (2012). "Impulsive predictive control of T1DM glycemia: an in-silico study". In: *2012 ASME 5th Annual Dynamic Systems and Control Conference (DSCC2012)*. Fort Lauderdale, FL, USA, p. 8550.

Chapman, C. and J. Mitchell (1965). "The physiology of exercise". *Sci. Am.* **212**, pp. 88–96.

Chiuso, A. (2007a). "On the relation between CCA and predictor-based subspace identification". *IEEE Trans. Automatic Control* **52**:10, pp. 1795–1812.

Chiuso, A. (2007b). "The role of vector autoregressive modeling in subspace identification". *Automatica* **43**:6, pp. 1034–1048.

Chiuso, A. (2008). "Choosing the future horizon in closed-loop CCA-type subspace algorithms". *Automatica* **30**, pp. 75–93.

Chiuso, A. and G. Picci (2005a). "Consistency analysis of some closed-loop subspace identification methods". *Automatica* **41**, pp. 377–391.

Chiuso, A. and G. Picci (2005b). "Prediction error vs. subspace methods in closed-loop identification". In: *Proc. 16th IFAC World Congress (IFAC2005)*. Prague, Czech Republic.

Chiuso, A. (2010). "On the asymptotic properties of closed-loop CCA-type subspace algorithms: equivalence results and role of the future horizon". *IEEE Trans. Autom. Control* **55**:3, pp. 624–649.

Clarke, W. and B. Kovatchev (2007). "Continuous glucose sensors–continuing questions about clinical accuracy". *J. Diabetes Sci. Technol.* **1**, pp. 164–170.

Clymer, A. (1959). "Direct system synthesis by means of computers". *Trans. AIEE* **77**, pp. 798–806.

Cobelli, C. and E. Carson (2008). *Introduction to Modeling in Physiology and Medicine*. Elsevier, New York.

Cobelli, C., C. Dalla Man, G. Sparacino, L. Magni, G. De Nicolao, and B. Kovatchev (2009). "Diabetes: models, signals and control". IEEE Reviews in Biomedical Engineering.

Cobelli, C., E. Renard, and B. Kovatchev (2011). "Artificial pancreas: past, present, future". **60**. Diabetes, pp. 2672–2682.

Dalla Man, C., A. Caumo, and C. Cobelli (2002). "The oral glucose minimal model: estimation of insulin sensitivity from a meal test". *IEEE Transactions on Biomedical Engineering* **49**:5, pp. 419–429.

Dalla Man, C., A. Caumo, R. Basu, R. Rizza, G. Toffolo, and C. Cobelli (2004). "Minimal model estimation of glucose absorption and insulin sensitivity from oral test: validation with a tracer method". *American Journal of Physiology Endocrinology Metabolism* **287**, E637–E643.

Dalla Man, C., K. E. Yarasheski, A. Caumo, H. Robertson, G. Toffolo, K. S. Polonski, and C. Cobelli (2005). "Insulin sensitivity by oral glucose minimal models: validation against clamp". *American Journal of Physiology Endocrinology Metabolism* **289**, E954–E959.

Dalla Man, C., M. Camilleri, and C. Cobelli (2006). "A system model of oral glucose absorption: validation on gold standard data". *IEEE Transactions on Biomedical Engineering* **53**:12, pp. 2472–2477.

Dalla Man, C., R. R. Rizza, and C. Cobelli (2007). "Meal simulation model of the glucose-insulin system". *IEEE Transactions on Biomedical Engineering* **54**:10, pp. 1740–1749.

Damiano, E., F. El-Khatib, H. Zheng, D. Nathan, and S. Russell (2013). "A comparative effectiveness analysis of three continuous glucose monitors". *Diabetes Care* **36**:2, pp. 251–259.

Dassau, E., H. Zisser, R. Harvey, M. Percival, B. Grosman, W. Bevier, E. Atlas, S. Miller, R. Nimri, L. Jovanovic, and D. F.J. (2013). "Clinical evaluation of a personalized artificial pancreas". *Diabetes Care* **36**:4, pp. 801–809.

De Gaetano, A. and O. Arino (2000). "Mathematical modelling of the intravenous glucose tolerance test". *Journal of Mathematical Biology* **40**, pp. 136–168.

De Nicolao, G., G. Sparacino, and C. Cobelli (1997). "Nonparametric input estimation in physiological systems: problems, methods and case studies". *Automatica* **33**:5, pp. 851–870.

De Nicolao, G., L. Magni, C. Dalla Man, and C. Cobelli (2011). "Modeling and control of diabetes: towards the artificial pancreas". In: *Proc. of the 18th IFAC World Congress (IFAC2011)*. Milano, Italy, pp. 7092–7101.

Deiss, D., J. Bolinder, J. Riveline, T. Battelino, E. Bosi, N. Tubiana- Rufi, D. Kerr, and M. Phillip (2006). "Improved glycemic control in poorly controlled patients with type 1 diabetes using real-time continuous glucose monitoring". *Diabetes Care* **29**, pp. 2730–2732.

Dexcom (2013). *Dexcom® SEVEN® PLUS*. `http://www.dexcom.com/seven-plus`.Page retrieved September 2013.

Di Ruscio, D. (1997). "Model based predictive control: an extended state space approach". In: *Proc. of the 36th Conference on Decision and Control (CDC1997)*. San Diego, CA, pp. 3210–3217.

DIAdvisor (2012). *The DIAdvisor^{TM}*. `http://www.diadvisor.eu`. Page retrieved May 2013.

Dong, J. and M. Verhaegen (2008a). "Model free probabilistic design with uncertain markov parameters identified in closed loop". In: *Proc. 47th Conference on Decision and Control (CDC2008)*. Cancun, Mexico, pp. 2637–2643.

Dong, J. and M. Verhaegen (2008b). "On the equivalence of closed-loop subspace predictive control with LQG". In: *Proc. 47th Conference on Decision and Control (CDC2008)*. Cancun, Mexico, pp. 4085–4090.

Dong, J., M. Verhaegen., and E. Holweg (2008). "Closed-loop subspace predictive control for fault tolerant MPC design". In: *Proc. 17th IFAC World Congress (IFAC2008)*. Seoul, South Korea, pp. 3216–3221.

Elleri, D., J. Allen, J. Harris, K. Kumareswaran, M. Nodale, L. Leelarathna, C. Acerini, A. Haidar, M. Wilinska, N. Jackson, A. Umpleby, M. Evans, D. Dunger, and R. Hovorka (2013a). "Absorption patterns of meals containing complex carbohydrates in type 1 diabetes". *Diabetologia* **56**, pp. 1108–1117.

Elleri, D., J. Allen, K. Kumareswaran, L. Leelarathna, M. Nodale, K. Caldwell, P. Cheng, C. Kollman, A. Haidar, H. Murphy, M. Wilinska, C. Acerini, D. Dunger, and R. Hovorka (2013b). "Closed-loop basal insulin delivery over 36 hours in adolescents with type 1 diabetes: randomized clinical trial". *Diabetes Care* **36**:4, pp. 838–844.

Eren-Oruklu, M., A. Cinar, L. Quinn, and D. Smith (2009). "Estimation of future glucose concentrations with subject-specific recursive linear models". *Diabetes Techn. Ther.* **11**:4, pp. 243–253.

Eren-Oruklu, M., A. Cinar, D. Rollins, and L. Quinn (2012). "Adaptive system identification for estimating future glucose concentrations and hypoglycemia alarms". *Automatica* **48**, pp. 1892–1897.

Facchinetti, A., G. Sparacino, and C Cobelli (2007). "Reconstruction of glucose in plasma from interstitial fluid continuous glucose monitoring data: role of sensor calibration". *Journal of Diabetes Science and Technology* **1**:5, pp. 617–623.

Facchinetti, A., G. Sparacino, and C. Cobelli (2010). "Modeling the error of continuous glucose monitoring sensor data: critical aspects discussed through simulation studies". *Journal of Diabetes Science and Technology* **4**:1, pp. 4–14.

Facchinetti, A., G. Sparacino, S. Guerra, Y. Luijf, J. De Vries, J. Mader, M. Ellmerer, C. Benesch, L. Heinemann, D. Bruttomesso, A. Avogaro, and C. Cobelli (2013). "Real-time improvement of continuous glucose-monitoring accuracy. The smart sensor concept." *Diabetes Care* **36**:4, pp. 793–800.

Favoreel, W., B. De Moor, P. Van Overschee, and M. Gevers (1999). "Model-free subspace-based LQG-design". In: *Proc. of the American Control Conference (ACC1999)*. San Diego, CA, pp. 3372–3376.

Fernandez, M., M. Villasana, and D. Streja (2007). "Glucose dynamics in type I diabetes: insights from the classic and linear minimal models". *Computers in Biology and Medicine* **37**, pp. 611–627.

Ferrannini, E. and C. Cobelli (1987). "The kinetics of insulin in man. general aspects." *Diabetes Metab Review* **3**, pp. 335–363.

Finan, D., J. Jørgensen, N. Poulsen, and H. Madsen (2010). "Robust model identification applied to type 1 diabetes". In: *Proc. of the 2010 American Control Conference (ACC2010)*. Baltimore, USA, pp. 2021–2026.

Finan, D., H. Zisser, L. Jovanovic, W. C. Bevier, and D. E. Seborg (2006). "Identification of linear dynamic models for type 1 diabetes: a simulation study". In: *Proc. of IFAC International Symposium on Advanced Control of Chemical Processes (ADCHEM2006)*. Gramado, Brazil.

Finan, D., H. Zisser, L. Jovanovic, W. C. Bevier, and D. E. Seborg (2007). "Practical issues in the identification of empirical models from simulated type 1 diabetes data". *Diabetes Technology and Therapeutics* **9**:5, pp. 438–450.

Finan, D., C. Palerm, F. Doyle, H. Zisser, L. Jovanovic, W. Bevier, and D. Seborg (2008). "Identification of empirical dynamic models from type 1 diabetes subject data". In: *Proc. of American Control Conference (ACC2008)*. Seattle, Washington, USA, pp. 2099–2104.

Finan, D., C. Palerm, J. Doyle, and D. Seborg (2009). "Effect of input excitation on the quality of empirical dynamic modes for type 1 diabetes". *Process Systems Engineering* **55**:5, pp. 1135–1146.

Galloway, J., C. Spradlin, R. Nelson, J. Wentworth, J. Davidson, and J. Swarner (1981). "Factors influencing the absorption, serum insulin concentration, and blood glucose responses after injections of regular insulin and various insulin mixtures". *Diabetes Care* **4**, pp. 366–376.

Gani, A, A. Gribok, L. Yinghui, W. Ward, R. Vigersky, and J. Reifman (2010). "Universal glucose models for predicting subcutaneous glucose concentration in humans". *IEEE Transactions on Information Technology in Biomedicine* **14**:1, pp. 157–165.

Gani, A., G. Andrei, R. Srinivasan, W. Kenneth, and R. Jaques (2009). "Predicting subcutaneous glucose concentration in humans: data-driven glucose modeling". *IEEE Transactions on Biomedical Engineering* **56**:2, pp. 246–254.

Garg, K., J. Smith, C. Beatson, B Lopez-Baca, M. Voelmle, and P. Gottlieb (2009). "Comparison of accuracy and safety of the seven and the navigator continuous glucose monitoring systems". *Diabetes Technol. Therapeutics* **11**, 65âĂŞ72.

Garg, S., H. Zisser, S. Schwartz, T. Bailey, R. Kaplan, S. Ellis, and L. Jovanovic (2006). "Improvement in glycemic excursions with a transcutaneous, real-time continuous glucose sensor". *Diabetes Care* **29**, pp. 44–50.

Garg, S., M. Voelmle, and P. Gottlieb (2010). "Time lag characterization of two continuous glucose monitoring systems". *Diabetes Res. Clin. Pract.* **87**, pp. 348–353.

Garnier, H., M. Mensler, and A. Richard (2003). "Continuous-time model identification from sampled data. implementation issues and performance evaluation". *International Journal of Control* **76**:13, pp. 1337–1357.

Garnier, H., L. Wang, and P. Young (2008). "Direct identification of continuous-time models from sampled data: issues, basic solutions and relevance". In: *Identification of Continuous-time Models from Sampled Data*. Springer-Verlag, London.

Golub, G. and C. Van Loan (1996). *Matrix Computations*. Ed. by T. Edition. The Johns Hopkins University Press, Baltimore, MD.

Grossman, P. (2004). "The lifeshirt: a multi-function ambulatory system monitoring health, disease, and medical intervention in the real world". *Studies in Health Technology and Informatics* **108**, pp. 133–141.

Guerra, S., A. Facchinetti, G. Sparacino, G. De Nicolao, and C. Cobelli (2012). "Enhancing the accuracy of subcutaneous glucose sensors: a real-time deconvolution-based approach". *IEEE Trans Biomed Eng.* **59**:6, pp. 1658–1669.

Hallouzi, R. (2008). *Multiple-Model Based Diagnosis for Adaptive Fault Tolerant Control*. PhD thesis. Delft Center for Systems and Control (DCSC), Delft Technical University.

Hamilton, J. (1994). *Time Series Analysis*. Princeton University Press, Princeton, NJ.

Hann, C., G. Chase, J. Lin, T. Lotz, C. Doran, and G. Shaw (2005). "Integral-based parameter identification for long-term dynamic verification of a glucose-insulin system model". *Computer Methods and Programs in Biomedicine* **77**, pp. 259–270.

Hannan, E. and M. Deistler (1988). *The Statistical Theory of Linear Systems*. John Wiley, New York.

Hannan, E. and D. Poskitt (1988). "Unit canonical correlations between future and past". *The Annals of Statistics* **16**:2, pp. 784–790.

Haverkamp, B. (2001). *State space identification: theory and practice*. PhD thesis. Delft University of Technology.

Haverkamp, B. and M. Verhaegen (1997). *SMI Toolbox: State space Model Identification software for multivariable dynamical systems*. 1.0. TU Delft. Delft, The Netherlands.

Hemocue (2013). *HemoCue®*. `http://www.hemocue.com/international/Products/Glucose-1160.html`.Page retrieved September 2013.

Ho, B. and R. Kalman (1966). "Effective construction of linear state-variable models from input/output functions". *Regelungstechn.* **14**, pp. 545–548.

Holst, J. (1977). *Adaptive Prediction and Recursive Estimation*. PhD thesis. Department of Automatic Control, Lund Institute of Technology, Sweden.

Horowitz, M., D. O'Donovan, K. Jones, C. Feinle, C. Rayner, and M. Samsom (2002). "Gastric emptying in diabetes: clinical significance and treatment". *Diabetic Medicine* **19**, pp. 177–194.

Hovorka, R. (2011). "Closed-loop insulin delivery: from bench to clinical practice". *Nat Rev Endocrinol* **7**:7, pp. 385–95.

Hovorka, R. (2005). "Management of diabetes using adaptive control". *Int. J. Adapt. Control and Signal Process.* **19**, pp. 309–325.

Hovorka, R., V. Canonico, L. Chassin, U. Haueter, M. Massi-Benedetti, M. Orsini Federici, T. Pieber, H. Schaller, L. Schaupp, T. Vering, and M. Wilinska (2004). "Nonlinear model predictive control of glucose concentration in subjects with type 1 diabetes". *Physiol. Meas.* **25**, pp. 905–920.

Humalog® (2013). `http://www.humalog.com`. Page retrieved September 2013.

Insulution (2013). *Daily Dose*. `http://www.insulution.com/en/insulution/`. Page retrieved September 2013.

International Organization for Standardization (ISO), Publication 15197 (2003). *In vitro diagnostic test systems: requirements for blood glucose monitoring systems for self-testing in managing diabetes mellitus*. Geneva.

Jansson, M. (2003). "Subspace identification and ARX modeling". In: *Proc. 13th IFAC Symposium on System Identification (SYSID2003)*. Rotterdam.

Johansson, R. (1993). *System Modeling and Identification*. Prentice Hall, Englewood Cliffs, NJ.

Johansson, R. (1994). "Identification of continuous-time models". *IEEE Transactions on Signal Processing* **4**:42, pp. 887–897.

Johansson, R. (2009). "Continuous-time model identification and state estimation using non-uniformly sampled data". In: *Proc. 15th IFAC Symposium on System Identification (SYSID2009), July, 2009, Saint-Malo, France*.

Johansson, R. (2010). "Continuous-time model identification and state estimation using non-uniformly sampled data". In: *Proc. 19th Int. Symp. Mathematical Theory of Networks and Systems (MTNS2010)*. Budapest, Hungary, pp. 347–354.

Johansson, R., M. Verhaegen, and C. T. Chou (1999). "Stochastic theory of continuous-time state-space identification". *IEEE Transactions on Signal Processing* **47**, pp. 41–51.

Johansson, R., M. Cescon, and F. Ståhl (2013). "Continuous-time model identification using non-uniformly sampled data". In: *11th IEEE AFRICON 2013 Conference*. Mauritius.

Kadali, R., B. Huang, and A. Rossiter (2003). "A data driven subspace approach to predictive controller design". *Control Eng. Practice* **11**, pp. 261–278.

Kailath, T. and B. Hassibi (2000). *Linear Estimation*. Prentice Hall, Upper Saddle River, NJ.

Kalman, R. (1960). "A new approach to linear filtering and prediction problems". *Trans. A.S.M.E. J. of Basic Engineering* **82**, pp. 35–45.

Katayama, T. (2005). *Subspace Methods for System Identification*. Springer-Verlag, London.

Katayama, T. (2006). "A system theoretic interpretation of LQ decomposition in subspace identification methods". In: *Proc. of the 17th Int. Symposium on Mathematical Theory of Networks and Systems (MTNS2006)*. Kyoto, Japan, pp. 1089–1095.

Katayama, T. and G. Picci (1999). "Realization of stochastic systems with exogenous inputs and subspace identification methods". *Automatica* **35**, pp. 1635–1652.

Keenan, B., J. Mastrototaro, G Voskanyan, and S. G.M. (2009). "Delays in minimally invasive continuous glucose monitoring devices: a review of current technology". *Journal of Diabetes Science and Technology* **3**:5, pp. 1207–1214.

Kildegaard, J., J. Randloev, J. U. Poulsen, and O. Hejlesen (2007). "The impact of non-model-related variability on blood glucose prediction". *Diabetes Technology and Therapeutics* **9**:4, pp. 385–393.

King, C., S. Anderson, M. Breton, W. Clarke, and B. Kovatchev (2007). "Modeling and calibration effectiveness and blood-to-interstitial glucose dynamics as potential confounders of the accuracy of continuous glucose sensors during hyperinsulinemic clamp". *journal of diabetes science and technology* **1**:3, pp. 317–322.

Kirchsteiger, H., S. Pölzer, R. Johansson, E. Renard, and L. del Re (2011a). "Direct continuous time system identification of MISO transfer function models applied to type 1 diabetes". In: *Proc. 50th Conference on Decision and Control and European Control Conference (CDC-ECC2011)*. Orlando, USA, pp. 5176–5181.

Kirchsteiger, H., G. Castillo Estrada, S. Pölzer, L. del Re, and E. Renard (2011b). "Estimating interval process models for type 1 diabetes for robust control design". In: *Proc. of the 18th IFAC World Congress (IFAC2011)*. Milano, Italy, pp. 11761–11766.

Kiriakidis, K. and R. O. Brien (2006). "Optimal estimation of blood insulin from blood glucose". In: *Proc. of ASME IMECE 2006*. Chicago, Illinois, USA.

Knobbe, E. J. and B. Buckingham (2005). "The extended Kalman filter for continuous glucose monitoring". *Diabetes Technology and Therapeutics* **7**:1, pp. 15–27.

Knudsen, T (2001). "Consistency analysis of subspace identification methods based on a linear regression approach". *Automatica* **37**:1, pp. 81–89.

Kollman, C., D. Wilson, T. Wysocki, W. Tamborlane, and R. Beck (2005). "Limitations of statistical measures of error in assessing the accuracy of continuous glucose sensors". *Diabetes Technology and Therapeutics* **7**:5, pp. 665–672.

Kolmogorov, A. (1939a). "Interpolation und extrapolation von stationaren zufalligen folgen". *Izv. Akad. Nauk U.R.S.S. Ser. Mat.* **5**, pp. 3–14.

Kolmogorov, A. (1939b). "Sur l'interpolation et extrapolation des suites stationnaires". *C.R. Acad. Sci. Paris* **208**, pp. 2043–2045.

Kovatchev, B., M. Breton, C. Dalla Man, and C. Cobelli (2008a). *In silico model and computer simulation environment approximating the human glucose/insulin utilization*. Master File MAF-1521. Food and Drug Administration (FDA), Silver Spring, MA.

Kovatchev, B., M. Breton, C. Cobelli, and C. Dalla Man (2008b). *Method, system and computer simulation environment for testing of monitoring and control strategies in diabetes*. Patent WO.

Kovatchev, B., D. Cox, L. Gonder-Frederick, and W. Clarke (1997). "Symmetrization of the blood glucose measurement scale and its applications". *Diabetes Care* **20**:11, pp. 1655–1658.

Kovatchev, B., L. Gonder-Frederik, D. Cox, and W. Clarke (2004). "Evaluating the accuracy of continuous glucose-monitoring sensors". *Diabetes Care* **27**:8, pp. 1922–1928.

Kovatchev, B., C. King, M. Breton, S. Anderson, and W. Clarke (2006). "Clinical assessment and mathematical modeling of the accuracy of continuous glucose sensors (CGS)". In: *Proc. 28th International Conference of the IEEE Engineering in Medicine and Biology Society (EMBS2008)*. New York City, USA, pp. 71–74.

Kulku, E., J. Tamada, G. Reach, R. Potts, and M. Lesho (2003). "Phisiological differences between interstitial glucose and blood glucose measured in human subjects". *Diabetes care* **26**:8, pp. 2405–2409.

Lantus® (2013). `http://www.lantus.com`. Page retrieved September 2013.

Larimore, W. (1990). "Canonical variate analysis in identification, filtering and adaptive control". In: *Proc. 29th IEEE Conference on Decision and Control (CDC1990)*. Honolulu, Hawaii, pp. 596–604.

Leal, Y., W. Garcia-Gabin, J. Bondia, E. Esteve, W. Ricart, J. Fernandez-Real, and J. Vehi (2010). "Real-time glucose estimation algorithm for continuous glucose monitoring using autoregressive models". *Journal of Diabetes Science and Technology* **4**:2, pp. 391–403.

Leelarathna, L., M. Nodale, J. Allen, D. Elleri, K. Kumareswaran, A. Haidar, K. Caldwell, M. Wilinska, C. Acerini, M. Evans, H. Murphy, D. Dunger, and R. Hovorka (2013). "Evaluating the accuracy and large inaccuracy of two continuous glucose monitoring systems." *Diabetes Technol. Ther.* **15**:2, p. 143149.

Lehmann, E. and T. Deutch (1992). "A physiological model of glucose-insulin interaction in type 1 diabetes mellitus". *Journal of Biomedical Engineering* **14**, pp. 235–242.

Lehmann, E., I. Hermanyi, and T. Deutch (1994). "Retrospective validation of a physiological model of glucose-insulin interaction in type 1 diabetes mellitus". *Med. Eng. and Phys.* **16**:4, pp. 351–352.

Levemir® (2013). `http://www.levemir.com`. Page retrieved September 2013.

Ljung, L. and T. McKelvey (1996). "Subspace identification from closed-loop data". *Signal Processing* **52**:2, pp. 209–215.

Ljung, L. (1999). *System identification: theory for the user*. Prentice-Hall, Upper Saddle River, NJ, USA.

Ljung, L. (2003). "Aspects and experiences of user choices in subspace identification". In: *Proc. 13th IFAC Symposium on System Identification (SYSID2003)*. Rotterdam, The Netherlands, pp. 1765–1770.

Lynch, S. and W. Bequette (2002). "Model predictive control of blood glucose in type I diabetics using subcutaneous glucose measurements". In: *Proc. of the American Control Conference (ACC2002)*. Anchorage, pp. 2714–2719.

Magni, L., D. Raimondo, L. Bossi, C. Dalla Man, G. De Nicolao, B. Kovatchev, and C. Cobelli (2007). "Model predictive control of type I diabetes: an *in Silico* trial". *Journal of Diabetes Science and Technology* **1**:6, pp. 804–812.

Magni, P., G. Sparacino, R. Bellazzi, and C. Cobelli (2006). "Reduced sampling schedule for the glucose minimal model: importance of Bayes estimation". *American Journal of Physiology Endocrinology Metabolism* **290**, E177–E184.

Makroglou, A., J. Li, and Y. Kuang (2006). "Mathematical models and software tools for the glucose-insulin regulatory system and diabetes: an overview". *Applied Numerical Mathematics* **56**, pp. 559–573.

Maran, A., C. Crepaldi, A. Tiengo, G. Grassi, E. Vitali, G. Pagano, S. Bistoni, G. Calabrese, F. Santeusanio, F. Leonetti, M. Ribaudo, U. Di Mario, G. Annuzzi, S. Genovese, G. Riccardi, M. Previti, D. Cucinotta, F. Giorgino, A. Bellomo, R. Giorgino, A. Poscia, and M. Varalli (2002). "Continuous subcutaneous glucose monitoring in diabetic patients". *Diabetes Care* **25**:2, pp. 347–352.

Markakis, M., G. D. Mitsis, and V. Z. Marmarelis (2008). "Computational study of an augmented minimal model for glycaemia control". In: *Proc. of 30th International Conference of the IEEE Engineering in Medicine and Biology Society (EMBC2008)*. Vancouver, British Columbia, Canada, pp. 5445–5448.

MathWorks (2013). *MathWorks*. `http://www.mathworks.com/products/matlab/`. Page retrieved May 2013.

Medtronic (2013a). *Guardian*®. `http://www.medtronicdiabetes.com/products/guardiancgm`. Page retrieved September 2013.

Medtronic (2013b). *MiniMed Pradigm® Revel^{TM}*. http://www.medtronicdiabetes.com/products/paradigmrevelinsulinpump. Page retrieved September 2013.

Menga, G. and E. Mosca (1980). *MUSMAR: Multivariable adaptive regulators based on multistep cost functionals*. Ed. by D.G. Lainiotis and N.S. Tzannes. D. Reidel Publishing Company, Dordrecht.

Miller, M and P. Strange (2007). "Use of Fourier models for analysis and interpretation of continuous glucose monitoring glucose profiles". *Journal of Diabetes Science and Technology* **1**, pp. 630–638.

Morbiducci, U., A. Tura, and M. Grigioni (2005). "Genetic algorithms for parameter estimation in mathematical modeling of glucose metabolism". *Computers in Biology and Medicine* **35**, pp. 862–874.

Mosca, E., G. Zappa, and J. Lemos (1989). "Robustness of multipredictor adaptive regulator: MUSMAR". *Automatica* **25**:4, pp. 521–529.

Naumova, V., S. Pereverzyev, and S. Sivananthan (2012). "A meta-learning approach to the regularized learning-case study: blood glucose prediction". *Neural Networks* **33**:9, pp. 181–193.

Normand, S., Y. Khalfallah, C. Louche-Pelissier, C. Pachiaudi, J. Antoine, S. Blanc, M. Desage, J. Riou, and M. Laville (2001). "Influence of dietary fat on postprandial glucose metabolism (exogenous and endogenous) using intrinsically (13)c-enriched durum wheat". *Br. J. Nutr.* **86**, pp. 3–11.

Novo Nordisk (2013a). *FlexTouch®*. http://www.novonordisk.com/diabetes_care/insulin_pens_and_needles/FlexTouch/. Page retrieved September 2013.

Novo Nordisk (2013b). *NovoPen® 4*. http://www.novonordisk.com/diabetes_care/insulin_pens_and_needles/novopen_4/. Page retrieved September 2013.

NovoLog® (2013). http://www.novolog.com. Page retrieved September 2013.

Nucci, G. and C. Cobelli (2000). "Models of subcutaneous insulin kinetics. a critical review". *Computer Methods and Programs in Biomedicine* **62**, pp. 249–257.

Nussey, S. and S. Whitehead (2001). *Endocrinology: An Integrated Approach*. BIOS Scientific Publishers Limited, Oxford.

Ohlsson, H. and L. Ljung (2011). "Identification of Piecewise Affine Systems Using Sum-of-Norms Regularization". In: *Proceedings of the 18th IFAC World Congress*, pp. 6640–6645.

Ohlsson, H. and L. Ljung (2013). "Identification of Switched Linear Regression Models using Sum-of-Norms Regularization". *Automatica* **49**:4, pp. 1045–1050.

Ohta, Y. and T. Kawai (2004). "Continuous-time subspace system identification using generalized orthonormal basis functions". In: *Proc. of the 16th Int. Symp. Mathematical Theory of Network and Systems (MTNS2004)*. Leuven, Belgium.

Palerm, C. and B. Bequette (2007). "Hypoglycemia detection and prediction using continuous glucose monitoring - a study on hypoglycemic clamp data". *Journal of Diabetes Science and Technology* **1**:5, pp. 624–629.

Palerm, C., J. Willis, J. Desemone, and B. Bequette (2005). "Hypoglycemia prediction and detection using optimal estimation". *Diabetes Technology and Therapeutics* **7**:1, pp. 3–14.

Palerm, C. C., M. Rodriguez-Fernandez, W. C. Bevier, H. Zisser, J. R. Banga, L. Jovanovic, and F. J. Doyle (2006). "Robust parameter estimation in a model for glucose kinetics in type 1 diabetes subjects". In: *Proc. 28th International Conference of the IEEE Engineering in Medicine and Biology Society (EMBS2006)*. New York City, USA, pp. 319–322.

Pappada, S., B. Cameron, and P. Rosman (2008). "Development of a neural network for prediction of glucose concentration in type 1 diabetes patients". *Journal of Diabetes Sciences and Technology* **2**:5, pp. 792–801.

Pappada, S., B. Cameron, P. Rosman, R. Bourey, T. Papadimos, W. Olorunto, and M. Borst (2011). "Neural network-based real-time prediction of blood glucose in patients with insulin-dependent diabetes". *Diabetes Techn. Ther.* **13**:2, pp. 135–141.

Percival, M., Y. Wang, B. Grosman, E. Dassau, H. Zisser, L. Jovanovic, and F. Doyle (2011). "Development of a multi-parametric model predictive control algorithm for insulin delivery in type 1 diabetes mellitus using clinical parameters". *Journal of Process Control* **21**:3, pp. 391–404.

Percival, M., W. Bevier, H. Zisser, L. Jovanovic, D. Seborg, and F. Doyle (2008). "Prediction of dynamic glycemic trends using optimal state estimation". In: *Proc. of 17th IFAC World Congress (IFAC2008)*. Seoul, South Korea, pp. 4222–4227.

Percival, M., W. Bevier, Y. Wang, E. Dassau, H. Zisser, L. Jovanovic, and F. Doyle (2010). "Modeling the effects of subcutaneous insulin administration and carbohydrate consumption on blood glucose". **4**:5. Journal of Diabetes Science and Technology, pp. 1214–1228.

Perez-Gandia, C., A. Facchinetti, G. Sparacino, C. Cobelli, E. Gomez, M. Rigla, A. de Leiva, and M. Hernando (2010). "Artificial neural network algorithm for online glucose prediction from continuous glucose monitoring". *Diabetes Technology and Therapeutics* **12**:1, pp. 81–88.

Perriello, G., P. De Feo, E. Torlone, C. Fanelli, F. Santeusanio, P. Brunetti, and G. Bolli (1991). "The dawn phenomenon in type 1 (insulin–dependent) diabetes mellitus: magnitude, frequency, variability and dependency on glucose counterregulation and insulin sensitivity". *Diabetologia* **34**, pp. 21–28.

Peternell, K (1995). *Subspace methods for subspcae identification*. PhD thesis. Tech. Univ. Vienna.

Pillonetto, G., G. Sparacino, and C. Cobelli (2003). "Numerical non-identifiability regions of the minimal model of glucose kinetics: superiority of bayesian estimation". *Mathematical Biosciences* **184**, pp. 53–67.

Reifman, J., S. Rajaraman, A. Gribok, and W. Ward (2007). "Predictive monitoring for improved management of glucose levels". *Journal of Diabetes Sciences and Technology* **1**:4, pp. 478–486.

Rivera-Montalvo, A., A. Stamps, and E. Gatzke (2008). "Application of dynamic optimization-based parameter estimation to a diabetes mellitus patient model". In: *Proc. of American Control Conference (ACC2008)*. Seattle, Washington, USA, pp. 1382–1387.

Robergs, R. and S. Roberts (2000). *Fundamentals Principles of Exercise Physiology for Fitness, Performance, and Health*. McGraw-Hill Companies.

Roy, A. and R. S. Parker (2006). "Dynamic modeling of free fatty acid, glucose, and insulin: an extended minimal model". *Diabetes Technology and Therapeutics* **8**:6, pp. 617–626.

Sanofi-Aventis (2013). *ClikSTAR®*. `http://en.sanofi.com/products/diabetes/diabetes.aspx`. Page retrieved September 2013.

Schmidt, S., D. Finan, A. K. Duun-Henriksen, J. Jørgensen, H. Madsen, H. Bengtsson, J. Holst, S. Madsbad, and K. Norgaard (2012). "Effects of everyday life events on glucose, insulin, and glucagon dynamics in continuous subcutaneous insulin infusion-treated type 1 diabetes: collection of clinical data for glucose modeling". *Diabetes Technology and Therapeutics* **14**:3, pp. 210–217.

Sinha, N. and G. Rao (1991). *Identification of continuous-time systems. Methodology and computer implementation*. Kluwer Academic Publishers, The Netherlands.

Sivananthan, S., V. Naumova, C. Dalla Man, A. Facchinetti, E. Renard, C. Cobelli, and S. Pereverzev (2011). "Assessment of blood glucose predictors: the prediction-error grid analysis (PRED-EGA)". *Diabetes Technol. Ther.* **13**:8, pp. 787–796.

Söderström, T. and P. Stoica (1989). *System Identification*. Prentice Hall, Upper Saddle River, NJ.

Sorensen, J. (1985). *A Physiologic Model of Glucose Metabolism in Man and Its Use to Design and Assess Improved Insulin Therapies for Diabetes*. PhD thesis. Massachussetts Institute of Technology, Department of Chemical Engineering.

Sparacino, G, A Facchinetti, A Maran, and C Cobelli (2008). "Continuous glucose monitoring time series and hypo/ hyper glycemia prevention: requirements, methods, open problems". *Current Diabetes Reviews* **4**:3, pp. 181–192.

Sparacino, G., F. Zanderigo, A. Maran, A. Facchinetti, and C. Cobelli (2007). "Glucose concentration can be predicted ahead in time from continuous glucose monitoring sensor time-series". *IEEE Transactions on Biomedical Engineering* **54**:5, pp. 931–937.

Spurr, G., A. Prentice, P. Murgatroyd, G. Goldberg, J. Reina, and N. Christman (1988). "Energy expenditure from minute-by-minute heart-rate recording: a comparison with indirect calorimetry". *The American Journal of Clinical Nutrition* **48**:3, pp. 552–559.

Ståhl, F. and R. Johansson (2008). "Short-term diabetes blood glucose prediction based on blood glucose measurements". In: *Proc. of 30th International Conference of the IEEE Engineering in Medicine and Biology Society (EMBC2008)*. Vancouver, British Columbia, Canada, pp. 291–294.

Ståhl, F. and R. Johansson (2009). "Diabetes mellitus modeling and short-term prediction based on blood glucose measurements". *Mathematical Biosciences* **217**, pp. 101–117.

Steil, G., K. Rebrin, F. Hariri, S. Jinagonda, S. Tadros, C. Darwin, and M. Saad (2005). "Interstitial fluid glucose dynamics during insulin-induced hypoglycemia". *Diabetologia* **48**, pp. 1833–1840.

Stemmann, M. (2013). *Predictive Control of Diabetic Glycemia*. Licentiate Thesis TFRT--3258--SE. Department of Automatic Control, Lund University, Sweden.

Stoica, P. and A. Nehorai (1989). "On multistep prediction error methods for time series models". *Journal of Forecasting* **8**, pp. 357–368.

The American Diabetes Association (2010). "Diagnosis and classification of diabetes mellitus". *Diabetes Care* **33**:Supplement 1, S11–S66.

The American Diabetes Association (2013). "Standards of medical care in diabetes 2013". *Diabetes Care* **36**:Supplement 1, S11–S66.

The Diabetes Control and Complications Trial Research Group (1993). "The effect of intensive treatment of diabetes on the development and progression of long-term complications in insulin-dependent diabetes mellitus". *N Eng J Med* **329**:14, pp. 977–986.

The Diabetes Control and Complications Trial/Epidemiology of Diabetes Interventions and Complications Study Research Group (2005). "Intensive diabetes treatment and cardiovascular disease in patients with rype 1 diabetes". *N Eng J Med* **353**:25, pp. 2643–2653.

The DIAdvisor Consortium (2012). "Final publishable summary report". `http://cordis.europa.eu/results/`.

The International Diabetes Federation (2013). *IDF diabetes atlas 5th edition 2012 update*. `http://www.idf.org`. Page retrieved May 2013.

Toumaz technologies. *Sensium^{tm} life pebble*. `http://www.toumaz.com/`. Page retrieved September 2013.

Truxal, T. (1955). *Control System Synthesis*. McGraw-Hill, New York.

Unbehauen, H. and G. Rao (1987a). *Identification of Continuous-Time Systems*. North-Holland, Amsterdam.

Unbehauen, H. and G. Rao (1987b). *Identification of Continuous-Time Systems*. Amsterdam: North-Holland.

Unbehauen, H. and G. Rao (1990). "Continuous-time approaches to system identification-a survey". *Automatica* **26**, pp. 23–35.

van Heudsen, K., E. Dassau, H. Zisser, D. Seborg, and F. Doyle (2012). "Control-relevant models for glucose control using a priori patient characteristics". **59**:7. IEEE Trans. Biomedical Eng., pp. 1839–1849.

Van Overschee, P. and B. De Moor (1994). "N4SID: subspace algorithms for the identification of combined deterministic-stochastic systems". *Automatica* **30**, pp. 75–93.

Van Overschee, P. and B. De Moor (1996). *Subspace Identification for Linear Systems : Theory-Implementation-Application*. Kluwer Academic Publishers, Boston.

Verdult, V. and M. Verhaegen (2002). "Subspace identification of multivariable linear parameter-varying systems". *Automatica* **38**:5, pp. 805–814.

Verhaegen, M. (1994). "Identification of the deterministic part of MIMO state space models given in innovations form from input-output data". *Automatica* **30**:1, pp. 61–74.

viliv (2013). *viliv S5*. `http://www.myviliv.com/v4/product/s5/s5.asp`. Page retrieved September 2013.

Wahren, J., G. Felig, G. Ahlborg, and L. Jorfeldt (1971). "Glucose metabolism during leg exercise in man". *J. Clin. Invest.* **50**, pp. 2715–2725.

Walsh, J. and R. Roberts (2012). *Pumping Insulin*. Ed. by 5th edition. Torrey Pines Press, San Diego, CA.

Wang, Y., H. Zisser, E. Dassau, L. Jovanovic, and F. Doyle J. III (2010). "Model predictive control with learning-type set-point: application to artificial pancreatic beta-cell". **56**:6. AIChE Journal, pp. 1510–1518.

Wiener, N. (1949). *The extrapolation interpolation and smoothing of stationary time series with engineering applications*. J. Wiley & Sons.

Wilinska, M., L. Chassin, H. Schaller, L. Schaupp, T. Pieber, and R. Hovorka (2005). "Insulin kinetics in type-1 diabetes: continuous and bolus delivery of rapid acting insulin". *IEEE Transactions on Biomedical Engineering* **52**:1, pp. 3–12.

Wilinska, M., L. Chassin, C. Acerini, J. Allen, D. Dunger, and R. Hovorka (2010). "Simulation environment to evaluate closed-loop insulin delivery systems in type 1 diabetes". *Journal of Diabetes Science and Technology* **4**:1, pp. 132–144.

Williams, G. and J. Pickup (1992). *Handbook of Diabetes second edition*. Blackwell Science, Oxford.

Woodley, B., J. How, and R. Kosut (2001). "Subspace based direct adaptive H_∞ control". *Int. J. Adapt. Control Signal Process.* **15**, pp. 535–561.

World Health Organization-International Diabetes Federation (2006). *Definition and diagnosis of diabetes mellitus and intermediate hyperglycemia-Report of a WHO/IDF consultation*. Tech. rep. World Health Organization.

Yellow Spring Instruments (2013). *YSI 2300 STAT Plus^{TM} Glucose Analyzer*. `http://www.ysilifesciences.com/index.php?page=ysi-2300-stat-plus-glucose-lactate-analyzer`. Page retrieved September 2013.

Young, P. (1981a). "Parameter estimation for continuous-time models - a survey". *Automatica* **17**:1, pp. 23–39.

Young, P. (1964). "In flight dynamic checkout - a discussion". *IEEE Transactions on Aerospace* **2**, pp. 1106–1111.

Young, P. (1969). "Applying parameter estimation to dynamic systems". *Control engineering* **16**, Oct 119–125, Nov 118–124.

Young, P. (1981b). "Parameter estimation for continuous-time models-a survey". *Automatica* **17**, pp. 23–29.

Young, P. and H. Garnier (2006). "Identification and estimation of continuous-time data-based mechanistic (DBM) models for environmental systems". *Environmental Modelling and Software* **21**:8, pp. 1055–1072.

Zecchin, C., A. Facchinetti, G. Sparacino, G. De Nicolao, and C. Cobelli (2011). "A new neural network approach for short-term glucose prediction using continuous glucose monitoring time-series and meal information". In: *Proc. of 33rd International Conference of the IEEE Engineering in Medicine and Biology Society (EMBC2011)*. Boston, Massachussets, USA.

Zecchin, C., A. Facchinetti, G. Sparacino, G. De Nicolao, and C. Cobelli (2012). "Neural network incorporating meal information improves accuracy of short-time prediction of glucose concentration". *IEEE Trans Biomed Eng.* **59**:6, pp. 1550–1560.

Zecchin, C., A. Facchinetti, G. Sparacino, and C. Cobelli (2013). "Reduction of number and duration of hypoglycemic events by glucose prediction methods: a proof-of-concept in silico study". *Diabetes Technol. Ther.* **15**:1, pp. 66–77.

Zhao, C., E. Dassau, L. Jovanovic, H. Zisser, F. Doyle, and D. Seborg (2013). "Predicting subcutaneous glucose concentration using a latent-variable-based statistical method for type 1 diabetes mellitus". *Journal of Diabetes Science and Technology* **6**:3, pp. 617–33.